UNIVERSIDAD COMPLUTENSE DE MADRID
FACULTAD DE CIENCIAS FÍSICAS

TESIS DOCTORAL

Development of dual-layer membranes and recycling of reverse osmosis membrane modules for water treatment

Desarrollo de membranas de doble capa y reciclaje de módulos de membrana de ósmosis inversa para tratamiento de aguas

MEMORIA PARA OPTAR AL GRADO DE DOCTOR

PRESENTADA POR

Jorge Contreras Martínez

Directores

Mohamed Khayet Souhaimi
María del Carmen García Payo

Madrid

UNIVERSIDAD COMPLUTENSE DE MADRID
FACULTAD DE CIENCIAS FÍSICAS

TESIS DOCTORAL

Development of dual-layer membranes and recycling of reverse osmosis membrane modules for water treatment

Desarrollo de membranas de doble capa y reciclaje de módulos de membrana de ósmosis inversa para tratamiento de aguas

MEMORIA PARA OPTAR AL GRADO DE DOCTOR

PRESENTADA POR

Jorge Contreras Martínez

DIRECTORES

Mohamed Khayet Souhaimi
María del Carmen García Payo

UNIVERSIDAD
COMPLUTENSE
MADRID

Development of dual-layer membranes and recycling of reverse osmosis membrane modules for water treatment

Desarrollo de membranas de doble capa y reciclaje de módulos de membrana de ósmosis inversa para tratamiento de aguas

Doctoral Thesis

Jorge Contreras Martínez

Supervisors

Mohamed Khayet Souhaimi

María del Carmen García Payo

Department of Structure of Matter, Thermal Physics and Electronics

Faculty of Physics

Madrid, 2021

“El agua anda descalza por calles mojadas”

Pablo Neruda

Siempre agradecido a todas las personas que
han hecho de esto una realidad.
A mi familia, que siempre está ahí.
A mis directores de tesis Carmen y Mohamed por
darme esta oportunidad y enseñarme tantas cosas.
A mis compañeros y amigos, simplemente por serlo.
Gracias a todos.

Index of contents

Appendix B: Supplementary Information of Chapter 6

Abstract

Nowadays, water scarcity is a problem that important organizations such as the United Nations (UN) warn about, indicating that only less than two-thirds of the world's population has adequate access to safe and drinking water. Membrane technologies and mainly desalination by reverse osmosis (RO) process, are being applied worldwide as mechanisms to obtain drinking water. However, RO has still some problems that require an immediate solution, such as the treatment and management of the produced brines and wastes caused by discarded RO membrane modules. Other membrane processes of emerging interest such as forward osmosis (FO), pervaporation (PV) or membrane distillation (MD), also need focused efforts for their proper development and subsequent large scale application.

The main objective of this PhD thesis is twofold. On one hand, dual-layer polymeric membranes (DLMs) are developed using different membrane preparation techniques in order to improve the performance of membrane separation processes of emerging interest such as PV and MD; and on other hand, attempts are made to recycle discarded RO modules in order to extend the useful life of their components making them suitable for water treatment by other membrane processes, contributing therefore to the circular economy of membrane science and protection of the environment.

Chapter 1 introduces the topic of the PhD. thesis, motivation and main objectives, as well as the membrane separation processes of emerging interest (PV, MD and FO) and the summary of the PhD. Thesis. In addition, a brief overview of RO in desalination field is given outlining its advantages and drawbacks, such as brines discharge into the environment and the high number of RO membrane modules disposed annually.

Chapter 2 is a state of the art review on the reuse and recycling of discarded RO membrane modules at the end of their useful life. It is reviewed the strategies currently applied as well as the different solutions proposed by the scientific community for their reuse and recycling in ultrafiltration (UF), nanofiltration (NF) and electrodialysis (ED) membranes. However, more efforts still need to be devoted to the development of new recycling procedures of discarded RO modules.

Chapter 3 deals with the development of DLMs composed of highly porous electrospun

polyvinylidene fluoride (PVDF) supports and a thin organophilic layer formed by the polymer of intrinsic microporosity PIM-1, for their application in n-butanol removal from water by PV. Compared to other membranes, these DLMs exhibit quite high permeate fluxes with very good separation factors. In addition, a numerical simulation study has been carried out by Aspen HYSYS applying these DLMs in hybrid PV systems with distillation columns for the production of biofuel. The numerical simulation shows how an increase of n-butanol concentration for a conventional distillation process as well as an increase in the separation factor of the membranes implies a reduction of the needed energy of the process for the separation of n-butanol from water.

Chapter 4 illustrates an experimental study on the design of DLMs hydrophobic/hydrophilic membranes composed of PVDF and polysulfone (PS) layers prepared by electrospinning for direct contact membrane distillation (DCMD) application. Compared to single-layer membranes prepared with PVDF under the same electrospinning time and the same DCMD operating conditions, these DLMs show higher permeate fluxes with very good salt (NaCl) rejection factors greater than 99.99%.

The knowledge acquired in the design, preparation and characterization of DLMs explored in Chapters 3 and 4, has facilitated to carry out the recycling and reuse of different elements of RO membrane modules. The recycling of the internal components of these modules like the membrane itself, the permeate spacer and the feed spacer, to prepare hydrophobic/hydrophilic DLMs has been proven in Chapter 5. The recycling of the permeate spacer, as a hydrophilic support of DLMs formed by an electrospun PVDF hydrophobic layer, improves the mechanical properties of this type of membranes and show DCMD permeate fluxes similar to those of commercial membranes applied under the same operating conditions, with high salt rejection factors (greater than 99%) during the treatment of high saline aqueous solutions, with concentrations up to 180 g/L, confirming their applicability in the concentration of RO brines. The use of RO membrane as support increases the liquid entry pressure (*LEP*) of the hydrophobic/hydrophilic DLMs, improves their salt rejection factors, but reduces their permeate fluxes. On the contrary, the use of the feed spacer as support results in a an irregular hydrophobic electrospun layer with large spaces between fibers, obtaining low salt rejection factors.

Another attempt of high interest for the circular economy is covered in Chapter 6. It deals with the recycling of discarded RO membranes converting them to FO membranes by applying the interfacial polymerization (IP) technique to form a new selective layer of PA or polyester (PE). These DLMs for FO applications are used for the treatment of humic acid model wastewater while RO brines of different concentrations are employed as osmotic solutions. The surface modification of this recycled membrane by IP using a mixture of

m-phenylenediamine (MPD) and trimethylamine (TEA) as an aqueous solution and trimesoyl chloride (TMC) as an organic solution, to form a thin layer of PA, improves the FO permeate fluxes and exhibits higher or comparable FO performance than those of the FO commercial membranes used under the same operating conditions.

The last chapter summarizes the most important conclusions of the present PhD. Thesis and presents the possible future research lines of interest opened in the UCM research group "*Membranes and Renewable Energies*".

Resumen

En la actualidad la escasez de agua es un problema del que alertan importantes organizaciones como la Organización de las Naciones Unidas (ONU), indicando que solo menos de dos tercios de la población mundial tiene acceso adecuado a agua potable y segura. Las tecnologías de membrana y principalmente la desalación mediante el proceso de separación ósmosis inversa (OI), están siendo aplicadas en todo el mundo como mecanismos para la obtención de agua potable. Sin embargo, la OI presenta algunos problemas que requieren una inmediata solución como el tratamiento y la gestión de las salmueras producidas y el adecuado manejo de los residuos ocasionados por los módulos de membrana desechados. Otros procesos de membrana de interés emergente como la osmosis directa (OD), la pervaporación (PV) o la destilación en membrana (DM), también necesitan la focalización de esfuerzos para su adecuado desarrollo y posterior aplicación a gran escala.

El objetivo principal de esta tesis doctoral es doble. Por un lado se estudia el desarrollo de membranas poliméricas de doble capa (MDCs) aplicando diferentes técnicas de preparación de membranas, con el objeto de mejorar el rendimiento de procesos de separación por membranas emergentes como la PV y la DM; y por otro lado se reciclan módulos de OI descartados con el objeto de alargar la vida útil de sus componentes para aplicaciones en otros procesos de membrana para el tratamiento de aguas, contribuyendo en la economía circular de la ciencia de membranas y protección del medio ambiente.

En el Capítulo 1 se introduce la temática de la tesis doctoral, motivación y objetivos principales, los procesos de separación por membranas de interés emergente (PV, DM y OD) y un resumen de la tesis. Además, se presenta una breve visión general de la OI en el campo de la desalación, indicando sus ventajas y sus problemáticas como la descarga de salmueras al medio ambiente y el elevado número de módulos de membranas de OI desechados anualmente.

El Capítulo 2 es una revisión del estado del arte en la reutilización y reciclaje de módulos de membranas de OI desechados al final de su vida útil. Se revisa las estrategias actualmente aplicadas, así como las diferentes soluciones propuestas por la comunidad científica para su reutilización y reciclaje en ultrafiltración (UF), nanofiltración (NF) y

electrodiálisis (ED). Sin embargo, aún es necesario centrar los esfuerzos para desarrollar nuevos procedimientos de reciclaje de los módulos de OI desechados.

En el Capítulo 3 se propone el desarrollo de MDCs compuestas por soportes de fluoruro de polivinilideno (PVDF) electrohilados altamente porosos y una fina capa organofílica formada por el polímero de microporosidad intrínseca PIM-1, para la separación de n-butanol del agua por PV. En comparación con otras membranas, estas MDCs exhiben unos flujos de permeado bastante altos con muy buen factor de separación. Mediante simulación numérica empleando Aspen HYSYS, se ha llevado a cabo un estudio aplicando estas MDCs en sistemas híbridos de PV con columnas de destilación para la producción de biocombustible. La simulación numérica muestra como un aumento en la concentración de n-butanol en el proceso destilación convencional, así como un aumento del factor de separación en los sistemas híbridos implican una reducción de la energía necesaria para la separación de n-butanol del agua.

En el Capítulo 4 se presenta un estudio experimental sobre MDCs hidrófoba/hidrofílicas compuestas por capas de PVDF y de polisulfona (PS) preparadas por electrohilatura para la desalación por destilación en membrana por contacto directo (DMCD). En comparación con las membranas de una sola capa preparadas con PVDF bajo el mismo tiempo de electrohilado y las mismas condiciones de operación DMCD, estas MDCs presentan mayores flujos de permeado con muy buenos factores de rechazo de sal (NaCl) superiores al 99.99%.

El conocimiento adquirido en el diseño, preparación y caracterización de MDCs recogidos en los Capítulos 3 y 4, ha ayudado en el reciclaje y reutilización de diferentes elementos de módulos de OI. En el Capítulo 5 se ha propuesto el reciclaje de los componentes internos de estos módulos como la membrana, el espaciador del permeado y el espaciador del alimento para preparar MDCs hidrófoba/hidrofílicas para DM. El reciclaje del espaciador del permeado, como soporte hidrofílico de MDCs con una capa hidrófoba electrohilada de PVDF, mejora las propiedades mecánicas de este tipo de membranas y presenta flujos de permeado DCMD similares a los obtenidos en membranas comerciales bajo las mismas condiciones de operación, con altos factores de rechazo de sal (superiores al 99%) utilizando disoluciones acuosas con altas concentraciones salinas de hasta 180 g/L confirmando su aplicabilidad en la concentración de salmueras de OI. El uso de la membrana de OI reciclada como soporte aumenta la presión de entrada de agua (*LEP*) de las MDCs hidrófoba/hidrofílicas, mejora el factor de rechazo de sal, pero reduce el flujo de permeado. Por el contrario, el uso del espaciador del alimento reciclado como soporte presenta una capa hidrófoba irregular con grandes espacios entre fibras obteniéndose bajos factores de rechazo de sal.

Otro intento de alto interés para la economía circular se recoge en el Capítulo 6 y es el reciclaje de las membranas de OI desechadas para convertirlas en membranas de OD aplicando la técnica de polimerización interfacial (PI) para formar una nueva capa selectiva de PA o poliéster (PE). Estas MDCs para OD se emplean para el tratamiento de aguas residuales modelo de ácido húmico aplicando como disolución osmótica salmueras de OI a diferentes concentraciones. La modificación superficial por PI utilizando una mezcla de m-fenilendiamina (MPD) y trimetilamina (TEA) como disolución acuosa y cloruro de trimesoilo (TMC) como disolución orgánica forma una fina capa de PA que mejora los flujos de permeado OD y muestra unos rendimientos en OD superiores o comparables a los ofrecidos por las membranas OD comerciales utilizadas bajo las mismas condiciones de operación.

En el último capítulo se resumen las conclusiones más importantes de esta tesis doctoral y se presentan las posibles futuras líneas de investigación de interés que se han abierto en el grupo de investigación UCM "*Membranas y Energías Renovables*".

Publications, research stays, conferences and awards

Publications derived from the PhD Thesis

1. *Dual-layered electrospun nanofibrous membranes for membrane distillation*
   Authors: M. Khayet, M. C. García-Payo, L. García-Fernández, J. Contreras-Martínez
   Journal: Desalination
   Volume: 426 (2018) 174-184
   Date: January 2018
   DOI: https://doi.org/10.1016/j.desal.2017.10.036

2. *Electrospun nanostructured membrane engineering using reverse osmosis recycled modules: membrane distillation application*
   Authors: J. Contreras-Martínez, C. García-Payo, M. Khayet
   Journal: Nanomaterials
   Volume: 11 (2021) 1601
   Date: June 2021
   DOI: https://doi.org/10.3390/nano11061601

3. *High-flux thin film composite PIM-1 membranes for butanol recovery: experimental study and process simulations*
   Authors: J. Contreras-Martínez, S. Mohsenpour, A. W. Ameen, P. M. Budd, C. García-Payo, M. Khayet, P. Gorgojo
   Journal: ACS Applied Materials & Interfaces
   Volume: 13 (2021) 42635-42649
   Date: September 2021
   DOI: https://doi.org/10.1021/acsami.1c09112

4. *Recycled reverse osmosis membranes for forward osmosis technology*
   Authors: J. Contreras-Martínez, C. García-Payo, P. Arribas, L. Rodríguez-Sáez, A. Lejarazu-Larrañaga, E. García-Calvo, M. Khayet
   Journal: Desalination
   Volume: 519 (2022) 115312
   Date: December 2021
   DOI: https://doi.org/10.1016/j.desal.2021.115312

Book chapters derived from the PhD Thesis

5. *Reuse and Recycling of End-of-Life Reverse Osmosis Membranes*
   Authors: J. Contreras-Martínez, J. A. Sanmartino, M. Khayet, M. C. García-Payo
   Book title: Advancement in Polymer-Based Membranes for Water Remediation
   Editors: Sanjay Kumar Nayak, Kingshuk Dutta, Jaydevsinh M. Gohil
   Editorial: Elsevier
   Chapter: 11
   ISBN: 978-0-323-88514-0
   Date: March 2021

Other publications

6. *Life Cycle Assessment application for emerging membrane recycling technologies: from reverse osmosis into forward osmosis*
   Authors: J. Senán-Salinas, J. Landaburu-Aguirre, J. Contreras-Martínez, E. García-Calvo
   Journal: Resources, Conservation and Recycling
   Volume: XXX
   Date: 2021 submitted, under revision.

Research stays during the PhD Thesis

1. ***Host Institution:*** *University of Manchester, School of Chemical Engineering*
   Supervisor: *Professor Patricia Gorgojo*
   Temporary stay: *from 01/10/19 to 01/01/20 (Three months)*

Conferences and congress contributions

1. *Innovación y reciclaje de membranas para el tratamiento de aguas residuales y salinas*
   Authors: J. Contreras-Martínez
   Congress: Jornadas de Doctorando UCM, Facultad Ciencias Físicas
   Place: Madrid (Spain)
   Type of contribution: Oral
   Date: 11 December 2017

2. *Innovación y reciclaje de membranas para el tratamiento de aguas residuales y salinas*
   Authors: J. Contreras-Martínez, C. García-Payo, M. Khayet
   Congress: PhDay 2017
   Place: Madrid (Spain)
   Type of contribution: Poster
   Date: 19-20 December 2017

3. *Recycling RO membrane modules for the treatment of high saline solutions by membrane distillation*
   Authors: J. Contreras-Martínez, P. Arribas, M. Khayet, M.C. García-Payo
   Congress: Euromembrane 2018
   Place: Valencia (Spain)
   Type of contribution: Poster
   Date: 11 July 2018

4. *Hydrophobic/hydrophilic composite nanofibrous membranes for direct contact membrane distillation*
   Authors: M. Khayet, M.C. García-Payo, L. García-Fernández, J. Contreras-Martínez
   Congress: Euromembrane 2018
   Place: Valencia (Spain)
   Type of contribution: Poster
   Date: 11 July 2018

5. *Interfacial polymerization study for recycling RO membranes in FO wastewater treatment*
   Authors: P. Arribas, J. Contreras-Martínez, M. C. García-Payo, M. Khayet
   Congress: Euromembrane 2018
   Place: Valencia (Spain)
   Type of contribution: Poster
   Date: 11 July 2018

6. *Life cycle assessment challenges in innovative recycling research. From reverse osmosis to forward osmosis*
   Authors: J. Senán-Salinas, J. Contreras-Martínez, J. Landaburu-Aguirre, E. García-Calvo
   Congress: SETAC Europe 24th LCA Symposium
   Place: Vienna (Austria)
   Type of contribution: Oral
   Date: 24-26 September 2018

7. *Recycled reverse osmosis discarded modules as membrane supports for membrane distillation technology*
   Authors: J. Contreras-Martínez, E. G. Merino, M.C. García-Payo, M. Khayet
   Congress: 6th International Conference on Engineering Research, Innovation and Education
   Place: Sylhet (Bangladesh)
   Type of contribution: Poster
   Date: 26-28 February 2021

8. *Recycled reverse osmosis membranes for forward osmosis technology*
   Authors: J. Contreras-Martínez, M.C. García-Payo, M. Khayet
   Congress: 6th International Conference on Engineering Research, Innovation and Education
   Place: Sylhet (Bangladesh)
   Type of contribution: Poster
   Date: 26-28 February 2021

Scientific awards

1. *Recycled reverse osmosis membranes for forward osmosis technology*
   Type: Poster award
   Authors: J. Contreras-Martínez, M.C. García-Payo, M. Khayet
   Congress: 6th International Conference on Engineering Research, Innovation and Education
   Place: Sylhet (Bangladesh)
   Date: 26-28 February 2021

Chapter 1

Introduction

1.1. Motivation and objectives

In 2010, a resolution of the General Assembly of the United Nations (UN) [1] admitted access to safe drinking water and sanitation as an essential human right. Nevertheless, in 2021, 2 billion people (approximately 25% of the world's population) do not have access to safe water [2]. This water scarcity causes the death of more than 2 million people each year [3]. Although more than 70% of the planet's surface is water, only 0.5% is adequate for human consumption. Moreover, this small percentage is not evenly distributed throughout the planet and it is not always managed properly [4]. In March 2021, UNICEF reported that the main causes of water crisis are the climate change, population growth and its associated increased water demand, conflicts and migration as well as poor water management [5]. In the same report, mobilizing business and technological innovations to improve the use, efficiency, quality and treatment of water is outlined as one of the four strategies required to solve this problem [5]. The other three indicated strategies to mitigate the worldwide water crisis are advocating for political commitment and policy change, accelerating financing and capacity development, and activating young people as champions and agents of change.

Since the presentation of the first asymmetric cellulose diacetate reverse osmosis (RO) membrane in 1963 by Loeb and Sourirajan [6] and the subsequent installation of the world's first RO pilot in Coalinga (California) [7], membrane separation technology has been presented as one of the technological solutions that can respond to water scarcity. Compared to conventional technologies, membrane separation processes exhibit various advantages for the treatment of water and wastewater, such as their better contaminants removal efficiencies, smaller sizes, suitability in developing countries and reduced energy consumption [3]. Different membrane separation technologies have been developed. Depending on the involved separation mechanism one can find microfiltration (MF), ultrafiltration (UF), nanofiltration (NF), reverse osmosis (RO), forward osmosis (FO), pressure retarded osmosis (PRO), membrane distillation (MD), electrodialysis (ED) and pervaporation (PV) among others. The membranes used in these processes are selective barriers able to separate compounds in liquid or vapour phases by means of an appropriate driving force. One of the provided classifications of membrane separation processes is according to their transmembrane driving force, the species that could separate or field of application. Table 1.1 summarizes some membrane technologies used for water treatment together with their driving force and main fileds of applications.

Table 1.1. *Membrane separation technologies together with their driving forces and main fields of applications [8, 9].*

	Driving force	Pore size (nm)	Applications
Microfiltration (MF)	Hydrostatic pressure gradient (0.1-2 MPa)	100–10,000	Pre-treatment Sterilization Removal of bacteria Clarification and biological stabilization
Ultrafiltration (UF)	Hydrostatic pressure gradient (1-10 MPa)	1–100	Pre-treatment Dewaxing De-asphalting Removal of macromolecules and virus
Nanofiltration (NF)	Hydrostatic pressure gradient (10-30 MPa)	0.5–2	Drinking water production Removal of ions Concentration/dewatering Water softening
Reverse Osmosis (RO)	Hydrostatic pressure gradient (15-80 MPa)	< 0.5	Desalination Drinking water production Wastewater treatment Petroleum industry
Forward Osmosis (FO)	Osmotic pressure gradient (concentration gradient)	< 5	Desalination Drinking water production Wastewater treatment Food industry
Pressure retarded osmosis (PRO)	Osmotic pressure gradient (concentration gradient)	< 5	Power generation Desalination
Membrane distillation (MD)	Vapour pressure gradient (temperature gradient, downstream pressure)	10-1,000	Desalination Ultrapure water production Extraction of volatile organic compounds Wastewater treatment
Electrodialysis (ED)	Electric potential gradient	< 1	Desalination Ultrapure water production Demineralization Table salt production Concentration of brines
Pervaporation (PV)	Vapour pressure gradient	< 0.5	Dehydration of organic solvents Removal of organic solvents from aqueous solutions Mix organic solvents separation

The first four filtration processes (MF, UF, NF and RO) presented in Table 1.1. use selective membranes and currently are mature solutions for water treatment with a quite high level of technological development and industrial implementation. These membrane processes are considered mainly for water pretreatments (MF and UF) or brackish water and seawater desalination (NF and RO), surpassing in annual production the conventional thermal technologies [3, 10, 11]. In fact, MF, UF or NF are commonly used as pretreatment processes in RO desalination plants [12]. Although these membrane processes are mature and well implemented in industry, improving their energy efficiency and water production rate as much as possible together with an adequate management of produced brines are necessary [13]. Because of the worldwide exponential growth of the number of desalination plants and the high rate of replacement of membrane modules due to severe fouling phenomena experienced by RO membranes, more than 840,000 RO membrane modules are discarded annually and usually disposed of in landfills [14]. The adequate handling of end-of-life RO membrane modules have also become an urgent problem to be solved in the interests of a circular economy while protecting the environment.

The other membrane separation processes (FO, PRO, MD, ED and PV shown in Table 1.1) of emerging interests during last decade for desalination and wastewater treatment, are still not fully implemented industrially although there are some small and large-scale pilot plants [11]. In recent years, the combination of FO, ED and MD technologies with the above mentioned filtration processes (MF, UF, NF and RO) for desalination has demonstrated the possibility of improving desalination efficiency (i.e. produced water quality), brines management and specific energy consumption among others [15]. Similarly, the integration of PV process has demonstrated its potential for the separation of organic solvents from water [16], and the production of biofuels [17]. To guarantee the economic viability and efficiency of these processes, a great effort is being made for the development of membranes with the most suitable characteristics for each process [3, 16].

Nowadays, there are different engineering strategies for the development of membranes for the above mentioned separation processes with improved characteristics. Various techniques have been adopted such as electrospinning, dip-coating and interfacial polymerization [3, 11, 18]. These techniques are detailed in the following sections 1.1.1, 1.1.2 and 1.1.3, respectively. Numerous dense and porous single-layer membranes have been developed by means of different techniques such as solvent evaporation, extrusion, rolling and stretching, sintering and phase inversion techniques such as non-solvent induced phase separation (NIPS) and thermally induced phase separation (TIPS) [3, 16, 18]. However, it was claimed that dual-layer membranes, for which different techniques are used to prepare each layer, exhibit optimized properties (i.e. good mechanical properties because of the thick

bottom layer acting as a support, high water production rates and separation factors because of the thin selective layer). In addition, these membranes can be easily tailored to meet the physico-chemical requirements of each process for a given application [18-25]. Details of the employed membrane preparation and modification techniques can be found in [9, 11, 24, 26].

The objective of the present thesis is the development of polymer dual-layer membranes using some of the above mentioned techniques to prepare FO, MD and PV membranes looking at the improvement of the performance of these process applied in water treatment (i.e. waste water, brine and n-butanol aqueous solution). In addition, both FO and MD membranes were designed taking into account the exposed problems of RO technology, brine discharge and end-of-life RO membrane modules management. The previous know-how acquired during the development of polymeric dual-layer membranes was applied to carry out the first attempts on the design, preparation and characterization of MD and FO membranes reusing different elements of RO membrane modules in order to implement the circular economy in the field of membrane science and technology as well as the protection of the environment.

1.1.1. Electrospinning

Electrospinning is a simple and reliable technique that allows the preparation of different types of nanofibers and nanofibrous membranes applying an electric voltage in the range of kVolts with few micro-Amps. The electrospun membranes exhibit a high void volume fraction even greater than 90%, nanofibers sizes in the range 20 – 1000 nm, controlled thickness through an adequate selection of electrospinning time, very high surface roughness, etc. The applied electric field (i.e. electric voltage), the distance between the metallic needle or spinneret (i.e. injector) and the collector, the internal diameter of the metallic needle, the environmental conditions (i.e. humidity and temperature), the type and structure of the collector, the composition and flow rate of the polymer solution are the main parameters affecting the morphology of the fibers and the resultant membrane structure [18, 27]. Both supported and unsupported membranes can be prepared using this technique. More details can be found elsewhere [9, 11, 18, 24, 27-29].

1.1.2. Dip-coating

Dip coating is a simple and reproducible technique used for membrane surface modification. A thin layer is coated on the surface of a substrate changing its chemical, thermal, structural or transport properties [30, 31]. This technique is carried out by immersing

the substrate in a specific liquid coating solution or by bringing only the surface of the substrate into contact with the coating solution, followed by gentle rinsing and adequate drying. The main parameters affecting the morphology of the produced thin film are the characteristics of the substrate, the immersion time in the liquid coating solution and the composition of the coating solution [32]. More details can be found in [9, 11, 24, 26, 32].

1.1.3. Interfacial polymerization

Thin polymeric film composite membranes are prepared by interfacial polymerization (IP) technique on either dense or porous substrates combining two immiscible liquid solutions of monomers (i.e. organic and aqueous solutions). The surface of the substrate is first soaked in the aqueous solution containing amine monomers for a certain time. Subsequently, the excess aqueous solution is removed and this substrate surface is brought into contact with an immiscible organic solution containing another amine monomer(s) for a certain time allowing polycondensation at the interface [9]. The used monomers, their concentration in the organic and aqueous solutions, the polymerization time and type of the substrate surface dictate the morphology and physico-chemical properties of the formed thin-film composite membranes [9, 33]. The considered monomers and details of the IP technique were reported in [3, 11, 19, 24, 34].

1.2. Pervaporation (PV)

PV technology is based on the use of selective dense membranes for the treatment of both liquid organic/organic and organic/water separation [16, 35]. The involved mechanism of such a selective separation is based on the sorption, diffusion, and desorption of the transported species through the membrane; since the feed mixture is introduced in the membrane module in liquid phase, while the permeate is collected in vapour phase by applying vacuum or sweeping gas at the membrane permeate side. Although in PV processes liquid-vapour phase change takes place, and it is necessary to provide latent heat of evaporation, this type of processes requires less energy than traditional distillation processes [20, 35, 36]. The mass transfer through the PV membrane is commonly described by the solution-diffusion model [35] and the permeate flux (J_i) of a given compound *i* is defined as [35]:

$$J_i = \frac{P_i}{\delta} \left(c_{i,feed} - c_{i,perm}\right) \quad (1.1)$$

where δ is the membrane thickness, $c_{i,feed}$ and $c_{i,perm}$ are the concentration of the compound *i* for the feed and permeate, respectively, and P_i is the permeability of the compound *i* defined as follows [35]:

$$P_i = S_i \cdot D_i \tag{1.2}$$

where S_i is the sorption coefficient and D_i is the diffusion coefficient of the compound *i*.

There are hydrophilic PV, organophilic PV and organo-selective PV processes defined depending on the hydrophilic or organophilic (i.e. hydrophobic) character of the used membrane. The organo-selective PV processes are used for organic/organic separation [16, 37]. The hydrophilic PV processes (Fig 1.1 a)) are considered for water removal from liquid aqueous mixtures while the organophilic PV processes (Fig 1.1 b)) are used for organic compounds removal from aqueous mixtures [16, 37].

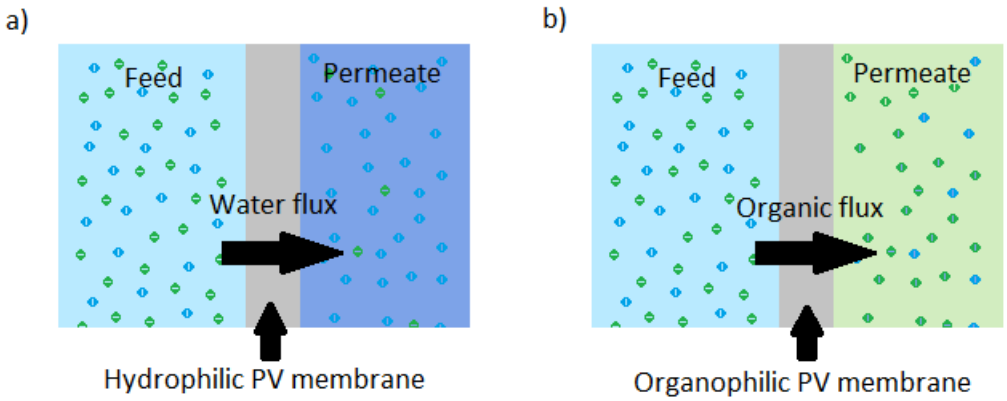

Figure 1.1. *Schematic representation of a) a hydrophilic PV process and b) an organophilic PV process.*

The major industrial PV applications are found for organic solvents dehydration, especially isopropanol and ethanol, using hydrophilic PV membranes. The organophilic PV processes are applied in pharmaceutical, cosmetic, food and biofuels industries to obtain organic concentrates from aqueous solutions with low concentrations of the target compound(s) [35, 36].

1.2.1. PV membranes

PV membranes can be classified in polymeric, inorganic and hybrid or mixed matrix membranes (i.e. inorganic filler(s) dispersed within a polymeric matrix). Polymeric membranes are more widely used than inorganic membranes mainly due to their lower cost

and ease of preparation, although their performance (i.e. permeate flux and selectivity) are worse than inorganic membranes. Mixed matrix membranes, which are not too expensive or difficult to prepare, also exhibit better PV performance than polymeric membranes [20, 35].

Polyvinyl alcohol (PVA), polyimide (PI), chitosan and sodium alginate are the materials most used in PV polymeric membrane engineering for hydrophilic PV processes. Zeolite, metal oxide or silica as inorganic fillers are commonly used together with the previous cited polymers to prepare mixed matrix membranes with better PV performance [35, 36]. For the hydrophobic (i.e. organophilic) PV processes, the most used polymeric materials are polydimethylsiloxane (PDMS), poly-1-trymetylsilyl-1-propylene (PTMSP), polyoctylmethylsiloxane (POMS) and polyether-block-polyamide (PEBA), while other hydrophobic polymers such as polypropylene (PP) and polyvinylidene fluoride (PVDF) are also used but to a lesser extent. [35, 36]. In recent years, the developed polymers of intrinsic microporosity (PIMs) have generated great interest for the improvement of the performance of PV membranes, mainly for the separation of alcohols from aqueous solutions [22]. PIMs are organophilic materials having good chemical, mechanical and thermal stability as well as a high permeability and a good selectivity because of their high free volume and hydrophobic character [22, 38, 39]. This type of PV membranes is generally prepared using only PIM [16, 39]. Recently, PIM mixed matrix membranes using nano-additives and dual-layer PIM membranes (i.e. thin-film composite PIM membranes) prepared primarily by dip-coating using porous substrates have been proposed for improved PV applications [16, 20, 38-40]. It is to be noted that among PIMs, PIM-1 is by far the most studied [38-41].

1.3. Membrane distillation (MD)

MD is a membrane separation process whose driving force is the difference of the vapour pressure established between the two sides of a porous and hydrophobic membrane, feed side and permeate side. The permeate flux (J) through de membrane is described by the following equation [42]:

$$J = C_m (P_f - P_p) \tag{1.3}$$

where C_m is the membrane mass transfer coefficient that depends on the membrane characteristics and the operating conditions, P_f and P_p are the water vapour pressure at the feed membrane surface and the permeate membrane surface, respectively.

The mass transport through the pores of the hydrophobic membrane occurs in vapour phase while heat is transferred by conduction through the membrane and as latent heat associated to mass transfer. Heat transfer by convection also takes place through the thermally boundary layers adjoining the feed and the permeate side of the membrane depending on the MD configuration, namely, direct contact MD (DCMD), sweeping gas MD

(SGMD), vacuum MD (VMD) and air gap MD (AGMD) [3, 16, 18]. A schema of the mechanism of DCMD transport through a porous hydrophobic single-layer membrane is presented as an example in Fig. 1.2.

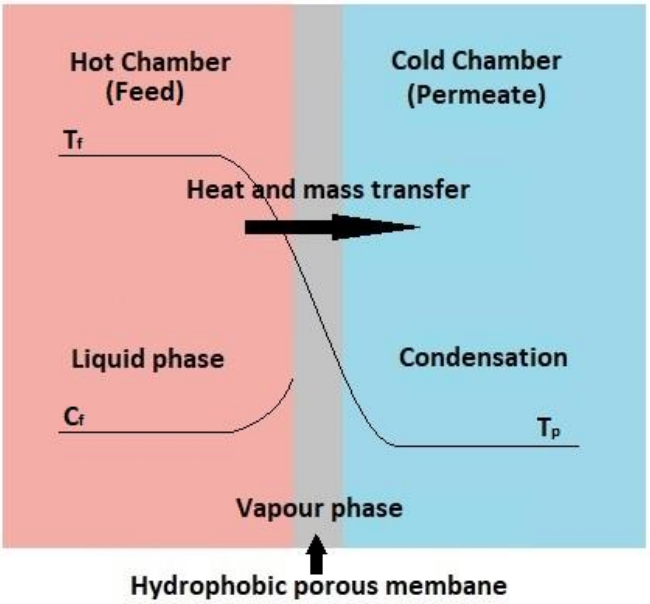

Figure 1.2. *Schematic representation of MD heat and mass transport through a porous hydrophobic single-layer membrane used for the treatment of an aqueous solution containing a non-volatile solute.*

Due to the heat transport through the membrane, a temperature polarization phenomenon (i.e. thermal boundary layers adjoining both membrane surfaces in Fig. 1.2) is generated reducing the driving force and subsequently the permeate flux. Similarly, due to the mass transport through the membrane, a concentration polarization phenomenon (i.e. concentration boundary layer adjoining the feed membrane surface in Fig. 1.2) is induced increasing the concentration of the non-volatile solute at the feed/membrane surface and reducing therefore the water vapour pressure and the permeate flux. By decreasing the thermal conductivity of the membrane matrix or increasing the void volume fraction of the membrane (i.e. porosity), the heat transfer by conduction through the membrane can be lowered improving the thermal efficiency of the MD process as consequence. In addition, the temperature and concentration polarization effects can be reduced by enhancing the hydrodynamic conditions at both sides of the membrane by means of the application of turbulent fluid flows or the use of turbulent promoters at both sides of the membrane [16, 18, 35] . These strategies can enhance the applied driving force and the MD performance as well [3, 18, 35].

One of the main advantages of MD technology is its capability to achieve more than 99% rejection of non-volatile solutes producing not only distilled water but also ultra-pure water. As it is not limited by the osmotic pressure of aqueous feed solutions, this technology is used for the treatment of aqueous solutions with high concentrations of non-volatile solutes up to their saturation (i.e. treatment of brines discharged by RO desalination plants as discussed later on in section 1.5). Provided that the MD driving force is not a hydrostatic pressure (i.e. MD is applied at atmospheric pressure), membranes in MD are less prone to fouling compared to other pressure-driven membrane separation processes (MF, UF, NF and RO). In addition, MD can be employed at temperatures ranging from 30ºC up to 90ºC, thus renewable energy sources such as solar energy can be considered. These cited characteristics make MD suitable for the treatment of water originated in different sectors such as pharmaceutical and food industries, other than desalination of brackish and seawater including the treatment of brines [3, 18]. To improve its industrial implementation, adequately designed modules and membranes specifically for MD, thorough water production costs analysis and energy consumption optimization are necessary [16, 18].

1.3.1. MD membranes

MD membranes should exhibit a high liquid entry pressure (*LEP*) to avoid wetting of its pores and guarantee the correct membrane separation efficiency, high permeability, good chemical and thermal stability, low thermal conductivity and adequate mechanical properties for safe packing in modules. Hydrophobic polymers are the most widely used materials for the preparation of single-layer MD membranes: Polyvinylidene fluoride (PVDF), polyethylene (PE), polypropylene (PP) and polytetrafluoroethylene (PTFE) [3, 16, 18, 28]. Surface modified hydrophilic membranes have also been proposed for MD applications [18, 35]. In fact, MD membranes can be classified as flat sheet, hollow fiber and nanofiber membranes; or as single, dual and multi-layer membranes also known as composite membranes. Phase inversion (Non-solvent induced phase separation, NIPs) and electrospinning are the most widely considered techniques for the preparation of MD membranes. To improve the MD performance, mixed matrix membranes have been proposed employing different nanomaterials such as silicon dioxide (SiO_2), titanium dioxide (TiO_2) and carbon-based nanoparticles among others (multi-walled carbon nanotube, MWCNT; graphene and its derivatives) [3, 18, 28].

The development of suitable dual-layer (hydrophobic/hydrophilic) membranes has proven its validity as a solution to enhance the DCMD permeate flux because of the thin hydrophobic layer (below 10 μm) that induces a reduction of the distance between the

liquid/vapor interfaces formed at both sides of the hydrophobic pores, to increase the *LEP* because of the smaller pore size of the hydrophobic layer (below 35 nm) compared to that of the hydrophilic layer, and to improve the thermal efficiency of the DCMD process because of the possibility to optimize the thickness of the hydrophilic layer and its void volume fraction [18, 43, 44].

1.4. Forward osmosis (FO)

Osmosis refers to the natural water transport through a selective permeable membrane due to the difference of the osmotic pressure at both sides of the membrane induced by a concentration difference. The selective membrane allows the passage of water but hinders the passage of most molecules or ions dissolved in water. Given two solutions at different concentrations, separated by a selective permeable membrane, the osmotic pressure difference ($\Delta\pi$) is the hydrostatic pressure that must be applied on the membrane side with the highest concentration (also called draw solution) to counteract the transport of water through the membrane (i.e. zero water permeate flux). In FO separation processes (Fig. 1.3), the applied hydrostatic pressure through the membrane is zero ($\Delta P = 0$) and the water permeate flux (J_w) occurs from the feed solution to be treated having lower osmotic pressure (π_f) and higher water chemical potential (μ_f) to the draw solution with higher osmotic pressure (π_{ds}) and lower water chemical potential (μ_{ds}) [3, 45, 46]. The following equation is normally used to describe J_w across the membrane [46]:

$$J_w = A \cdot \Delta\pi \tag{1.4}$$

where A is the water permeability coefficient.

An undesirable reverse solute diffusion flux (J_s) also appears through the membrane from the draw solution to the feed solution. This solute(s) transport is related to the characteristics of the FO membrane and results in a decline of $\Delta\pi$ and J_w as consequence. In addition, the concentration polarization phenomenon plays an important role on J_w as it is due not only to the external concentration boundary layer adjacent to the membrane surface but also to the internal concentration polarization effect inside the FO membrane, which is normally a thin film composite membrane [3, 28, 45, 47]. Fig. 1.3 shows a schema of the mass transport in FO separation process.

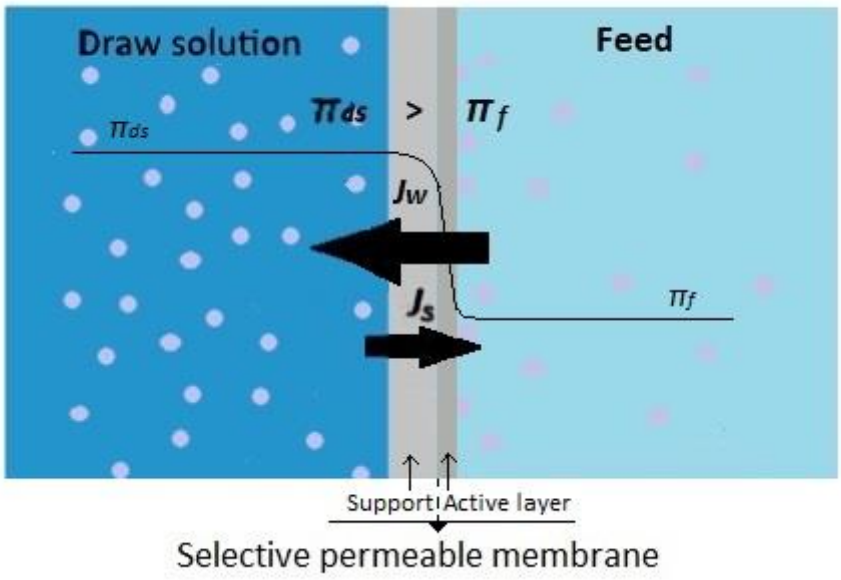

Figure 1.3. *Schematic representation of mass transport through a FO membrane.*

The selection of a solute or solutes for the preparation of the draw solution necessary to establish the driving force is also crucial for FO process. Other than the high osmotic pressure, the draw solution must be cheap, non-toxic, and its solute(s) should be highly soluble with an adequate molecular size to prevent its passage through the membrane [45, 46, 48].

In general, FO processes are suitable for wastewater treatment and exhibit high rejection to solutes with sizes greater than the molecular weight cut off (MWCO) of the used membrane, which has low propensity to fouling compared to pressure-driven membrane separation processes (MF, UF, NF, RO). In addition, the high $\Delta\pi$ existing between aqueous solutions with high and low salinity makes FO processes very appropriate for the treatment of brines discharged from RO desalination plants [3, 46, 48].

1.4.1. FO membranes

The membranes used in FO can be classified as phase inversion single-layer membranes, supported and unsupported membranes, thin film composite (TFC) membranes and mixed matrix membranes [3]. These can be found as flat sheet and hollow fiber membranes [3]. An FO membrane must be chemically and mechanically stable, must exhibit high permeate fluxes and good rejection factors of the solutes present in both the feed and draw solutions. In addition, it must have a high fouling resistance and induces a low internal concentration polarization effect [19, 45].

The polymeric materials most commonly used to prepare FO membranes by the phase inversion technique are cellulose triacetate (CTA) and cellulose acetate (CA). Although these membranes show high hydrophilicity together with good chemical and mechanical resistances, their rejection of inorganic salts such as sodium chloride (NaCl) or magnesium sulfate ($MgSO_4$) are not high enough [3, 34, 49].

TFC membranes consist on a thin layer of a selective dense polymer prepared on a porous support. The phase inversion technique is mainly employed for the preparation of the porous support, although electrospinning has been proposed during last decade as an adequate technique to prepare tailored supports with high void volume fractions and appropriate iner-fiber spaces for TFC FO membranes. Hydrophilic polymers such as polysulfone (PSF) and polyethersulfone (PES) and to a lesser extent polyacrylonitrile (PAN) are the materials used for the preparation of these supports. The thin film layers are commonly formed by the IP technique using two monomers, one dissolved in the organic phase and the other in the aqueous phase. Generally, trimesoyl chloride (TMC) in the organic phase and m-phenylenediamine (MPD) in the aqueous phase are the monomers used to form polyamide (PA) thin film layer. Other monomers such as piperazine (PIP), p-phenylene diamine (PPD) and triethanolamine (TEOA) in the aqueous phase have also been tested [3, 19, 34].

Mixed matrix membranes, both phase inversion and TFC membranes, consist on the incorporation a certain nano-additive in the polymeric matrix of the FO membrane. Various types of nano-additives such as titanium dioxide (TiO_2), silicon dioxide (SiO_2), zeolites, graphene oxide (GO), multi-walled carbon nanotube (MWCNT) and silver nanoparticle (Ag) have been employed to improve the mechanical properties or FO permeate fluxes, although in most cases these result in a decline of the separation factors [19, 34, 49, 50]. Since its patent in 2010 [51], the development of biomimetic membranes based on the incorporation of aquaporins to the selective thin layer of TFC membranes showed a high FO performance, but its poor mechanical stability and high manufacturing cost are important issues to be resolved [19, 33].

1.5. Reverse osmosis (RO): brine discharge and end-of-life RO membrane modules

RO is the most widely considered technology for water desalination worldwide. However, the correct management of the RO brines having 60 to 85 g/L total dissolved solids (TDS) is crucial for protecting the natural environment [52]. In fact, the discharge of these brines mainly into surface and coastal waters causes serious environmental impacts on nearby ecosystems [53]. Some adopted management strategies are sewer discharge, deep-

well injection, evaporation pound or land application do not improve the existing problem but aggravate it rendering it more expensive [13].

Recently, the proposed innovative strategies for the proper management of brines are their concentration by membrane processes (MD, FO, PRO, ED) increasing the rate of the recovered water looking at zero-liquid discharge (ZLD) to the environment [53, 54].

1.5.1. FO an MD technology for RO brine treatment

FO and MD processes have shown good potential for the treatment of brines and therefore both were proposed as promising solutions to be integrated to RO desalination process increasing not only its water production rate but also the quality of the produced water [13, 53, 55, 56]. A full development of these integrated technologies is still necessary.

FO process in combination with RO has been studied for the regeneration or concentration of RO brines [53, 55]. When RO brine is used as a draw solution for wastewater treatment by FO, the feed wastewater is concentrated while the brine is diluted reducing its salinity and hence returning it back to the RO process for its regeneration or rendering it more environmentally friendly to be discharged [57, 58]. When a draw solution with a higher osmotic pressure than that of the brine is used in FO process, RO brine can be concentrated and zero-liquid discharge treatment becomes possible [13, 53, 54].

MD technology, thanks to its ability to treat high salinity solutions, has been proposed for zero-liquid discharge treatment process of RO brines. This is also attributed to its low tendency to inorganic fouling and biofouling. However, more research studies must be done before the industrial integration of MD and RO technologies, especially in the design of adequate MD membranes and modules with high permeate fluxes and *LEP* at high saline solutions [13, 53, 54, 59].

1.5.2. End-of-life RO membrane modules

Annually, 14.000 tonnes of RO membrane modules are discarded after their useful life [60]. Currently, the common strategy for managing these discarded RO membrane modules is its disposal in nearby landfills. Since RO is a worldwide growing technology, more than two million RO membrane modules are expected to be discarded by 2025 [61]. The current environmental crisis makes it necessary to change the current linear life-cycle scheme (made-use-discarded) of discarded membrane modules towards a circular economy [62].

As it is detailed in Chapter 2, different proposals for the reuse and recycling of end-of-life membrane modules have been presented. The direct reuse of discarded RO membrane modules is very limited as indicated in few publications [63-65]. In the last decade, some

procedures for recycling and modifying RO membrane modules on a pilot or laboratory scale have been proposed to extend their useful life in UF, NF, ED and membrane biofilm reactor (MBfR) [14, 66-69].

1.6. Thesis overview

This thesis is focused on the design, preparation and characterization of dual-layer membranes for water treatment by PV, MD and FO separation processes. Three membrane preparation techniques were considered: dip-coating, electrospinning and interfacial polymerization (IP). Some of these dual-layer membranes were prepared using different parts of end-of-life RO membrane modules extending their lifetime and contributing therefore to a circular economy and sustainability in membrane science and related materials.

In Chapter 2, a state of the art review on the reuse and recycling of end-of-life RO membrane modules is presented. Currently, a large number of end-of-life RO membrane modules are disposed in nearby landfills due to the faced irreversible membrane fouling and loss of RO performance. The different proposed methods and followed protocols for their reuse, recycling and applications, mainly in other membrane processes for water remediation, are reviewed.

The need to increase the permeate flux of PV membranes is necessary for the further industrial advance of this technology [35, 36]. Chapter 3 of the present thesis is devoted to the development of dual-layer membranes composed by a highly porous electrospun hydrophobic PVDF support and an organophilic thin film selective layer formed by a polymer of intrinsic microporosity, PIM-1. These membranes are characterized and applied for the recovery of n-butanol from water because of the high interest of this process in the production of biofuels. Compared to PV membranes reported in the literature, the dual-layer membranes developed in this PhD. thesis show very high permeate fluxes. In addition, for sake of comparison of the energy consumption and economic costs of conventional distillation column and hybrid systems (i.e. PV prior distillation column), a numerical simulation using Aspen HYSYS has been carried out.

The development of dual-layer hydrophobic/hydrophilic nanofibrous MD membranes using the hydrophobic polymer PVDF for the bottom layer and the hydrophilic polymer PSF for the top layer is presented in Chapter 4. Different thicknesses of each layer have been explored by changing the electrospinning time of each polymer solution and maintaining the total electrospinning time at 3 h. Compared to electrospun single-layer MD membranes prepared with each polymer, the dual-layer hydrophobic/hydrophilic membranes exhibit better MD characteristics and DCMD desalination performance.

The knowledge acquired in the development of polymeric dual-layer membranes reported in Chapters 3 and 4, has facilitate to carry out the first attempts in the recycling and reuse of different elements of RO membrane modules.

In Chapter 5, the possibility to recycle and reuse the internal components of the end-of-life RO membrane modules, the RO feed and permeate spacers as well as the RO membrane, is explored. After passive cleaning, these recycled components were reused as supports for the preparation of dual-layer MD membranes composed by a PVDF nanofibrous layer prepared by electrospinning technique. These membranes have been characterized and tested for the treatment of RO brines, proving the suitability and performance stability over time at high salt concentrations of the membranes supported by the RO permeate spacer or the RO membrane. Comparison with other supported and unsupported MD nanofibrous membranes have made.

The possibility to recycle discarded membranes from end-of-life RO modules for the preparation of FO membranes is shown in Chapter 6. The RO membrane is first cleaned and then transformed by means of dip-coating technique to form a thin layer of PA or polyester (PE) on its top surface in order to improve its FO transport properties in wastewater treatment (i.e. humic acid aqueous solutions in the present PhD. thesis). RO brines are considered as a draw solution. The obtained FO results of the developed dual-layer membranes are better or at least comparable to those of the commercial (TFC-HTI and CTA-HTI, supplied by Hydration Technology Innovations HTI™, LLC, Albany, USA) used under the same operating conditions. The results indicated that it is possible to use discarded RO membranes in FO technology

Finally, Chapter 7 summarizes the most important conclusions of the research studies performed in this PhD. thesis and presents possible future research lines in the field of membrane engineering and RO membrane modules recycling.

1.7. References

[1] United Nations, The Human Right to Water and Sanitation, A/RES/64/292, United Nations General Assembly, New York, in, 2010.
[2] UN-Water, Summary Progress Update 2021 – SDG 6 – water and sanitation for all., in, Geneva, Switzerland, 2021.
[3] N.P. Hankins, R. Singh, Emerging Membrane Technology for Sustainable Water Treatment, Elsevier, Boston, 2016.
[4] H.T. El-Desouky, H.M. Ettouney, Fundamentals of salt water desalination, Elsevier, 2002.
[5] Programme Division United Nations Children's Fund (UNICEF), Reimagining WASH: Water security for all, in, New York, 2021.
[6] S. Loeb, S. Sourirajan, Sea Water Demineralization by Means of an Osmotic Membrane, in: Saline Water Conversion—II, AMERICAN CHEMICAL SOCIETY, 1963, pp. 117-132.
[7] D. Stevens, S. Loeb, Reverse osmosis desalination costs derived from the Coalinga pilot plant operation, Desalination, 2 (1967) 56-74.

[8] P. Arribas, M. Khayet, M.C. García-Payo, L. Gil, 8 - Novel and emerging membranes for water treatment by hydrostatic pressure and vapor pressure gradient membrane processes, in: A. Basile, A. Cassano, N.K. Rastogi (Eds.) Advances in Membrane Technologies for Water Treatment, Woodhead Publishing, Oxford, 2015, pp. 239-285.
[9] D.M. Warsinger, S. Chakraborty, E.W. Tow, M.H. Plumlee, C. Bellona, S. Loutatidou, L. Karimi, A.M. Mikelonis, A. Achilli, A. Ghassemi, L.P. Padhye, S.A. Snyder, S. Curcio, C.D. Vecitis, H.A. Arafat, J.H. Lienhard, A review of polymeric membranes and processes for potable water reuse, Progress in Polymer Science, 81 (2018) 209-237.
[10] IDAGWI DesalData, IDA Water Security Handbook 2019–2020, IDA and GWI DesalData, (2019) 14-41.
[11] P. Pal, Membrane-Based Technologies for Environmental Pollution Control, Elsevier, 2020.
[12] M. Qasim, M. Badrelzaman, N.N. Darwish, N.A. Darwish, N. Hilal, Reverse osmosis desalination: A state-of-the-art review, Desalination, 459 (2019) 59-104.
[13] M.N. Soliman, F.Z. Guen, S.A. Ahmed, H. Saleem, M.J. Khalil, S.J. Zaidi, Energy consumption and environmental impact assessment of desalination plants and brine disposal strategies, Process Safety and Environmental Protection, 147 (2021) 589-608.
[14] R. García-Pacheco, J. Landaburu-Aguirre, A. Lejarazu-Larrañaga, L. Rodríguez-Sáez, S. Molina, T. Ransome, E. García-Calvo, Free chlorine exposure dose (ppm·h) and its impact on RO membranes ageing and recycling potential, Desalination, 457 (2019) 133-143.
[15] S. Lee, J. Choi, Y.-G. Park, H. Shon, C.H. Ahn, S.-H. Kim, Hybrid desalination processes for beneficial use of reverse osmosis brine: Current status and future prospects, Desalination, 454 (2019) 104-111.
[16] M. Kumar Purkait, R. Singh, P. Mondal, D. Haldar, Thermal Induced Membrane Separation Processes, Elsevier, 2020.
[17] P. Zheng, C. Li, N. Wang, J. Li, Q. An, The potential of pervaporation for biofuel recovery from fermentation: An energy consumption point of view, Chinese Journal of Chemical Engineering, 27 (2019) 1296-1306.
[18] M. Khayet, T. Matsuura, Membrane distillation: principles and applications, (2011).
[19] Z. Alihemati, S.A. Hashemifard, T. Matsuura, A.F. Ismail, N. Hilal, Current status and challenges of fabricating thin film composite forward osmosis membrane: A comprehensive roadmap, Desalination, 491 (2020) 114557.
[20] X. Cheng, F. Pan, M. Wang, W. Li, Y. Song, G. Liu, H. Yang, B. Gao, H. Wu, Z. Jiang, Hybrid membranes for pervaporation separations, Journal of Membrane Science, 541 (2017) 329-346.
[21] Z. Huang, G. Yang, J. Zhang, S. Gray, Z. Xie, Dual-layer membranes with a thin film hydrophilic MOF/PVA nanocomposite for enhanced antiwetting property in membrane distillation, Desalination, 518 (2021) 115268.
[22] G. Liu, W. Jin, Pervaporation membrane materials: Recent trends and perspectives, Journal of Membrane Science, 636 (2021) 119557.
[23] O. Makanjuola, F. Ahmed, I. Janajreh, R. Hashaikeh, Development of a dual-layered PVDF-HFP/cellulose membrane with dual wettability for desalination of oily wastewater, Journal of Membrane Science, 570-571 (2019) 418-426.
[24] J. Meier-Haack, M. Müller, K. Lunkwitz, Polymer Membranes for Sustainable Technologies, in: P. Eyerer, M. Weller, C. Hübner (Eds.) Polymers - Opportunities and Risks II: Sustainability, Product Design and Processing, Springer Berlin Heidelberg, Berlin, Heidelberg, 2010, pp. 281-297.
[25] Y.K. Ong, T.-S. Chung, Chapter 19 - High performance dual-layer hollow fiber fabricated via novel immiscibility-induced phase separation (I2PS) process for dehydration of ethanol☆, in: T.-S. Chung, Y. Feng (Eds.) Hollow Fiber Membranes, Elsevier, 2021, pp. 407-430.
[26] Q.-C. Xia, M.-L. Liu, X.-L. Cao, Y. Wang, W. Xing, S.-P. Sun, Structure design and applications of dual-layer polymeric membranes, Journal of Membrane Science, 562 (2018) 85-111.
[27] F.E. Ahmed, B.S. Lalia, R. Hashaikeh, A review on electrospinning for membrane fabrication: Challenges and applications, Desalination, 356 (2015) 15-30.

[28] J. Ravi, M.H.D. Othman, T. Matsuura, M. Ro'il Bilad, T.H. El-badawy, F. Aziz, A.F. Ismail, M.A. Rahman, J. Jaafar, Polymeric membranes for desalination using membrane distillation: A review, Desalination, 490 (2020) 114530.
[29] S.S. Ray, S.-S. Chen, N.C. Nguyen, H.T. Nguyen, Chapter 9 - Electrospinning: A Versatile Fabrication Technique for Nanofibrous Membranes for Use in Desalination, in: S. Thomas, D. Pasquini, S.-Y. Leu, D.A. Gopakumar (Eds.) Nanoscale Materials in Water Purification, Elsevier, 2019, pp. 247-273.
[30] J. Baghdachi, Smart Coatings, in: Smart Coatings II, American Chemical Society, 2009, pp. 3-24.
[31] M.F. Montemor, Functional and smart coatings for corrosion protection: A review of recent advances, Surface and Coatings Technology, 258 (2014) 17-37.
[32] N.Y. Abu-Thabit, A.S.H. Makhlouf, Chapter 1 - Fundamental of smart coatings and thin films: synthesis, deposition methods, and industrial applications, in: A.S.H. Makhlouf, N.Y. Abu-Thabit (Eds.) Advances in Smart Coatings and Thin Films for Future Industrial and Biomedical Engineering Applications, Elsevier, 2020, pp. 3-35.
[33] W. Xu, Q. Chen, Q. Ge, Recent advances in forward osmosis (FO) membrane: Chemical modifications on membranes for FO processes, Desalination, 419 (2017) 101-116.
[34] H. Jain, M.C. Garg, Fabrication of polymeric nanocomposite forward osmosis membranes for water desalination—A review, Environmental Technology & Innovation, 23 (2021) 101561.
[35] A. Basile, A. Figoli, M. Khayet, Pervaporation, vapour permeation and membrane distillation: principles and applications, Elsevier, 2015.
[36] B. Van der Bruggen, P. Luis, Chapter Four - Pervaporation, in: S. Tarleton (Ed.) Progress in Filtration and Separation, Academic Press, Oxford, 2015, pp. 101-154.
[37] W.P. Silvestre, N.F. Livinalli, C. Baldasso, I.C. Tessaro, Pervaporation in the separation of essential oil components: A review, Trends in Food Science & Technology, 93 (2019) 42-52.
[38] M. Alberto, R. Bhavsar, J.M. Luque-Alled, A. Vijayaraghavan, P.M. Budd, P. Gorgojo, Impeded physical aging in PIM-1 membranes containing graphene-like fillers, Journal of Membrane Science, 563 (2018) 513-520.
[39] L. Gao, M. Alberto, P. Gorgojo, G. Szekely, P.M. Budd, High-flux PIM-1/PVDF thin film composite membranes for 1-butanol/water pervaporation, Journal of Membrane Science, 529 (2017) 207-214.
[40] M. Alberto, R. Bhavsar, J.M. Luque-Alled, E. Prestat, L. Gao, P.M. Budd, A. Vijayaraghavan, G. Szekely, S.M. Holmes, P. Gorgojo, Study on the formation of thin film nanocomposite (TFN) membranes of polymers of intrinsic microporosity and graphene-like fillers: Effect of lateral flake size and chemical functionalization, Journal of Membrane Science, 565 (2018) 390-401.
[41] J.M. Luque-Alled, A.W. Ameen, M. Alberto, M. Tamaddondar, A.B. Foster, P.M. Budd, A. Vijayaraghavan, P. Gorgojo, Gas separation performance of MMMs containing (PIM-1)-functionalized GO derivatives, Journal of Membrane Science, 623 (2021) 118902.
[42] H.C. Duong, L. Xia, Z. Ma, P. Cooper, W. Ela, L.D. Nghiem, Assessing the performance of solar thermal driven membrane distillation for seawater desalination by computer simulation, Journal of Membrane Science, 542 (2017) 133-142.
[43] M. Khayet, T. Matsuura, J.I. Mengual, Porous hydrophobic/hydrophilic composite membranes: Estimation of the hydrophobic-layer thickness, Journal of Membrane Science, 266 (2005) 68-79.
[44] M. Khayet, J.I. Mengual, T. Matsuura, Porous hydrophobic/hydrophilic composite membranes: Application in desalination using direct contact membrane distillation, Journal of Membrane Science, 252 (2005) 101-113.
[45] D.L. Shaffer, J.R. Werber, H. Jaramillo, S. Lin, M. Elimelech, Forward osmosis: Where are we now?, Desalination, 356 (2015) 271-284.
[46] S. Zhao, L. Zou, C.Y. Tang, D. Mulcahy, Recent developments in forward osmosis: Opportunities and challenges, Journal of Membrane Science, 396 (2012) 1-21.

[47] S.K. Singh, C. Sharma, A. Maiti, A comprehensive review of standalone and hybrid forward osmosis for water treatment: Membranes and recovery strategies of draw solutions, Journal of Environmental Chemical Engineering, 9 (2021) 105473.
[48] R. Valladares Linares, Z. Li, S. Sarp, S.S. Bucs, G. Amy, J.S. Vrouwenvelder, Forward osmosis niches in seawater desalination and wastewater reuse, Water Research, 66 (2014) 122-139.
[49] W.A. Suwaileh, D.J. Johnson, S. Sarp, N. Hilal, Advances in forward osmosis membranes: Altering the sub-layer structure via recent fabrication and chemical modification approaches, Desalination, 436 (2018) 176-201.
[50] M. Qasim, N.A. Darwish, S. Sarp, N. Hilal, Water desalination by forward (direct) osmosis phenomenon: A comprehensive review, Desalination, 374 (2015) 47-69.
[51] Peter Holme Jensen, Danielle Keller, Claus Hélix Nielsen, Membrane for filtering of water, in: U.S. Patent (Ed.), Aquaporin A/S, Copehhagen N (DK) 2010.
[52] A. Panagopoulos, K.-J. Haralambous, Environmental impacts of desalination and brine treatment - Challenges and mitigation measures, Marine Pollution Bulletin, 161 (2020) 111773.
[53] A. Panagopoulos, K.-J. Haralambous, M. Loizidou, Desalination brine disposal methods and treatment technologies - A review, Science of The Total Environment, 693 (2019) 133545.
[54] A.S. Bello, N. Zouari, D.A. Da'ana, J.N. Hahladakis, M.A. Al-Ghouti, An overview of brine management: Emerging desalination technologies, life cycle assessment, and metal recovery methodologies, Journal of Environmental Management, 288 (2021) 112358.
[55] C.R. Martinetti, A.E. Childress, T.Y. Cath, High recovery of concentrated RO brines using forward osmosis and membrane distillation, Journal of Membrane Science, 331 (2009) 31-39.
[56] H.S. Son, S. Soukane, J. Lee, Y. Kim, Y.-D. Kim, N. Ghaffour, Towards sustainable circular brine reclamation using seawater reverse osmosis, membrane distillation and forward osmosis hybrids: An experimental investigation, Journal of Environmental Management, 293 (2021) 112836.
[57] S. Adham, M. Oppenheimer, M.L. Liu, M.M. Kumar, Dewatering Reverse Osmosis Concentrate from Water Reuse Applications Using Forward Osmosis WateReuse Foundation, in, 2007.
[58] S. Liyanaarachchi, V. Jegatheesan, S. Muthukumaran, S. Gray, L. Shu, Mass balance for a novel RO/FO hybrid system in seawater desalination, Journal of Membrane Science, 501 (2016) 199-208.
[59] N. Dow, J. Zhang, M. Duke, J.-d. Li, S.R. Gray, E. Ostarcevic, Membrane distillation of brine wastes, (2008).
[60] J. Landaburu-Aguirre, R. García-Pacheco, S. Molina, L. Rodríguez-Sáez, J. Rabadán, E. García-Calvo, Fouling prevention, preparing for re-use and membrane recycling. Towards circular economy in RO desalination, Desalination, 393 (2016) 16-30.
[61] J. Senán-Salinas, A. Blanco, R. García-Pacheco, J. Landaburu-Aguirre, E. García-Calvo, Prospective Life Cycle Assessment and economic analysis of direct recycling of end-of-life reverse osmosis membranes based on Geographic Information Systems, Journal of Cleaner Production, 282 (2021) 124400.
[62] S.E. McMillan, "Closing the Loop": THE EUROPEAN UNION & THE CIRCULAR ECONOMY, Scitech Lawyer, 15 (2019) 4-8.
[63] E. Ould Mohamedou, D.B. Penate Suarez, F. Vince, P. Jaouen, M. Pontie, New lives for old reverse osmosis (RO) membranes, Desalination, 253 (2010) 62-70.
[64] M. Pontié, Old RO membranes: solutions for reuse, Desalination and Water Treatment, 53 (2015) 1492-1498.
[65] C. Prince, M. Cran, P. Le-Clech, K. Uwe-Hoehn, M. Duke, Reuse and recycling of used desalination membranes, proceedings of OzWater, 11 (2011) 1-8.
[66] R. García-Pacheco, Q. Li, J. Comas, R.A. Taylor, P. Le-Clech, Novel housing designs for nanofiltration and ultrafiltration gravity-driven recycled membrane-based systems, Science of The Total Environment, 767 (2021) 144181.

[67] A. Lejarazu-Larrañaga, S. Molina, J.M. Ortiz, R. Navarro, E. García-Calvo, Circular economy in membrane technology: Using end-of-life reverse osmosis modules for preparation of recycled anion exchange membranes and validation in electrodialysis, Journal of Membrane Science, 593 (2020) 117423.
[68] M.R. Moradi, A. Pihlajamäki, M. Hesampour, J. Ahlgren, M. Mänttäri, End-of-life RO membranes recycling: Reuse as NF membranes by polyelectrolyte layer-by-layer deposition, Journal of Membrane Science, 584 (2019) 300-308.
[69] J. Morón-López, L. Nieto-Reyes, S. Aguado, R. El-Shehawy, S. Molina, Recycling of end-of-life reverse osmosis membranes for membrane biofilms reactors (MBfRs). Effect of chlorination on the membrane surface and gas permeability, Chemosphere, 231 (2019) 103-112.

Chapter 2

Reuse and Recycling of End-of-life Reverse Osmosis Membranes

Reverse osmosis (RO) is a mature membrane separation technology that is still expanding for seawater desalination. In addition to seeking solutions inherent to this technology problems (i.e. energy consumption, permeate flux reduction, brine discharge), a proper management of the large number of end-of-life discarded RO modules is necessary. Because of membrane irreversible fouling and the loss of RO performance, modules are discarded and mostly disposed in nearby landfills. Recently, different methods and processes have been proposed and optimized for their reuse, recycling and applications mainly in other membrane processes for water remediation. In this sense, ultrafiltration and microfiltration are the foremost applications considered. RO discarded membrane transformation techniques were also studied for their use in electrodialysis and membrane biofilm reactors processes.

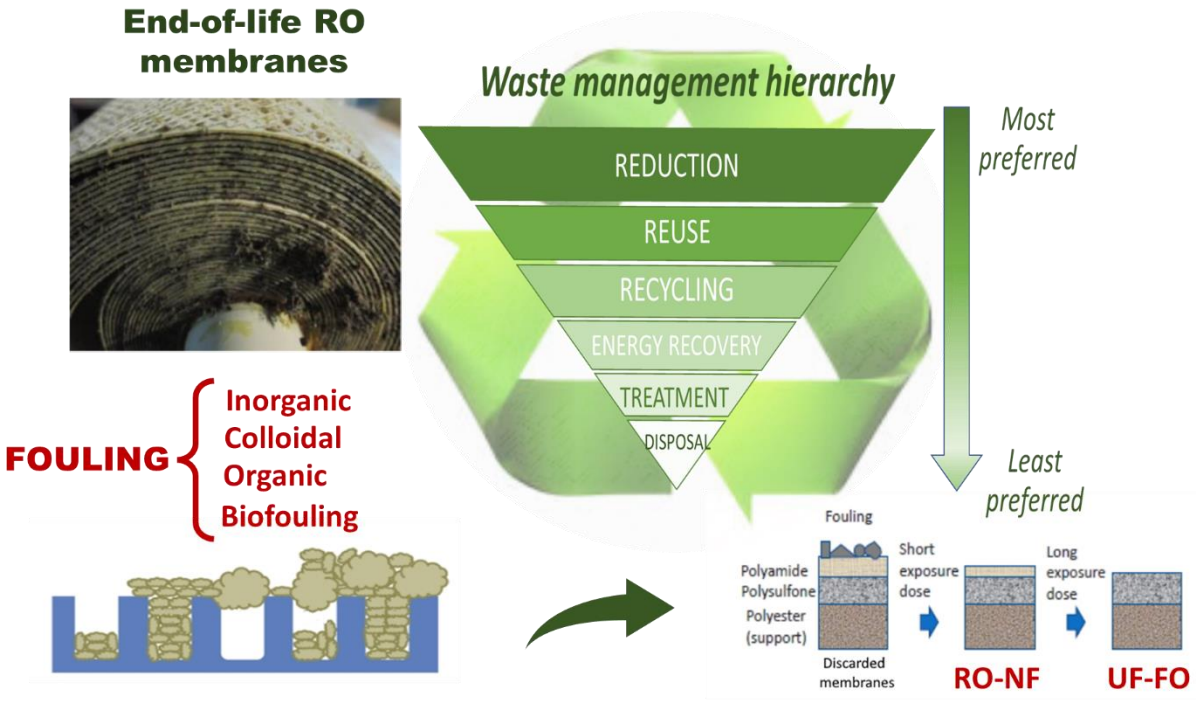

2.1. Introduction

It is an unquestionable issue that climate change is one of the biggest problems of the coming years. Human activity generates a large number of greenhouse gases, which is one of the main causes of climate change [1]. Therefore, mitigating the climatic impact of human activity is a necessity today. One of the emerging tools to carry out this task is the circular economy based on reduction, reuse, recycling and recovering, so that the use of resources is established within a closed loop, reducing pollution and at the same time maintaining the growth of economy [2,3]. This tool must be applied to all aspects of human activity. One of these aspects under study nowadays is the discarded reverse osmosis membrane modules in desalination plants [4–6].

The lack of accessibility to drinking water for human consumption is a problem in numerous countries all around the World. According to the report published by the World Health Organization (WHO) and the United Nations Children's Fund (UNICEF) [7], this problem affected 29% of the world's population in 2017. In 2020, the report by United Nations (UN) [8] included other than the problems of deforestation, water pollution, industrialization and agricultural activities, the consequences of climate change. This new report not only does not present any improved vision compared to the previous report, but it adds greater uncertainty about access of people to adequate drinking water sources. This shows that water stress is increasing and the prospects for the future are dramatic because water demand exceeds its availability.

Among the different measures adopted by authorities, RO desalination has been presented for years as a viable and mature solution to supply fresh water. Its growth since the first sustainable desalination plants during the period 1929-1938 [9] has been exponential. In 2019, 142 million of m^3 per day of drinkable water was produced by RO desalination [10]. Even though it is a technology with a high energy consumption, it is by far more competitive than other traditional thermal, evaporation and condensation, technologies. Various techniques have been adopted to reduce the energy consumption and water production cost including the use of renewable energy sources [11]. If the growth and volume of desalination by RO separation process are compared with those of other desalination technologies, RO is the most widely implemented technology with the greatest water production capacity [12,13].

Although RO is a mature and extensively implemented technology, it also has various drawbacks to overcome other than the reduction of energy consumption [11], such as the discharge of brines [12] and the management of the high volume of wastes generated by the discarded membrane modules. This last disadvantage is caused by the short average life span

of RO membrane modules (5-8 years) [14]. More than 14,000 tonnes of membrane modules are disposed annually around the world [5].

In this chapter, an overview of the different procedures adopted and techniques developed, to avoid the disposal of discarded RO membrane modules in landfills and to recycle or reuse them in other applications, are presented.

2.2. Reverse osmosis membrane technology

RO separation process makes use of a permeable and selective membrane that separates a solute from its solvent using an external hydrostatic pressure greater than the osmotic pressure (π) of the feed solution (Fig. 2.1). The mechanism of separation and the related transport theories have been widely reviewed [15–18].

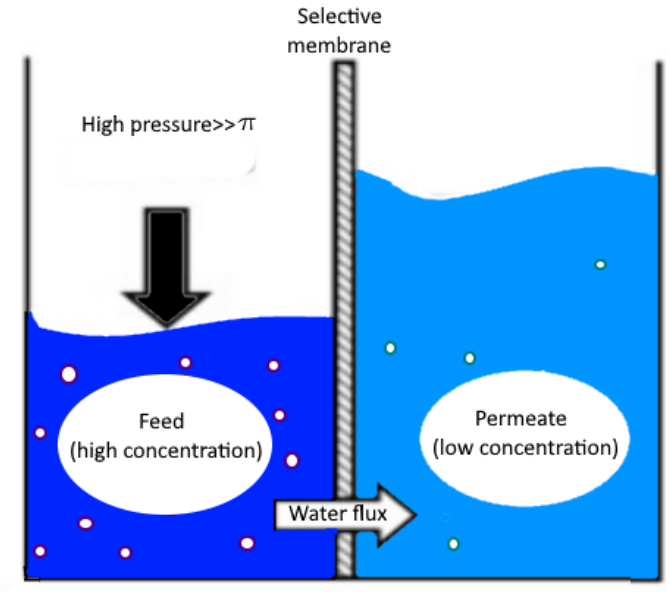

Figure 2.1. *Schematic of RO membrane process.*

RO separation process is used in numerous applications, for instance wastewater and leachate of landfill treatment, medical, pharmaceutical, food and hydrogen production industries to obtain clean water. However, the main application of this process is the sea or brackish water desalination [19]. In 2019, 74% of the world's desalination plants used RO technology [12]. Nevertheless, RO desalination presents some environmental problems that are already being addressed by the scientific community. Different configurations and combinations with other technologies have been developed to improve the desalination performance and reduce the environmental impact of RO technology [20]. Fig. 2.2 shows, as an example, the general operating schema of a typical RO desalination plant.

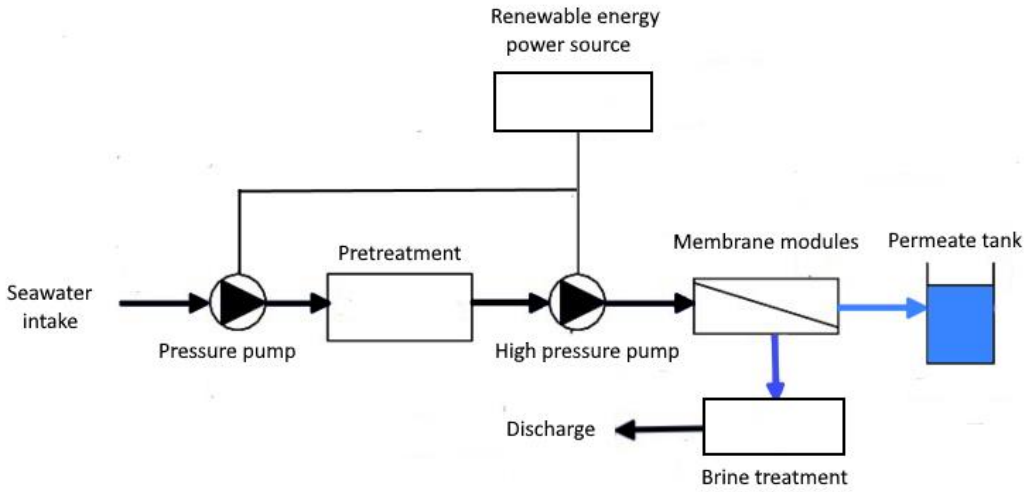

Figure 2.2. *Operational schema of a typical RO desalination plant.*

Microfiltration (MF) and ultrafiltration (UF) are commonly considered as pre-treatment methodologies to the RO process. These permit to remove a large part of major components from feed solutions so that the efficiency of the RO process is enhanced as both the working hydrostatic pressure at the entrance of the RO membrane modules and membrane fouling are reduced, extending their useful life as a consequence [21–24]. With the same purpose, other conventional pre-treatment methods are also used in RO plants such as disinfection, pH adjustment, coagulation, flocculation, sedimentation, flotation, filtration and dechlorination [21].

Different procedures and technologies have been tested for the treatment of RO brines looking at the creation of a sustainable process. Currently, the most common disposal methods are the surface water discharge in open water bodies, the sewer discharge, the deep-well injection and the evaporation pond; but these methods have environmental disadvantages that should be solved without increasing water production costs [25]. Different membrane technologies, such as forward osmosis, pressure retarded osmosis, membrane distillation, electrodialysis and reverse electrodialysis have been proposed for the treatment of RO brines [12,24–27].

In order to reduce costs and environmental impacts due to consumption of fossil fuels, different configurations for energizing by renewable energies and energy recovery systems have been proposed. Khan *et al.* [11] reviewed the potential of wind and photovoltaic technologies as possible electrical energization technologies for RO desalination. It was stated that the difficulty of the direct application of both technologies lay in the intermittency of both natural resources, either wind or sun, and it was claimed that the best energy solution was the mixture of different technologies (i.e., renewable, non-renewable and storage

systems), which guaranteed a stable and continuous electricity supply. As energy recovery systems, the Pelton wheel turbine and the pressure exchanger are widely coupled at the brine outlets of RO membrane modules [28]. The use of solar thermal energy coupled to RO membrane process has also been proposed, but it is still far from commercialization [29,30].

2.3. Reverse osmosis membranes and modules

In 1959 Reid and Breton [31] successfully synthesized the first cellulose acetate membrane for water desalination. This membrane exhibited a high salt rejection factor, but it showed an extremely low water permeate flux. Later, in 1963, Loeb and Sourirajan [32] presented an asymmetric cellulose diacetate membrane that improved both the salt rejection factor and the water permeate flux obtained by Reid and Breton. In the following years, cellulose triacetate membranes were developed with greater resistances to chemical and biological attacks, but prone to compaction even at low pressures (<30 bar) [33]. Later on, Richter and Hoehn [34] proposed the use of polyamide (PA) as a material to manufacture membranes. In 1979, Cadotte [35] developed the first thin film composite (TFC) membrane that consisted on a porous substrate as a support or a backing material and a thin selective layer of PA. Up to date, the TFC PA membranes remain the most widely used commercial RO membranes and are present in 95% of RO desalination plants in the world [36].

A typical TFC PA membrane (Fig. 2.3) is composed of a mechanical support of a non-woven polyester material over which a porous substrate of polysulfone is deposited by phase inversion (PI) method. The active PA layer is then formed by interfacial polymerization (IP) method as a thin film on the porous polysulfone layer [37–39]. The latest generations of commercial TFC PA membranes exhibit water permeabilities for seawater and brackish water between 1-2 LMH/bar and 2-8 LMH/bar, respectively. The salt rejection factors of these membranes are higher than 99.7% [40].

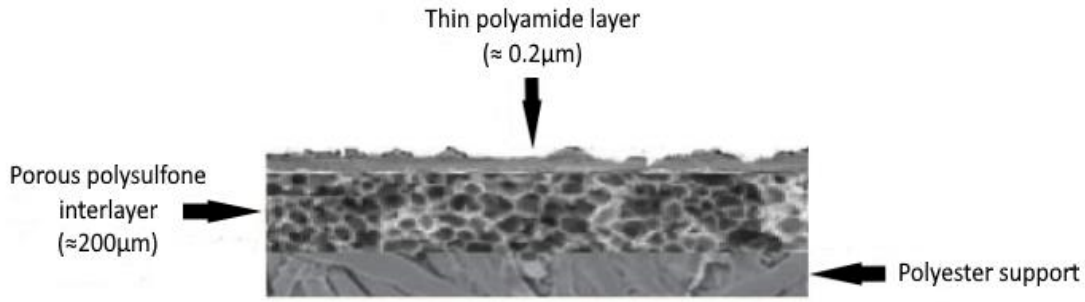

Figure 2.3. *Schematic illustration of common TFC PA membrane adapted from [38.]*

To improve the permeate flux of water together with the salt rejection factor, different monomers have been investigated. In 1981 Cadotte [35] was able to synthesize a high-water permeability (0.75 LMH/bar) and high salt rejection factor (99.5%) membrane by IP using 1,3-diaminobenzene (m-phenylenediamine, MPDA) and trimesoyl chloride (TMC). Currently, the TFC PA membranes produced by IP of MPD and TMC are the most commercially used ones [6]. Different studies propose the use of other combinations of monomers for the synthesis of the PA layer. In very few cases it was possible to increase the water permeate flux without scarifying the salt rejection factor achieved by Cadotte. Uemura *et al.* [41] by using MPDA and 1,3,5-trisaminobenzene (TAB) and a mixture of TMC and terephthaloyl chloride (TCL) obtained a water permeability of 2.8 LMH/bar and a salt rejection factor of 99.6%. Liu *et al.* [42] synthesized the PA layer using MPDA and 5-isocyanate-isophthaloyl chloride (ICIC) and obtained a higher water permeability (3.65 LMH/bar) but a value of the salt rejection factor (98.6%) lower than that reported by Cadotte.

In recent years, different modification strategies have been proposed to improve the performance of the TFC PA membranes. These look at the increase of the water permeate fluxes without reducing the salt rejection factors and the improvement of the anti-fouling properties of the membranes as well. For this purpose, various manufacturing control technologies have been applied to fix specific thicknesses for the different layers of the membrane as well as their porosities and hydrophilic properties, surface modifications of both the support layer and the PA active layer and the addition of nano-additives in the different layers among others [37,39,43–45].

In general, in RO desalination plants, TFC PA membranes are packed in a spiral wound membrane (SWM) module configuration as can be seen in Fig. 2.4 [46]. Inside the module generally fabricated using fiberglass are located the membrane together with the spacers of the feed and the permeate designed adequately to allow the liquid circulation while minimizing the concentration polarization layer as much as possible [47]. The spacer for the permeate is located between two membranes with their active layers facing each other. The membrane sheets are sealed with glue on three of their edges. The open edge is connected to the perforate central collector tube. Between each of these sets of two membranes and a permeate spacer is located the feed spacer. The configuration of the SWM module and its material composition are presented in Fig. 2.4a and 2.4b, respectively.

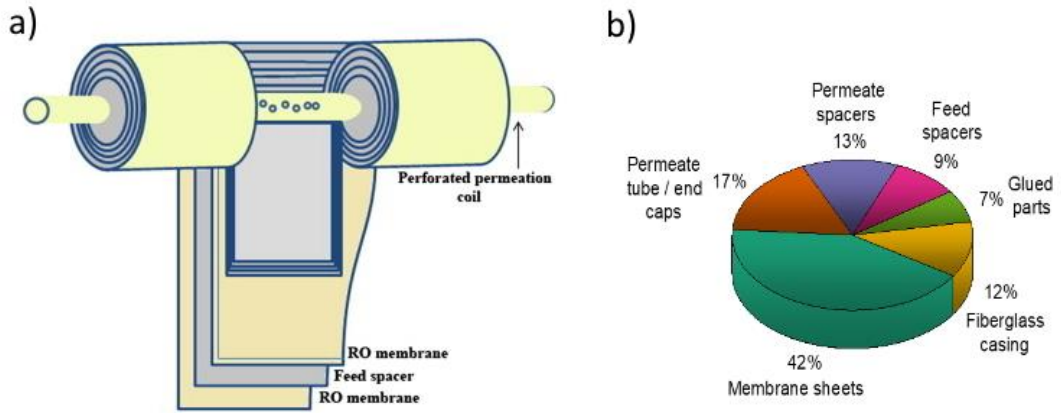

Figure 2.4. *a) Configuration of spiral wound membrane modules [38] and b) its composition adapted from [6].*

Currently, the standard dimension of these types of membrane modules is 8-inch diameter and 40-inch length. Efforts are currently being made to fabricate larger modules (16-, 18 and 24-inch) in order to increase the performance of the RO membrane process because these modules would reduce the energy required per liter of produced fresh water [47].

2.4. Fouling in RO separation process: problem, prevention and cleaning protocols

It is already known that the RO membrane separation process is limited by the increase of the osmotic pressure of the feed solution to be treated due to the corresponding increase of the feed solution concentration and the concentration polarization during the desalination process. However, there are some limiting factors like membrane fouling and membrane deterioration [48], that reduce considerably the RO performance. Membrane deterioration refers to the damage of the membrane active layer due to the utilization of different oxidants in the feed water pre-treatment and chemicals during the cleaning procedures [48]. This results in a decline of the rejection capability and an irreversible membrane destruction.

Membrane fouling, which is an unavoidable phenomenon affecting both membrane surface and its pores, leads to severe permeability losses and drastic enhancements of water production costs in RO desalination [49–51]. Generally, fouling depends on membrane characteristics, feed solution and RO operating conditions. During the RO process, the convective and diffusive transport of non-dissolved colloidal or biologic matter and precipitated inorganic material creates a continuous fouling layer on the membrane surface (i.e., surface fouling) or within the pores of the membrane (i.e., internal fouling), as shown in

Fig. 2.5 [50,52]. When RO membranes get fouled, the developed fouling layer increases the pressure loss along the membrane and induces an additional resistance to water permeation together with a reduction of the rejection factor affecting therefore the membrane lifetime [48,50,52,53].

As RO membranes are relatively compact in comparison to microporous membranes, the major fouling mechanism is often associated with surface fouling in contrast to internal fouling [54]. Fouling includes precipitation of inorganic salts, accumulation of suspended particulate matter, and formation of biofilms [54,55]. Hence, four major types of membrane fouling can be distinguished based on the foulant type, namely: crystalline or inorganic fouling, particulate or colloidal fouling, organic fouling and microbiological fouling or biofouling [18,48,54,56–62].

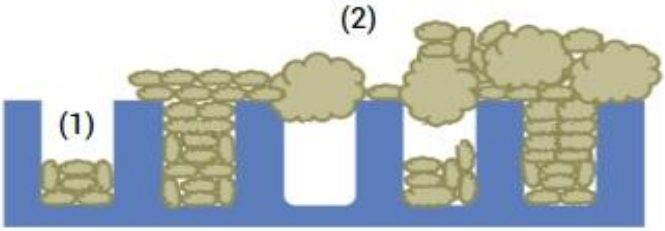

Figure 2.5. *(1) Internal (within membrane pores) and (2) external (on membrane surface) membrane fouling. Adapted from [55].*

2.4.1. Inorganic fouling

Crystalline or inorganic fouling, which generally refers to mineral scaling, consists in the deposition of inorganic material precipitating on a membrane surface [50], causing one of the major membrane fouling problems in water treatment and membrane desalination processes [47] due to the high amount of total dissolved solids in feed aqueous solutions and the very high salt rejection factors [57].

Common scaling substances can be mainly categorized into metal ions and silica-based scales due to their chemical components [48,60,61,63]. Carbonates like $CaCO_3$, phosphates like $Ca_3(PO_4)_2$ and sulphates like $CaSO_4$ and $BaSO_4$, among others, are usually formed by crystallization. Crystal growth is usually divided into three stages as shown in Fig. 2.6a. The starting step takes place when salts concentration is over their solubility and the ions start colliding to form ion pairs and clusters. Then, some ion clusters align in an orderly way to form stable nuclei. Finally, crystals grow gradually from nuclei in an irreversible process [48,60,61]. The formation of silica-based scale is a complex, which depends on multiple factors, including pH, temperature, ionic strength, multivalent ions, silica concentration, etc. [61].

In RO processes membrane scaling can be divided into bulk (homogeneous) and surface (heterogeneous) crystallization, as shown in Fig. 2.6b [15,54,60,61,63]. It is known that the high recovery rates of RO in water desalination results in high concentration of sparingly soluble salts from feed water over their solubility limit, favoring the formation of salt crystals in the bulk solution and their subsequent deposition on the membrane surface causing membrane blocking and deterioration of membrane performance [60,61,64,65]. On the other hand, salt crystals can be directly formed and grown on the membrane surface under a high concentration polarization and salt supersaturation [60,61]. Regardless of their origin, scaling dramatically reduces the RO membrane permeate flux.

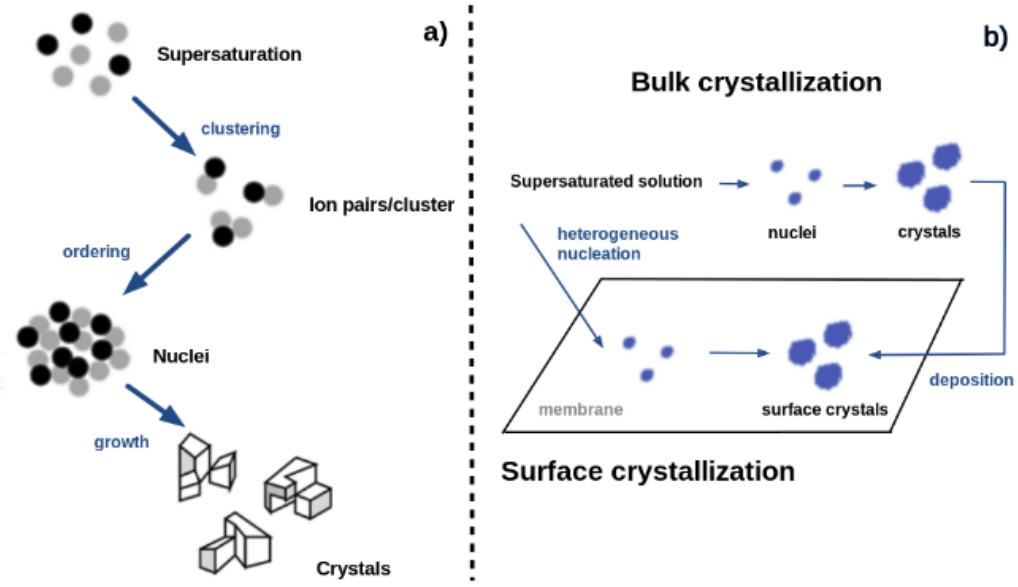

Figure 2.6. *Stages of crystals growth (a) and bulk and surface crystallization processes (b).*

2.4.2. Colloidal fouling

Particulate or colloidal fouling refers to the accumulation of particles, intermediate in size between suspended solids and true dissolved solids, on membrane surface and within its pores [48–50,66]. Colloidal particles are difficult to remove by filtration pre-treatment procedures because of their small size. These accumulate on the membrane surface causing a fouling layer [67]. It is worth noting that despite of the well-known pre-treatments in RO plants that remove most of particulate matter, this type of fouling still occurs in RO seawater desalination [68]. The most common colloidal particles can be divided into inorganic colloids (i.e., silica, iron and aluminum oxides), organic colloids (i.e., proteins, natural organic matter (NOM) and polysaccharides) and biological colloids (i.e., microorganisms) [48–50,66].

This type of fouling and its reversibility or irreversibility can be controlled by foulant-foulant and foulant-membrane interactions [49,69,70]. The colloidal fouling layer increases the concentration polarization near the membrane surface, enhances the corresponding osmotic pressure and reduces the water permeate flux [49,71]. Additionally, the increase of the overall thickness through which the water must permeate reduces the membrane permeability, making necessary a higher operational hydrostatic pressure to maintain a constant permeate flux [49].

2.4.3. Organic fouling

Seawater RO desalination membranes are mainly fouled by organic matter [17,51]. Organic fouling results from the deposition of NOM on the membrane surface [50,66,72]. The principal components of NOM are humic substances, in particular humic acid (HA), produced by the degradation of NOM [48,72], followed by carbohydrates (including polysaccharides), proteins and a variety of acidic and low molecular weight species [55,72]. HA, which is usually present in natural waters, surface and ground waters and seawater, can form chelates with metal ions and generates a gel like fouling layer by complexation of multivalent ions [48]. It has been identified as one of the major foulants for RO membranes [73].

HA follows an adsorption-desorption mechanism to migrate through the membrane pores, as shown in Fig. 2.7. It involves an initial deposition on the membrane governed by the interactions between HA and the membrane surface, and the subsequent development of a gel or cake layer governed by the interactions between the deposited HA and HA in the bulk solution [48,53]. Later, hydrogen bonding between water and HA is formed and then weakened as water vapor moves through the membrane, re-adsorpting HA onto the membrane and inducing pore wetting [72].

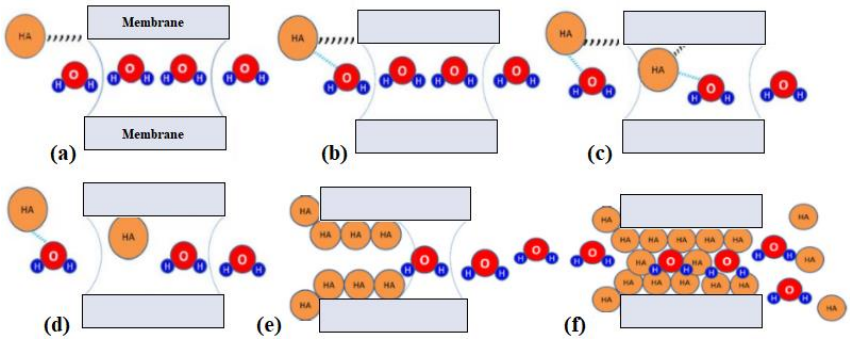

Figure 2.7. *Adsorption-desorption mechanism for HA migration through a membrane pore. (a) adsorption of HA onto membrane surface; (b) hydrogen bonding between water and HA; (c, d) weakening of hydrogen bond as water vapor moves through the membrane; (e) re- adsorption of HA onto the membrane and (f) pore wetting phenomenon [72].*

The adsorption of theses organics on the membrane surface is further influenced by the physico-chemical properties of organic foulant(s) and the membrane and the operating conditions [53]. In general, this type of fouling results in permeability decline, which can be an irreversible process.

2.4.4. Biofouling

Biofouling or microbiological fouling of RO membranes has been recognized as one of the most severe problems that reduces the efficiency of the RO desalination process [50,62,74]. This type of fouling is referred to as the unwanted reversibly or irreversibly deposition (adhesion and accumulation) and growth of microorganisms onto the membrane surface or within its pores [50,62]. While reversibly attached microorganisms (i.e., planktonic organisms) can be removed easily by chemical treatments that cause microbial inactivation, irreversibly attached microorganisms induce biofilms formation that cannot be removed by gentle rinsing or water circulation. Among the microorganisms that have potential to form biofilm on the membrane surface are mycobacterium, flavobacterium, pseudomonas, bacillus, cytophaga and lactobacillus [50]. A biofilm is an assemblage of surface-associated microbial cells covered by self-produced extracellular polymeric substances (EPS), resistant to biocides and antibiotics [50,55,62,72,75]. EPS are composed of polysaccharides, proteins, glycoproteins, lipoproteins and other macromolecules of microbial origin, forming a slime matrix, which glues the cells to the membrane surface and keep the biofilm together [75]. The general development of a biofilm takes place in three phases [50,66] as is schematized in Fig. 2.8.

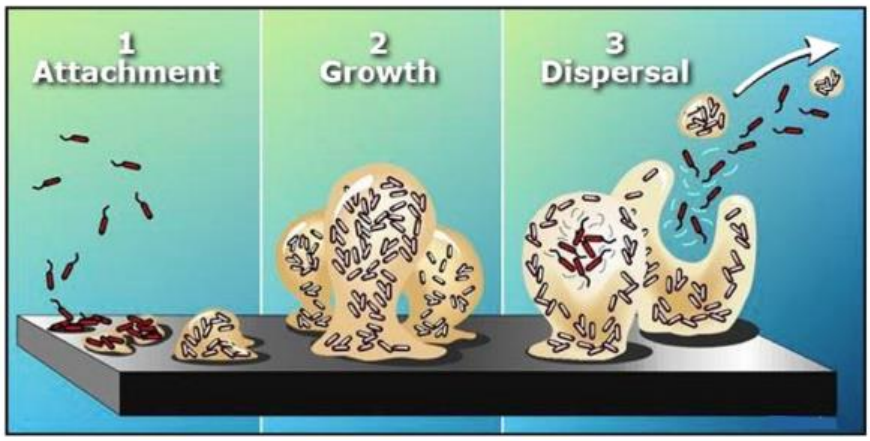

Figure 2.8. *Biofilm formation process. (1) Attachment of microorganisms to membrane surface, colonization and EPS production. (2) EPS development and biofilm growth (3) Plateau phase and biofilm propagation [50].*

The first step, named the induction phase, is probably the most important for the prevention of any biofilm development. This stage is characterized by an initial rapid primary colonization, followed by a primary plateau. The adhesion is essentially proportional to the cell density in water phase and it occurs owing to weak physico-chemical interactions [50,66]. Then, a logarithmical growth takes place when cell growth on the membrane surface contributes more to biofilm accumulation than does the adhesion of planktonic cells. When biofilm growth (adhesion and multiplication), the cell detachment and cellular senescence are in balance. This last phase is mainly known as plateau phase, and when it is reached the original surface properties of the membrane are masked by the biofilm [50,66].

It can be stated that biofouling takes place when biofilms are present in the wrong place and at the wrong times. For example, on a separation membrane, the biofilm acts as a secondary membrane that participates in water purification process, producing a long-term flux decline and enhanced concentration polarization resulting in a decrease of the salt rejection factor that cannot be recovered fully by the hydraulic cleaning of the membrane [50]. Thus, while the first three types of fouling can be reduced by means of pre-treatments, it is difficult to effectively control biofouling by any pre-treatment in RO process because the deposited microbial cells can grow, multiply and relocate [66].

2.4.5. Fouling prevention and mitigation

As it is already mentioned in the previous section, membrane fouling is unavoidable in membrane separation processes. However, there exist some strategies to prevent or reduce it. To mitigate the appearance of fouling a pre-treatment of feed solution, an optimization of the RO operating conditions and the development of adequate membranes using materials resistant to fouling or surface modification of membranes using nanomaterials with structural and chemical properties less prone to fouling [54,55].

Feed water pre-treatment prior to RO desalination to minimize membrane fouling by removing foulants and/or adjusting the feed water chemistry is widely considered and studied by numerous researchers. The typical or conventional pre-treatment approaches include screening, coagulation-flocculation, media filtration, UF/MF and their combinations [54,55]. Screening is a prior step to remove large and suspended solids in water. Coagulants and flocculants are mainly utilized to enhance the settlement of suspended solids in the feed water in order to achieve higher removal rates. Typical coagulants and flocculants include ferric chloride, ferric sulphate and cationic polymers [54]. Their efficiency was confirmed in different studies. For instance, Mitrouli *et al.* 2008, who used polyaluminum chloride, ferric chloride and ferric chlorosulphate as coagulants, observed up to 88% reduction of water

turbidity. To control biofouling, Wei Ma and Yaqian Zhao [76] proposed coagulation with Fe (VI) followed by UF and achieved 98% of algae and microbial removal rate.

Media filtration is employed to eliminate different types of particles smaller than those removed by screening. Various type of materials can be utilized like activated carbon, expanded clay and anthracite coal, among others. For example, Mitrouli *et al.* [77] by using different filters like expanded clay and anthracite coal with similar particle range to pre-treat seawater under different operating conditions, could reduce water turbidity and silt. Moreover, Van der Hoek *et al.* [78], who used biologically activated carbon and slow sand filtration, observed an excellent RO feed water and a very stable operating RO parameters overtime, with only a 16% permeate flux reduction in 11 months.

MF/UF are the most popular for the pre-treat of feed water as both can remove a variety of foulants, such as biomass flocs, individual bacterial cells, colloidal particles and macromolecular organics depending on the membrane pore size and the foulant molecular weight [54,55]. After a previous coagulation, an UF membrane was used by Ma *et al.* [76] as pre-treatment step to diminish RO feed water pollution, achieving a 98% reduction of algae and microbes. Kim *et al.* [62] carried out a comparative study of the MF and UF membranes as pre-treatment method for high-pressure membranes for the reclamation of biologically treated wastewater effluents. Compared to MF pre-treatment, it was found that the UF pre-treatment allowed a lower permeate flux reduction in the subsequent RO process and less RO membrane fouling due to a higher rejection of colloidal substances, organic matter and polysaccharides.

The above mentioned methods are focused on the feed water foulants removal. Nevertheless, other methodologies aim to optimize the feed water chemistry (i.e., pH, hardness, ionic strength, etc.) because the solution chemistry influences the interactions between foulant and membrane and between foulants with each other, in addition to the influence of the inorganic scale precipitation and the biological activity of microorganisms [55]. For example, the pH adjustment is extensively considered to control the inorganic scaling. Van der Hoek *et al.* tried to avoid scaling problems with barium sulphate ($BaSO_4$) and calcium carbonate ($CaCO_3$) by acidifying the feed water with hydrochloric acid (HCl), achieving a recovery of 85% in the RO separation process. Maartens and Swart [79] achieved a significant reduction of NOM adsorption on membrane surface by adjusting the pH at 7 with HCl and sodium hydroxide (NaOH).

Another way to reduce fouling risk, both organic and inorganic, is to remove or diminish water hardness (i.e., reduce calcium and magnesium salts concentrations). In this case, the ionic exchange is the most followed technique. Huang *et al.* [80] by using magnetic ion exchange (MIEX), coagulation and UF, could reduce organic fouling in RO membranes to

values between 87% and 99.9% when treating humic substances. Moreover, Apell and Boyer [81] combined both anion and cation exchange treatments in a single and completely mixed reactor for the simultaneous removal of 70% of dissolved organic carbon in feed water and at least a 55% of water hardness.

It must be mentioned that the limitation of nutrients present in water is an effective strategy for biofouling control. For this purpose, C.M. Kim *et al.* [82] discovered that the phosphate limitation in feed water greatly reduced microbial growth and biofilm formation.

Most of the used chemicals in the pre-treatment processes are coagulants/flocculants for the enhancement of suspended solids removal, and acids for the pH adjustment. Scaling inhibitors or anti-scalants are also mostly considered. These are formulated using polyacrylic acid, carboxylic acid or phosphonates [54]. Lyster *et al.* [83] used two different commercial anti-scalants (PC-504T and Flocon 260) to retard the nucleation and crystal growth of a RO feed water. Van der Hoek *et al.* [78] added Flocon 100 anti-scalant in combination with sulfuric acid (H_2SO_4) dosage to recover up to 90% of RO water. However, some anti-scalants in feed water showed risks of increasing biofouling potential as well as an enhancement of organic fouling [78,84].

Besides feed water pre-treatments, RO operational conditions must be chosen and optimized, within the design limitations of different RO membrane modules, in terms of temperature, operating pressure and feed flow rate to mitigate fouling phenomenon [54,55]. Separation performance is improved with temperature in RO systems. However, an elevated temperature also affects fouling formation on the membrane surface, favoring crystal nucleation [64] and biofilms growth [85,86]. In addition, the operating hydrostatic pressure in RO separation process is also a very important parameter that allows to control membrane fouling [63,87]. A high-pressure result in a higher initial permeate flux hence promoting fouling development due to an increase in the concentration polarization effect [54]. Furthermore, a high-pressure may result in the compaction of foulants onto the membrane surface by increasing the hydraulic resistance of the foulant(s) layer [88], making irreversible their removal by any subsequent physical cleanings [89]. In general, membrane fouling can be reduced at high feed flow rate or low permeate flux. A greater feed flow rate induces a high shear force on the membrane surface that can result in less foulant(s) deposition and concentration polarization effect [55]. In addition, the permeate flux decline overtime is lower for higher feed flow rates. This fact can be directly related to lower organic fouling, inorganic fouling and biofilms development [90,91].

TFC membranes, which is generally composed of an ultrathin PA layer on a porous support, are the widely used RO membranes because of the excellent physicochemical properties of PA [92]. It was reported that membrane fouling is closely related to membrane

surface characteristics such as smoothness and hydrophilicity [44]. Accordingly, membrane modification is considered one of the main strategy followed to reduce membrane fouling. Among the considered approaches to design fouling resistant TFC membranes, one can find the increase of the hydrophilic character of the RO membrane active layer with reduced roughness and the nano-enhanced TFC membranes (NEMs) by incorporating nano-additives (nanoparticles or nanotubes) in their active layer due to their excellent antifouling properties as well as the impressive water transport properties.

To date, surface modification is the most promising way of biofouling control in RO systems and includes physical modification (adsorption or coating) and chemical modification (covalent attachment of antifouling polymer chains or grafting) [54,93,94]. While the most promising technique for membrane surface coating is plasma treatment [54,95], surface grafting can be achieved by using a single or a mixture of monomers. Different methods like atom transfer radical polymerization (ATRP), chemical coupling and free radical graft polymerization, among others, are considered [54]. However, most of the proposed studies are based on the active layer modification and only few researches consider the support layer modification [39]. This is because membrane fouling occurs mainly at the membrane surface and in the active layer near the feed solution. Surface modification can be effective to mitigate external fouling, but may has little effect on the internal fouling control and sometimes reduces membrane water permeability because an additional layer is formed on the membrane surface [55].

As it is mentioned previously, some research studies were focused on the improvement of the membrane surface by adding nanomaterials into the PA layer to produce NEMs, such as carbon nanotubes or halloysite nanotubes [96,97]. Another way to tune the structure and physicochemical properties of RO membranes to improve the permeate flux and the fouling resistance is by adding nano-sized ceramic and metal particles, such as TiO_2 [98], silver [99] and silica [100], among others. A complete study on surface modification and incorporation of nanoparticles in membrane surfaces for the improvement of antifouling properties was reported by Goh *et al.* [54].

Some research studies were also carried out on feed spacers (i.e., thickness [101], geometry [102] or even surface modification [103]), as an integrated part in RO spiral wound modules [54]. In fact, spacers inserted in the feed flow play an important role in fouling mitigation. These help to provide turbulent flow and less concentration polarization effect [55,104], resulting in an enhancement in mass transfer, better mixing, and less membrane fouling initiated by particle depositions [105,106].

2.5. End-of-life RO membrane modules: reuse and recycling techniques

A membrane module reaches the end of its useful life when its performance, both water permeate flux and salt rejection factor, decline below the minimum operating levels established by the manufacturer and it is no longer possible to apply any cleaning treatment to recover the required values of production. A common indicator of the decline in an RO system performance is an increase in the feed inlet pressure to keep constant the water permeate flux. This degradation in membrane performance is generally due to irreversible fouling and chemical damage of the membrane material suffered during its operational life [5]. Therefore, the annual module replacement rate in RO plants was estimated to be between 10 and 20% [17,107]. Consequently, thousands of tons of wastes are generated per year. It is worth noting that prior to the disposal of discarded RO membrane modules, cleaning protocols are being developed to extend the useful life of these modules or finally to prepare them for reuse or recycling.

2.5.1. Cleaning strategies adopted for RO fouled membranes and discarded modules

Because of the nature of filtration, fouling in RO membrane separation process is unavoidable and shortens membrane life imposing therefore a large economic burden on RO membrane plant operation [48,50]. One of the major goals of the RO desalination industry has been the enhancement, or at least the maintenance of the water permeate flux without sacrificing the salt rejection factor over long periods in order to increase the efficiency and reduce the operation costs. For that, effective, sustainable and periodical cleaning strategies of each RO desalination plant must be programmed and performed [51]. Cleaning processes aim to restore the membrane performance when the expected permeate flux decreases by about 10% [48,50].

RO membrane cleaning is usually performed in three different ways: physical, chemical and biological [55,108]. The physical cleaning methods mainly include membrane surface flushing and backwashing [49,55,109]. The first one is based on an enhanced crossflow velocity along the membrane surface. Even though it has been demonstrated to be effective against membrane fouling, this cleaning method consumes high amount of clean water during flushing, which would in turn reduce the actual water recovery [55]. On the other hand, membrane backwashing consists on reversing the water permeation direction and using the permeation drag force to detach and remove the deposited foulant(s) on the membrane surface [55]. This is carried out by applying a larger pressure on the permeate side, hence the osmotic pressure causes the permeate water to flow in the opposite direction with

a given force to remove the deposited foulant(s) [49]. For this reason, RO membranes must withstand hydrostatic pressures in both directions. Finally, ultrasonic techniques have also been applied for membrane cleaning. Ultrasounds causes cavitation, which refers to the formation of bubbles in liquid, that grow and lastly collapse, aiding membrane cleaning. However, one drawback of this applied technique is the cost while the other is the vulnerability of the RO membrane to be damaged due to the high cavitational collapse depending on the applied power density, frequency, and time of ultrasound [49].

Chemical cleaning aims to remove impurities by means of chemical agents that weaken the adhesion force between foulant(s) and membrane [55]. A large number of chemical cleaning agents have been used: alkalis, acids (hydrochloric acid-HCl, nitric acid-HNO_3, H_2SO_4), bases (like NaOH), metal chelating agents (such as sodium ethylene diamine tetra acetic acid-EDTA), surfactants (such as sodium dodecyl sulphate-SDS, oxidation agents (like sodium hypochlorite–NaClO or hydrogen peroxide-H_2O_2) and their combinations [49,55,108,110]. Despite the fact that chemical cleaning is able to achieve a high efficiency against organic fouling and biofouling, it could not remove foulant(s) from membrane pores.

Although it has been claimed that both physical and chemical cleaning are effective against membrane fouling, the former consumes a large amount of water and can cause damage to membrane integrity, while the later generates a large waste of chemical reagents that can cause environmental problems, and uses corrosive substances such as NaClO or H_2O_2 that may be detrimental to membranes and also exert negative influences on microbial community [55,110]. To overcome these impacts, biological cleaning that involves the use of bioactive agents for foulant(s) removal has be suggested [55,111]. Among the different biological cleaning strategies reported in the literature, enzymatic cleaning is the most widely used [55,110]. In this case, environmental friendly enzymes can specifically interact with the biopolymeric foulant(s) (i.e., proteins and lipids) and break up the foulant(s) layer on the membrane surface, thus preventing the physical and chemical destruction of the membrane materials [110]. One advantage of using enzymes for membrane cleaning is its normal operation conditions (i.e., pH, temperature and concentration) that are not harmful for RO membranes [112]. Nevertheless, the use of enzymes alone for cleaning RO fouled membranes can result more of a liability than a solution since enzymes could become additional foulants on the membrane surface reducing its permeability as well. Therefore, enzymatic cleaning should be combined with other cleaning procedures (physical and/or chemical) to address other types of fouling for an effective cleaning of RO modules used in seawater desalination [49]. Table 2.1 summarizes different cleaning strategies of RO fouled membranes.

Table 2.1. *Cleaning procedures of RO fouled membranes.*

Fouling type	*Membrane*	*Cleaning method*	*Cleaning agents*	*Procedure*	*Improvement*	*Reference*
Organic fouling/ biofouling	TFC polyamide	Osmotic backwashing	NaCl	1.5 M NaCl flushes into the feed water, at 13.8 bar	70–90% reduction of biofouling. 63% original flux recovery	[113]
Organic fouling/ biofouling	TFC polyamide	Surface flushing + chemical + osmotic backwashing	EDTA and NaCl	Flushing with DI water (45 min) + Chemical cleaning with 5 mM (EDTA) at pH 11 (45 min) + Osmotic backwashing with 32 to 96 g/L NaCl. (10 min) + Flushing with DI water	Increase permeate flux and permeation rates after cleaning increased with solution salinity (32, 64 and 96 g/L NaCl).	[114]
Organic fouling/ biofouling	TFC polyamide	Surface flushing	NaCl	50mM NaCl cleaning solution (15min)	70% permeate flux recovery	[109]
Organic fouling/ biofouling	LFC polyamide		Monovalent cations (Na^+, K^+, Cs^+, NH_4^+)	25 mM and 100 mM	75% cleaning efficiency for NaCl at 25 mM and ~ 90% for all the salts at 100 mM	[115]
Organic fouling/ biofouling	Cellulose acetate	Chemical and biological	Enzyme + EDTA + dispersant. Bactericidal agent + anionic detergent	Chemicals dissolved in a 100 mM phosphate buffer at pH7.	70-90% biofilm removal	[116]
Organic fouling/ biofouling	BTESE-derived organosilica membranes	Physical (immersion and agitation)	DI water	3 cleaning steps at 1000 rpm. First at 298K and the others at 353K a	Total recovery of membrane	[117]
Organic fouling/ biofouling	TFC polyamide	Biological	Subtilisin (protease and lipase) + dextranase + polygalacturonase	Doses of 50, 100, and 150 ppm. at neutral pH (~7) during 18-36h	Restored the hydrophobicity and roughness of the TFC RO surface to its initial condition	[118]
Inorganic fouling ($CaCO_3$)	TFC polyamide	Osmotic backwashing	NaCl	Backwashing immediately after salt precipitation	Initial permeate flux recovery	[119]
Inorganic and organic fouling /biofouling	Polyamide	Physical and chemical	NaOH + SDS + HCl	10 min DI water +10 min chemicals at 0.5bar	Removal of most of the deposited materials from the membrane surface	[108]
organic and organic fouling /biofouling	Polyamide	Physical (ultrasounds)	-	20 kHz frequency and 2.8 W/cm^2 power intensity	50–250% permeate flux increase with no compromise in salt rejection	[120]

TFC: Thin film composite; EDTA: ethylene diamine tetra acetic acid; LFC: Low fouling composite; BTESE: bis(triethoxysilyl)ethane; DI: deionized water.

To study and verify the causes of performance loss of the discarded RO membrane modules at the end of their useful life, autopsies of the modules were performed by different authors [121–127]. Pontier et al. [128] described different tools available for the characterization of discarded RO membrane modules such as gravimetry, permeability and rejection of solutes, as well as different scanning and microscopy techniques necessary for the analysis and surface characterization of RO membranes.

In specific studies aimed at the possible recycling of the discarded RO membrane modules, a clear difference has been observed for the type of fouling existing in the discarded modules depending on the type of feed water used, seawater or brackish water. The characterization of the membranes discarded during autopsy of the end-of-life RO modules has shown similar characteristics to UF membranes. [4,129–132]. When seawater was used as feed, the type of membrane fouling was more organic and biofouling, while for brackish water used as feed, the most abundant fouling type was clay matrix [4,127,133,134].

2.5.2. Reuse of discarded RO membrane modules

Following the waste management hierarchy shown in Fig. 2.9, reduction together with reuse or recycling should be prioritized for an adequate management of RO discarded membrane modules. Nevertheless, it is not always possible to reduce wastes. Therefore, strategies to reuse and recycle discarded RO membrane modules become of great importance.

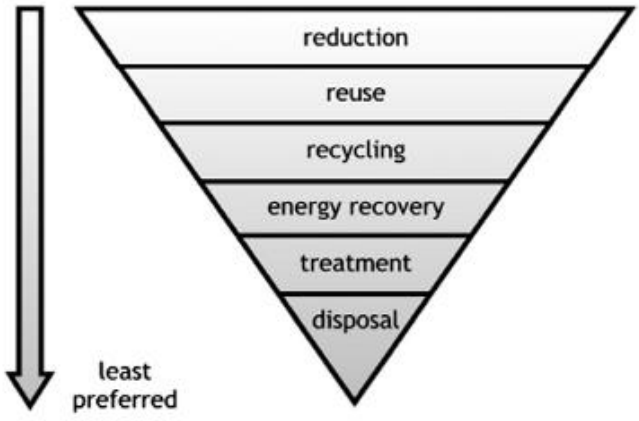

Figure 2.9. *Waste management hierarchy [6].*

The potential reuse of discarded RO membrane modules is very scarce as only few reports has been found in the membrane literature [129–131]. For example, Mohamedou *et al.* [129] verified that a discarded RO membrane could be a useful nanofiltration (NF) membrane valid in less demanding filtration processes. It was also proposed the use of spacers and the discarded RO membrane as a geotextile in gardens (root entry protective layer in drainage sublayer). Prince *et al.* [131], after studying the characteristics of discarded RO membranes from seawater RO modules, proposed their reuse in RO separation of lower solute concentrations (i.e., for selective demineralization of brackish water or NF as RO pre-treatment). The external and internal elements of the RO membrane modules have been proposed for reuse in various applications such as geotextile, mouse pad, support for children drawings, protection from snake attack, and aromatic herbs containers in familial kitchen [130].

2.5.3. Recycling discarded RO membrane modules

Different chemical procedures have been proposed to recycle discarded RO membrane modules. The degradation of the PA layer of TFC membranes by certain oxidizing agents has been widely investigated [135,136]. This method has been used for the total or partial elimination of the PA layer where the irreversible fouling is located [103]. NaClO is one of the most used chemical agent [6,137]. Other considered chemical agents for PA layer degradation are H_2O_2, sodium dodecyl sulphate (SDS), acetone, N-methyl-2-pyrrolidone, potassium permanganate ($KMnO_4$), tannic acid and NaOH [5,107,132,138–142]. Any of these chemicals can be applied following an active procedure in which the oxidant solutions are pumped through the discarded RO membrane modules, or a passive procedure by immersing the discarded RO membrane modules in the oxidizing solution without any type of pumping. The exposure time of the discarded membrane modules in the oxidant solution and its concentration determine the degradation speed of the PA layer. For this reason, both parameters (exposure time and oxidant concentration) have been the investigated in the following studies [134,138–140,143]. Both parameters were merged as the exposure dose (ppm·h) defined as the concentration of the oxidizing agent in parts per million (ppm) multiplied by the exposure time in hours (h). In addition, it was reported the decisive role of the pH basic of the oxidant solutions in the degradation of the PA layer [141,144,145]. Fig. 2.10 shows the degradation schema of the PA layer of the discarded RO TFC membrane as a function of the applied dose of the oxidizing agent.

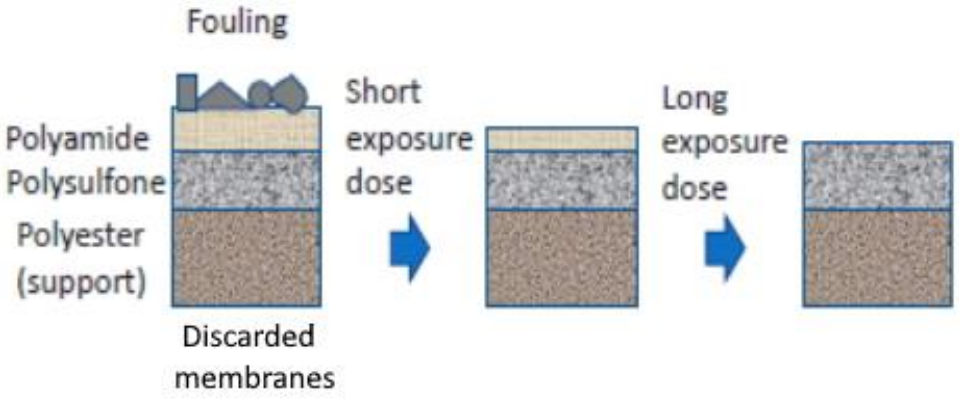

Figure 2.10. *Degradation of the PA layer of discarded RO TFC membrane as a function of the oxidizing agent dose.*

Analyzing the attenuated total Reflectance-Fourier transform infrared (ATR-FTIR) spectra of RO discarded membranes subjected to different exposure doses in the recycling process, it was confirmed the dependence of the degradation of the PA layer on the exposure dose of the oxidizing agent. Fig. 2.11 shows the spectra of seawater and brackish water discarded membranes and those exposed to different exposure doses. If the characteristic peaks of PA amide I and amide II are observed at 1664 and 1542 cm^{-1} respectively, the different degrees of degradation of the PA layer are clearly detected. Due to the difference of fouling layers present on the discarded membranes that generally depend on the type of feed water used, for the same exposure dose the discarded membrane from brackish water desalination suffers greater degradation of the PA layer than the membrane previously used in seawater desalination. It was claimed a complete degradation of the PA layer around 300,000 ppm·h exposure doses for the discarded membranes previously used in seawater desalination and 50,000 ppm.h for those applied in brackish water desalination [134].

The surface of discarded RO membranes and those subjected to a recycling process with different exposure doses of NaClO were studied by SEM. Fig. 2.12 shows the removal of fouling and the progressive degradation of the PA layer from the surface of the RO membrane with the increase of the exposure dose of the oxidizing agent [146].

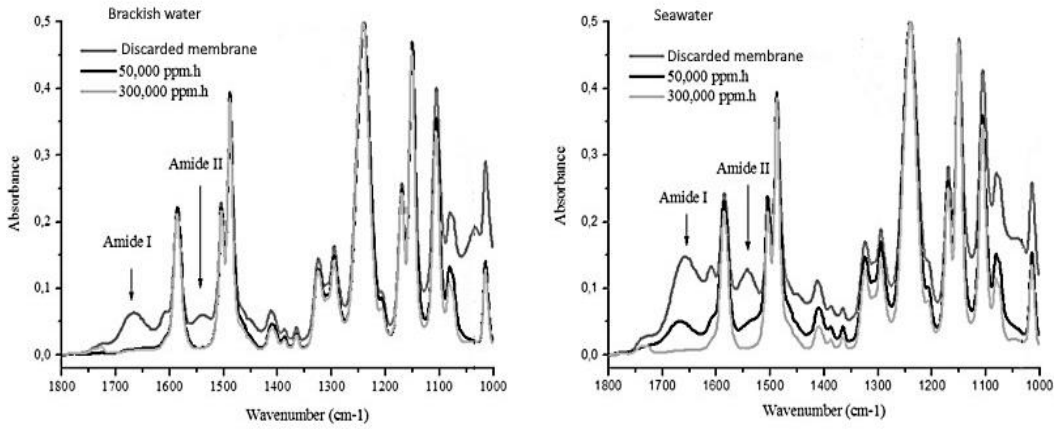

Figure 2.11. *ATR-FTIR spectra of recycled membranes from brackish water and seawater desalination plants after different exposure doses [134].*

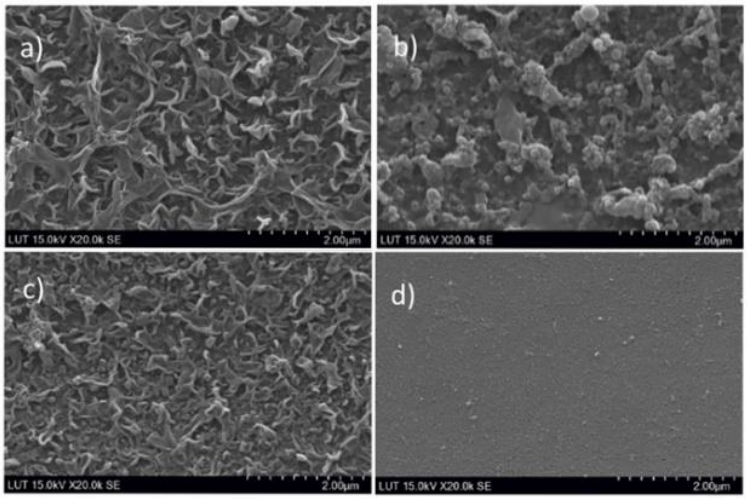

Figure 2.12. *SEM images of PA TFC RO seawater desalination membrane surface a) pristine, b) end-of-life, c) exposed to 94,250 ppm·h of NaClO solution and d) exposed to 240,500 ppm·h of NaClO solution. Adapted from [146].*

It is worth noting that most of the above mentioned recycling procedures have been reported on a laboratory scale. However, a pilot plant has been proposed for passive simultaneous recycling of six membrane modules [147]. As can be seen in Fig. 2.13, this consists of a cylindrical polypropylene container filled with the oxidizing solutions. It is equipped with low pressure pumps, valve circuits, a container to store the oxidant solutions and a container to carry out the neutralization of NaClO with sodium bisulphite in order to maintain constant the NaClO concentration.

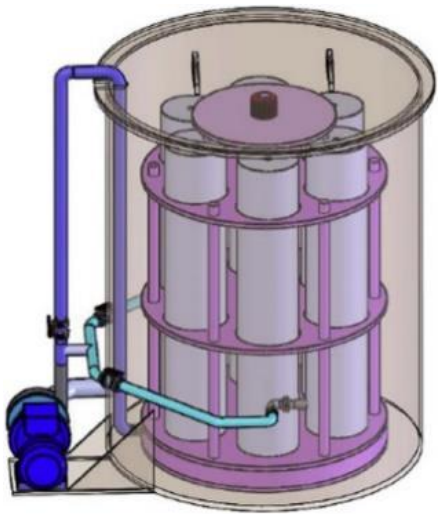

Figure 2.13. *Pilot scale used to recycle simultaneously 6 membrane modules [147].*

Headed for the industrialization and standardization of membrane module recycling, García-Pacheco *et al.* [148] developed and tested two other housing designs for recycling membrane modules. This design only replaces the endcaps (lids for feed and permeate inlet and outlet of the RO modules) adapting the recycled end-of-life RO modules to use in ultra-low-pressure gravity-driven membrane systems with acceptable results.

In addition to the chemical recycling processes mentioned above, various transformations have been adopted to the discarded RO membranes for their use in other applications. These transformations were carried out directly on the discarded membranes or after the chemical recycling process [146,149–153]. For instance, Moradi *et al.* [146] investigated the deposition of polyelectrolyte multilayers after chemical recycling using NaClO aqueous solution and could improve the performance of recycled membranes in UF separation process. With the same purpose, Rodríguez-Sáez *et al.* [149] reported on the modification of the active layer of recycled membranes by passive cleaning with NaClO dissolution and dip-coting technique using catechol and polyethyleneimine. Morrón *et al.* [150–152] used both discarded and recycled membranes treated with NaClO to grow a cyanobacterial biofilm in its active layer for use in membrane biofilms reactor process (MBfR). Lejarazu-Larrañaga *et al.* [153] used membranes recycled by passive cleaning with NaClO as a support to prepare anion exchange membranes for electrodialysis (ED) separation process.

Few reports have evaluated energy recovery as an alternative to the disposal of modules discarded in landfills [131,132]. Pontié *et al.* [132] reported the use of pyrolysis and show a reduction of 48.5% in the mass of waste and an energy recovery of 2210 kWh. These

results showed an environmental improvement with respect to landfill disposal but not with respect to reuse or recycling for the modules.

Nowadays, discarded RO membrane modules are disposed in landfills and it is necessary to propose other alternatives. It is necessary to study whether recycling, reuse or any of the proposed techniques improve current procedures environmentally and economically. Lawler *et al.* [14] presented a comparative life cycle assessment (LCA) study reporting the environmental impact produced by the different alternatives to landfill disposal of discarded RO membrane modules. It was claimed that reuse is the most environmentally friendly option. Recycling also seems a favorable option, but it is necessary to know its new useful life in order to assess it properly. The disposal of discarded membrane modules in landfills is presented as the least favorable alternative for the environment.

2.6. Applications of RO recycled membranes in other membrane processes

Taking into consideration the type of membranes commonly used in the RO process, a relatively simple conversion of the dense membrane into a porous material is possible through the degradation of the PA active layer [6]. In this way, recycled RO membranes could then be expected to comply with the characteristics, hydraulic permeabilities and separation performances comparable to commercially available filtration membranes [6]. The application of RO recycled membrane modules and membranes in filtration processes mainly refers to NF and UF technologies. The difference between these two membranes, NF or UF, lies in the PA layer degradation. For NF only a low degradation of the PA layer is necessary, thus a low exposure dose to the oxidizing agent is needed. However, for UF membranes a higher exposure dose is needed to ensure the total degradation of the PA layer [134,138–140,143,145].

Few authors have reported on the use of recycled RO membranes in MBfR, membrane distillation (MD), ED and photocatalytic membrane reactor (PMR). For these applications, RO recycled membranes require some additional transformations to adapt their characteristics to those of the new application. These are explained in detail in section 2.5.3. Table 2.2 summarizes the different alternatives reported in literature for the application of recycled RO membranes in other membrane separation processes.

Table 2.2. *Different alternatives reported for the application of recycled RO membranes in other membrane separation processes.*

RO membrane	*Oxidant agent*	*Cleaning type*	*Transformation*	*New application*	*Results*	*Reference*
-	$KMnO_4$	Peeling by oxidizing solution (1000 mg/L) at 4.4 bar (1-2 h) + Neutralization by SBS (18 h)	-	Filtration prior to RO desalination	94% suspended solids reduction (turbidity) before further RO treatment	[142]
TFC PA	NaClO	Exposure to NaClO solution of 6.25 g/L (48 h), equivalent to 300,00 ppm.h	-	UF	MWCO between 10-100 kDa. Similar protein rejection than UF commercial of PES (10 kDa)	[139,145]
TFC PA	NaClO	62,500 ppm for 3 h	-	UF	UF 10 kDa MWCO membrane was prepared	[130]
TFC PA	NaClO, acetone or NMP	124 ppm NaClO, 10,000 ppm acetone, 10,000 ppm NMP for 0.8, 20 and 92 h + NaClO 124 ppm from 1 to 410 h	-	UF and NF	NaClO was the most effective reagent. Up to 122 h of NaClO, membranes showed NF properties and from 242 h, MF properties	[141]
TFC PA	-	-	Old RO spacers of PP + low density PP to elaborate a new flat sheet membrane by IP	MD	Membrane characteristics (contact angle, porosity, thickness and roughness) were those of a typical MD membrane	[132]
TFC PA	NaClO	Passive process in pilot scale plant at different exposure doses from 6200 to 1,700,000 ppm·h	-	NF and MF	80% salt rejection factor in long term experiments with UF-like recycled membranes	[147]
TFC PA	NaClO	Exposure dose ranging from 13,000 to 240,500 ppm·h	Deposition of polyelectrolyte multilayers	NF	Mg SO_4 rejection 98.3%. The permeability and rejection greater than those values for commercial membranes	[146]
TFC PA	NaClO	Exposure dose at 6,200 and 300,000 ppm·h	-	MBfR	Chlorination process could eliminate previous incrustations and improve the binding of the desired bacteria in MBfR	[151]
TFC PA	-	-	Discarded RO membranes as a support material to biofilm layer of microcystins	MBfR	Microcystins-degrading biofilm on discarded RO membranes removed 2 $mg \cdot L^{-1}$ of microcystin in 24 h.	[150]
TFC PA	NaClO	Exposure dose at 6,200 ppm·h	Discarded RO membranes as a support material to grow natural cyanobacterial	MBfR	Microcystins removal rate of 0.021 h^{-1}	[152]

Table 2.2. (continuation) *Different alternatives reported for the application of recycled RO membranes in other membrane separation processes.*

RO membrane	*Oxidant agent*	*Cleaning type*	*Transformation*	*New application*	*Results*	*Reference*
TFC PA	NaClO	Passive immersion at ~300,000 ppm.h at room temperature	PMR composed of TiO_2 nanoparticles and UF like recycled RO membrane	PMR and MBR	60% of organic matter of the MBR permeate was discomposed in the PMR	[154]
TFC PA	NaClO	Passive process at 800,000 ppm.h	Recycled anion exchange membranes prepared by casting and phase inversion using discarded RO modules as membrane support. Use of PP components (feed spacers, end plates and compartments) as ED stacks	ED	Highly permselective (87% higher than commercial membrane). 84.5% salt rejection of membranes tested by brackish water desalination experiments in the assembled electrodialysis	[153]
TFC PA	NaClO	Passive immersion at 6,000-26,500 ppm.h for NF-like recycled membranes and 300,000 ppm.h for UF-like recycled membranes.	Housing (end caps) designs for NF and UF gravity-driven recycled membrane-based systems	NF and UF	NF-like recycled membranes: ~1.7 L $m^{-2}h^{-1}bar^{-1}$ permeability and >81% DOC rejection UF-like recycled membranes: >74% biopolymers rejection and 18-fold higher permeate rate than NF-like recycled membranes	[148]
TFC PA	NaClO	Passive process at 350,000 ppm.h	Active layer modification by dip-coating using CA and PEI	UF	Flow recovery ratio of 1.38 and a relative permeability (individual permeability over average permeability) of 1.12	[149]

CA: catechol; DOC: dissolved organic carbon; ED: electrodialysis; MBfR: membrane biofilms reactors; MBR: membrane bioreactor; MD: membrane distillation; MF: Microfiltration; MWCO: molecular weight cut-off; NF: nanofiltration; NMP: N-methyl-2-pyrrolidone; PEI: polyethyleneimine; PES: polyethersulfone; PMR: photocatalytic membrane reactor; PP: polypropylene; RO: reverse osmosis; SBS: sodium bisulphite solution; TFC PA: thin film composite polyamide; UF: Ultrafiltration.

2.6.1. RO recycled membranes in UF and MF process

The most considered applications for RO recycled membranes have been UF and MF. These applications do not require any transformation of the membranes after recycling by means of an oxidizing agent. Since the first published paper on the recycling of discarded RO membrane modules in 2002 and 2003 [142,155], some researchers proposed improvements to the recycling process in order to improve the performance of these membranes in their subsequent filtration applications. Rodriguez *et al.* [142] reported their best results for the recycling process using KMnO4 in aqueous solution at 1,000 mg / L as an oxidizing agent. In a first step, the oxidant solution was circulated at 4.4 bar during 1-2 hours, then a sodium bisulphite solution (SBS) was circulated to neutralize the oxidant solution. Later, Veza and Rodriguez-Gonzalez [155] tested recycled membrane modules for wastewater secondary effluent filtration treatment prior to RO treatment. In addition to the reduction of suspended solids by 94%, the RO unit reduced 98.5% the electrical conductivity at a 60% recovery ratio.

During the past decade (2010-2020) and due to the implementation of the waste treatment method based on circular economy, the idea of membrane recycling was recovered. Lawer *et al.* [139,145] reported similar properties of the recycled membranes to those of the commercial Pall Omega 10 kDa PES-UF membrane by using an exposure dose of 300,000 ppm.h of NaClO as an oxidizing agent to the discarded RO membranes. It was emphasized the remarkable importance of the storage conditions of the discarded RO membrane modules. The storage of the membrane modules before and after recycling in dry conditions produced an irrecoverable decrease of the permeate flux. Similarly, for the same RO membrane modules, it was observed a variable membrane performance caused by differences in fouling. Garcia-Pacheco *et al.* [156] defined a gravimetric method that allows the classification of the discarded RO membrane modules according to their fouling degree, in order to apply the most suitable recycling procedure, and thus the recycled modules could present a more homogeneous performance. Garcia-Pacheco *et al.* [141,143] made optimized studies of the adequate exposure dose in NaClO solutions as an oxidizing agent together with the adequate pH in the recycling processes. They also reported the first pilot scale plant for recycling end-of-life RO membrane modules [147]. Based on the operating data of this pilot plant, Senan *et al.* [157] reported a comparative LCA and cost-effectiveness analysis. This comparison highlighted the environmental and economic viability of recycling discarded RO membrane modules.

Recently, two research studies have been published [146,149] with the main objective to improve the filtration pefromance by transforming the recycled RO membranes using NaClO as an oxidizing solution. Moradi *et al.* [146] deposited multilayers of SC498/KE253

polyelectrolyte after the recycling process of the RO membrane. The electrolyte layers were deposited by circulation of the polyelectrolytic solution (1 g/L polyelectrolyte and 0.05 M NaCl) through the RO membrane module by fluidic assembly technique. The NF membrane composed of eight bilayers of polyelectrolytes deposited on the recycled RO membrane exhibited an improved saltwater permeability of 11 L/m^2.h.bar with maximum NaCl and $MgSO_4$ rejection factors of 92% and 98%, respectively. By applying the dip-coating technique, Rodriguez-Sáez *et al.* [149] modified recycled RO membranes (350,000 ppm·h of exposure dose) transforming it into NF membranes. The best parameters reported for the transformation of the active layer of the recycled membranes was using catechol (1 g/L) and polyethyleneimine (1 g/L) at 30ºC for 2 hours. Under these conditions a flow recovery ratio of 1.38 and a relative permeability (individual permeability over average permeability) of 1.12 were obtained.

2.6.2. RO recycled membranes in MD, MBfR and ED separation processes

In recent years, several reports have been focused on the application of recycled RO membranes in other membrane separation processes rather than filtration systems. In this case, transforming the recycled RO membranes in order to adapt their characteristics to those required by the new applications is necessary.

Morón *et al.* [150–152] reported the use of discarded and recycled RO membranes as a support material to create a biofilm layer of microcystins-degrading. In their first report [151], it was studied the feasibility of using recycled RO membranes as a support to prepare biofilm reactor membranes, and it was finally confirmed their suitability. In their second report [150], a biofilm layer of microcystins-degrading (Sphingopyxis sp. strain IM-1) was prepared on the active layer of a discarded RO membrane. These new recycled membranes, when tested for microcystin-degradation in an MBfR system, were able to remove 2 mg/L of microcystin in 24 h. In their latest report [152], both discarded and recycled RO membranes were used to generate a biofilm layer using natural cyanobacterial. In MBfR system, these membranes exhibited a removal rate of 0.021 h^{-1}.

Lejarazu-Larrañaga *et al.* [153] proposed the application of recycled RO membranes in ED process. These were used as a support material for the preparation of anion exchange membranes. The necessary transformation was performed using two combined methods: casting and PI. A mixture of anion exchange resin with a solution of polymerized polyvinylchloride in tetrahydrofuran (1: 1 (w / w)) was used. After studying the impact of various manufacturing parameters (i.e., thickness and solvent evaporation time) on the membrane performance, the membrane prepared with 800 µm thickness and 60 min solvent

evaporation time was the one that presented the best characteristics and performance (84.5% salt removal) comparable to those of commercial membranes (AMH-PES for anion exchange and CMH-PES for cation exchange from RALEX®).

For these applications, a more advanced development is still necessary to make feasible the evaluation of economic and environmental costs produced by the transformations carried out based on the performance and new useful life provided to the discarded RO membranes. In addition, developing more standardized protocols for the transformed and/or recycled membranes is necessary.

In addition to the use of recycled RO membranes in the above mentioned water remediation processes, future research trends should be focused on the direct reuse of end-of-life RO membrane modules as part of the pre-filtration step in RO desalination plants, making the process more sustainable. Furthermore, their other plastic parts of the modules should be reused for the manufacture of new RO modules. There is also an open window for new development and transformation of discarded membranes and their reutilization as supports. Current membrane recycling methodologies must be improved in terms of ecology and performance in order to open the range of use of recycled RO membranes in other water remediation processes for their implementation at an industrial level.

2.7. Conclusions

RO is the most common technology applied for desalination worldwide due to its low cost and high-water production rate compared to other available techniques. It is expected that from 2025 around two million of RO spiral-wound modules will be discarded per year due to membrane fouling and other associated problems. Based on an adequate waste management hierarchy, different strategies have been adopted during last years to revalue discarded RO membrane modules. These alternatives include reuse and recycling of RO membrane modules for their use in other membrane processes, such as NF, UF, biofilm-membrane reactors or ED. In this sense, the oxidation and removal of the polyamide (PA) layer by means of different chemicals is the most studied method to convert the dense RO membrane into a porous one. Moreover, the recycling of discarded RO membrane modules as pre-filters in RO desalination plants, the utilization of the support layer of RO membranes for new membranes development or even the use of plastic parts for other purposes have been considered. Nevertheless, these other ways are still under study.

Efforts should be focused into an intensive research along the following lines. First, in the direct reutilization of RO discarded membrane modules within the desalination plants themselves as pre-filters, contributing to a circular economy, since less waste and lower

associated costs would be generated. On the other hand, into the improving of recycling techniques and protocols, to be able to use the RO membrane modules and the recycled membranes in other membrane processes and improve the performance of the current ones to make the leap from labs to industry.

2.8. References

[1] T.F. Stocker, D. Qin, G.-K. Plattner, M. Tignor, S.K. Allen, J. Boschung, A. Nauels, Y. Xia, V. Bex, P.M. Midgley, IPCC, 2013: Climate Change 2013: The Physical Science Basis. Contribution of Working Group I to the Fifth Assessment Report of the Intergovernmental Panel on Climate Change, 2013.

[2] M. Sarja, T. Onkila, M. Mäkelä, A systematic literature review of the transition to the circular economy in business organizations: Obstacles, catalysts and ambivalences, J. Clean. Prod. 286 (2021) 125492.

[3] J.P. Schöggl, L. Stumpf, R.J. Baumgartner, The narrative of sustainability and circular economy - A longitudinal review of two decades of research, Resour. Conserv. Recycl. 163 (2020) 105073.

[4] R. García-Pacheco, W. Lawler, J. Landaburu-Aguirre, E. García-Calvo, P. Le-Clech, 4.14 End-of-Life Membranes: Challenges and Opportunities, in: E. Drioli, L. Giorno, E. Fontananova (Eds.), Compr. Membr. Sci. Eng. (Second Ed., Elsevier, Oxford, 2017: pp. 293–310.

[5] J. Landaburu-Aguirre, R. García-Pacheco, S. Molina, L. Rodríguez-Sáez, J. Rabadán, E. García-Calvo, Fouling prevention, preparing for re-use and membrane recycling. Towards circular economy in RO desalination, Desalination. 393 (2016) 16–30.

[6] W. Lawler, Z. Bradford-Hartke, M.J. Cran, M. Duke, G. Leslie, B.P. Ladewig, P. Le-Clech, Towards new opportunities for reuse, recycling and disposal of used reverse osmosis membranes, Desalination. 299 (2012) 103–112.

[7] WHO, UNICEF, Progress on Drinking Water, Sanitation and Hygiene, 2017.

[8] United Nations World Water Assessment Programme, The United Nations World Water Development Report 2020, 2020.

[9] B. Rahimi, H.T. Chua, Chapter 1 - Introduction to Desalination, in: B. Rahimi, H.T. Chua (Eds.), Low Grade Heat Driven Multi-Effect Distill. Desalin., Elsevier, Amsterdam, 2017: pp. 1–17.

[10] IDA and GWI desalData, The IDA Water Security Handbook 2019–2020, 2019.

[11] M.A.M. Khan, S. Rehman, F.A. Al-Sulaiman, A hybrid renewable energy system as a potential energy source for water desalination using reverse osmosis: A review, Renew. Sustain. Energy Rev. 97 (2018) 456–477.

[12] A. Panagopoulos, K.-J. Haralambous, Environmental impacts of desalination and brine treatment - Challenges and mitigation measures, Mar. Pollut. Bull. 161 (2020) 111773.

[13] A.H. Haidari, S.G.J.J. Heijman, W.G.J.J. van der Meer, Optimal design of spacers in reverse osmosis, Sep. Purif. Technol. 192 (2018) 441–456.

[14] W. Lawler, J. Alvarez-Gaitan, G. Leslie, P. Le-Clech, Comparative life cycle assessment of end-of-life options for reverse osmosis membranes, Desalination. 357 (2015) 45–54.

[15] M. Qasim, M. Badrelzaman, N.N. Darwish, N.A. Darwish, N. Hilal, Reverse osmosis desalination: A state-of-the-art review, Desalination. 459 (2019) 59–104.

[16] A.F. Ismail, T. Matsuura, Progress in transport theory and characterization method of Reverse Osmosis (RO) membrane in past fifty years, Desalination. 434 (2018) 2–11.

[17] L.F. Greenlee, D.F. Lawler, B.D. Freeman, B. Marrot, P. Moulin, Reverse osmosis desalination: Water sources, technology, and today's challenges, Water Res. 43 (2009) 2317–2348.

[18] L. Malaeb, G.M. Ayoub, Reverse osmosis technology for water treatment: State of the art review, Desalination. 267 (2011) 1–8.

[19] A. Ahsan, M. Imteaz, 15 - Application and Future Prospects of Reverse Osmosis Process, in: A. Ahsan, A.F.B.T.-N. in W. and W.T. Ismail (Eds.), Micro Nano Technol., Elsevier, 2019: pp. 297–301.

[20] B. Peñate, L. García-Rodríguez, Current trends and future prospects in the design of seawater reverse osmosis desalination technology, Desalination. 284 (2012) 1–8.
[21] J. Kavitha, M. Rajalakshmi, A.R. Phani, M. Padaki, Pretreatment processes for seawater reverse osmosis desalination systems—A review, J. Water Process Eng. 32 (2019) 100926.
[22] S.H. Joo, B. Tansel, Novel technologies for reverse osmosis concentrate treatment: A review, J. Environ. Manage. 150 (2015) 322–335.
[23] L. Henthorne, B. Boysen, State-of-the-art of reverse osmosis desalination pretreatment, Desalination. 356 (2015) 129–139.
[24] F.E. Ahmed, R. Hashaikeh, N. Hilal, Hybrid technologies: The future of energy efficient desalination – A review, Desalination. 495 (2020).
[25] A. Panagopoulos, K.-J. Haralambous, M. Loizidou, Desalination brine disposal methods and treatment technologies - A review, Sci. Total Environ. 693 (2019) 133545.
[26] M.O. Mavukkandy, C.M. Chabib, I. Mustafa, A. Al Ghaferi, F. AlMarzooqi, Brine management in desalination industry: From waste to resources generation, Desalination. 472 (2019) 114187.
[27] S. Lee, J. Choi, Y.G. Park, H. Shon, C.H. Ahn, S.H. Kim, Hybrid desalination processes for beneficial use of reverse osmosis brine: Current status and future prospects, Desalination. 454 (2019) 104–111.
[28] H. Nassrullah, S.F. Anis, R. Hashaikeh, N. Hilal, Energy for desalination: A state-of-the-art review, Desalination. 491 (2020) 114569.
[29] G. Kosmadakis, D. Manolakos, S. Kyritsis, G. Papadakis, Design of a two stage Organic Rankine Cycle system for reverse osmosis desalination supplied from a steady thermal source, Desalination. 250 (2010) 323–328.
[30] A.S. Nafey, M.A. Sharaf, Combined solar organic Rankine cycle with reverse osmosis desalination process: Energy, exergy, and cost evaluations, Renew. Energy. 35 (2010) 2571–2580.
[31] C.E. Reid, E.J. Breton, Water and ion flow across cellulosic membranes, J. Appl. Polym. Sci. 1 (1959) 133–143.
[32] S. Loeb, S. Sourirajah, Sea water demineralization by means of an osmotic membrane, in saline water conversion-Ⅱ: advances in chemistry series number 28, in: ACS Publications (Ed.), Saline Water Conversion-Ⅱ, Washington, DC: American Chemical Society, 1963: pp. 117–132.
[33] K.P. Lee, T.C. Arnot, D. Mattia, A review of reverse osmosis membrane materials for desalination—Development to date and future potential, J. Memb. Sci. 370 (2011) 1–22.
[34] J.W. Richter, H.H. Hoehn, Permselective, aromatic, nitrogen-containing polymeric membranes, 1971.
[35] J.E. Cadotte, Interfacially synthesized reverse osmosis membrane, (1981).
[36] G.M. Geise, H.-S. Lee, D.J. Miller, B.D. Freeman, J.E. McGrath, D.R. Paul, Water purification by membranes: The role of polymer science, J. Polym. Sci. Part B Polym. Phys. 48 (2010) 1685–1718.
[37] R.H. Hailemariam, Y.C. Woo, M.M. Damtie, B.C. Kim, K.-D. Park, J.-S. Choi, Reverse osmosis membrane fabrication and modification technologies and future trends: A review, Adv. Colloid Interface Sci. 276 (2020) 102100.
[38] S.S. Shenvi, A.M. Isloor, A.F. Ismail, A review on RO membrane technology: Developments and challenges, Desalination. 368 (2015) 10–26.
[39] T.A. Otitoju, R.A. Saari, A.L. Ahmad, Progress in the modification of reverse osmosis (RO) membranes for enhanced performance, J. Ind. Eng. Chem. 67 (2018) 52–71.
[40] Y. Okamoto, J.H. Lienhard, How RO membrane permeability and other performance factors affect process cost and energy use: A review, Desalination. 470 (2019) 114064.
[41] T. Uemura, Y. Himeshima, M. Kurihara, Interfacially synthesized reverse osmosis membrane, 1988.
[42] M. Liu, D. Wu, S. Yu, C. Gao, Influence of the polyacyl chloride structure on the reverse osmosis performance, surface properties and chlorine stability of the thin-film composite polyamide membranes, J. Memb. Sci. 326 (2009) 205–214.

[43] D.L. Zhao, S. Japip, Y. Zhang, M. Weber, C. Maletzko, T.S. Chung, Emerging thin-film nanocomposite (TFN) membranes for reverse osmosis: A review, Water Res. 173 (2020) 115557.
[44] M. Asadollahi, D. Bastani, S.A. Musavi, Enhancement of surface properties and performance of reverse osmosis membranes after surface modification: A review, Desalination. 420 (2017) 330–383.
[45] G.R. Xu, J.N. Wang, C.J. Li, Strategies for improving the performance of the polyamide thin film composite (PA-TFC) reverse osmosis (RO) membranes: Surface modifications and nanoparticles incorporations, Desalination. 328 (2013) 83–100.
[46] J. Johnson, M. Busch, Engineering Aspects of Reverse Osmosis Module Design, Desalin. Water Treat. 15 (2010) 236–248.
[47] A.J. Karabelas, M. Kostoglou, C.P. Koutsou, Modeling of spiral wound membrane desalination modules and plants - review and research priorities, Desalination. 356 (2015) 165–186.
[48] C. Fritzmann, J. Löwenberg, T. Wintgens, T. Melin, State-of-the-art of reverse osmosis desalination, Desalination. 216 (2007) 1–76.
[49] A. Matin, T. Laoui, W. Falath, M. Farooque, Fouling control in reverse osmosis for water desalination & reuse: Current practices & emerging environment-friendly technologies, Sci. Total Environ. 765 (2020) 142721.
[50] A. Matin, Z. Khan, S.M.J. Zaidi, M.C. Boyce, Biofouling in reverse osmosis membranes for seawater desalination: Phenomena and prevention, Desalination. 281 (2011) 1–16.
[51] S. Daly, A. Allen, V. Koutsos, A.J.C. Semião, Influence of organic fouling layer characteristics and osmotic backwashing conditions on cleaning efficiency of RO membranes, J. Memb. Sci. 616 (2020) 118604.
[52] S. Hong, M. Elimelech, Chemical and physical aspects of natural organic matter (NOM) fouling of nanofiltration membranes, J. Memb. Sci. 132 (1997) 159–181.
[53] Y. Zhao, L. Song, S.L. Ong, Fouling of RO membranes by effluent organic matter (EfOM): Relating major components of EfOM to their characteristic fouling behaviors, J. Memb. Sci. 349 (2010) 75–82.
[54] P.S. Goh, W.J. Lau, M.H.D. Othman, A.F. Ismail, Membrane fouling in desalination and its mitigation strategies, Desalination. 425 (2018) 130–155.
[55] Q. She, R. Wang, A.G. Fane, C.Y. Tang, Membrane fouling in osmotically driven membrane processes: A review, J. Memb. Sci. 499 (2016) 201–233.
[56] J.S. Vrouwenvelder, J.A.M. van Paassen, L.P. Wessels, A.F. van Dam, S.M. Bakker, The Membrane Fouling Simulator: A practical tool for fouling prediction and control, J. Memb. Sci. 281 (2006) 316–324.
[57] B. Andrews, B. Davé, P. López-Serrano, S.P. Tsai, R. Frank, M. Wilf, E. Koutsakos, Effective scale control for seawater RO operating with high feed water pH and temperature, Desalination. 220 (2008) 295–304.
[58] G.D. Kang, Y.M. Cao, Development of antifouling reverse osmosis membranes for water treatment: A review, Water Res. 46 (2012) 584–600.
[59] S. Jiang, Y. Li, B.P. Ladewig, A review of reverse osmosis membrane fouling and control strategies, Sci. Total Environ. 595 (2017) 567–583.
[60] A. Matin, F. Rahman, H.Z. Shafi, S.M. Zubair, Scaling of reverse osmosis membranes used in water desalination: Phenomena, impact, and control; future directions, Desalination. 455 (2019) 135–157.
[61] W. Yu, D. Song, W. Chen, H. Yang, Antiscalants in RO membrane scaling control, Water Res. 183 (2020) 115985.
[62] H.S. Kim, J.Y. Lee, S.Y. Ham, J.H. Lee, J.H. Park, H.D. Park, Effect of biofilm inhibitor on biofouling resistance in RO processes, Fuel. 253 (2019) 823–832.
[63] Y. Oh, S. Lee, M. Elimelech, S. Lee, S. Hong, Effect of hydraulic pressure and membrane orientation on water flux and reverse solute flux in pressure assisted osmosis, J. Memb. Sci. 465 (2014) 159–166.

[64] A. Jawor, E.M.V. Hoek, Effects of feed water temperature on inorganic fouling of brackish water RO membranes, Desalination. 235 (2009) 44–57.
[65] T. Tran, B. Bolto, S. Gray, M. Hoang, E. Ostarcevic, An autopsy study of a fouled reverse osmosis membrane element used in a brackish water treatment plant, Water Res. 41 (2007) 3915–3923.
[66] H.C. Flemming, Reverse osmosis membrane biofouling, Exp. Therm. Fluid Sci. 14 (1997) 382–391.
[67] P. Aimar, P. Bacchin, Slow colloidal aggregation and membrane fouling, J. Memb. Sci. 360 (2010) 70–76.
[68] S. Gutiérrez Ruiz, J.A. López-Ramírez, M. Hassani Zerrouk, A. Egea-Corbacho Lopera, J.M. Quiroga Alonso, Study of reverse osmosis membranes fouling by inorganic salts and colloidal particles during seawater desalination, Chinese J. Chem. Eng. 28 (2020) 733–742.
[69] C.Y. Tang, T.H. Chong, A.G. Fane, Colloidal interactions and fouling of NF and RO membranes: A review, Adv. Colloid Interface Sci. 164 (2011) 126–143.
[70] E.M. Vrijenhoek, H. Seungkwan, E. Menachem, Influence of membrane surface properties on initial rate of colloidal fouling of reverse osmosis and nanofiltration membranes, in: J. Memb. Sci., ACS Division of Environmental Chemistry, 2001: pp. 281–283.
[71] Y. Ju, S. Hong, Nano-colloidal fouling mechanisms in seawater reverse osmosis process evaluated by cake resistance simulator-modified fouling index nanofiltration, Desalination. 343 (2014) 88–96.
[72] M. Laqbaqbi, J.A. Sanmartino, M. Khayet, C. García-Payo, M. Chaouch, Fouling in membrane distillation, osmotic distillation and osmotic membrane distillation, Appl. Sci. 7 (2017) 334.
[73] C.Y. Tang, Y.N. Kwon, J.O. Leckie, Fouling of reverse osmosis and nanofiltration membranes by humic acid-Effects of solution composition and hydrodynamic conditions, J. Memb. Sci. 290 (2007) 86–94.
[74] H.J. Lee, J. Seo, M.S. Kim, C. Lee, Inactivation of biofilms on RO membranes by copper ion in combination with norspermidine, Desalination. 424 (2017) 95–101.
[75] H. Flemming, G. Schaule, T. Griebe, J. Schmitt, A. Tamachkiarowa, Biofouling the Achilles heel of membrane processes, Desalination. 113 (1997) 215–225.
[76] W. Ma, Y. Zhao, L. Wang, The pretreatment with enhanced coagulation and a UF membrane for seawater desalination with reverse osmosis, Desalination. 203 (2007) 256–259.
[77] S.T. Mitrouli, S.G. Yiantsios, A.J. Karabelas, M. Mitrakas, M. Follesdal, P.A. Kjolseth, Pretreatment for desalination of seawater from an open intake by dual-media filtration: Pilot testing and comparison of two different media, Desalination. 222 (2008) 24–37.
[78] J.P. van der Hoek, J.A.M.H. Hofman, P.A.C. Bonné, M.M. Nederlof, H.S. Vrouwenvelder, RO treatment: selection of a pretreatment scheme based on fouling characteristics and operating conditions based on environmental impact, Desalination. 127 (2000) 89–101.
[79] A. Maartens, P. Swart, E.P. Jacobs, Feed-water pretreatment: methods to reduce membrane fouling by natural organic matter, J. Memb. Sci. 163 (1999) 51–62.
[80] H. Huang, H. Cho, K. Schwab, J.G. Jacangelo, Effects of feedwater pretreatment on the removal of organic microconstituents by a low fouling reverse osmosis membrane, Desalination. 281 (2011) 446–454.
[81] J.N. Apell, T.H. Boyer, Combined ion exchange treatment for removal of dissolved organic matter and hardness, Water Res. 44 (2010) 2419–2430.
[82] C.M. Kim, S.J. Kim, L.H. Kim, M.S. Shin, H.W. Yu, I.S. Kim, Effects of phosphate limitation in feed water on biofouling in forward osmosis (FO) process, Desalination. 349 (2014) 51–59.
[83] E. Lyster, M. man Kim, J. Au, Y. Cohen, A method for evaluating antiscalant retardation of crystal nucleation and growth on RO membranes, J. Memb. Sci. 364 (2010) 122–131.
[84] A. Sweity, Z. Ronen, M. Herzberg, Induced organic fouling with antiscalants in seawater desalination, Desalination. 352 (2014) 158–165.
[85] J.M.Y. Chiu, V. Thiyagarajan, M.M.Y. Tsoi, P.Y. Qian, Qualitative and quantitative changes in marine biofilms as a function of temperature and salinity in summer and winter, Biofilms. 2 (2005) 183–195.

[86] S.R. Toleti, Comparative effect of temperature on biofilm formation in natural and modified marine environment, Aquat. Ecol. 44 (2010) 463–478.
[87] Q. She, X. Jin, Q. Li, C.Y. Tang, Relating reverse and forward solute diffusion to membrane fouling in osmotically driven membrane processes, Water Res. 46 (2012) 2478–2486.
[88] Y.N. Wang, C.Y. Tang, Protein fouling of nanofiltration, reverse osmosis, and ultrafiltration membranes-The role of hydrodynamic conditions, solution chemistry, and membrane properties, J. Memb. Sci. 376 (2011) 275–282
[89] M. Xie, J. Lee, L.D. Nghiem, M. Elimelech, Role of pressure in organic fouling in forward osmosis and reverse osmosis, J. Memb. Sci. 493 (2015) 748–754.
[90] S. Mattaraj, W. Phimpha, P. Hongthong, R. Jiraratananon, Effect of operating conditions and solution chemistry on model parameters in crossflow reverse osmosis of natural organic matter, Desalination. 253 (2010) 38–45.
[91] A.I. Radu, J.S. Vrouwenvelder, M.C.M. van Loosdrecht, C. Picioreanu, Effect of flow velocity, substrate concentration and hydraulic cleaning on biofouling of reverse osmosis feed channels, Chem. Eng. J. 188 (2012) 30–39.
[92] Y. Wang, Z. Wang, X. Han, J. Wang, S. Wang, Improved flux and anti-biofouling performances of reverse osmosis membrane via surface layer-by-layer assembly, J. Memb. Sci. 539 (2017) 403–411.
[93] A. Nguyen, S. Azari, L. Zou, Coating zwitterionic amino acid l-DOPA to increase fouling resistance of forward osmosis membrane, Desalination. 312 (2013) 82–87.
[94] H.Y. Yu, Y. Kang, Y. Liu, B. Mi, Grafting polyzwitterions onto polyamide by click chemistry and nucleophilic substitution on nitrogen: A novel approach to enhance membrane fouling resistance, J. Memb. Sci. 449 (2014) 50–57.
[95] L. Zou, I. Vidalis, D. Steele, A. Michelmore, S.P. Low, J.Q.J.C. Verberk, Surface hydrophilic modification of RO membranes by plasma polymerization for low organic fouling, J. Memb. Sci. 369 (2011) 420–428.
[96] T.H. Lee, M.Y. Lee, H.D. Lee, J.S. Roh, H.W. Kim, H.B. Park, Highly porous carbon nanotube/polysulfone nanocomposite supports for high-flux polyamide reverse osmosis membranes, J. Memb. Sci. 539 (2017) 441–450.
[97] M. Ghanbari, D. Emadzadeh, W.J. Lau, T. Matsuura, A.F. Ismail, Synthesis and characterization of novel thin film nanocomposite reverse osmosis membranes with improved organic fouling properties for water desalination, RSC Adv. 5 (2015) 21268–21276.
[98] A. Nguyen, L. Zou, C. Priest, Evaluating the antifouling effects of silver nanoparticles regenerated by TiO2 on forward osmosis membrane, J. Memb. Sci. 454 (2014) 264–271.
[99] X. Liu, S. Qi, Y. Li, L. Yang, B. Cao, C.Y. Tang, Synthesis and characterization of novel antibacterial silver nanocomposite nanofiltration and forward osmosis membranes based on layer-by-layer assembly, Water Res. 47 (2013) 3081–3092.
[100] S.G. Kim, J.H. Chun, B.H. Chun, S.H. Kim, Preparation, characterization and performance of poly(aylene ether sulfone)/modified silica nanocomposite reverse osmosis membrane for seawater desalination, Desalination. 325 (2013) 76–83.
[101] R. Valladares Linares, S.S. Bucs, Z. Li, M. AbuGhdeeb, G. Amy, J.S. Vrouwenvelder, Impact of spacer thickness on biofouling in forward osmosis, Water Res. 57 (2014) 223–233.
[102] V.A. Haaksman, A. Siddiqui, C. Schellenberg, J. Kidwell, J.S. Vrouwenvelder, C. Picioreanu, Characterization of feed channel spacer performance using geometries obtained by X-ray computed tomography, J. Memb. Sci. 522 (2017) 124–139.
[103] P.A. Araújo, J.C. Kruithof, M.C.M. Van Loosdrecht, J.S. Vrouwenvelder, The potential of standard and modified feed spacers for biofouling control, J. Memb. Sci. 403–404 (2012) 58–70.
[104] H. Mo, H.Y. Ng, An experimental study on the effect of spacer on concentration polarization in a long channel reverse osmosis membrane cell., Water Sci. Technol. a J. Int. Assoc. Water Pollut. Res. 61 (2010) 2035–2041.

[105] S.R. Suwarno, X. Chen, T.H. Chong, V.L. Puspitasari, D. McDougald, Y. Cohen, S.A. Rice, A.G. Fane, The impact of flux and spacers on biofilm development on reverse osmosis membranes, J. Memb. Sci. 405–406 (2012) 219–232.
[106] P.R. Neal, H. Li, A.. Fane, D.. Wiley, The effect of filament orientation on critical flux and particle deposition in spacer-filled channels, J. Memb. Sci. 214 (2003) 165–178.
[107] S. Muñoz, R. Frank, I. Pilar, C. Pérez, F.X. Simón, Life+ Remembrane: End-of-life recovery of reverse osmosis, FuturEnviro. (2014) 1–5.
[108] S.S. Madaeni, S. Samieirad, Chemical cleaning of reverse osmosis membrane fouled by wastewater, Desalination. 257 (2010) 80–86.
[109] B. Mi, Menachem Elimelech, Organic fouling of forward osmosis membranes: Fouling reversibility and cleaning without chemical reagents, J. Memb. Sci. 348 (2010) 337–345.
[110] Z. Wang, J. Ma, C. Tang, K. Kimura, Q. Wang, X. Han, Membrane Cleaning in Membrane Bioreactors : A Review, J. Memb. Sci. 468 (2014) 276–307.
[111] A. Maartens, P. Swart, E.P. Jacobs, An enzymatic approach to the cleaning of ultrafiltration membranes fouled in abattoir effluent, J. Memb. Sci. 119 (1996) 9–16.
[112] M.A. Argüello, S. Álvarez, F.A. Riera, R. Álvarez, Utilization of enzimatic detergents to clean inorganic membranes fouled by whey proteins, Sep. Purif. Technol. 41 (2005) 147–154.
[113] E. Bar-Zeev, M. Elimelech, Reverse Osmosis Biofilm Dispersal by Osmotic Back-Flushing: Cleaning via Substratum Perforation, Environ. Sci. Technol. Lett. 1 (2014) 162–166.
[114] G.Z. Ramon, T.V. Nguyen, E.M.V. Hoek, Osmosis-assisted cleaning of organic-fouled seawater RO membranes, Chem. Eng. J. 218 (2013) 173–182.
[115] S. Lee, M. Elimelech, Salt cleaning of organic-fouled reverse osmosis membranes, Water Res. 41 (2007) 1134–1142.
[116] C. Whittaker, H. Ridgway, B. Olson, Evaluation of Cleaning Strategies for Removal of Biofilms from Reverse-Osmosis Membranes, Appl. Environ. Microbiol. 48 (1984) 395–403.
[117] S.M. Ibrahim, H. Nagasawa, M. Kanezashi, T. Tsuru, Chemical-free cleaning of fouled reverse osmosis (RO) membranes derived from bis(triethoxysilyl) ethane (BTESE), J. Memb. Sci. 601 (2020) 117919.
[118] M. Khan, S. Danielsen, K. Johansen, L. Lorenz, S. Nelson, A. Camper, Enzymatic cleaning of biofouled thin-film composite reverse osmosis (RO) membrane operated in a biofilm membrane reactor, Biofouling. 30 (2013) 153–167.
[119] A. Sagiv, R. Semiat, Backwash of RO spiral wound membranes, Desalination. 179 (2005) 1–9.
[120] D. Feng, J.S.J. van Deventer, C. Aldrich, Ultrasonic defouling of reverse osmosis membranes used to treat wastewater effluents, Sep. Purif. Technol. 50 (2006) 318–323.
[121] F.H. Butt, F. Rahman, U. Baduruthamal, Identification of scale deposits through membrane autopsy, Desalination. 101 (1995) 219–230.
[122] R.P. Carnahan, L. Bolin, W. Suratt, Biofouling of PVD-1 reverse osmosis elements in the water treatment plant of the City of Dunedin, Florida, Desalination. 102 (1995) 235–244.
[123] L.Y. Dudley, E.G. Darton, Membrane autopsy — a case study, Desalination. 105 (1996) 135–141.
[124] F.H. Butt, F. Rahman, U. Baduruthamal, Characterization of foulants by autopsy of RO desalination membranes, Desalination. 114 (1997) 51–64.
[125] L. Dudley, Membrane autopsies for reversing fouling in reverse osmosis, Membr. Technol. 1998 (1998) 9–12.
[126] J.S. Vrouwenvelder, D. Van Der Kooij, Diagnosis, prediction and prevention of biofouling of NF and RO membranes, Desalination. 139 (2001) 65–71.
[127] M. Karime, S. Bouguecha, B. Hamrouni, RO membrane autopsy of Zarzis brackish water desalination plant, Desalination. 220 (2008) 258–266.
[128] M. Pontié, S. Rapenne, A. Thekkedath, J. Duchesne, V. Jacquemet, J. Leparc, H. Suty, Tools for membrane autopsies and antifouling strategies in seawater feeds: A review, Desalination. 181 (2005) 75–90.

[129] E. Ould Mohamedou, D.B. Penate Suarez, F. Vince, P. Jaouen, M. Pontie, New lives for old reverse osmosis (RO) membranes, Desalination. 253 (2010) 62–70.
[130] M. Pontié, Old RO membranes: solutions for reuse, Desalin. Water Treat. 53 (2015) 1492–1498.
[131] C. Prince, M. Cran, P. Le-Clech, K. Uwe-Hoehn, M. Duke, Reuse and recycling of used desalination membranes, Proc. OzWater. 11 (2011) 1–8.
[132] M. Pontié, S. Awad, M. Tazerout, O. Chaouachi, B. Chaouachi, Recycling and energy recovery solutions of end-of-life reverse osmosis (RO) membrane materials: A sustainable approach, Desalination. 423 (2017) 30–40.
[133] L. Fortunato, A.H. Alshahri, A.S.F. Farinha, I. Zakzouk, S. Jeong, T.O. Leiknes, Fouling investigation of a full-scale seawater reverse osmosis desalination (SWRO) plant on the Red Sea: Membrane autopsy and pretreatment efficiency, Desalination. 496 (2020) 114536.
[134] S. Molina, J. Landaburu-Aguirre, L. Rodríguez-Sáez, R. García-Pacheco, J.G. de la Campa, E. García-Calvo, Effect of sodium hypochlorite exposure on polysulfone recycled UF membranes and their surface characterization, Polym. Degrad. Stab. 150 (2018) 46–56.
[135] G.D. Kang, C.J. Gao, W.D. Chen, X.M. Jie, Y.M. Cao, Q. Yuan, Study on hypochlorite degradation of aromatic polyamide reverse osmosis membrane, J. Memb. Sci. 300 (2007) 165–171.
[136] S.T. Mitrouli, A.J. Karabelas, N.P. Isaias, Polyamide active layers of low pressure RO membranes: Data on spatial performance non-uniformity and degradation by hypochlorite solutions, Desalination. 260 (2010) 91–100.
[137] E. Coutinho de Paula, M.C. Santos Amaral, Environmental and economic evaluation of end-of-life reverse osmosis membranes recycling by means of chemical conversion, J. Clean. Prod. 194 (2018) 85–93.
[138] M.K. Da Silva, A. Ambrosi, G.M. Dos Ramos, I.C. Tessaro, Rejuvenating polyamide reverse osmosis membranes by tannic acid treatment, Sep. Purif. Technol. 100 (2012) 1–8.
[139] W. Lawler, T. Wijaya, A. Antony, G. Leslie, P. Le-Clech, Reuse of reverse osmosis desalination membranes, in: IDA World Congr., Perth Convention and Exhibition Centre Perth, Western Australia, 2011.
[140] A. Ambrosi, I.C. Tessaro, Study on Potassium Permanganate Chemical Treatment of Discarded Reverse Osmosis Membranes Aiming their Reuse, Sep. Sci. Technol. 48 (2013) 1537–1543.
[141] R. García-Pacheco, J. Landaburu-Aguirre, S. Molina, L. Rodríguez-Sáez, S.B. Teli, E. García-Calvo, Transformation of end-of-life RO membranes into NF and UF membranes: Evaluation of membrane performance, J. Memb. Sci. 495 (2015) 305–315.
[142] J.J. Rodríguez, V. Jiménez, O. Trujillo, J. Veza, Reuse of reverse osmosis membranes in advanced wastewater treatment, Desalination. 150 (2002) 219–225.
[143] R. García-Pacheco, J. Landaburu-Aguirre, A. Lejarazu-Larrañaga, L. Rodríguez-Sáez, S. Molina, T. Ransome, E. García-Calvo, Free chlorine exposure dose (ppm·h) and its impact on RO membranes ageing and recycling potential, Desalination. 457 (2019) 133–143.
[144] H.D. Raval, V.R. Chauhan, A.H. Raval, S. Mishra, Rejuvenation of discarded RO membrane for new applications, Desalin. Water Treat. 48 (2012) 349–359.
[145] W. Lawler, A. Antony, M. Cran, M. Duke, G. Leslie, P. Le-Clech, Production and characterisation of UF membranes by chemical conversion of used RO membranes, J. Memb. Sci. 447 (2013) 203–211.
[146] M.R. Moradi, A. Pihlajamäki, M. Hesampour, J. Ahlgren, M. Mänttäri, End-of-life RO membranes recycling: Reuse as NF membranes by polyelectrolyte layer-by-layer deposition, J. Memb. Sci. 584 (2019) 300–308.
[147] R. García-Pacheco, J. Landaburu-Aguirre, P. Terrero-Rodríguez, E. Campos, F. Molina-Serrano, J. Rabadán, D. Zarzo, E. García-Calvo, Validation of recycled membranes for treating brackish water at pilot scale, Desalination. 433 (2018) 199–208.
[148] R. García-Pacheco, Q. Li, J. Comas, R.A. Taylor, P. Le-Clech, Novel housing designs for nanofiltration and ultrafiltration gravity-driven recycled membrane-based systems, Sci. Total Environ. 767 (2021) 144181.

[149] L. Rodríguez-Sáez, J. Landaburu-Aguirre, S. Molina, C. García-Payo, E. García-Calvo, Study of surface modification of recycled ultrafiltration membranes using statistical design of experiments, Surfaces and Interfaces. (2021) 100978.
[150] J. Morón-López, L. Nieto-Reyes, J. Senán-Salinas, S. Molina, R. El-Shehawy, Recycled desalination membranes as a support material for biofilm development: A new approach for microcystin removal during water treatment, Sci. Total Environ. 647 (2019) 785–793.
[151] J. Morón-López, L. Nieto-Reyes, S. Aguado, R. El-Shehawy, S. Molina, Recycling of end-of-life reverse osmosis membranes for membrane biofilms reactors (MBfRs). Effect of chlorination on the membrane surface and gas permeability, Chemosphere. 231 (2019) 103–112.
[152] J. Morón-López, L. Nieto-Reyes, S. Molina, M.Á. Lezcano, Exploring microcystin-degrading bacteria thriving on recycled membranes during a cyanobacterial bloom, Sci. Total Environ. 736 (2020) 139672.
[153] A. Lejarazu-Larrañaga, S. Molina, J.M. Ortiz, R. Navarro, E. García-Calvo, Circular economy in membrane technology: Using end-of-life reverse osmosis modules for preparation of recycled anion exchange membranes and validation in electrodialysis, J. Memb. Sci. 593 (2020) 117423.
[154] C.P.M. de Oliveira, M.M. Viana, G.R. Silva, L.S. Frade Lima, E. Coutinho de Paula, M.C.S. Amaral, Potential use of green TiO2 and recycled membrane in a photocatalytic membrane reactor for oil refinery wastewater polishing, J. Clean. Prod. 257 (2020) 120526.
[155] J.M. Veza, J.J. Rodriguez-Gonzalez, Second use for old reverse osmosis membranes: wastewater treatment, Desalination. 157 (2003) 65–72.
[156] F.J.R. R. García-Pacheco, P. Terrero, S. Molina Martínez, D. Martínez, E. Campos, R. García-Pacheco, J. Rabadán, P. Terrero, S. Molina Martínez, D. Martínez, E. Campos, F. Molina, L. Rodríguez-Sáez, A. Ortíz de Lejarazu, J. Landaburu-Aguirre, D. Zarzo, E. García-Calvo, Life+13 transfomem: a recycling example within the desalination world, XI AEDYR Int. Congr. VAL-112-16 (2016) VAL-112-16.
[157] J. Senán-Salinas, R. García-Pacheco, J. Landaburu-Aguirre, E. García-Calvo, Recycling of end-of-life reverse osmosis membranes: Comparative LCA and cost-effectiveness analysis at pilot scale, Resour. Conserv. Recycl. 150 (2019) 104423.

Chapter 3

High Flux Thin Film Composite PIM-1 Membranes for Butanol Recovery: Experimental Study and Process Simulation

Thin film composite (TFC) membranes of the prototypical polymer of intrinsic microporosity (PIM-1) have been prepared by dip coating on a highly porous electrospun polyvinylidene fluoride (PVDF) nanofibrous support. Prior to coating, the support was impregnated in a non-solvent to avoid the penetration of PIM-1 inside the PVDF network. Different non-solvents were considered and the results were compared with those of the dry support. When applied for the separation of n-butanol/water mixtures by pervaporation (PV), the developed membranes exhibited very high permeate fluxes, in the range of 16.1-35.4 kg m^{-2} h^{-1}, with an acceptable n-butanol/water separation factor of about 8. The PV separation index (PSI) of the prepared membranes is around 115, which is among the highest PSI values that have been reported so far. Hybrid PV-distillation systems have been designed and modelled in Aspen HYSYS using Aspen Custom Modeler for setting up the PIM-1 TFC and commercial PDMS membranes as a benchmark. The butanol recovery cost for the hybrid systems is compared with a conventional standalone distillation process used for n-butanol/water separation and a 10% reduction in recovery cost was obtained.

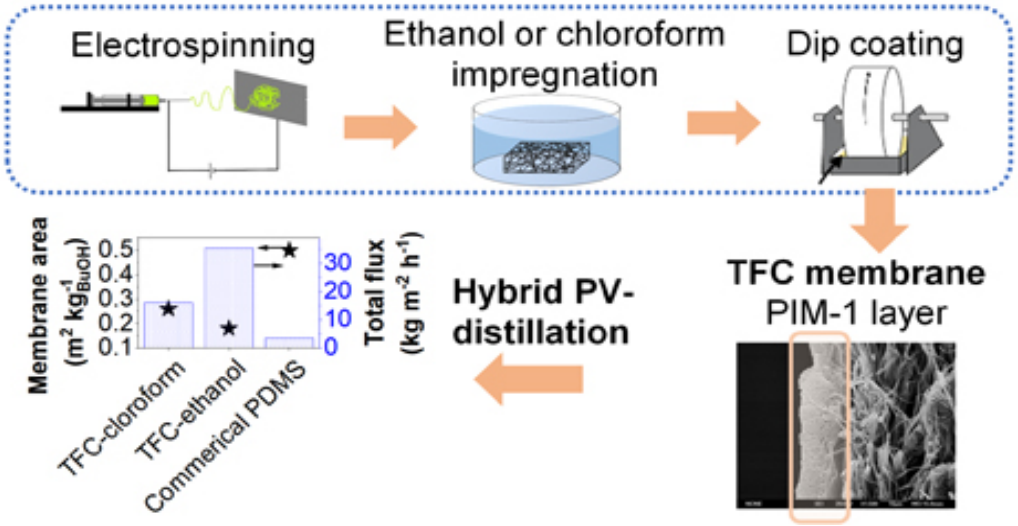

3.1. Introduction

In recent decades, there has been a lot of effort to mitigate greenhouse gas emissions in the sectors with high fossil fuel consumption, including transportation and electricity. In 2017, the transport and electricity sectors were responsible for 55% of greenhouse gas emissions. While electricity can be produced using renewable energy sources such as water, wind and solar energy, liquid fuel is still necessary [1]. In addition, the availability of agricultural based biomass makes biofuels, such as biodiesel and bioalcohols (biomethanol, bioethanol, and biobutanol), an interesting alternative to fossil fuels [2-4] Methanol (MeOH) is usually employed in biodiesel production because it is less expensive compared to other alcohols. However, biobutanol (n-butanol, BuOH) is less toxic and easy to handle compared to MeOH. Moreover, compared to bioethanol, BuOH is less corrosive, has lower Reid vapor pressure, and higher blending ratio with gasoline and energy density [5]. Therefore, it is a promising candidate to replace fossil fuels. It has been reported that using pure n-butanol or its blend with diesel can improve the fuel-air mixing and reduce NO_x, CO_2, and soot emissions in diesel engines [6, 7]. The physical properties of biofuels and gasoline are summarized in Table 3.1 [8, 9].

***Table 3.1**. Physical properties of gasoline, diesel, and biofuels.*

Parameter	Gasoline	Diesel	Methanol	Ethanol	n-Butanol
Energy density (MJ L^{-1})	32	45.5	16	19.6	29.2
Auto-ignition temperature (°C)	246-280	220-260	470	422	343-345
Air-fuel ratio	9	14.5	6.5	14.6	11.2
Boiling point (°C)	27-221	64	64.7	78	117
Heat of vaporization (MJ kg^{-1})	0.36	1.2	1.2	0.92	0.43
Research octane number	91-99	20-30	136	129	96
Motor octane number	81-89	20-30	104	102	78

It is worth noting that biobutanol can be produced by the acetone-butanol-ethanol (ABE) fermentation process at an average mass ratio of 3:6:1 [10]. However, low yields of n-butanol in the fermenter tank, and high costs in product recovery are the main drawbacks

towards the widespread commercial implementation of the process [11]. It has been reported that a butanol concentration above 13 g/L in the fermentation broth leads to product inhibition; however research in the optimization of lignocellulosic biomass pretreatment processes to reduce the formation of microbial inhibitors, the use of inhibitor tolerant strain(s) or the continuous recovering of butanol using membranes may allow higher butanol yields [12]. Various separation techniques have been investigated so far for product recovery, including gas stripping [13], liquid-liquid extraction [14], pervaporation (PV), distillation or combinations of them [15]. Among these separation techniques, PV is an energy-efficient membrane process with a high potential to separate water-alcohol mixtures. PV can be used for the dehydration of solvents (i.e. hydrophilic PV) [16-18] or the recovery of organics from aqueous solutions (i.e. hydrophobic PV) as well as for the separation of mixtures of organic solvents. PV can be integrated into the n-butanol production system to recover n-butanol at the end of the fermentation process [9, 19, 20]. However, high purity n-butanol cannot be produced by a stand-alone PV unit. Matsumura et al. [21] reported the possibility of energy saving of a PV-distillation hybrid system for n-butanol/water separation using an oleyl alcohol liquid membrane. Wyk et al. [22], by simulating a PV-distillation process in Aspen HYSYS, showed the feasibility of the hybrid system to reduce the energy consumption of n-butanol purification compared to the conventional distillation column. However, the performance of the PV unit in a large-scale simulation was considered the same as the one obtained in the experimental results, and the effect of feed temperature reduction due to the permeate evaporation was not considered in the simulation.

Investigations on alcohol purification by the PV process have been carried out using hydrophobic freestanding and thin film composite (TFC) membranes, including polydimethylsiloxane (PDMS) [22, 23], poly[1-(trimethylsilyl)−1-propyne] (PTMSP) [24], polyether block amide (PEBA) [25], polytetrafluoroethylene (PTFE) [26], polyvinylidene fluoride (PVDF) [27], and PIM-1 [28]. A comprehensive study on alcohol selective PV membranes was presented by Zao and Jin [29] and it was concluded that there was a need to find advanced membrane materials and tailor specific membrane structures to make the process more competitive.

PIM-1 is a glassy polymer with an intrinsic microporosity and high free volume that shows good selectivity towards organophilic components, and higher permeate flux than other more conventional glassy polymers. In PV and other pressure-driven membrane processes, the transmembrane permeate flux is inversely related to the membrane thickness, and therefore in order to reduce the required membrane area for a given separation process thin film composite (TFC) membranes must be produced. PIM-1 TFC membranes have been prepared on macroporous supports [30] and poly(vinylidene fluoride) (PVDF) supports

produced by phase inverstion [31, 32] for PV applications. Polyacrylonitrile (PAN) [33, 34], Ultem 1000 [35], and cross-linked P84 polyimide [36], support membranes have been also used as supports for PIM-1 layers in organic solvent separations.

In the present study, TFC membranes have been designed by coating PIM-1 on a PVDF electrospun support for n-butanol recovery from water by PV. PVDF has been selected for the preparation of the supports because of its hydrophobic character, good thermal and chemical stability. Electrospinning has been used for the preparation of the nanofibrous PVDF supports rather than phase inversion technique, in order to produce substrates with a high void volume fraction (i.e. high porosity) [37], that can reduce mass transfer resistance during permeation of butanol in the PV process. In order to avoid penetration of PIM-1 (more likely due to the high porosity of the support) during membrane formation via dip-coating, different non-solvents have been used to impregnate the PVDF electrospun support prior coating, and the effect on the n-butanol recovery from aqueous solutions via PV has been investigated. Moreover, hybrid PV-distillation systems and the conventional stand-alone distillation processes have been simulated in Aspen HYSYS (V8.8) to allow comparisons of the energy demand of n-butanol purification in both processes.

3.2. Experimental

3.2.1. Materials

Polyvinylidene fluoride (PVDF, M_w=275 kg/mol), tetrafluoroterephthalonitrile (TFTPN), and 1-4 dioxane (≥99.8%) were supplied from Sigma Aldrich (UK). 5,5',6,6'-tetrahydroxy3,3,3',3'-tetramethyl-1,1'-spirobisindane (TTSBI) was purchased from Alfa Aesar (UK). N,N-dimethyl acetamide (DMAc, synthesis grade) was provided from Merck. Potassium carbonate (K_2CO_3), toluene (synthesis grade), isopropyl alcohol (IPA), chloroform, acetone, n-butanol (BuOH used for PV experiments), ethanol (EtOH), and methanol (MeOH) were purchased from Fisher Chemical. Deionized water used for PV experiments was produced by a Milli-Q integral system (Merck Millipore, Ireland).

3.2.2. Synthesis and characterization of PIM-1

The PIM-1 synthesis was carried out following the steps reported by Ameen et al. [38]. First, TFTPN (4 g), TTSBI (7.02 g), and K_2CO_3 (8.28 g) were left under agitation to react in the solvent mixture containing anhydrous DMAc (40 mL) and toluene (20 mL). The mixture was heated from room temperature to 140 °C under N_2 atmosphere. After 25 min reaction, a highly viscous solution with yellow color was obtained. The solution was precipitated in MeOH

and left overnight. The formed solid was recovered by vacuum filtration, dissolved in chloroform and subsequently precipitated in MeOH again. The precipitate was recovered and soaked in deionized water for 16 h. Then the polymer was filtered and washed with 1-4-dioxane and acetone. Finally, it was washed with MeOH three times and dried at 20 °C under vacuum for 48 h.

The average molecular weight (M_w) of the synthesized PIM-1 was determined by gel permeation chromatography (GPC) as described in our previous work 32 and the obtained value was 45,561 g mol^{-1} with a polydispersity (M_w/M_n) of 1.7.

3.2.3. Preparation of electrospun nanofibrous PVDF support

The PVDF nanofibrous membrane support was fabricated by electrospinning using a dope solution containing 25 wt.% PVDF, 15 wt.% acetone and 60 wt.% DMAc, according to the research study reported by Essalhi and Khayet [39]. The mixture was stirred for 24 h at 50 °C prior to electrospinning using the set-up presented in Fig. 3.1. The flow rate of the dope solution (Fig. 3.1 (c)) was set at 1.23 mL h^{-1} using an electric pump (KD Scientific 200P Two-Syringe Infusion Pump (USA), Fig. 3.1 (b)). The internal diameter of the stainless-steel needle (Fig. 3.1 (d)) was 0.6 mm. The electric voltage was set at 20 kV and the distance between the tip of the metallic needle and the collector (i.e. air gap horizontal length) (Fig. 3.1 (e)) was 19.5 cm. The electrospinning jet moved from the needle (higher potential) towards the stainless-steel collector (lower potential) for 70 min. The prepared nanofibrous membrane support was finally dried in an oven at 80 °C for 30 min. The SEM image of the top surface of the electrospun nanofibrous support is shown in Fig. 3.1 (f).

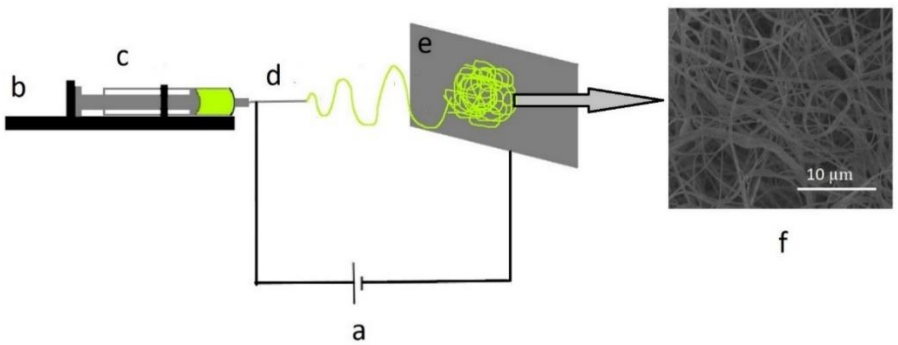

Figure 3.1. *Schematic of the electrospinning set-up: a) high electric voltage source, b) pump for circulation of the polymer solution, c) syringe holding the polymer dope solution, d) stainless steel needle, e) stainless steel collector, and f) top surface SEM image of the prepared PVDF membrane support.*

3.2.4. Preparation of PIM-1 TFC membranes

TFC membranes were prepared via dip-coating of the PVDF supports with a 4 wt% PIM-1 solution (in choroform), for 2 s at room temperature. In order to avoid excessive penetration of the polymer solution into the support, during the dip-coating process the support was first impregnated in a non-solvent of PVDF for 2 s. The time lag between support impregnation and the dip-coating was reduced as much as possible to minimize evaporation. Three non-solvents were tested: chloroform, MeOH and EtOH, and the TFC membranes prepared with each of these non-solvent-impregnated supports were denoted as TFC-C, TFC-M, and TFC-E, respectively. For comparison, a TFC membrane was also prepared using a non-impregnated PVDF support (TFC-N).

3.2.5. Characterization of PVDF nanofibrous support and TFC membranes

A Quanta FEG650 scanning electron microscope (SEM, USA) was used to study the morphological structure of the surfaces and cross-sections of the prepared PVDF nanofibrous support and the TFC membranes. Previously, the samples were coated with a 6-8 nm layer of platinum using an MTM 10 Thickness Monitor (Cressington, USA). An open source image analysis software (UTHSCSA Image Tool) was used to measure the nanofiber diameters of the electrospun PVDF support. In conjunction with SEM images, energy dispersive X-ray spectroscopy maps (EDX) were collected using AZtec 3.3 SP1 software to analyze the interface between PIM-1 and the support layer. The thicknesses (l) of the support and the TFC membranes were measured by a digital micrometer having an accuracy of ±1 µm (Helios-Preisser Instruments 1724-502 series (Germany)). For each TFC membrane, the thickness measurement was carried out at twenty different points and the average value was reported together with its standard deviation. To prevent the deformation of the sample under the micrometer pressure, a thick (1 mm) plastic film was used for thickness measurements. The hydrophobic character of both PVDF nanofibrous support and the TFC membranes was studied by water contact angle (CA) measurement at room temperature. An Optical Contact Angle Meter CAM 100 was used to capture the water drop images and then CAM 200-software ver. 3.992 KSV Instruments (USA) was employed to calculate the CA. Twenty images were analyzed for each sample and the average values were reported together with their standard deviation.

Liquid entry pressure of distillate water (LEP_W) is defined as the minimum transmembrane pressure that is applied on distilled water before its penetration into the membrane pores. It depends on both the hydrophobicity and the maximum pore size of the membrane. 40 LEP_W was measured for the PVDF support according to the method described

by Smolders and Franken [41] and the obtained value is given in section 8.1 in the Appendix A.

The porosity or void volume fraction (ε) of the PVDF nanofibrous support was determined using a pycnometer and two liquids of different surface tensions, distilled water and IPA. In this method, the hydrophobic PVDF support is submerged in water and IPA. The former liquid does not wet the support pores whereas and the latter one penetrates into its pores. The densities of the support (ρ_m) and the polymer material (ρ_{pol}) were calculated according to the following equations [41].

$$\rho_{\mathrm{m}} = \frac{\rho_{\mathrm{W}} * w_{\mathrm{DM}}}{w_{\mathrm{P+W}} + w_{\mathrm{DM}} - w_{\mathrm{P+W+M}}} \tag{3.1}$$

$$\rho_{\mathrm{pol}} = \frac{\rho_{\mathrm{IPA}} * w_{\mathrm{DM}}}{w_{\mathrm{P+I}} + w_{\mathrm{DM}} - w_{\mathrm{P+I+M}}} \tag{3.2}$$

where w_{DM} and w_{P+W} are the weight of the dry support and the pycnometer with water, respectively; while w_{P+W+M} is the weight of the pycnometer with water and support. ρ_W and ρ_{IPA} are the densities of water (0.99 g cm^{-3}) and IPA (7.86 g cm^{-3}) at 20 ºC. w_{P+I} and w_{P+I+M} are the weight of the pycnometer with IPA and the weight of the pycnometer with IPA and the support, respectively. Once the densities of the support and the polymeric material were determined, Equation (3.3) was used to determine the porosity (%) [41].

$$\varepsilon = \left(1 - \frac{\rho_{\mathrm{m}}}{\rho_{\mathrm{pol}}}\right) * 100 \tag{3.3}$$

3.2.6. Pervaporation (PV)

PV was carried out in a set-up described in more detail elsewhere [42]. An aqueous solution containing 5 wt.% of n-butanol at 65 °C was used as feed for all the PV experiments for ease of comparison with our previous studies [31, 32, 42]. A vacuum pressure of the membrane permeate side, 10 mbar, was applied using a vacuum pump (vacuumbrand^{TM} MD 4 NT VARIO diaphragm pump), as it has been reported that vacuum pressures below10 mbar is unlikely to be achievable on the industrial scale [43]. The effective membrane area was 2.54 cm^2. To allow the system to attain a steady state condition, the permeate was collected 30 min after starting the experiment. The permeate was collected using two liquid nitrogen traps. The total permeate flux (J_T, kg m^{-2} h^{-1}) was determined using Equation (3.4):

$$J_{\mathrm{T}} = \frac{m}{A\,t} \tag{3.4}$$

where m (kg) is the mass of the collected permeate, A (m^2) is the effective membrane area and t (h) is the permeate collection time.

Water mass fraction in the collected permeate ($x_{w,perm}$) was determined using an 899 Coulometer titration system (Metrohm, Switzerland). The n-butanol permeate flux (J_{BuOH}, kg m^{-2} h^{-1}) and n-butanol/water separation factor ($\beta_{BuOH/w}$) were calculated as follows:

$$J_{\mathrm{BuOH}} = x_{\mathrm{BuOH,perm}} \cdot J_{\mathrm{T}} \tag{3.5}$$

$$\beta_{\mathrm{BuOH/w}} = \frac{(x_{\mathrm{BuOH,perm}}/x_{\mathrm{w,perm}})}{(x_{\mathrm{BuOH,feed}}/x_{\mathrm{w,feed}})} \tag{3.6}$$

where, $x_{BuOH,perm}$ and $x_{w,perm}$ are the mass fractions of n-butanol and water in the collected permeate, respectively; and $x_{BuOH,feed}$ and $x_{w,feed}$ are the initial mass fractions of n-butanol and water in the feed, respectively.

PV separation index (*PSI*) is a relative measure of the separation ability of a given membrane. It can be used as a guideline for designing the PV system and for selecting the optimum combination of flux and separation factor [44]. PSI was calculated as follows:

$$PSI = J_{\mathrm{T}} \cdot \left(\beta_{\mathrm{BuOH/w}} - 1\right) \tag{3.7}$$

3.3. Simulation studies

3.3.1. Pervaporation membrane separation process

The PV process simulation was carried out using Aspen HYSYS (V8.8). Aspen Custom Modeler (ACM) (V8.8) was used to model a PV membrane in cross-flow mode and no pressure drop in the feed and the permeate sides. The membrane was discretized into n cells according to Fig. 3.2. Each cell was assumed to be at steady state, with one inlet (i.e. the feed) and two outlets (i.e. the retentate and the permeate).

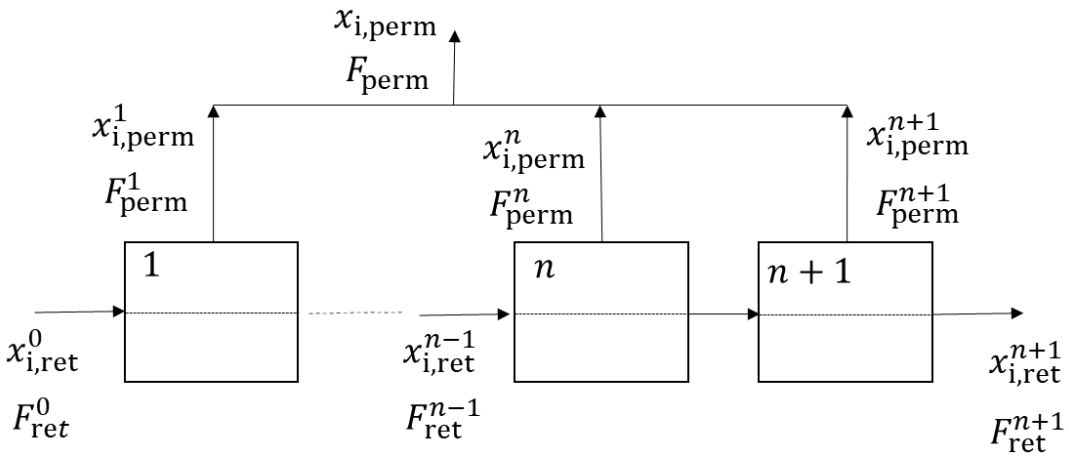

Figure 3.2. *Schematic of the discretized PV membrane.*

In Fig. 3.2, *n* is the cell number and its initial value (*n*=0) refers to the feed stream. For all cells *n* > 1, the feed was the retentate of the previous cell (*n*-1). The permeate streams of all cells were combined in one outlet stream considered as the outlet permeate of the membrane. $x^{n}_{i,\mathrm{ret}}$ and $x^{n}_{i,\mathrm{perm}}$ are the mass fractions of component i, in the retentate (liquid phase) and the permeate (vapor phase) streams for the cell number *n*. F^{n}_{perm} and F^{n}_{ret} are the mass flow rates (kg h^{-1}) of the permeate and the retentate of the cell number *n*, respectively. F_{perm} and $x_{\mathrm{i,perm}}$ are the permeate mass flow rate and mass fraction of component *i* of the permeate after mixing all the permeate streams of all cells. Equations (3.8) and (3.9) were set for each cell to obtain the transmembrane flow rate of the involved components.

$$F^{n}_{\mathrm{perm}} . x^{n}_{\mathrm{i,perm}} = A_{\mathrm{cell}} . J^{n}_{\mathrm{i}} \tag{3.8}$$

$$\sum_{\mathrm{i=1}}^{\mathrm{No.of\ components}} x^{n}_{\mathrm{i,perm}} = 1 \tag{3.9}$$

where, A_{cell} is the cell area (m^2), and J^{n}_{i} (kg m^{-2} h^{-1}) is the transmembrane permeate flux of component i of the cell number *n*. In a large-scale simulation, both the composition and temperature of the feed stream change for each cell due to the permeate evaporation and consequently the transmembrane permeate flux (J_{i}) is not constant for each cell. Generally, the temperature dependence of the PV permeate flux follows an Arrhenius type of dependence (Equation (3.10)) [45].

$$J_{\mathrm{i,1}} = J_{\mathrm{i,2}} \exp\left[\frac{-E_{\mathrm{i}}}{R}\left(\frac{1}{T_2} - \frac{1}{T_1}\right)\right] \tag{3.10}$$

where $J_{i,1}$ and $J_{i,2}$ are the transmembrane permeate fluxes of component i at the temperature T_1 (K) and T_2 (K), which are the inlet and the outlet temperature of each cell, respectively. E is the activation energy (kJ mol^{-1}) of component i and R is the gas constant (0.008314 kJ mol^{-1} K^{-1}. The activation energies of n-butanol and water obtained in a previous study are 70.6 and 34.5 kJ mol^{-1}, respectively [32]. The permeate fluxes of the components for the first cell were taken the same as the experimental results and then changed according to Equation (3.10) for the following cells. It was assumed that the permeate fluxes were independent of the variation of the concentration along the membrane since the experimental permeate fluxes in the batch PV system were obtained as an average from the final permeate mass measurement. Only the change of the feed concentration was considered. For instance, it has been reported that n-butanol mass fraction in the retentate changed from 5 wt.% to 4.5 wt.% for PIM-1 TFC membrane after 1 h of PV operation [31].

To obtain the composition and mass flow rates of the retentate and permeate streams in each cell, general and components mass balances were set around each cell according to Equations (3.11) and (3.12), respectively.

$$F_{\mathrm{ret}}^{n-1} = F_{\mathrm{perm}}^{n} + F_{\mathrm{ret}}^{n} \tag{3.11}$$

$$F_{\mathrm{ret}}^{n-1}.\, x_{\mathrm{i,ret}}^{n-1} = x_{\mathrm{i,perm}}^{n}.\, F_{\mathrm{perm}}^{n} + x_{\mathrm{i,ret}}^{n}.\, F_{\mathrm{ret}}^{n} \tag{3.12}$$

The flow rate and composition of the final permeate stream (after mixing), were obtained according to Equations (3.13) and (3.14).

$$F_{\mathrm{perm}} = \sum_{n=1}^{\mathrm{No.of\ cells}} F_{\mathrm{perm}}^{n} \tag{3.13}$$

$$F_{\mathrm{perm}}.\, x_{\mathrm{i,perm}} = \sum_{n=1}^{\mathrm{No.of\ cells}} F_{\mathrm{perm}}^{n}.\, x_{\mathrm{i,perm}}^{n} \tag{3.14}$$

An energy balance was established around each cell by means of Equation (3.15). Moreover, it was considered that the temperatures of the permeate and retentate streams are equal for each cell (Equation (3.16)) because of the low evaporation rate in each cell.

$$F_{\mathrm{perm}}^{n}.\left(H_{\mathrm{perm}}^{n} - H_{\mathrm{ret}}^{n-1}\right) = C_{\mathrm{Pl,ret}}^{n-1}.\, F_{\mathrm{ret}}^{n-1}.\, T_{\mathrm{ret}}^{n-1} - C_{\mathrm{Pl,ret}}^{n}.\, F_{\mathrm{ret}}^{n}.\, T_{\mathrm{ret}}^{n} \tag{3.15}$$

$$T^{n}_{\text{perm}}=T^{n}_{\text{ret}} \tag{3.16}$$

where, $C^{n-1}_{\text{Pl,ret}}$ and $C^{n}_{\text{Pl,ret}}$ (kJ kg^{-1} K^{-1}) are the heat capacities of the feed and retentate (i.e. liquid phase) for the cell number *n*; and $H^{n}_{\text{perm}}$and H^{n-1}_{ret} (kJ kg^{-1}) are the specific enthalpies of the permeate and retentate for each cell. The heat capacities and the specific enthalpies were calculated by Aspen Properties using property procedures in ACM based on NRTL thermodynamic model. The temperature of the final permeate stream (after mixing) was calculated by Richman mixing rule [46].

$$T_{\text{perm}}=\frac{\sum_{n=1}^{\text{No.of cells}} F^{n}_{\text{perm}}.C^{n}_{\text{Pv,perm}}.T^{n}_{\text{perm}}}{\sum_{n=1}^{\text{No.of cells}} F^{n}_{\text{perm}}.C^{n}_{\text{Pv,perm}}} \tag{3.17}$$

$C^{n}_{\text{Pv,perm}}$ and T^{n}_{perm} are the heat capacity and temperature of the permeate (i.e. vapor phase) for the cell number *n*. The equations (3.8-3.17) were solved simultaneously to calculate the temperature, composition and mass flow rates of the final permeate and retentate streams of the membrane.

3.3.2. Distillation process

A distillation process for n-butanol recovery from n-butanol/water mixtures was simulated in Aspen HYSYS (v8.8) using an NRTL thermodynamic model. This model can accurately predict the vapor-liquid equilibrium data for the n-butanol/water mixture. According to the vapor-liquid phase diagram at *P*=1 bar Fig. 3.3), obtained from Aspen Properties (V8.8), n-butanol/water forms an azeotropic mixture at a n-butanol mass fraction of 0.57. If the mass fraction of n-butanol in the distillation column feed is higher than 0.57, the bottom product can be pure n-butanol (*T*=117.4 °C) and the overhead product can be at an azeotrope composition and temperature. In contrast, for an n-butanol mass fraction lower than 0.57 the bottom product is pure water (*T*=99.6 °C) and the overhead product is at the azeotrope condition. The liquid-liquid equilibrium data were obtained from [47] (Fig. 3.3). When the concentration of n-butanol in the feed is between n-butanol lean-phase and n-butanol-rich phase, it means the solution is in the two-phase region.

Matsumura et al. [21] calculated the energy demand of n-butanol purification using one decanter (to separate the liquid-liquid mixture) and two distillation columns. It was found that the n-butanol energy recovery decreased by increasing n-butanol concentration in the feed stream. For instance, this energy at the feed concentration of 40 wt.% n-butanol was

3.2 MJ $\mathrm{kg}_{\mathrm{BuOH}}^{-1}$, which was one twenty-fifth of separation energy for a feed solution containing 0.5 wt.% n-butanol (79.5 MJ $\mathrm{kg}_{\mathrm{BuOH}}^{-1}$) [21, 48]. In order to make the separation more energy efficient at low concentrations of n-butanol, a water-stripper column was used before the decanter [49]. In the present study, the distillation process has been simulated using a decanter, two water columns, and one n-butanol column according to Fig. 3.4. The columns were simulated as a distillation column with a reboiler and a condenser. The decanter was simulated as a three-phase separator in which the vapor phase flow rate is zero. The feed with a flow rate 250 kg h^{-1} and temperature 40 °C was introduced in the first water column (30 stages, 1 bar) to remove water. The overhead product was fed to the decanter. The feed is separated into n-butanol phase (lighter liquid, x_{BuOH} > 0.57) and the aqueous phase (heavier liquid, x_{BuOH} < 0.57) that were then introduced to n-butanol and water columns (10 stages, 1 bar), respectively. The reflux ratio of the columns was set to 0.1. A heat exchanger (HE) was used before the first water column to recover the heat of the bottom product. The feed temperature increased from 40 °C to 90 °C (Fig. 3.4). The energy demand for n-butanol recovery was calculated by summing the reboiler and condenser energies.

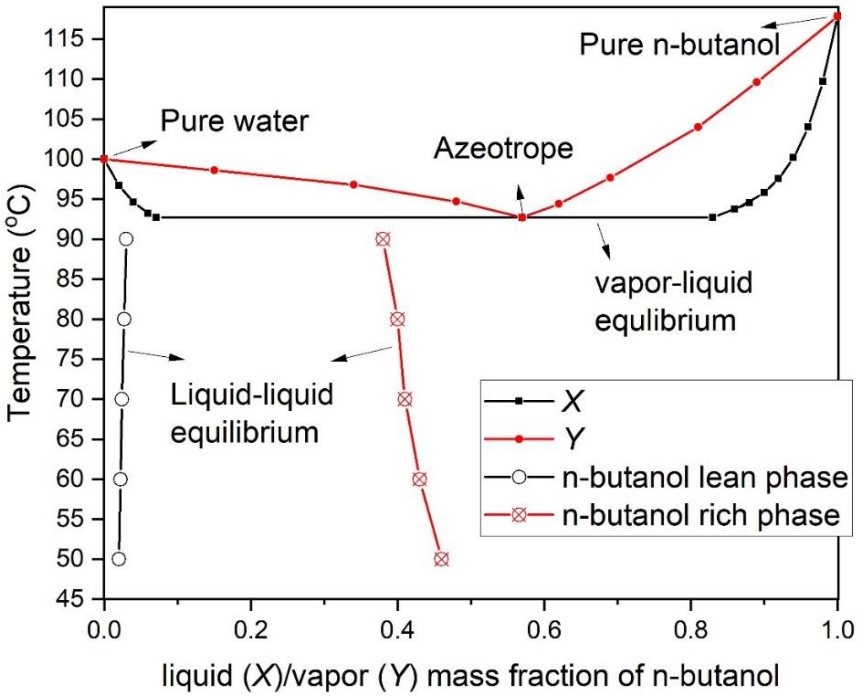

Figure 3.3. *Phase diagram of n-butanol-water at a pressure of 1 bar.*

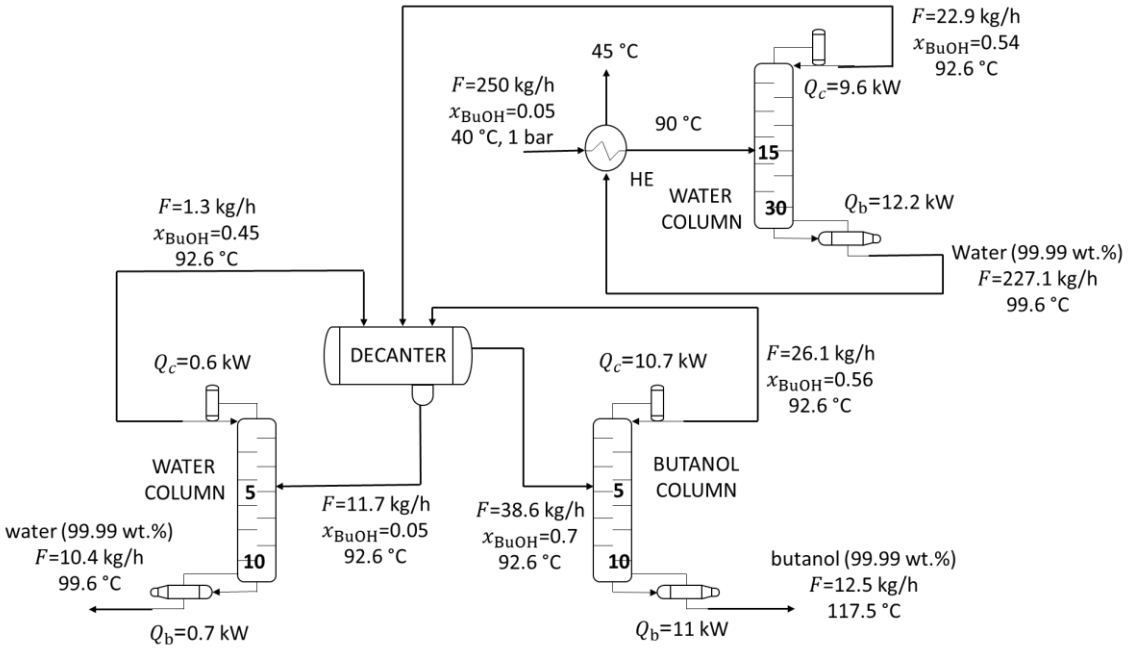

Figure 3.4. *Schematic of a conventional distillation column for n-butanol/water separation (n-butanol: BuOH).*

3.3.3. PV-distillation hybrid system

As mentioned in the previous section, the energy required for the purification of n-butanol in a conventional distillation process decreases as the n-butanol concentration in the feed increases. Thus, the use of a membrane PV unit has been investigated to increase the n-butanol mass fraction that goes into the distillation system. A schematic of the proposed hybrid system is shown in Fig. 3.5. The PV membrane separation has been simulated in Aspen HYSYS as a component splitter column using the results (composition, mass flow rates, and temperatures of permeate and retentate streams) obtained from the previously explained Aspen Custom Modeler (ACM) in section 3.3.1. The feed temperature decreases along the membrane due to the heat required for feed evaporation (permeate), which causes a reduction of the permeate flux of the two components, n-butanol and water. Therefore, two PV units with a heater in between them have been used to control the feed temperature.

The feed and permeate pressures used in the simulations were 1 and 0.01 bar, respectively. The vacuum pump energy, *W*, was calculated in J mol^{-1} according to Equation (3.18) [21].

$$W = \frac{RT_1}{k-1}\left[1 - \frac{P_2^{\frac{k-1}{k}}}{P_1}\right] \tag{3.18}$$

where, P_1 is the inlet pressure (0.01 bar), P_2 is the outlet pressure (1 bar), $k = 1.3$ is the isentropic coefficient, T_1 is the vacuum pump working temperature (temperature of permeate stream), and R (8.314 J mol^{-1} K^{-1}) is the gas constant. It is assumed that 98% of the permeate is condensed and the residual should be removed by the vacuum pump [48]. The presence of non-condensable gases leads to high vacuum pump costs and it should be considered in the economic assessment. To consider this parameter we need an estimation of the molar flow rate of non-condensable gases in the permeate gas. It is reported 3.95 mol of CO_2 and 3.41 mol H_2 are generated per mole of butanol in the fermentation tank. However, most of them are removed by the fermentation tank exhaust line [50]. In this study, the feed flow rate is considered 250 kg h^{-1} which contains 5 wt.% (0.168 kmol h^{-1}) butanol. Therefore the mole flow rate of CO_2 and H_2 in the fermentation tank is 0.67 kmol h^{-1} and 0.4 kmol h^{-1}. It is assumed 10 % of the non-condensable gases (0.107 kmol h^{-1}) pass through the membrane and need to be removed by the vacuum pump. It should be noted that the non-condensable gases have not been considered in the simulation and just the effect on the vacuum pump energy is studied. The pump shown in Fig. 3.5 is the centrifuge pump to increase the pressure of condensate from 0.01 to 1 bar. The vacuum pump is not shown in Fig. 3.5. The feed flow rate and temperature are the same as in the conventional distillation process, 250 kg h^{-1} and 40 °C, respectively. The inlet temperature of the PV units was set at 65 °C (same as the temperature of the PV experiment). As shown in Fig. 3.5, the retentate could be recycled back to the fermenter tank after passing through a heat recovery system to increase the temperature of the feed (HE-2). The permeate streams from both PV units were mixed (Mix-1) and then condensed at 5.4 °C. The condensate pressure was increased to 1 bar because the distillation columns operating pressure is 1 bar and the upstream pressure cannot be lower than the downstream pressure. It should be mentioned that no pressure drop was considered in the simulation. Similar to the conventional distillation column, the pressurized liquid flowed to a decanter and then separated into two phases. Both distillation columns (10 stages, 1 bar) were simulated as a reboiler absorber column (without condenser). The bottom products of the columns were water and n-butanol (99.99 wt.%). After condensation, the overhead products (i.e. vapor phase) were recycled to the decanter, and the heat of condensation was recovered to increase the feed temperature of the PV membrane (HE-1).

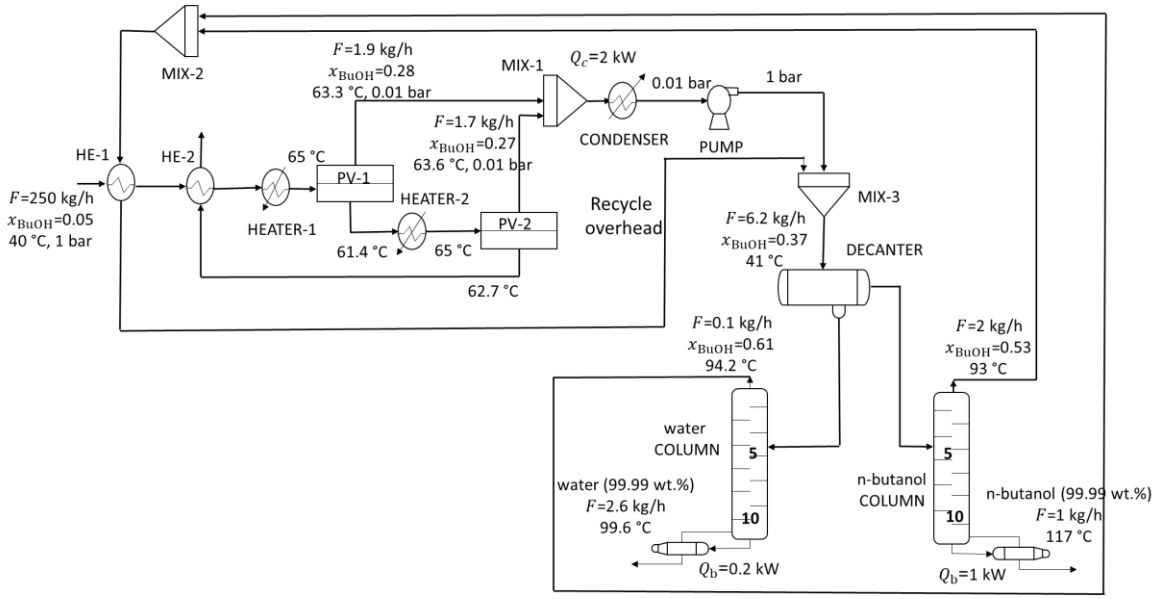

Figure 3.5. *Schematic of the PV (TFC-C)-distillation process for the removal of n-butanol from an n-butanol/water mixture (n-butanol: BuOH).*

3.4. Results and discussion

3.4.1. Membrane characterization

The morphology of the electrospun PVDF support was studied by SEM. As seen in Fig. 8.1 a in the Appendix A the top surface micrograph reveals a bead-free nanofibrous mesh. The nanofiber size distribution is shown in Fig. 8.1 b.

The void volume fraction of the electrospun PVDF supports was found to be 87 ± 1 %, which is close to the value reported in a previous study by Essalhi and Khayet [39], and much higher than that of PVDF porous supports commonly prepared by the conventional phase inversion technique (i.e. for these membranes the porosity varies from 52 % [51, 52] to 75% [53] depending on the preparation conditions, including nonsolvent bath temperature, humidity and polymer concentration).

The water CA values and thicknesses of the prepared TFC membranes and the PVDF support are summarized in Table 3.2. The high water CA value of the electrospun PVDF support (130 ± 4˚) indicates its highly hydrophobic character and the obtained water CA value is in accordance with others reported for nanofibrous PVDF membranes (128˚, 143˚, 140˚ and 139˚) [39, 54]. The higher water CA values of TFC-M and TFC-E can be justified by the presence of some cracks and pinholes (shown later on the SEM top surface images), which make the surface of these TFC membranes heterogeneous. According to Cassie's law [55], the water CA of the heterogeneous TFC membrane is higher than the homogenous PIM-1 membrane because the PVDF support has higher water CA. The previously reported water CA values of a

free standing PIM-1 membrane and a TFC membrane prepared on a phase inversion PVDF support were 87.8° and 92°, respectively [32, 42], which are close to those of TFC-M and TFC-E membranes prepared in this study.

Table 3.2. *Thickness (l) and water CA of the TFC membranes and PVDF nanofibrous support.*

	TFC-N[a]	TFC-C[b]	TFC-M[c]	TFC-E[d]	PVDF support
l (µm)	119 ± 10	120 ± 13	118 ± 11	118 ± 10	115 ± 9
CA (°)	80.7 ± 0.7	75.5 ± 0.5	92.4 ± 0.7	91.1 ± 0.3	130 ± 4

[a] Non-impregnated support
[b] Chloroform-impregnated support
[c] MeOH-impregnated support
[d] EtOH-impregnated support

The average thickness of the prepared PVDF supports was 115 ± 9 µm. The TFC-N and TFC-C membranes were slightly thicker than TFC-M and TFC-E ones. It seems that penetration of the coating solution into the PVDF support could increase the thickness of the TFC membranes due to the PVDF support swelling effect. However, the detected difference is small if the standard deviations are taken into consideration. The obtained high standard deviations are attributed mainly to the high roughness of the nanofiber PVDF support. The estimated PIM-1 layer thickness was found to be in the range of 3-5 µm. A lower concentration of PIM-1 in the coating solutions (2 wt% in chloroform) was used, as well as shorter coating times in order to reduce the thickness of the PIM-1 layer, but it did not lead to a stable and homogenous film.

The PIM-1 dope solution penetrates the PVDF support because of its high porosity and open inter-fiber space. This was confirmed by digital images (20x magnification) of both the top and bottom sides of the prepared TFC membranes are shown in Fig. 3.6. The backside of the TFC-N and TFC-C had yellow color, which demonstrated that the PIM-1 solution penetrated the support. The penetration in TFC-C was less than in TFC-N, as some parts of this last membrane was free of PIM-1 solution. This may be due partly to the fact that the PVDF support was previously impregnated with chloroform. On the contrary, the bottom side of two TFC membranes, TFC-M and TFC-E, maintained the typical color of the electrospun PVDF nanofibers, indicating the absence of PIM-1 solution. This is due to the fact that the PVDF support was impregnated with MeOH or EtOH for 2 s prior to PIM-1 coating, hindering the penetration of the PIM-1 solution inside the inter-fiber space of the PVDF support. It can be stated that the penetration of PIM-1 solution inside the inter-fiber space of the PVDF

support could decrease the thickness of the coated PIM-1 layer and in some cases induces the formation of defects on the PIM-1 top layer [34].

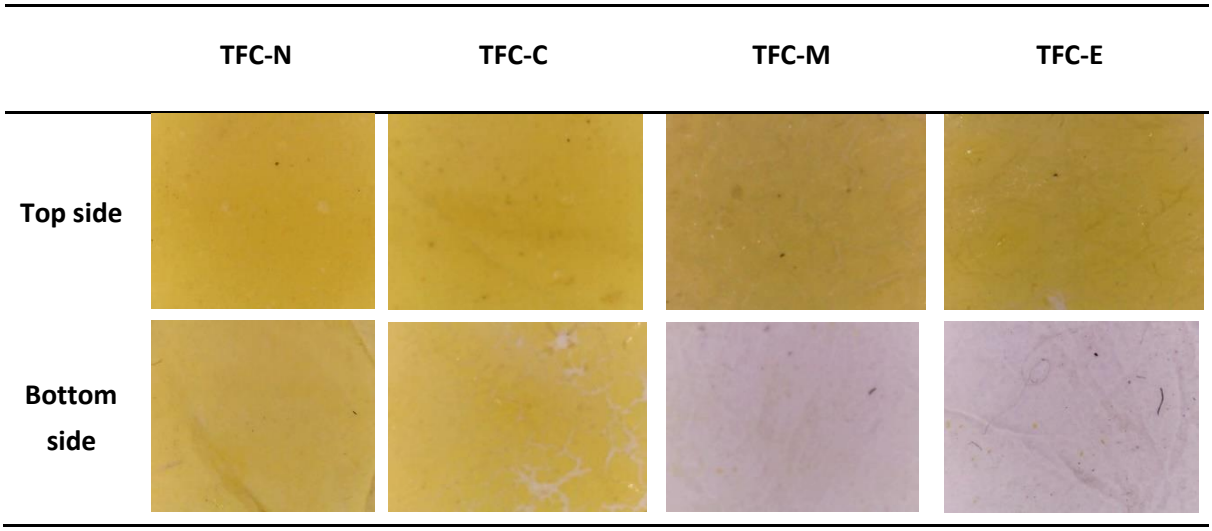

Figure 3.6. *Digital images (20x magnification) of the top and bottom sides of the prepared TFC membranes. The supports used in the fabrication of TFCs were non-impregnated in solvent (TFC-N), chloroform-impregnated (TFC-C), MeOH-impregnated (TFC-M), and EtOH-impregnated (TFC-E).*

The cross-section SEM and surface SEM images of the TFC membranes are presented in Fig. 3.7. The SEM images of the TFC-M and TFC-E (Fig. 3.7 (c) and (d)) membranes clearly show an interface between the support and the formed PIM-1 top layer without penetration of PIM-1 solution into the support inter-fiber space. However, as can be seen in Fig. 3.7 (a) and (b), for the TFC-N and TFC-C membranes such an interface is not evident and the PIM-1 layer thickness cannot be measured from their cross-section SEM images. These results agree with the structure reported for PIM-1 TFC membranes by Li et al. [34], where the infiltration of PIM-1 solution into the surface pores improved the attachment of the PIM-1 layer to the support, decreasing its thickness and resulting in the creation of possible defects.

The thickness of the PIM-1 layers in the membranes TFC-M and TFC-E is ~10 µm, which is higher than the thickness measured by the digital micrometer (Table 3.2). Electrospun supports are soft films and they can deform under the pressure of the digital micrometer, so a 1 mm thick plastic film was used to minimize this deformation. On the other hand, thickness measurements from SEM images are not always representative of the whole sample due to the difficulty to break it perpendicularly to its surface and to the small scale of cross-section SEM images, which does not represent the whole membrane and also, the difficulty in distinguishing the PIM-1 layer from the support [56]. It is worth noting that the cross-section structure of TFC-C membrane is different from the other prepared membranes due to the presence of chloroform in the support which is a solvent for PIM-1.

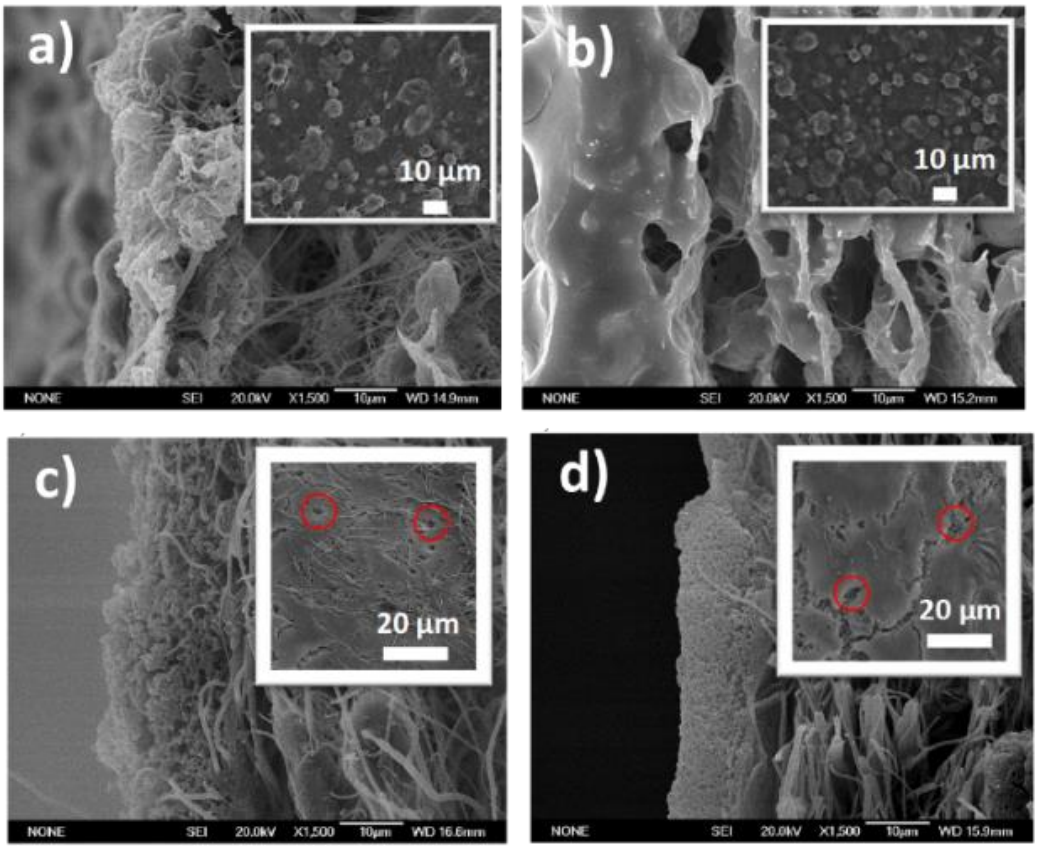

Figure 3.7. *Cross section SEM images of a) TFC-N, b) TFC-C, c) TFC-M, and d) TFC-E membranes (Insets show SEM images of the top surface of TFC membranes).*

To achieve a high PV performance, the thin top layer must be free of defects. However, cracks and small pinholes were observed on the surface of TFC-E and TFC-M membranes (see red circles in SEM images in Figure 3.7 (c) and (d)). The presence of small pinholes has been previously reported on thin PIMs layers prepared on ultrafiltration polymeric supports due to the fast evaporation of the solvent during dip coating [35]. Cook et al. [35] studied the influence of MeOH (1 wt.%) or EtOH (1 wt.%) as a co-solvent of chloroform on the morphology of PIM-1 membrane fabricated on PAN and crosslinked Ultem 1000. For both chloroform/MeOH and chloroform/EtOH solvents, pinholes appeared on the top surface of TFC membranes. This was attributed to the formation of minimum boiling point azeotropes and increasing evaporation rate of chloroform/MeOH and chloroform/EtOH mixtures. The vapor-liquid equilibrium data of chloroform/EtOH and chloroform/MeOH mixtures are shown in Fig. 8.2 of the Appendix A. At 1 wt.% of each mixture, compared to chloroform solvent, the boiling point of chloroform/MeOH and chloroform/EtOH solvent mixtures decreases 1.5 °C and 5 °C, respectively.

In our study, the PIM-1 coating solution was prepared by dissolving PIM-1 in chloroform only, and either MeOH or EtOH was used to fill the inter-fiber space of the PVDF

nanofibrous support, therefore chloroform/MeOH and chloroform/EtOH are not totally mixed and it is complicated to predict if they form an azeotropic solution at the interface. The interaction between two solvents may be related to their Hansen solubility parameters (HSP) (Table 8.1 of the Appendix A). The HSP value of chloroform is closer to that of EtOH and therefore, chloroform has more affinity to EtOH. In addition, PIM-1 has stronger interaction with EtOH than with MeOH [34, 35]. In order to study the behavior of the PIM-1 solution when in contact with the alcohols used to impregnate the support, 5 µl MeOH or EtOH were added to a 2 mL PIM-1 solution (4 wt.% polymer/chloroform). This was done without stirring to simulate the dip coating process, and in both cases, local precipitation of PIM-1 was observed in the point where the non-solvent was added. In TFC-M and TFC-E membranes, chloroform can diffuse into both MeOH and EtOH and vice versa. This induces instant solidification of PIM-1 facilitating the formation of small pinholes and cracks during TFC-M and TFC-E preparation. Larger cracks were observed on the TFC-E membrane surface (Figure 3.7 (d)), due to the higher affinity of EtOH with both PIM-1 and chloroform, which results in a higher permeate flux in PV (Table 3.3). Another mechanism of pinhole formation may be the uneffective support of the PIM-1 layer due to large size of the surface pores in the electrospun support mesh.

Nevertheless, the water/butanol feed during PV can swell the PIM-1 film and close the micro-pores and heal small defects, as it was reported by Bruggen et al. [57] for commercial membranes, with deswelling of the membranes in dry conditions leading to cracks. The surface SEM images of the prepared membranes before and after the PV test (when the membrane is dry) are shown in Fig. 8.3 of the Appendix A, showing some evidence of the reduction in size of small cracks and pores. Furthermore, it should be noted that TFC-E and TFC-M were fragile and special care had to be taken when placing them in the PV system.

Energy-dispersive X-ray spectroscopy (EDX) was carried out and mappings of carbon (C), oxygen (O) and fluorine (F) elements are depicted in the Appendix A in Fig. 8.4 and 8.5 of the Appendix A for TFC-N and TFC-E, respectively. The mapping was performed in cross-sections of the membranes of about 20 µm high starting at the top surface of the TFC membrane where the selective PIM-1 layer should have been formed. O and F atoms where selected as relevant elements in the TFC structure as O atom belongs only to PIM-1, whereas F atom is only present in PVDF. For the TFC-E membrane (i.e. ethanol-impregnated support), Fig. 8.5 of the Appendix A shows high intensities of O and F atoms at both the top and bottom sides of the selected area suggesting a clear interface between the PIM-1 layer and the PVDF support. However, for the TFC-N membrane (non-impregnated support), the intensity of O atom at the top and middle of the mapping (shown in Fig. 8.4 of the Appendix A) is almost the same, indicating infiltration of PIM-1 into the support.

3.4.2. Pervaporation performance of TFC membranes

The PV performance of the prepared TFC membranes for n-butanol recovery from an aqueous solution was evaluated by means of the total permeate flux, the n-butanol separation factor, and the permeate flux of n-butanol. As shown in Table 3.3, compared to other PV membranes [35], all prepared TFC membranes showed high total permeate fluxes greater than 16 kg m^{-2} h^{-1}, the highest one being for membrane TFC-E (35.4 kg m^{-2} h^{-1}), followed by TFC-M (30.2 kg m^{-2} h^{-1}), TFC-N (19.4 kg m^{-2} h^{-1}), and TFC-C (16.1 kg m^{-2} h^{-1}). However, the separation factor followed the order, TFC-C (8)> TFC-N (7.1)> TFC-M=TFC-E (4.8). The higher permeate flux of TFC-E and TFC-M membranes could be justified by the lower penetration of PIM-1 into the inter-fiber space of the PVDF support, which reduces the mass transfer resistance during the PV experiment. Infiltration of PIM-1 into the PVDF support is not observed in the backside images of TFC-E and TFC-M membranes (digital pictures of both the top and bottom sides after PV experiments are shown in Fig. 8.6 of the Appendix A). Their lower n-butanol/water separation factors may be attributed to the presence of few cracks and pinholes at the surface of the TFCs, as discussed in the previous section. Furthermore, it was observed that the PIM-1 layer was stable and did not detach from the PVDF during the PV tests (Fig. 8.6 of the Appendix A).

The total permeate flux values reported for the PIM-1 TFC membranes prepared on phase inversion PVDF supports [35] are lower than the values summarized in Table 3.3. In previous studies, the reported total permeate fluxes were 4 kg m^{-2} h^{-1} [32] and 9 kg m^{-2} h^{-1} [31] with an n-butanol/water separation factor of about 13. Therefore, the use of a highly porous support results in higher permeate fluxes. This has been already observed for polyamide (PA) and polyvinyl alcohol (PVA) TFC membranes developed for engineered osmosis applications using electrospun nanofibrous supports [58, 59]. This was attributed to the high porosity and pore interconnectivity in this type of support.

Table 3.3. *PV performance of the prepared PIM-1 TFC membranes on electrospun PVDF nanofibrous support. The feed aqueous solution was 5 wt.% of n-butanol/water mixture at 65°C.*

	J_T (kg^{-2} h^{-1})	J_{BuOH} (kg m^{-2} h^{-1})	$\beta_{BuOH/w}$	*PSI* (kg m^{-2} h^{-1})
TFC-N	19.4 ± 0.7	5.0 ± 0.2	7.1 ± 0.4	118.3 ± 7.8
TFC-C	16.1 ± 0.7	4.6 ± 0.1	8.0 ± 0.1	112.7 ± 1.7
TFC-M	30.2 ± 0.3	6.0 ± 0.1	4.8 ± 0.1	114.8 ± 3.0
TFC-E	35.4 ± 1.8	7.2 ± 0.7	4.8 ± 0.2	134.5 ± 7.5

Table 8.2 of the Appendix A presents a comparison of PV performance of the considered membranes for the dehydration of n-butanol solution. It should be noted that the feed temperature and composition highly affect the separation performance of PV membranes, therefore the feed concentration and temperature are also mentioned in Table 8.2 of the Appendix A. In Fig. 3.8, separation factor $\beta_{BuOH/w}$ of the prepared PIM-1 TFC membranes was plotted as a function of the corresponding total permeate flux (J_T), together with the values of other membranes reported in the literature for the PV separation of n-butanol from water mixtures. All membranes indicated in Fig. 3.8 have been tested at a feed temperature and composition of 50-70 °C and 5-6 wt.% of n-butanol in water (almost similar to the experimental conditions of this study), respectively. The best membranes should correspond to those exhibiting high total permeate flux and $\beta_{BuOH/w}$ (i.e. top right in Fig. 3.8).

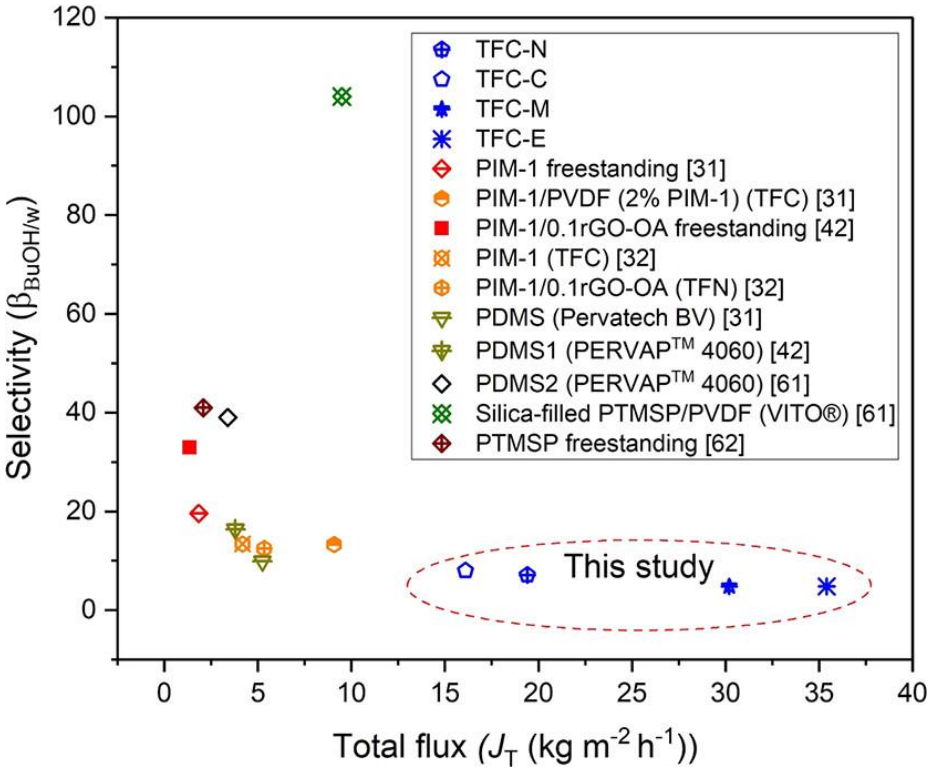

Figure 3.8. *PV separation factor ($\beta_{BuOH/w}$) vs. total permeate flux (J_T) of the prepared TFC membranes and other hydrophobic membranes reported in the PV literature for n-butanol/ water separation [31, 32, 42, 61, 62].*

Up to date, the best n-butanol selective membrane is the silica-filled PTMSP/PVDF from VITO®, with a remarkable $\beta_{BuOH/w}$ value of 104, and J_T of 9.5 kg m^{-2} h^{-1}. The PTMSP freestanding, PIM-1/alkylamine-functionalized reduced GO (GO-OA) (0.1 wt%) membrane and the commercial PDMS2 (PERVAP™ 4060) membrane are among those membranes showing reasonably high separation factor ($32.9 < \beta_{BuOH/w} < 41$), although the total permeate flux is lower than 3.4 kg m^{-2} h^{-1}. All other membranes reported similar $\beta_{BuOH/w}$ values to the prepared PIM-1 TFC membranes in this study. The most selective PIM-1 TFC membrane was

found to be TFC-C, having a total permeate flux of 16.1 kg m^{-2} h^{-1}, which represents a 69 % increase of the permeate flux compared to the VITO® membrane. The other PIM-1 TFC membranes were found to be less selective (TFC-M and TFC-E have a $\beta_{BuOH/w}$ value of 4.8) but the highest total permeate fluxes up to 30 kg m^{-2} h^{-1}, which represents an increase up to 270 % compared to the permeate flux of the VITO® membrane. In general, the developed PIM-1 TFC membranes in this study exhibit a much higher permeate flux with a comparable $\beta_{BuOH/w}$ to other PV membranes. The higher permeate flux is attributed to the lower mass transfer resistance of the electrospun support and the intrinsic microporosity of the PIM-1 layer formed on its top surface, whereas the reasonable obtained separation factor is due to the relatively compact and defect-free PIM-1 structure selective layer formed onto the nanofibrous PVDF support. It should be noted that the neat support on its own cannot be used as a PV membrane, because the liquid feed permeates across the membrane due to the transmembrane pressure difference and big pore size.

For sake of comparison, the PV separation index, *PSI*, is more useful as it provides quantitative information of the PV membrane performance since it takes into account its permeability and separation factor. Table 8.2 of the Appendix A shows the *PSI* values of the prepared PIM-1 TFC membranes and other PV membranes reported in the literature. A comparison is made in Fig. 3.9 for PV at a similar temperature and composition. As expected, the silica-filled PTMSP/PVDF (VITO®) membrane showed much higher *PSI* value (978 kg m^{-2} h^{-1}) because of its high $\beta_{BuOH/w}$ and total permeate flux. The *PSI* values are inversely proportional to the PIM-1 layer thickness, and despite freestanding PIM-1 membranes having a higher separation factor, their TFC counterparts (Table 8.2) show higher *PSI* values. The prepared PIM-1 TFC membranes in this study exhibited greater *PSI* values than the other reported PIM-1 TFC membranes in the PV literature due to their higher permeate flux attributed partially to the higher support porosity. Their *PSI* values are similar to that of the commercial PDMS2 (PERVAP™ 4060) membrane. Consequently, it can be concluded that the PIM-1 TFC membranes supported on PVDF nanofibrous supports have an outstanding and improved PV performance for n-butanol/water separation. Among these PIM-1 TFC membranes, TFC-E has a remarkable permeate flux (35.4 kg m^{-2} h^{-1}) and *PSI* value (134.5 kg m^{-2} h^{-1}).

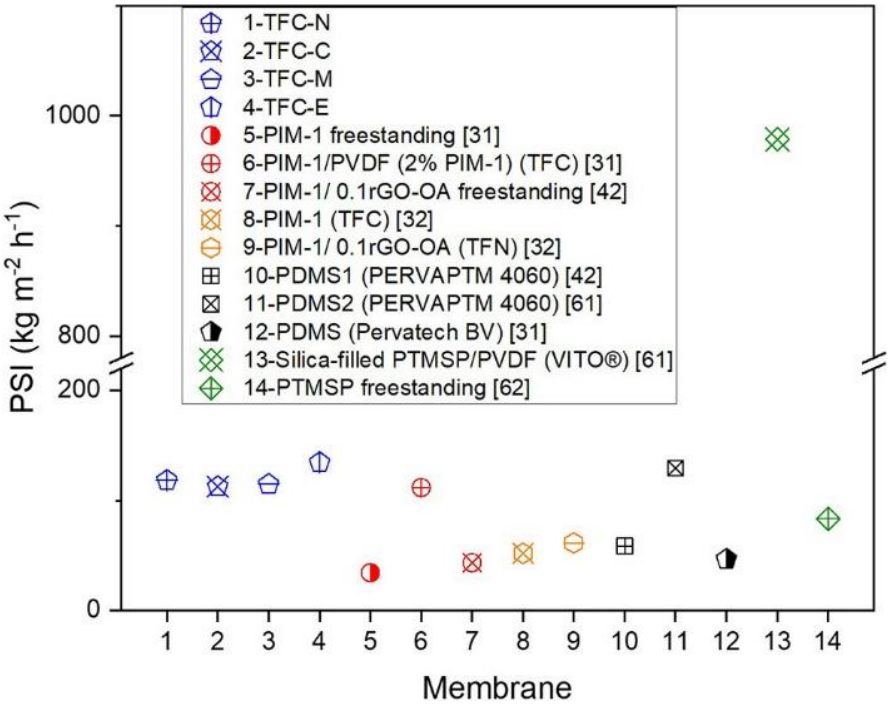

Figure 3.9. *PSI values of the prepared TFC membranes and other hydrophobic membranes reported in the PV literature for n-butanol/ water separation [31, 32, 42, 61, 62].*

3.4.3. Hybrid PV-distillation system versus distillation

The simulation of a conventional distillation process for n-butanol/water separation (Fig. 3.4) shows that the required energy decreases significantly when increasing the n-butanol concentration in the feed aqueous solution. This obtained energy per kg of produced n-butanol was 40, 22.9, 16, and 13.2 MJ $\mathrm{kg}_{\mathrm{BuOH}}^{-1}$ for n-butanol feed mass fractions ($x_{\mathrm{BuOH,feed}}$) 0.005, 0.01, 0.02, and 0.05, respectively. Van Heck et al. [49], who simulated the conventional distillation column using the same configuration as the one considered in the present study, reported separation energy of 21.4 MJ $\mathrm{kg}_{\mathrm{BuOH}}^{-1}$ for 2 wt.% n-butanol in water. This value is similar to the simulated values obtained in this study for the same concentration of n-butanol. The difference (30%) can be due to different reflux ratios in the columns, the number of distillation columns trays and the heat integration process

The TFC-E and TFC-C membranes, showing the highest permeate flux and n-butanol/water separation factor, respectively, of the TFC membranes prepared in this work, are considered for the simulation in the PV-distillation hybrid system. Different commercial PDMS membranes at different temperatures are also simulated [32, 61]. The energy demand for n-butanol recovery in the hybrid system using TFC-C and TFC-E is compared with other hydrophobic PV membranes reported in the literature for n-butanol/water separation. It is to be noted that the performance of the hybrid systems, in terms of energy saving, should be compared at the same operating conditions. However, these are rarely the same for the

membranes taken from open literature. Therefore, experimental values of the feed temperature and composition, the activation energy of the components, and the pressure at the permeate side (i.e. vacuum pressure) found in the literature for each membrane are used in the simulation (see Table 8.3 of the Appendix A). For n-butanol/water PV separation, the required energy per kg of produced n-butanol is listed in Table 3.4. The energy of n-butanol/water separation in the PV-distillation hybrid system was calculated as the involved energy in the condenser used to condense the permeate coming out from the membrane modules, the energy required in the reboilers of all the distillation columns, the vacuum pump energy, and the energy demand of the heaters (see all these energies values in Table 3.4). Due to different permeate pressures, the applied temperature of the condenser for PDMS2 (PERVAP^{TM} 4060) and Silicalite/Silicon membranes is -54 ˚C, and 0.5 ˚C, respectively; while for the other membranes it is slightly higher, 5.4 ˚C. The obtained energies of the distillation columns and the condenser are 4.1 (MJ $\mathrm{kg}_{\mathrm{BuOH}}^{-1}$) and 7.1 (MJ $\mathrm{kg}_{\mathrm{BuOH}}^{-1}$) for TFC-C membrane, and 4.8 (MJ $\mathrm{kg}_{\mathrm{BuOH}}^{-1}$) and 11.7 (MJ $\mathrm{kg}_{\mathrm{BuOH}}^{-1}$) for TFC-E membrane, respectively. The lower energy demand of the TFC-C membrane is attributed to its higher n-butanol separation factor, which induces a higher n-butanol mass fraction in the permeate. Consequently, less permeate is condensed to produce 1 kg of n-butanol. A heat exchanger (not shown in Fig. 3.5) is used before the condenser to recover the heat associated to the permeate and cool it down by using the condenser outlet stream. The PDMS2 (PERVAP 4060) membrane ($x_{\mathrm{BuOH.permeate}} = 0.67$, T_{permeate} = 49.3 ºC) [61] exhibits the lowest energy of the condenser and distillation column, 2.2 and 3.2 MJ $\mathrm{kg}_{\mathrm{BuOH}}^{-1}$, respectively. In addition, it was observed that the energy of the vacuum pump is almost the same for different membranes. This can be justified by the higher molar flow rate of non-condensable gases in comparison with butanol/water flow rate. Furthermore, the required energy of the centrifugal pump (to increase the pressure of permeate after condenser), is 5×10^{-4} MJ $\mathrm{kg}_{\mathrm{BuOH}}^{-1}$, which is negligible compared to the energy of the distillation columns and the condenser.

Table 3.4. *Total permeate flux (J_T), n-butanol separation factor ($\beta_{BuOH/w}$), total membrane area ($_{AMembrane}$), permeate temperature (T_{Perm}) and its composition ($x_{BuOH,perm}$) used in PV-distillation simulation and the obtained energy of the distillation columns ($Q_{Distillation}$), condenser ($Q_{Condenser}$), heater (Q_{Heater}) and vacuum pump ($Q_{Vacuum\ Pump}$) to produce 1 kg h^{-1} of n-butanol.*

Membrane	J_T (kg m^{-2} h^{-1})	$\beta_{BuOH/w}$	$A_{Membrane}$ (m^2 kg_{BuOH}^{-1})	T_{Perm} (°C)	$x_{BuOH,perm}$	$Q_{Distillation}$ (MJ kg_{BuOH}^{-1})	$Q_{Condenser}$ (MJ kg_{BuOH}^{-1})	Q_{Heater} (MJ kg_{BuOH}^{-1})	$Q_{Vacuum\ Pump}$ (MJ kg_{BuOH}^{-1})	Ref
TFC-C	16.1	8	0.26	63.35	0.2735	4.1	7.1	8.3	0.55	This work
TFC-E	35.4	4.8	0.18	62.28	0.1879	4.8	11.7	12.5	0.56	This work
PIM-1 (TFC)	4.19	13.4	0.63	63.44	0.0.4030	3.5	4.4	5.8	0.54	[32]
PIM-1/PVDF	9.08	13.3	0.32	63.92	0.4036	3.4	4.3	5.4	0.55	[31]
PDMS (Pervatech BV)	5.25	9.9	0.7	62.42	0.3346	3.6	5.7	7.1	0.55	[31]
PDMS1 (PERVAP 4060)	3.8	16.4	0.6	63.61	0.4593	3.3	3.6	5.3	0.55	[32]
PDMS2 (PERVAP 4060)	3.4	39	0.5	49.28	0.6707	3.2	2.1	2.9	0.57	[61]
PDMS/Ceramic	0.50	25	14	38.38	0.1767	5.6	12.4	5.4	0.56	[62]
PDMS/20% ZIF-7	1.68	65	4	58.79	0.3381	4.1	5.6	5.9	0.55	[63]
Silicalite/Silicon	0.09	90	28	76.43	0.4143	3.8	4.3	5.3	0.56	[64]

The required membrane area and energy demand of n-butanol recovery from aqueous solution, for distillation columns and the PV unit in the hybrid systems mentioned in Table 3.4, are compared with the standalone distillation column energy in Fig. 3.10. The PV unit energy is the summation of energies of condenser, vacuum pump, and heaters. For the membranes, TFC-C and TFC-E, the necessary energy for n-butanol recovery from 5 wt.% n-butanol aqueous solution is 20 and 29.5 MJ $\mathrm{kg}_{\mathrm{BuOH}}^{-1}$, respectively. These are about 55% and 80% of the n-butanol energy content (36.1 MJ $\mathrm{kg}_{\mathrm{BuOH}}^{-1}$ [22]). It was found that, among the membranes applied under the same operating conditions, the PDMS2 (PERVAP 4060) membrane exhibiting the highest n-butanol separation factor needed lower n-butanol recovery energy. The required energy of the standalone distillation columns at the feed mass fraction 5 wt % n-butanol is 13.2 MJ $\mathrm{kg}_{\mathrm{BuOH}}^{-1}$, which is lower than the energy required for the TFC-C and TFC-E membranes.

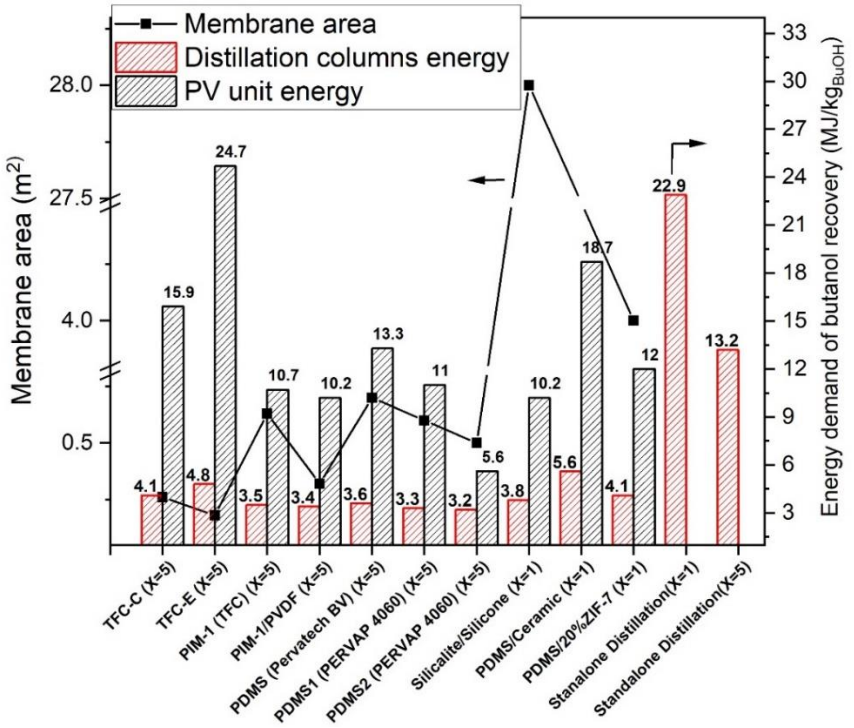

Figure 3.10. *Energy of n-butanol recovery from aqueous solutions at $x_{BuOH,feed}$=1 wt.% and $x_{BuOH,feed}$=5 wt.%) in the PV-distillation hybrid system and the conventional distillation column.*

Compared to the other membranes, the main advantage of using TFC-C membrane in the PV-distillation hybrid system is the small membrane area required to produce 1 kg n-butanol. For instance, the membrane area needed to produce 1 kg h^{-1} n-butanol using PDMS2 (PERVAP 4060) (0.5 m^2) membrane is twice that of TFC-C (0.26 m^2) membrane. In addition, as the membrane area increases, the installation and maintenance costs, which include membrane replacement due to possible fouling or any other damage, increase [65].

In this regard, the capital costs and operation costs of TFC-C/distillation and PDMS2 (PERVAP 4060)/distillation hybrid systems and the standalone distillation unit have been compared. Also, the optimum membrane area that minimizes the total butanol recovery cost is calculated for TFC-C and PDMS2 PERVAP4060 membranes. In section 3.3.3, to decrease the simulation running time and also to be sure the feed concentration does not change significantly, the feed flow rate and butanol production rate were considered 250 kg h^{-1} and 1 kg h^{-1}, respectively. However, 250 kg h^{-1} is lower than the feed flow rate of a real industrial plant, therefore for economic assessment simulations, it was considered 250 metric tons h^{-1}.

The PV unit consists of the membrane, a condenser, heat exchangers, membrane modules, and a vacuum pump. It has been estimated that the cost of freestanding thick membranes is in the range of 50-500 $\$.m^{-2}$ however, the cost of TFC membranes is between 1-10 $\$\ m^{-2}$ [66]. In this study, the cost of PIM-1 TFC membrane is considered 50 $\$\ m^{-2}$ (see section 8.6 of Appendix A). Also, the membrane module cost is assumed 50 $\$\ m^{-2}$. The factorial method [67] has been used to estimate the cost of common plant equipment including the distillation columns (i.e vertical vessel, trays, condenser, and reboiler), and the heat exchangers. The details of the calculations are mentioned in the Appendix A section 8.6.

For TFC-C and PDMS2 (PERVAP4060) membranes, the effect of membrane area on butanol recovery cost is calculated and shown in Fig. 3.11 (a) and (b). The total cost is the summation of capital and operating costs. The capital cost ($\$\ year^{-1}$) is the summation of purchase and installation costs of the main equipment based on 10 years depreciation time. The operating cost ($\$\ year^{-1}$) includes the utilities, equipment maintenance, and membrane replacement. It is assumed that the membrane should be changed every year. The minimum butanol separation cost ($\$\ kg_{BuOH}^{-1}$) for TFC-C and PDMS2 (PERVAP 4060) is 0.075 and 0.032 ($\$\ kg_{BuOH}^{-1}\ year^{-1}$), respectively which were obtained at membrane areas of 1500 m^2 and 4500 m^2. The butanol recovery cost for the standalone distillation column and the hybrid systems at the optimum area is compared in Fig. 3.11 (c). PDMS2 (PERVAP 4060)/distillation system exhibited both the lowest capital and operational cost among the compared systems which is around 10 percent lower than the standalone distillation column unit. The details of the cost calculations are mentioned in Table 8.6 of the Appendix A.

It is important to note that all calculations have been carried out considering constant permeate fluxes and separation factors that have been taken from short-term pervaporation tests. It would be necessary in a future work to validate the obtained values with long-term PV experiments in a continuous mode, as compaction, aging or swelling effects may alter the initial performance of PIM-1 membranes.

a)

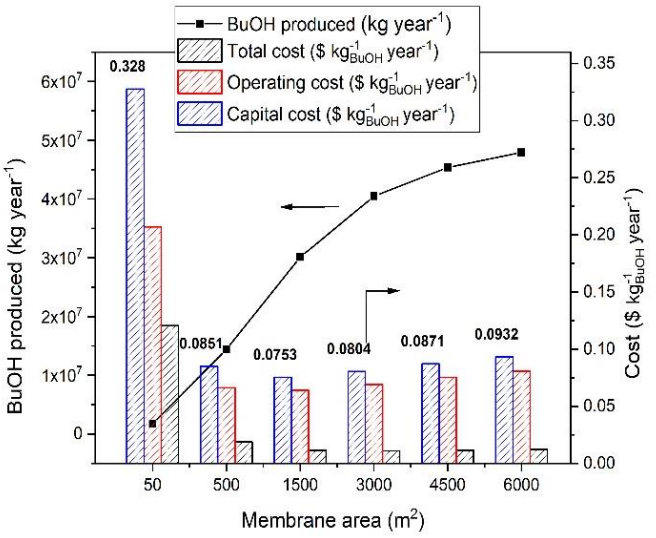

b)

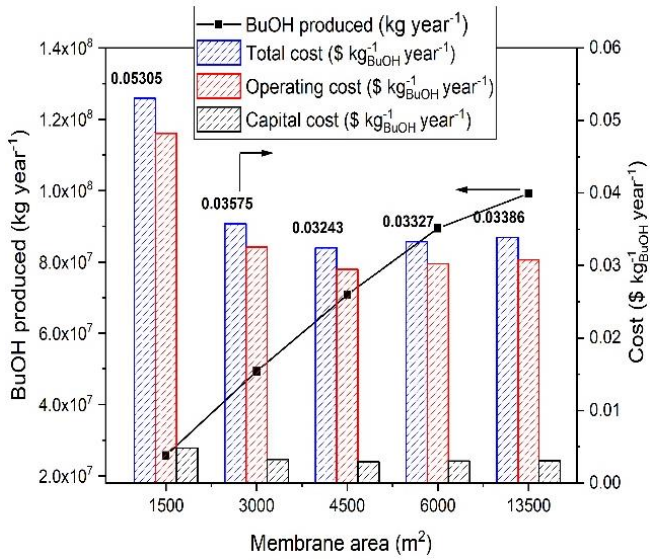

c)

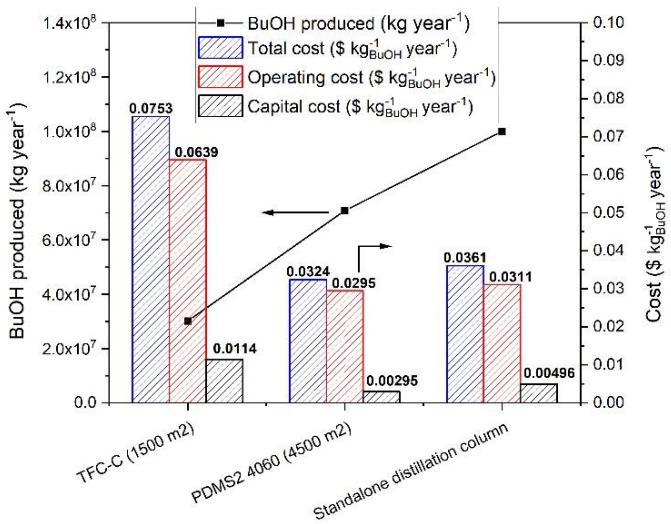

Figure 3.11. *Effect of membrane area on the annual butanol separation cost for a) TFC-C/distillation and b) PDMS2 (PERVAP 4060)/distillation hybrid systems. C) An economic comparison of the annual butanol separation cost of the hybrid systems at the optimum area with the standalone distillation column.*

3.5. Conclusions

In this work, thin film composite membranes of polymer of intrinsic microporosity PIM-1 have been prepared on polyvinylidene fluoride electrospun supports. The high porosity of the support and the thin layer of organophilic PIM-1 aids in having an exceptionally high flux membrane for the separation of butanol from water in pervaporation.

Penetration of PIM-1 into the support during the fabrication of thin film composite membranes by dip-coating plays an important role in the PV membrane performance. By impregnating the PVDF nanofibrous support with ethanol or methanol prior to coating it was possible to avoid infiltration but small pinholes were created upon the formation of the PIM-1 thin layer, leading to decreased n-butanol/water separation factors. The impregnation of the support with chloroform led to the formation of a thin and non-fragile PIM-1 layer, which resulted in a membrane with an improved n-butanol/water separation factor of 8.

The prepared PIM-1 TFC membranes had total permeate flux ranged between 16.1 and 35.4 kg m^{-2} h^{-1}, and n-butanol/water separation factors in the range 4.8-8. This confirms the synergistic effect of the low resistance to mass transfer of electrospun PVDF nanofibrous substrate, and the microporous layer of PIM-1. Under similar PV operating conditions, the calculated PV separation index *PSI* of the prepared PIM-1 TFCs is higher than most commercial membranes.

To evaluate the impact of these new TFCs for the recovery of n-butanol and assess potential reductions in energy requirements, PV-distillation and conventional stand-alone distillation processes were simulated using Aspen HYSYS. In the stand-alone distillation process, it was found that the energy demand for the separation process decreases by increasing the n-butanol concentration in the feed aqueous solution. Therefore, it is sensible to use an organophilic membrane to pre-concentrate the n-butanol before it enters the distillation column. In the simulated hybrid process (membrane separation/distillation) the energy demand decreases as the membrane n-butanol/water separation factor increases; for the TFC prepared with a chloroform-impreganted support (TFC-C) the energy demand is 20 MJ $\mathrm{kg}_{\mathrm{BuOH}}^{-1}$, which is 55% of the n-butanol energy content (36.1 MJ $\mathrm{kg}_{\mathrm{BuOH}}^{-1}$). Herein, the developed high flux PIM-1 TFCs allow the use of smaller membrane areas in the butanol recovery process, cutting down fabrication, maintenance, and installation costs. However, in order to decrease the energy demand it would be needed to improve the separation factor.

3.6. References

[1] Correa, D. F.; Beyer, H. L.; Fargione, J. E.; Hill, J. D.; Possingham, H. P.; Thomas-Hall, S. R.; Schenk, P. M., Towards the Implementation of Sustainable Biofuel Production Systems. Renew. Sust. Energ. Rev. 2019, 107, 250-263.

[2] Nyambo, C.; Mohanty, A. K.; Misra, M., Polylactide-based Renewable Green Composites from Agricultural Residues and their Hybrids. Biomacromolecules 2010, 11 (6), 1654-1660.

[3] Maiti, S.; Gallastegui, G.; Suresh, G.; Brar, S. K.; LeBihan, Y.; Drogui, P.; Buelna, G.; Ramirez, A. A.; Verma, M.; Soccol, C. R., Two-phase Partitioning Detoxification to Improve Biobutanol Production from Brewery Industry Wastes. Chem. Eng. J. 2017, 330, 1100-1108.

[4] Jin, C.; Yao, M.; Liu, H.; Chia-fon, F. L.; Ji, J., Progress in the Production and Application of n-Butanol as a Biofuel. Renew. Sust. Energ. Rev. 2011, 15 (8), 4080-4106.

[5] Bouaid, A.; El boulifi, N.; Hahati, K.; Martinez, M.; Aracil, J., Biodiesel Production from Biobutanol. Improvement of Cold Flow Properties. Chem. Eng. J. 2014, 238, 234-241.

[6] No, S.-Y., Application of Biobutanol in Advanced CI Engines – A Review. Fuel 2016, 183, 641-658.

[7] Zhen, X.; Wang, Y.; Liu, D., Bio-butanol as a New Generation of Clean Alternative Fuel for SI (Spark Ignition) and CI (Compression Ignition) Engines. Renew. Energy 2020, 147, 2494-2521.

[8] Baral, N. R. Techno-Economic Analysis of Butanol Production through Acetone-Butanol-Ethanol Fermentation. The Ohio State University, 2016.

[9] Bharathiraja, B.; Jayamuthunagai, J.; Sudharsanaa, T.; Bharghavi, A.; Praveenkumar, R.; Chakravarthy, M.; Yuvaraj, D., Biobutanol–An Impending Biofuel for Future: A Review on upstream and downstream processing tecniques. Renew. Sust. Energ. Rev. 2017, 68, 788-807.

[10] Van der Merwe, A.; Cheng, H.; Görgens, J.; Knoetze, J., Comparison of Energy Efficiency and Economics of Process Designs for Biobutanol Production from Sugarcane Molasses. Fuel 2013, 105, 451-458.

[11] Huang, Q.; Niu, C. H.; Dalai, A. K., Production of Anhydrous Biobutanol Using a Biosorbent Developed from Oat Hulls. Chem. Eng. J. 2019, 356, 830-838.

[12] Baral, N. R.; Shah, A., Microbial Inhibitors: Formation and Effects on Acetone-Butanol-Ethanol Fermentation of Lignocellulosic Biomass. Appl Microbiol Biotechnol 2014, 98 (22), 9151-72.

[13] Cai, D.; Chang, Z.; Gao, L.; Chen, C.; Niu, Y.; Qin, P.; Wang, Z.; Tan, T., Acetone–Butanol–Ethanol ABE) Fermentation Integrated with Simplified Gas Stripping Using Sweet Sorghum Bagasse as Immobilized Carrier. Chem. Eng. J. 2015, 277, 176-185.

[14] Dadgar, A. M.; Foutch, G. L., Improving the Acetone-Butanol Fermentation Process with Liquid-Liquid Extraction. Biotechnol. Prog. 1988, 4 1), 36-39.

[15] Cai, D.; Chen, H.; Chen, C.; Hu, S.; Wang, Y.; Chang, Z.; Miao, Q.; Qin, P.; Wang, Z.; Wang, J.; Tan, T., Gas Stripping–Pervaporation Hybrid Process for Energy-Saving Product Recovery from Acetone–Butanol–Ethanol (ABE) Fermentation Broth. Chem. Eng. J. 2016, 287, 1-10.

[16] Ji, C.-H.; Xue, S.-M.; Xu, Z.-L., Novel Swelling-Resistant Sodium Alginate Membrane Branching Modified by Glycogen for Highly Aqueous Ethanol Solution Pervaporation. ACS Appl. Mater. Inter. 2016, 8 (40), 27243-27253.

[17] Zuo, J.; Shi, G. M.; Wei, S.; Chung, T.-S., The Development of Novel Nexar Block Copolymer/Ultem Composite Membranes for C2–C4 Alcohols Dehydration via Pervaporation. ACS Appl. Mater. Inter. 2014, 6 (16), 13874-13883.

[18] Ying, Y.; Liu, D.; Zhang, W.; Ma, J.; Huang, H.; Yang, Q.; Zhong, C., High-Flux Graphene Oxide Membranes Intercalated by Metal–Organic Framework with Highly Selective Separation of Aqueous Organic Solution. ACS Appl. Mater. Inter. 2017, 9 (2), 1710-1718.

[19] Abdehagh, N.; Tezel, F. H.; Thibault, J., Separation Techniques in Butanol Production: Challenges and Developments. Biomass Bioenerg. 2014, 60, 222-246.

[20] Zheng, P.; Li, C.; Wang, N.; Li, J.; An, Q., The Potential of Pervaporation for Biofuel Recovery from Fermentation: An Energy Consumption Point of View. Chin. J. Chem. Eng. 2019, 27 (6), 1296-1306.

[21] Matsumura, M.; Kataoka, H.; Sueki, M.; Araki, K., Energy Saving Effect of Pervaporation Using Oleyl Alcohol Liquid Membrane in Butanol Purification. Bioprocess Eng. 1988, 3 (2), 93-100.
[22] Van Wyk, S.; Van der Ham, A.; Kersten, S., Pervaporative Separation and Intensification of Downstream Recovery of Acetone-Butanol-Ethanol (ABE). Chem. Eng. Process. 2018, 130, 148-159.
[23] Si, Z.; Li, G.; Wang, Z.; Cai, D.; Li, S.; Baeyens, J.; Qin, P., A Particle-Driven, Ultrafast-Cured Strategy for Tuning the Network Cavity Size of Membranes with Outstanding Pervaporation Performance. ACS Appl. Mater. Inter. 2020, 12 (28), 31887-31895.
[24] Vopička, O.; Pilnáček, K.; Friess, K., Separation of Methanol-Dimethyl Carbonate Vapour Mixtures with PDMS and PTMSP Membranes. Separ. Purif. Technol. 2017, 174, 1-11.
[25] Liu, Q.; Li, Y.; Li, Q.; Liu, G.; Liu, G.; Jin, W., Mixed-Matrix Hollow Fiber Composite Membranes Comprising of PEBA and MOF for Pervaporation Separation of Ethanol/Water Mixtures. Separ. Purif. Technol. 2019, 214, 2-10.
[26] Vrana, D. L.; Meagher, M. M.; Hutkins, R. W.; Duffield, B., Pervaporation of Model Acetone-Butanol-Ethanol Fermentation Product Solutions Using Polytetrafluoroethylene Membranes. Sep. Sci. Technol. 1993, 28 (13-14), 2167-2178.
[27] Genduso, G.; Farrokhzad, H.; Latré, Y.; Darvishmanesh, S.; Luis, P.; Van der Bruggen, B., Polyvinylidene Fluoride Dense Membrane for the Pervaporation of Methyl Acetate–Methanol Mixtures. J. Membr. Sci. 2015, 482, 128-136.
[28] Žák, M.; Klepic, M.; Štastná, L. Č.; Sedláková, Z.; Vychodilová, H.; Hovorka, Š.; Friess, K.; Randová, A.; Brožová, L.; Jansen, J. C., Selective Removal of Butanol from Aqueous Solution by Pervaporation with a PIM-1 Membrane and Membrane Aging. Separation and Purification Technology 2015, 151, 108-114.
[29] Zhao, J.; Jin, W., Manipulation of Confined Structure in Alcohol-Permselective Pervaporation Membranes. Chin. J. Chem. Eng. 2017, 25 (11), 1616-1626.
[30] Budd, P. M., Polymers of Intrinsic Microporosity and their Potential in Process Intensification. In Sustainable Nanoscale Engineering, Szekely, G.; Livingston, A., Eds. Elsevier: 2020; pp 231-264.
[31] Gao, L.; Alberto, M.; Gorgojo, P.; Szekely, G.; Budd, P. M., High-Flux PIM-1/PVDF Thin Film Composite Membranes for 1-Butanol/Water Pervaporation. J. Membr. Sci. 2017, 529, 207-214.
[32] Alberto, M.; Bhavsar, R.; Luque-Alled, J. M.; Prestat, E.; Gao, L.; Budd, P. M.; Vijayaraghavan, A.; Szekely, G.; Holmes, S. M.; Gorgojo, P., Study on the Formation of Thin Film Nanocomposite (TFN) Membranes of Polymers of Intrinsic Microporosity and Graphene-Like Fillers: Effect of Lateral Flake Size and Chemical Functionalization. J. Membr. Sci. 2018, 565, 390-401.
[33] Gorgojo, P.; Karan, S.; Wong, H. C.; Jimenez-Solomon, M. F.; Cabral, J. T.; Livingston, A. G., Ultrathin Polymer Films with Intrinsic Microporosity: Anomalous Solvent Permeation and High Flux Membranes. Adv. Funct. Mater. 2014, 24 (30), 4729-4737.
[34] Li, J.; Zhang, M.; Feng, W.; Zhu, L.; Zhang, L., PIM-1 Pore-Filled Thin Film Composite Membranes for Tunable Organic Solvent Nanofiltration. J. Membr. Sci. 2020, 601, 117951.
[35] Cook, M.; Gaffney, P. R.; Peeva, L. G.; Livingston, A. G., Roll-to-Roll Dip Coating of Three Different PIMs for Organic Solvent Nanofiltration. J. Membr. Sci. 2018, 558, 52-63.
[36] Gao, J.; Japip, S.; Chung, T.-S., Organic Solvent Resistant Membranes Made from a Cross-Linked Functionalized Polymer with Intrinsic Microporosity (PIM) Containing Thioamide Groups. Chem. Eng. J. 2018, 353, 689-698.
[37] Raghavan, P.; Zhao, X.; Manuel, J.; Shin, C.; Heo, M.-Y.; Ahn, J.-H.; Ryu, H.-S.; Ahn, H.-J.; Noh, J.-P.; Cho, G.-B., Electrochemical Studies on Polymer Electrolytes Based on Poly (vinylidene fluoride-co-hexafluoropropylene) Membranes Prepared by Electrospinning and Phase Inversion—A Comparative Study. Mater. Res. Bull. 2010, 45 (3), 362-366.
[38] Ameen, A. W.; Ji, J.; Tamaddondar, M.; Moshenpour, S.; Foster, A. B.; Fan, X.; Budd, P. M.; Mattia, D.; Gorgojo, P., 2D Boron Nitride Nanosheets in PIM-1 Membranes for CO2/CH4 Separation. Journal of Membrane Science 2021, 119527.

[39] Essalhi, M.; Khayet, M., Self-Sustained Webs of Polyvinylidene Fluoride Electrospun Nano-Fibers: Effects of Polymer Concentration and Desalination by Direct Contact Membrane Distillation. J. Membr. Sci. 2014, 454, 133-143.
[40] Alkhudhiri, A.; Hilal, N., Membrane Distillation—Principles, Applications, Configurations, Design, and Implementation. In Emerging Technologies for Sustainable Desalination Handbook, Elsevier: 2018; pp 55-106.
[41] Smolders, K.; Franken, A., Terminology for Membrane Distillation. Desalination 1989, 72 (3), 249-262.
[42] Alberto, M.; Luque-Alled, J. M.; Gao, L.; Iliut, M.; Prestat, E.; Newman, L.; Haigh, S. J.; Vijayaraghavan, A.; Budd, P. M.; Gorgojo, P., Enhanced Organophilic Separations with Mixed Matrix Membranes of Polymers of Intrinsic Microporosity and Graphene-Like Fillers. J. Membr. Sci. 2017, 526, 437-449.
[43] Van Hecke, W.; De Wever, H., High-Flux POMS Organophilic Pervaporation for ABE Recovery Applied in Fed-Batch and Continuous Set-Ups. Journal of Membrane Science 2017, 540, 321-332.
[44] Cheng, C.; Li, P.; Zhang, T.; Wang, X.; Hsiao, B. S., Enhanced Pervaporation Performance of Polyamide Membrane with Synergistic Effect of Porous Nanofibrous Support and Trace Graphene Oxide Lamellae. Chem. Eng. Sci. 2019, 196, 265-276.
[45] Liu, F.; Liu, L.; Feng, X., Separation of Acetone–Butanol–Ethanol (ABE) from Dilute Aqueous Solutions by Pervaporation. Separ. Purif. Technol. 2005, 42 (3), 273-282.
[46] Mach, E., Principles of the Theory of Heat: Historically and Critically Elucidated. Springer Science & Business Media: 2012; Vol. 17.
[47] Prochazka, O.; Suška, J.; Pick, J., Phase Equilibria in the Methanol-Water-1-Butanol Dystem. Collect. Czechoslov. Chem. Commun. 1975, 40 (3), 781-786.
[48] Rom, A.; Miltner, A.; Wukovits, W.; Friedl, A., Energy Saving Potential of Hybrid Membrane and Distillation Process in Butanol Purification: Experiments, Modelling and Simulation. Chem. Eng. Process. 2016, 104, 201-211.
[49] Van Hecke, W.; Vandezande, P.; Claes, S.; Vangeel, S.; Beckers, H.; Diels, L.; De Wever, H., Integrated Boprocess for Long-Term Continuous Cultivation of Clostridium Acetobutylicum Coupled to Pervaporation with PDMS Composite Membranes. Bioresour. Technol. 2012, 111, 368-377.
[50] Van Hecke, W.; Joossen-Meyvis, E.; Beckers, H.; De Wever, H., Prospects & Potential of Biobutanol Production Integrated with Organophilic Pervaporation–A Techno-Economic Assessment. Appl. Energy 2018, 228, 437-449.
[51] Mohsenpour, S.; Safekordi, A.; Tavakolmoghadam, M.; Rekabdar, F.; Hemmati, M., Comparison of the Membrane Morphology Based on the Phase Diagram Using PVP as an Organic Additive and TiO2 as an Inorganic Additive. Polymer 2016, 97, 559-568.
[52] Mohsenpour, S.; Khosravanian, A., Influence of Additives on the Morphology of PVDF Membranes Based on Phase Diagram: Thermodynamic and Experimental Study. J. Appl. Polym. Sci. 2018, 135 (21), 46225.
[53] Eykens, L.; De Sitter, K.; Dotremont, C.; Pinoy, L.; Van der Bruggen, B., Membrane Synthesis for Membrane Distillation: A Review. Separ. Purif. Technol. 2017, 182, 36-51.
[54] Prince, J.; Singh, G.; Rana, D.; Matsuura, T.; Anbharasi, V.; Shanmugasundaram, T., Preparation and Characterization of Highly Hydrophobic Poly (vinylidene fluoride)–Clay Nanocomposite Nanofiber Membranes (PVDF–Clay NNMs) for Desalination Using Direct Contact Membrane Distillation. J. Membr. Sci. 2012, 397, 80-86.
[55] Zhang, B.; Wang, J.; Liu, Z.; Zhang, X., Beyond Cassie Equation: Local Structure of heterogeneous Surfaces Determines the Contact Angles of Microdroplets. Sci. Rep. 2014, 4, 5822.
[56] Lin, L.; Feng, C.; Lopez, R.; Coronell, O., Identifying Facile and Accurate Methods to Measure the Thickness of the Active Layers of Thin-Film Composite Membranes–A Comparison of Seven Characterization Techniques. Journal of membrane science 2016, 498, 167-179.

[57] Van der Bruggen, B.; Jansen, J. C.; Figoli, A.; Geens, J.; Boussu, K.; Drioli, E., Characteristics and Performance of a "Universal" Membrane Suitable for Gas Separation, Pervaporation, and Nanofiltration Applications. The Journal of Physical Chemistry B 2006, 110 (28), 13799-13803.
[58] Bui, N.-N.; Lind, M. L.; Hoek, E. M.; McCutcheon, J. R., Electrospun Nanofiber Supported Thin Film Composite Membranes for Engineered Osmosis. J. Membr. Sci. 2011, 385, 10-19.
[59] Park, M. J.; Gonzales, R. R.; Abdel-Wahab, A.; Phuntsho, S.; Shon, H. K., Hydrophilic Polyvinyl Alcohol Coating on Hydrophobic Electrospun Nanofiber Membrane for High Performance Thin Film Composite Forward Osmosis Membrane. Desalination 2018, 426, 50-59.
[60] Fadeev, A.; Selinskaya, Y. A.; Kelley, S.; Meagher, M.; Litvinova, E.; Khotimsky, V.; Volkov, V., Extraction of Butanol from Aqueous Solutions by Pervaporation through Poly (1-trimethylsilyl-1-propyne). J. Membr. Sci. 2001, 186 (2), 205-217.
[61] Claes, S.; Vandezande, P.; Mullens, S.; De Sitter, K.; Peeters, R.; Van Bael, M. K., Preparation and Benchmarking of Thin Film Supported PTMSP-Silica Pervaporation Membranes. J. Membr. Sci. 2012, 389, 265-271.
[62] Gongping, L.; Dan, H.; Wang, W.; Xiangli, F.; Wanqin, J., Pervaporation Separation of Butanol-Water Mixtures Using Polydimethylsiloxane/Ceramic Composite Membrane. Chin. J. Chem. Eng. 2011, 19 (1), 40-44.
[63] Wang, X.; Chen, J.; Fang, M.; Wang, T.; Yu, L.; Li, J., ZIF-7/PDMS Mixed Matrix Membranes for Pervaporation Recovery of Butanol from Aqueous Solution. Separ. Purif. Technol. 2016, 163, 39-47.
[64] Qureshi, N.; Meagher, M.; Hutkins, R. W., Recovery of Butanol from Model Solutions and Fermentation Broth Using a Silicalite/Silicone Membrane. J. Membr. Sci. 1999, 158 (1-2), 115-125.
[65] Van Hoof, V.; Van den Abeele, L.; Buekenhoudt, A.; Dotremont, C.; Leysen, R., Economic Comparison between Azeotropic Distillation and Different Hbrid Systems Combining Distillation with Pervaporation for the Dehydration of Isopropanol. Separ. Purif. Technol. 2004, 37 (1), 33-49.
[66] Baker, R. W.; Lokhandwala, K., Natural Gas Processing with Membranes: an Overview. Ind. Eng. Chem. Res. 2008, 47 (7), 2109-2121.
[67] Sinnott, R.; Towler, G., Chemical Engineering Design: SI Edition. Butterworth-Heinemann: 2019.

Chapter 4

Dual-Layered Electrospun Nanofibrous Membranes for Membrane Distillation

Dual-layered electrospun nanofibrous membranes (DL-ENMs) were prepared using the hydrophobic polymer polyvinylidene fluoride (PVDF) and the hydrophilic one polysulfone (PSF). The thickness of each layer was varied by changing the electrospinning time of each polymer solution maintaining the total electrospinning time at 3h. The characteristics of the DL-ENMs and those of each layer were studied by means of different techniques and the results were compared to the single layer PVDF and PSF ENMs (i.e. SL-ENMs). The prepared DL-ENMs were tested in desalination by direct contact membrane distillation (DCMD) using different sodium chloride feed aqueous solutions. The DCMD permeate flux of the DL-ENMs was found to be higher than that of the PVDF SL-ENM and it increased with the decrease of the PVDF layer due not only to the reduction of the total thickness and to the increase of both the inter-fiber space and the void volume fraction, but also to the reduction of the path between the liquid/vapour interfaces formed at both side of the DL-ENMs. Compared to the proposed SL-ENMs in DCMD, it is better to use DL-ENMs adequately designed with hydrophobic and hydrophilic polymers than SL-ENM with only a hydrophobic polymer.

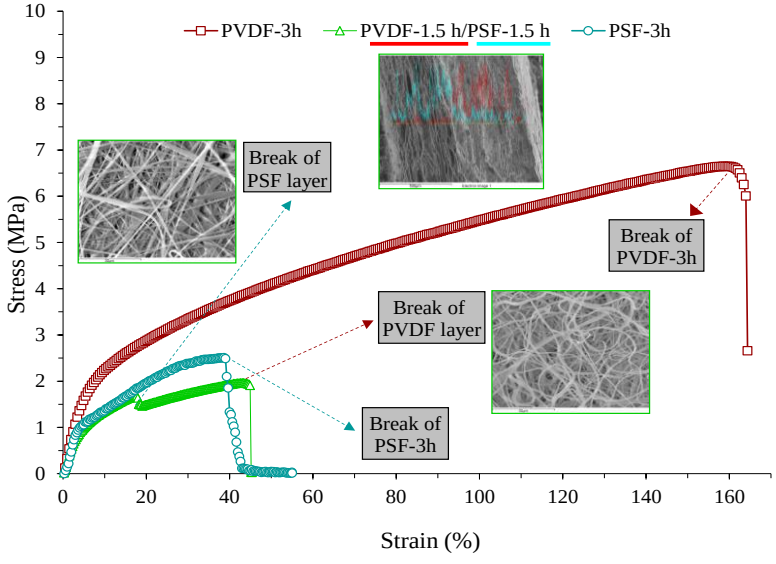

4.1. Introduction

Nanofibrous materials exhibit several important characteristics such as a very high surface area to volume ratio that can be as high as 100 times that of microfibrous materials, tunable and very high void volume fraction or "porosity" that can reach more than 90%, inter-fiber space or "pore size" that can range from ten nanometers to several micrometers, flexibility in surface functionalities, interconnected open structure, good mechanical performance and possibility to construct a wide variety of fiber sizes and shapes (e.g. beaded, ribbon, porous and core-shell nanofibers). Therefore, nanofibrous materials have received extensive research interest for many potential applications in diverse fields as drug delivery carriers, optical and chemical sensors, stimuli-responsive materials, bioreactors, tissue engineering scaffolds, electronic and semi-conductive materials, photovoltaic cells, battery applications, reinforced nano-composites, affinity membranes for different separation processes, etc. [1-11]

Polymer nanofibers have been fabricated by means of different physical, chemical, thermal and electrostatic techniques including template synthesis [12], liquid-liquid phase separation [13], self-assembly [14], vapour-phase polymerization [15] and electrospinning [11]. Among all these techniques, electrospinning is the most considered for the preparation of submicrometer-sized polymeric fibers because of its simplicity, cost and versatility permitting to organize nanofibers of various types (e.g. porous, hollow and core/sheath) into three-dimensional network. A lot of attention has been devoted to this technology using both natural and synthetic polymers and copolymers to produce fibers with different diameters from few micrometers down to tens of nanometers by adjusting electrospinning process parameters [16].

In membrane science and nanotechnology, electrospun nanofibrous membranes (ENMs) have been applied in different membrane separation processes such as microfiltration (MF), ultrafiltration (UF), engineered osmosis (EO) and membrane distillation (MD) [17-26]. For this last process ENMs offer interesting and attractive characteristics such as the high void volume fraction that provides large space for evaporation improving the water production rate, high hydrophobicity and less susceptibility to wetting by the feed water solutions if the inter-fiber space is adequately designed (i.e. high liquid entry pressure, *LEP*), high surface roughness and low thermal conductivity reducing therefore the heat loss by conduction (i.e. in MD the heat transfer by conduction through the fibers of the ENMs following Fourier's law is heat lost as no water vapour is associated to this heat) [27,28].

Both unsupported (i.e. non-woven mats) [29-32] and supported (i.e. backing material) [33-35] ENMs have been considered in different MD configurations. In fact, adequate supports should not enhance the mass transfer resistance but must provide the membrane with the necessary mechanical properties preventing its rupture when assembled in modules [10,21,27]. Essalhi and Khayet [36] observed an improvement of the mechanical properties of poly(vinylidene fluoride) (PVDF) SL-ENMs with the increase of the thickness (i.e. increase electrospinning time) but the MD permeate flux was reduced because the permeate flux is inversely proportional to the membrane thickness. Various surface or bulk modifications of ENMs including post-heat treatment have been studied in order to improve the physico-chemical and mechanical characteristics of the ENMs required in MD [26,36,34,35,37-48]. It is worth quoting that most of the prepared unsupported ENMs for MD are single hydrophobic layer obtained from a single hydrophobic polymer such as PVDF or the copolymer polyvinylidene fluoride-co-hexafluoropropylene (PVDF-HFP) with or without nanoadditives or mixed polymers such as polydimethylsiloxane (PDMS) and poly (methyl methacrylate) (PMMA) or PDMS and PVDF [25,29-32,36-46]. A supported triple layered hydrophobic/hydrophilic composite membrane has also been proposed for air gap membrane distillation (AGMD) applications [35]. This has been prepared using a PVDF electrospun nanofiber layer as the top layer (i.e., the active layer facing the feed), a PVDF cast middle microporous layer and a commercial backing support (polyethylene terephtalate, PET). It was claimed that the permeate flux of this triple layered membrane was 1.5 times higher (15.2 kg/m^2.h) than that of the dual layer membrane (i.e. membrane without the nanofiber selective layer).

Three research studies have been published so far on unsupported double-layered hydrophobic/hydrophilic ENMs for desalination by AGMD and direct contact membrane distillation (DCMD) [34,47,48]. Liao et al. [34] proposed a double-layered membrane with a thin superhydrophobic layer comprising PVDF and silica nanoparticles (i.e. 72 μm thick, 154º water contact angle) electrospun on a porous PVDF nanofibrous support. This membrane exhibited a stable permeate flux of 24.6±1.2 kg/m^2.h when using a feed NaCl aqueous solution of 3.5 wt% during 25 h DCMD operation. Woo et al. [47] studied the effects of different hydrophilic nanofibrous supports on the desalination AGMD performance. The top layer, which faced the feed side was made of hydrophobic nanofibers (i.e. PVDF-HFP) while the bottom layer was made of hydrophilic nanofibers (i.e. polyacrylonitrile, PAN; polyvinyl alcohol, PVA or nylon-6, N6). The PVDF-HFP and support layer thickness ratio was maintained at 50/50. When using 3.5 wt% NaCl feed aqueous solution, it was observed permeate fluxes of the single and double-layered ENMs of 11 – 15.5 kg/m^2.h, which were greater than those of commercial PVDF membrane (i.e. about 5 kg/m^2.h under the same operating conditions).

It was claimed that the hydrophilic ENM layer enhanced the permeate flux depending on its wettability and characteristics. The double-layered membrane prepared with N6 as ENM support exhibited the highest permeate flux (15.5 kg/m^2.h) with 99.5% salt rejection factor. Tijing et al. [48] prepared the same type of ENMs membrane (PVDF-HFP/PAN) with two different thickness ratio (50/50 and 25/75) being the total thickness 80 μm. The thickness of the membrane layers was controlled by manipulating the electrospinning time between 1.5 and 6 h. The two membranes exhibited the same membrane characteristics (i.e. void volume fraction, 90%; contact angle, 150/100º, surface pore size 0.6-2.5/6-16 μm; average fiber diameter 0.21/1.7 μm) except a slight difference of the liquid entry pressure (*LEP*), 85 and 94 kPa for the 50/50 and 25/75 PVDF-HFP/PAN membranes, respectively. These membranes were used in desalination by DCMD and a higher permeate flux was obtained (i.e. about 30 kg/m^2.h) with a salt rejection factor greater than 98.5%. This result was attributed to the thicker PAN layer, which decreased the mass transfer resistance. It was claimed that a thinner top ENM hydrophobic layer with high void volume fraction would lead to better DCMD permeate flux.

In fact, porous composite hydrophobic/hydrophilic flat sheet and hollow fiber membranes have been proposed for DCMD because of their high performance compared to single layer hydrophobic ones [27,28,49-56]. The hydrophobic thin layer is the responsible of the mass transfer and separation whereas the optimized thicker hydrophilic layer having bigger pores not only acts as support by increasing the mechanical properties of the membrane, but also reduces its heat transfer by conduction and improves the mass transfer [50-52]. For this type of membranes, the permeate liquid penetrates inside the bigger pores of the hydrophilic layer reducing therefore the distance between the liquid/vapour interfaces formed at each side of the hydrophobic thin layer. In addition, although the hydrophobic layer exhibited smaller pore size (i.e. an order of magnitude smaller than that of the commercial membranes used in MD), the observed improved DCMD permeate flux of this type of membranes is due to the Knudsen type of flow instead of the combined Knudsen/Molecular diffusion mechanism that occurs in commercial microporous membranes. In the case of ENMs, Essalhi and Khayet [57] demonstrated that Knudsen contribution increased with the increase of the ratio of the mean electrospun fiber diameter to the inter-fiber space. Because of the web configuration of ENMs, collisions occur between water vapour molecules and nanofibers together with collisions between water vapour molecules and each other's and between water vapour molecules and air present inside the void volume space of the ENMs. It was found that Knudsen diffusion 17.9–37.4 times greater than molecular diffusion. In addition, the heat transfer by conduction through the ENMs was found to be less than 20% of the total heat transferred through each ENM.

In this study, dual-layered ENMs (DL-ENMs) are prepared by electrospinning using the hydrophobic polymer polyvinylidene fluoride (PVDF) and the hydrophilic one polysulfone (PSF). In contrast to the three previously published studies [34,47,48], in the present paper a systematic experimental study on the effects of the thickness of each layer on the characteristics of the DL-ENMs and the DCMD desalination performance are carried out under different operating conditions. The thickness of the two layers was controlled by varying the electrospinning time maintaining the total electrospinning duration 3 h. The DCMD performance is compared to SL-ENMs prepared by either PVDF or PSF and to the other types of unsupported ENMs published so far for desalination by MD.

4.2. Experimental

4.2.1. Materials

The hydrophobic PVDF polymer (Sigma-Aldrich Chemical Co.; M_w = 275 kg/mol and M_n =107 kg/mol) and the hydrophilic PSF polymer (UDEL P-3500 LCD, Solvay Specialty Polymers; M_w = 79 kg/mol; ρ = 1.24 g/cm^3) were used for the preparation of the ENMs. Due to the hydrophilic character of PSF and the possible influence of ambient humidity, this polymer was first dried at 120 ºC overnight using a vacuum desiccator composed of a vacuum pump (Vacuubrand brand,model MZ2C), a desiccant (Afora) and a heating mantle (Selecta).

The dope solutions were prepared by a mixture of solvents, acetone and *N,N*-dimethyl acetamide (DMAC). Isopropyl alcohol (IPA) used to determine both the void volume fraction and the inter-fiber space, and the sodium chloride (NaCl) used in liquid entry pressure (*LEP*) measurements and DCMD experiments. All the chemical products were purchased from Sigma-Aldrich Chemical Co.

4.2.2. SL-ENMs and DL-ENMs fabrication

Two polymer solutions were prepared by dissolving 25 wt% PVDF or PSF in the solvent mixture acetone/DMAC (20/80 wt%). The polymer was added to the solvent mixture and kept at 55ºC in under an orbital shaker thermostatic bath (Stuart SBS40) at the same temperature during 24 h and then under a stirring magnetic agitation (IKA, RCT basic) of 120 rpm for about 4 h until it was totally dissolved. The dope solutions were characterized by measuring the surface tension (σ), electrical conductivity (χ) and viscosity (μ). The surface tension was measured by the pendant drop shape analysis using an Optical Contact Angle Meter (CAM200). The electrical conductivity was measured using the conductivity meter (Cyber Scan

con11 Conductivity/TDS/1C, Eutech Instruments). The viscosity was measured using a digital Viscosimeter (Brookfield, DV-Iþ) connected to a thermostat (Model HETO21-DT-1, Rego S.A). Details of the mentioned measurements are described elsewhere [31]. Prior to characterization and electrospinning, the polymer solutions were degassed overnight at room temperature. All measurements were carried out at 24.0 ± 0.5 ºC and the values of σ, χ and μ are summarized in Table 4.1.

Table 4.1*. Surface tension (σ), electrical conductivity (χ) and viscosity (μ) of the PVDF and PSF dope solutions used in the preparation of the ENMs.*

Polymer solution	σ (mN/m)	χ (μS/cm)	μ (Pa·s)
PVDF	32.2 ± 0.8	9.56 ± 0.02	3.02 ± 0.09
PSF	38.9 ± 0.5	2.51 ± 0.02	2.14 ± 0.07

The electrospinning system used to prepare the ENMs was presented in detail elsewhere [36]. In this study, an electric voltage of 27 kV was applied to both PVDF and PSF solutions using a stainless steel needle of 0.6/0.9 mm inner/outer diameters connected to a glass syringe (Nikepal, 50 mL) by a Teflon tube. The flow rate of the polymer solutions was 1.23 mL/h and the air gap between the needle tip and the metallic collector was 27.5 cm. The temperature and the humidity was 23ºC and 36%, respectively. During electrospinning, the solvents are evaporated while the polymer fiber is stretched, elongated, whipped and finally deposited on the form of a non-woven mat on the grounded metallic collector. To prepare the DL-ENMs, the electrospinning time of each polymer solution was varied from 0.5 h to 2.5 h starting from the PVDF layer as the electrical conductivity of PVDF solution is greater than that of PSF solution permitting the dissipation of the electric charge to the collector and resulting in more packed fiber web. In contrast, when the electrospun PSF layer was first electrospun before PVDF layer, the PSF layer acts as an insulator getting loosely packed web. The SL-ENMs were prepared from each polymer solution during 3 h electrospinning time. The electrospinning time of each ENM is indicated in Table 4.2. After electrospinning, the ENMs were dried in oven at 120ºC for 0.5 h (i.e. post-treatment).

Table 4.2. *Electrospinning time of each layer and the membrane code used for the ENMs prepared in this study.*

Membrane	Electrospinning time (h)	
	Bottom layer (PVDF)	Top layer (PSF)
PVDF-3h	3	-
CENM-1	2.5	0.5
CENM-2	2	1
CENM-3	1.5	1.5
CENM-4	1	2
CENM-5	0.5	2.5
PSF-3h	-	3

4.2.3. ENMs characterization and DCMD experiments

The surface and the cross-section of the ENMs were studied by a field emission scanning electron microscope (SEM, JEOL Model JSM-6335F). The samples were first fractured in liquid nitrogen and then placed over a support and coated with gold under vacuum conditions. Both the fiber size distribution and the mean fiber diameter (d_f) were determined from these SEM images using the UTHSCSA Image Tool free software. About 100 fibers of each ENM sample were considered. X-ray Energy Dispersive Spectroscopy (EDX, Oxford Instruments X-Max) was considered to determine the elemental composition of sulfur (PSF) and fluorine (PVDF) along the cross-section of the membrane sample.

The thickness (δ) of the ENMs was measured by the micrometer (Schut Geometrical Metrology) on different points of each membrane sample. At least 50 values were obtained and the average values together with their standard deviations were reported.

The water contact angle (ϑ_w) of the surface of each ENM was measured at room temperature (23ºC) by a computerized optical system CAM200, equipped with a CCD camera, frame grabber and image analysis software [36].

Differential scanning calorimetry (DSC) (Mettler Toledo, DSC 1 Star^e System) was used to study the thermal properties of the prepared ENMs together with the polymers PVDF and PSF. The melting temperature (T_m), the enthalpy of melting (ΔH_m), the crystallization

temperature (T_c) and the heat of crystallization (ΔH_c) of both the PVDF polymer and ENMs (SL-ENMS and DL-ENMs) were determined by Star^e software (Version 10.00d Build 3690). The DL-ENMs were tested without separating the PSF and PVDF layers. The glass transition temperature (T_g) was also determined for the PSF polymer and some of the ENMs.

The mechanical properties of the DL-ENMs and SL-ENMs were investigated according to ASTM D 3379-75 specifications using an Instron dynamometer (model 3366) at 23ºC and a cross-head speed of 22 mm/min. The Young´s modulus, the tensile stress at break and the strain at break were determined for all the prepared ENMs.

The void volume fraction (ε) of the ENMs was determined by measuring the density of each ENM using isopropyl alcohol (IPA), which penetrates inside the inter-fiber space of the ENMs, and distilled water, which does not enter in the inter-fiber space. The applied method was reported elsewhere [27].

The inter-fiber space (i.e. maximum, mean and minimum size) of the ENMs was determined following the wet/dry method using the set-up and the procedure detailed in [36].

The liquid entry pressure (*LEP*) of water measurements were carried out using the system detailed elsewhere [36]. The container was filled first with 0.2 L distilled water or NaCl aqueous solution and then the pressure was applied gradually by means of a nitrogen cylinder on the aqueous solution, which was facing the PVDF layer of the ENMs. The temperature was 23ºC. The minimum registered applied pressure before the liquid penetrates into the inter-fiber space is the *LEP* value.

The experimental system used to carry out the DCMD experiments through ENMs is detailed in [52]. In this study, the experiments were conducted first with distilled water as feed and then with salt NaCl aqueous solutions of different concentrations (12 and 30 g/L). The feed solutions were brought in contact with the PVDF layer of the DL-ENMs while the PSF layer was maintained in contact with the permeate cold water. The feed temperature was 80ºC while that of the permeate was 20ºC and both the feed and permeate circulation rates were 500 rpm.

4.3. Results and discussions

4.3.1. Structural and morphological characteristics of the prepared ENMs

The SEM images of the cross-section and surface of each layer of the prepared DL-ENMs are shown in Fig. 4.1 together with the corresponding EDX analysis of the cross-section and the distribution of the fiber diameter and those of the PSF and PVDF SL-ENMs for sake of

comparison. The total thickness (δ_t) and that of each layer (δ_{PSF} or δ_{PVDF}), the mean fiber diameter (d_f) and the water contact angle (θ_w) of each layer of the DL-ENMs and those of the PVDF and PSF SL_ENMs are presented in Table 4.3. A strong cohesive fibrous structure with a random fiber distribution and without beads formation was obtained for all prepared ENMs. This indicates the adequate post-treatment considered for 30 min at a temperature of 120 ºC to prepare the ENMs, which were below the melting and crystallization temperatures of PVDF polymer as it will be discussed later on based on the DSC results. From the obtained SEM images, it can be seen that the PSF layer of the same DL-ENM exhibits more open web structure than the PVDF layer (see Fig. 4.1). Moreover, it seems that there is a slight systematic decrease of the d_f of both the PVDF and PSF layers with the decrease of the PVDF electrospinning time (i.e. increase of the PSF layer) of the DL-ENMs, and the d_f of the PSF layer is smaller than that of PVDF. However, if the standard deviation is taken into account no significant change of d_f should be considered. The smaller d_f of the PSF layer than that of PVDF layer may be attributed to the lower viscosity of the PSF polymer solution compared to that of the PVDF polymer solution (see Table 4.1) although the PSF polymer solution exhibits higher surface tension. Under the same electrospinning parameters, polymer solutions with high surface tension results in greater d_f values at the tip of the metallic needle while low viscosity leads to small d_f values due to the stretching of the electrospun fiber through the electrified jet along the gap between the needle tip and the metallic collector. In this case, the dominant effect is the viscosity.

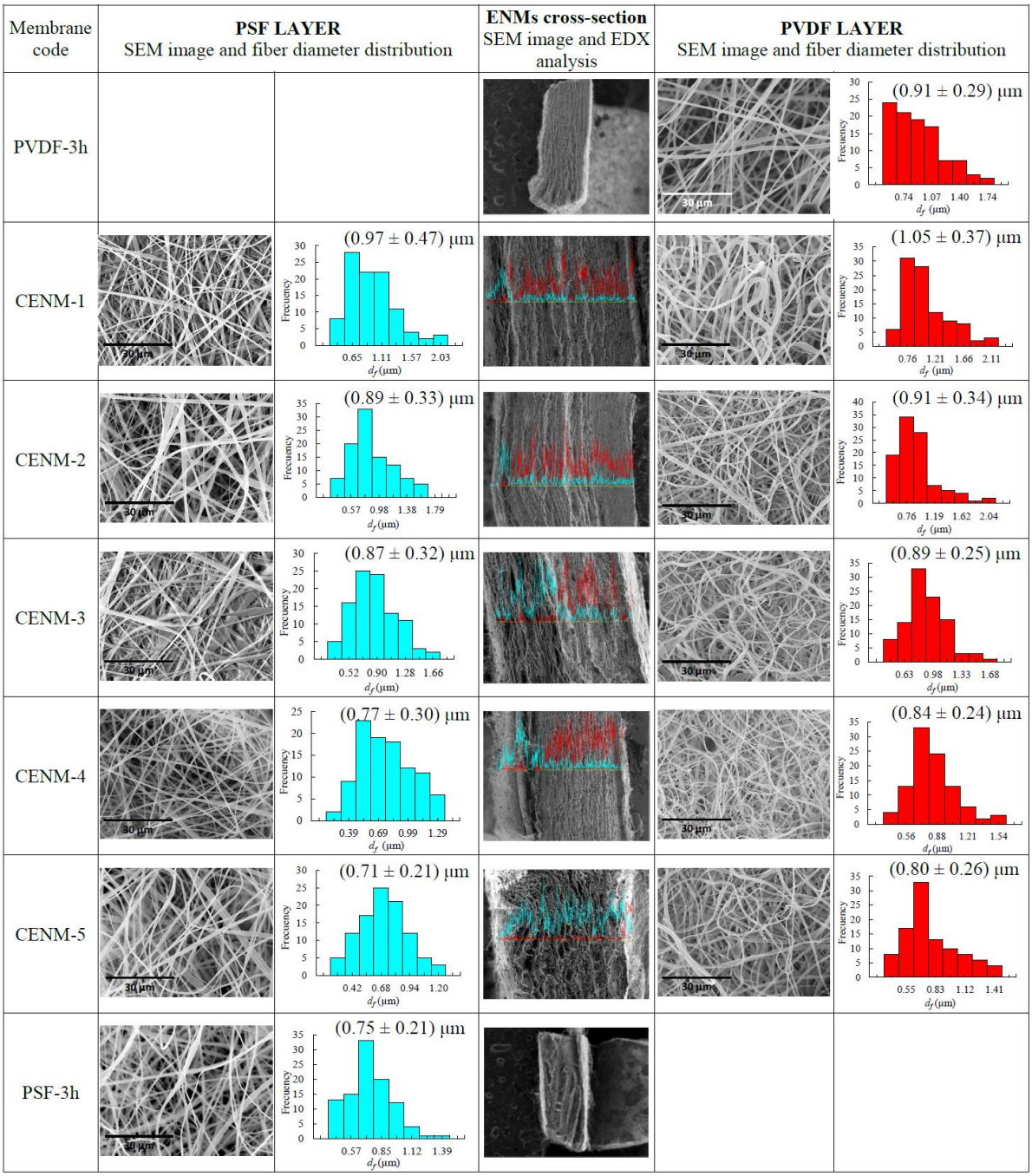

Figure 4.1. *SEM images of the PSF and PVDF surfaces with the corresponding distribution of their fiber diameters, and SEM images and EDX analysis of the cross-section of the prepared ENMs membranes. Cyan and red colors correspond to the PSF and PVDF layer, respectively.*

Table 4.3. *Thickness (δ), mean fiber diameter (df) and water contact angle (ϑw) of the PSF and PVDF layers of the prepared ENMs and the total thickness (δt) of the PVDF and PSF SL-ENMs as well as DL-ENMs.*

Membrane	Top layer (PSF)			Bottom layer (PVDF)			δ_t (μm)
	δ_{PS} (μm)	$(d_f)_{PSF}$ (μm)	$(\vartheta_w)_{PSF}$ (º)	δ_{PVDF} (μm)	$(d_f)_{PVDF}$ (μm)	$(\vartheta_w)_{PVDF}$ (º)	
PVDF-3h	-	-	-	-	0.9 ± 0.3	142.5 ± 0.1	847 ± 46
CENM-1	88 ± 8	0.9 ± 0.5	129.3 ± 1.2	626 ± 56	1.1 ± 0.4	146.5 ± 1.3	714 ± 62
CENM-2	153 ± 8	0.9 ± 0.3	135.3 ± 2.0	464 ± 40	0.9 ± 0.3	137.7 ± 2.0	617 ± 74
CENM-3	226 ± 9	0.9 ± 0.3	132.4 ± 1.5	220 ± 29	0.9 ± 0.3	136.4 ± 1.7	446 ± 99
CENM-4	270 ± 9	0.8 ± 0.3	134.7 ± 0.8	115 ± 12	0.8 ± 0.2	138.1 ± 0.4	415 ± 95
CENM-5	350 ± 8	0.7 ± 0.2	131.9 ± 1.2	56 ± 9	0.8 ± 0.3	140.5 ± 0.8	407 ± 80
PSF-3h	-	0.8 ± 0.2	138.7 ± 0.5	-	-	-	564 ± 37

As it is expected, there is an increase of the PSF layer thickness with the increase of the electrospinning time of the PSF polymer solution (see τ in Table 4.3 and the EDX profile in Fig. 4.1). However, although the total electrospinning time of the DL-ENMs was maintained at 3 h, the total thickness was decreased with the increase of the PSF layer (see τ_t in Table 4.3). This may be attributed to lower viscosity and higher surface tension of PSF solution compared to PVDF one. As it was planned, the thickness of the PSF layer of the DL-ENMs increased gradually from 88.5 to 350.4 μm with increasing electrospinning time of the PSF polymer solution approaching that of the PSF SL-ENM (i.e. 563.9 μm), whereas the thickness of the PVDF layer was reduced from that of the PVDF SL-ENM (i.e. 847.1) to 56.4 μm of the CENM-5 prepared with only half an hour of PVDF electrospinning time. Almost similar results were obtained by Essalhi and Khayet [36] for PVDF SL-ENMs, whose thickness was increased significantly with the increase of the electrospinning time (i.e. when the electrospinning time was increased from 1 h to 3h the thickness of the PVDF ENMs was increased from 144.5 to 833.4 μm, which are almost similar to the obtained results for the CENM-4 and PVDF-3h).

The water contact angle (θ_w) of both the PSF and PVDF layers of the DL-ENMs did not show any clear trend with the change of the electrospinning time of the two polymer

solutions. However, the θ_w values of the PVDF layer of the DL-ENMs are greater than those of the PSF layer. This is attributed partly to the PSF that is more hydrophilic than PVDF and to the roughness of the ENMs since the electrospinning operation conditions were maintained the same for both polymer solutions. The obtained θ_w of the PSF ENM are due to the web structure and high roughness of the top membrane surface. Arribas et al. [19] demonstrated this fact by measuring and comparing the θ_w of the PSF flat sheet membrane and the PSF ENMs (i.e. 82.3 $\pm$ 2.1 and 121.8, respectively), both prepared with same polymer solution. It was observed that the θ_w of the PSF ENMs was higher (i.e. average of 121.8º) than that of the PSF phase inversion membrane (i.e. 82.3º $\pm$ 2.1º). The θ_w values of the PVDF layer of the DL-ENMs and PVDF SL-ENMs prepared in this study are quite similar to those reported by Esslahi and Khayet [36] but are greater than those of the PVDF ENMs reported by Feng et al. [19,20] and Prince et al. [21] (128º).

The DSC results of both the DL-ENMs and the SL-ENMs together with the PVDF and PSF polymers are summarized in Table 4.4 and the obtained heating and cooling curves are plotted in Fig. 4.2. The melting temperature (T_m) increased slightly with the addition of the PSF layer of the DL-ENMs, whereas the crystallization temperature (T_c) was similar to that of PVDF polymer whose exothermic crystallization peak was registered around 141ºC. However, the enthalpy of melting (ΔH_m) and the enthalpy of crystallization (ΔH_c) were clearly decreased with increasing the PSF layer thickness of the DL-ENMs. This is expected since the polymer PSF is amorphous as it can be seen in Fig. 4.2. It is worth quoting that Essalhi and Khayet [36] obtained a similar T_m value (159.3$\pm$ 0.2ºC) for PVDF SL-ENM; Prince et al. [37] reported a slightly higher T_m value (164.21ºC) for a PVDF ENM of 300 μm thickness; but Feng et al. [29] reported a smaller T_m value (153ºC). These variations may be due to the type of PVDF polymer and solvent(s) used as well as to the applied electrospinning conditions.

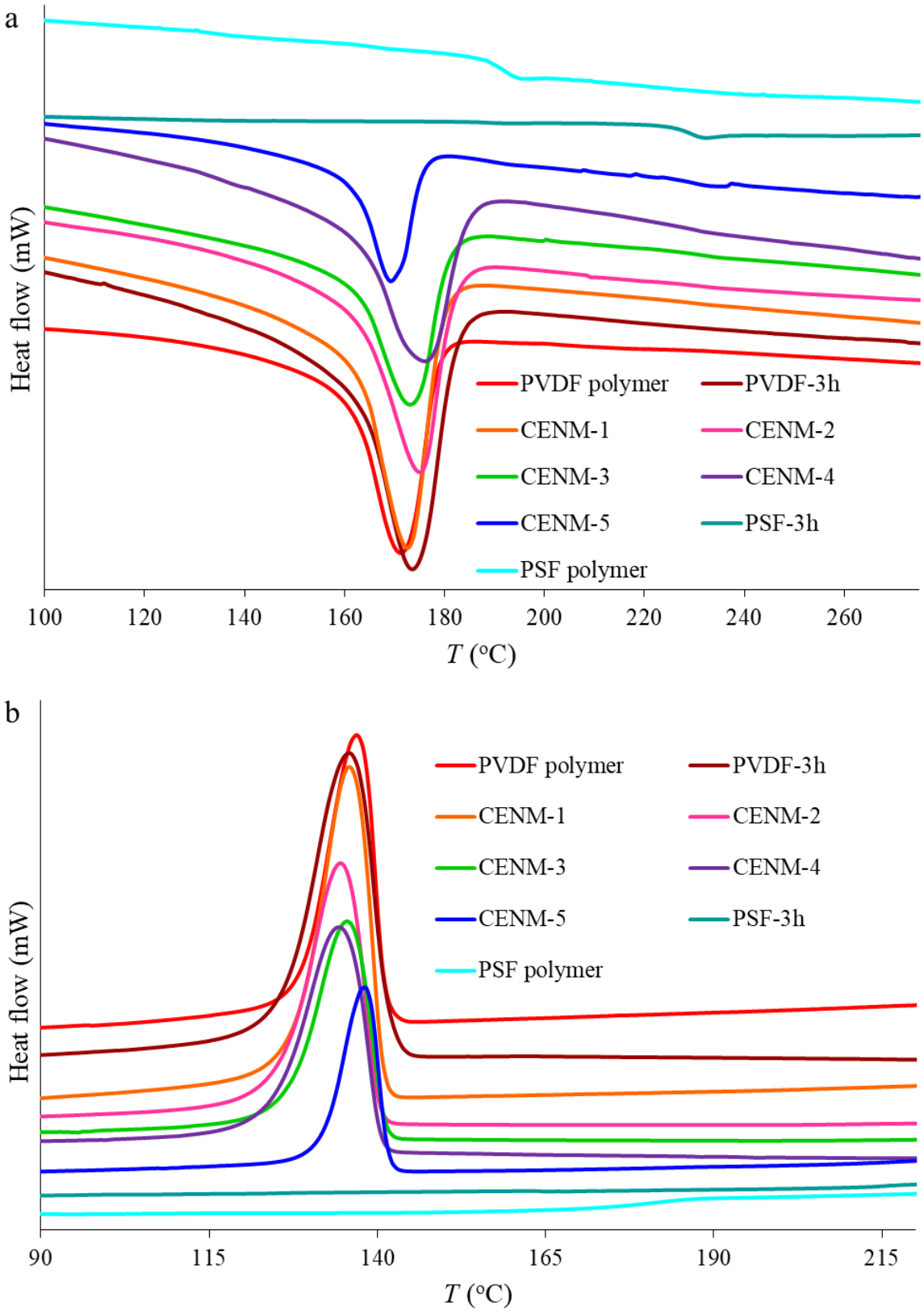

Figure 4.2. *DSC thermograms for (a) heating and (b) cooling of the polymers PVDF and PSF, the DL-ENMs and the PSF and PVDF SL-ENMs.*

Table 4.4. *DSC results: melting temperature (Tm), crystallization temperature (Tc), enthalpy of melting (ΔHm), enthalpy of crystallization (ΔHc), degree of crystallinity of melting (Xm), degree of crystallinity of crystallization (Xc) and glass transition temperature (Tg) of both the PVDF and PSF polymers and the prepared SL-ENMs and DL-ENMs.*

Membrane	T_m (ºC)	ΔH_m (J/g)	X_m (%)	T_c (ºC)	ΔH_c (J/g)	X_c (%)	T_g (ºC)
PVDF polymer	159.7 ± 0.8	40.0 ± 0.5	38.3 ± 0.4	141.14 ± 0.12	39.5 ± 0.5	37.8 ± 0.7	-
PVDF-3h	159.1 ± 0.6	40.8 ± 0.3	39.0 ± 0.3	140.6 ± 0.4	40.4 ± 0.6	38.7 ± 0.6	-
CENM-1	160.3 ± 0.3	39.1 ± 0.8	37.4 ± 0.7	141.7 ± 0.2	39.5 ± 0.3	37.7 ± 0.3	-
CENM-2	161.1 ± 0.1	36.9 ± 0.2	35.3 ± 0.2	141.6 ± 0.4	37.8 ± 0.4	36.2 ± 0.4	-
CENM-3	161.1 ± 0.2	33.6 ± 0.5	32.1 ± 0.5	141.25 ± 0.2	34.9 ± 0.3	33.4 ± 0.3	-
CENM-4	161.3 ± 0.3	29.6 ± 0.8	28.3 ± 0.3	141.10 ± 0.04	31.9 ± 0.4	30.5 ± 0.4	-
CENM-5	161.0 ± 0.1	24.7 ± 0.8	23.7 ± 0.8	141.47 ± 0.2	26.8 ± 0.3	25.6 ± 0.3	228.6 ± 0.4
PSF-3h	-	-	-	-	-	-	228.6 ± 0.3
PSF polymer	-	-	-	-	-	-	197.8 ± 0.6

The degree of crystallinity of the DL-ENMs, SL-ENMs and PVDF polymer was determined from the melting and crystallization DSC scans, X_m and X_c, respectively [58]:

$$X_m = \frac{\Delta H_m}{\Delta H^*} 100 \quad (4.1)$$

$$X_c = \frac{\Delta H_c}{\Delta H^*} 100 \quad (4.2)$$

where ΔH^* is the heat of fusion of pure crystalline PVDF (104.6 kJ/kg [59]). As shown in Table 4.4 the degree of crystallinity of the DL-ENMs was reduced with the increase of PSF layer of the DL-ENMs provided that PSF is an amorphous polymer. The glass transition temperature (T_g) could not be detected for PVDF polymer, PVDF SL-ENM and DL-ENMs prepared with PVDF electrospinning time of PVDF solution higher than 0.5 h (see Fig. 4.2(b) and Table 4.4), because PVDF has a negative T_g of about -35ºC, which is out of the DSC temperature range.

The tensile stress/strain behavior of the DL-ENMs and the PSF and PVDF SL-ENMs is presented in Fig. 4.3 and the corresponding mechanical data are summarized in Table 4.5. The decrease of the thickness of the PVDF layer resulted in a gradual enhancement of the Young´s modulus of the DL-ENMs towards that of the PSF SL-ENM. It is to point out that Young´s modulus of the PVDF SL-ENM is higher than that of the PSF SL-ENM, and all DL-ENMs have lower Young´s modulus than those of PSF and PVDF SL-ENMs. From the stress-strain curves plotted in Fig. 4.3 it can be seen for all DL-ENMs an echelon corresponding to the breaking of the PSF layer before the PVDF layer. This echelon was not detected for the SL-ENMs, PSF-3h and PVDF-3h. Therefore, from the observed echelon the tensile stress and strain at break of the PSF layer of the DL-ENMs were determined whereas those of the PVDF layer were determined from the end of the stress-strain curve. A sharp decrease of both the tensile stress and the strain at break were observed for the PVDF layer of the DL-ENMs with the reduction of its electrospinning time (i.e. decrease of the thickness of the PVDF layer) approaching values lower than those of the PSF SL-ENM. On the contrary, although the thickness of the PSF layer was increased, the tensile stress of the PSF layer of the DL-ENMs was decreased. This may be attributed to the more open structure of the PSF layer compared to PVDF layer or which is the same to the better mechanical resistance of the PVDF layer. No clear trend could be detected between the thickness of the PSF layer and the strain at break (Table 4.5). The tensile stress and the strain at break of the PVDF SL-ENM (i.e. PVDF-3h ENMs) are 1.7 and 2.7 times greater than that of the CENM-1, which was prepared by only 0.5 h electrospinning time of PSF (i.e. τ = 88.5 μm). In addition, the CENM-3 membrane that was prepared with the same electrospinning time of both polymer solutions (i.e. both PSF and PVDF layers have almost the same thickness), exhibited a PVDF layer with greater tensile stress and strain at break than the PSF layer. Essalhi and Khayet [36] observed better mechanical properties for thicker PVDF ENMs. In MD technology, although thicker membranes improve both the mechanical properties and the thermal efficiency (i.e. based on Fourier´s law the heat transfer by conduction is smaller) the permeate flux is lower as the membrane permeability is inversely proportional to the thickness. Therefore, the thickness of the ENMs must be optimized in order to design an adequate membrane for MD [60].

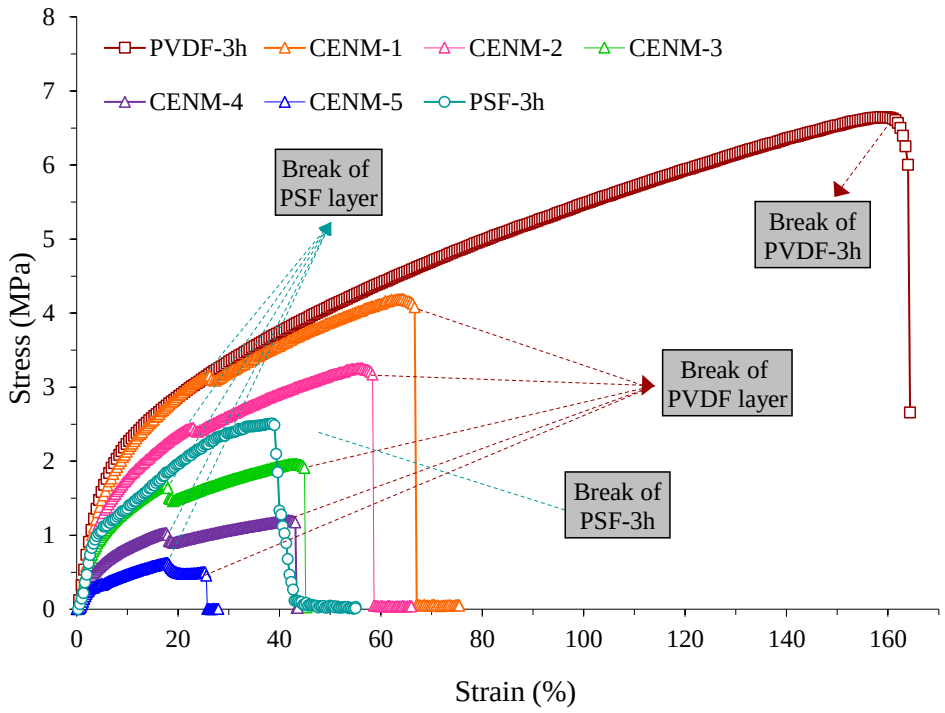

Figure 4.3. *Stress–strain curves of the prepared DL-ENMs as well as the PSF and PVDF SL-ENMs.*

Table 4.5. *Mechanical properties of the prepared DL-ENMs and SL-ENMs.*

Membrane	Young's modulus (MPa)	PSF layer		PVDF layer	
		Tensile stress at break (MPa)	Strain at break (%)	Tensile stress at break (MPa)	Strain at break (%)
PVDF-3h	58.4 ± 1.0	-	-	6.9 ± 0.4	165 ± 9
CENM-1	20.2 ± 1.3	3.08 ± 0.10	22.4 ± 2.8	4.11 ± 0.12	62 ± 4
CENM-2	26.1 ± 0.3	2.25 ± 0.07	21.6 ± 1.4	3.1 ± 0.2	53 ± 5
CENM-3	28.1 ± 1.6	1.55 ± 0.18	18.9 ± 1.7	1.92 ± 0.06	45 ± 3
CENM-4	37.7 ± 1.8	1.12 ± 0.12	20.3 ± 2.6	1.25 ± 0.07	43 ± 2
CENM-5	43 ± 3	0.60 ± 0.04	17.5 ± 0.6	0.47 ± 0.05	26.1 ± 1.1
PSF-3h	47.2 ± 0.6	2.6 ± 0.4	38.5 ± 0.3	-	-

The void volume fraction (ε), the mean size of the inter-fiber space (r) and the *LEP* values of the DL-ENMs and those of the PVDF and PSF SL-ENMs are summarized in Table 4.6. The ε values of the DL-ENMs increased gradually with the increase of the PSF layer. This result

agrees with the observed open structure of PSF from the SEM images and it may be attributed to the fact that the first deposited ENM layer over the metallic collector acts as an electric insulator affecting the dissipation of the electric charges to the collector and causes the formed fibers to repel each other resulting in a loosely packed fibrous web and a higher void volume fraction. In other words, when ENM is thin, the electric charges will dissipate easily to the metallic collector reducing the repulsion among fibers and resulting in a tightly packed ENM structure. Moreover, PSF is less electrically conductive than PVDF (see Table 4.1). Therefore, as the PSF thickness layer is increased, the ENM is less packed and therefore the void volume fraction is enhanced. Essalhi and Khayet [36] obtained an ε value for a PVDF ENM prepared with 3 h electrospinning time similar to that of the single layer PVDF membrane (87.5%). However, Feng et al. [29,32] and Prince et al. [37] reported smaller ε values (76% and 81-82%, respectively) for PVDF ENMs.

Table 4.6. *Void volume fraction (ε), mean size of the inter-fiber space (r) and liquid entry pressure (LEP) of distilled water, 12 g/L NaCl and 30 g/L NaCl aqueous solutions of the prepared DL-ENMs as well as PSF and PVDF SL-ENMs.*

Membrane code	ε (%)	r (nm)	*LEP* H_2O (10^4 Pa)	*LEP* 12 g/L (10^4 Pa)	*LEP* 30 g/L (10^4 Pa)
PVDF-3h	87.5 ± 0.3	1041 ± 34	8.9 ± 0.2	11.00 ± 0.14	9.8 ± 0.3
CENM-1	77 ± 2	509 ± 10	17.4 ± 0.3	17.90 ± 0.14	18.4 ± 0.2
CENM-2	80 ± 3	525 ± 20	15.0 ± 0.3	15.50 ± 0.14	16.30 ± 0.14
CENM-3	84.1 ± 1.7	632 ± 26	12.3 ± 0.3	12.85 ± 0.07	13.30 ± 0.14
CENM-4	87.8 ± 0.3	771 ± 28	10.0 ± 0.3	10.50 ± 0.14	11.0 ± 0.3
CENM-5	92.0 ± 1.6	945 ± 34	7.9 ± 0.4	8.30 ± 0.14	9.80 ± 0.14
PSF-3h	89.3 ± 1.1	1885 ± 48	2.9 ± 0.3	2.3 ± 0.3	1.9 ± 0.3

The inter-fiber space (i.e. maximum, mean and minimum size) of the prepared ENMs is shown in Fig. 4.4. It can be seen a gradual increase of the inter-fiber space of the DL-ENMs with the increase of the PSF layer thickness according to the void volume fraction results. This is attributed to the observed open structure of the PSF layer. The higher values of the inter-fiber space of the SL-ENMs compared to those of the DL-ENMs can be due to the coupling of the PSF and PVDF layers. When the PSF nanofibers were deposited on the PVDF nanofibers, because the same solvent was used, a very thin PVDF nanofibrous layer may be dissolved partially permitting the two types of nanofibers to fuse together resulting in a more compact

inter-layer than the PVDF and PSF layers. Feng et al. [29,32] and Prince et al. [37] reported smaller sizes of inter-fiber space than those obtained in this study. This may be attributed partly to the characterization technique used, to the electrospinning conditions and to the PVDF polymer solution.

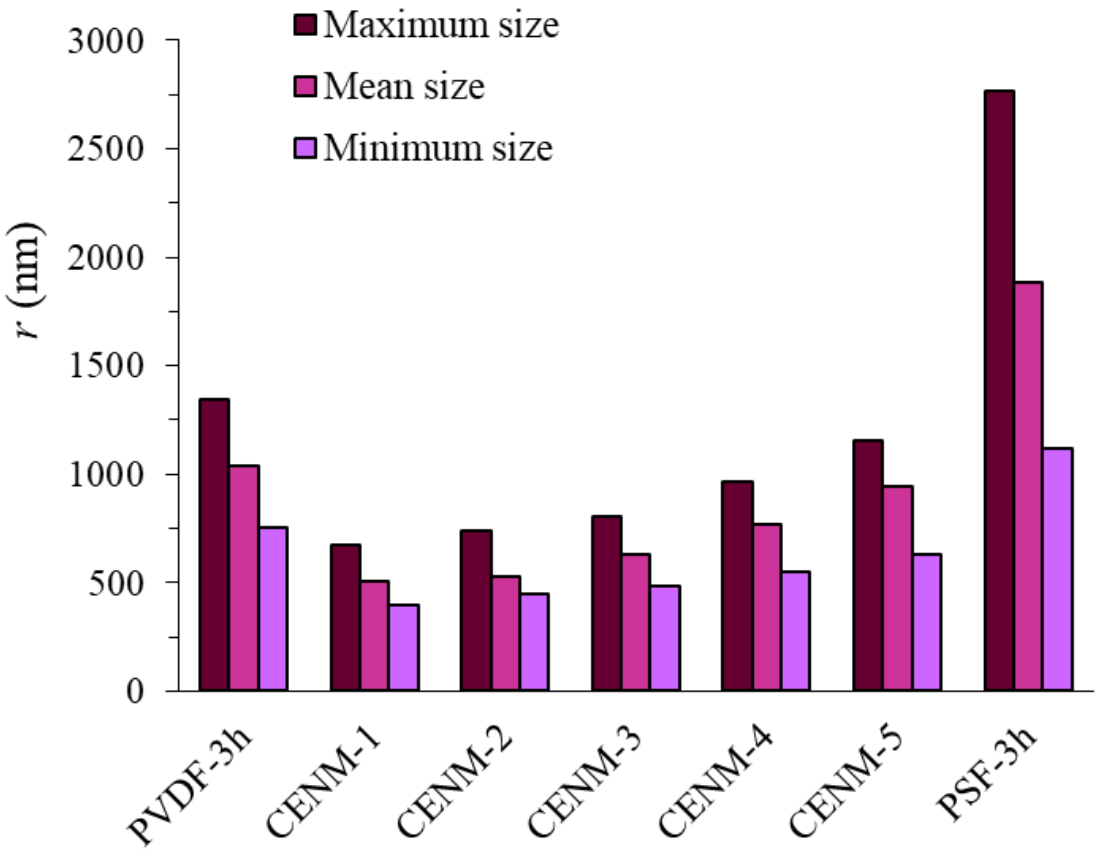

Figure 4.4. *Maximum, mean and minimum size of inter-fiber space of the DL-ENMs and SL-ENMs of PSF and PVDF.*

The measured *LEP* values of all ENMs are higher for aqueous solutions containing greater NaCl concentrations. This is attributed to the increase of the surface tension with the increase of the NaCl concentration [61]. The decrease of the *LEP* values of the DL-ENMs with the increase of the thickness of the PSF layer is attributed to the increase of the maximum size of the inter-fiber space as can be seen in Fig. 4.4 provided that the hydrophobic character of the PVDF layer is almost similar for all DL-ENMs as it was discussed previously (see θ_w in Table 4.3). Moreover, the *LEP* of the PSF SL-ENM is much smaller than that of the PVDF SL-ENM and DL-ENMs. This is attributed to the greater maximum inter-fiber space and to the less hydrophobic character of the PSF SL-ENM compared to that of the PVDF SL-ENM. It is worth quoting that Essalhi and Khayet [37] obtained a slightly lower water *LEP* value (i.e. 85

kPa) for a PVDF ENM prepared with 3h electrospinning time compared with the single layer PVDF ENM, Feng et al. [29,32] reported a higher value (i.e. 121.35 kPa) for PVDF ENM and Prince et al. [37] found a quite similar value (i.e. 90 kPa). These differences are due to the distinct PVDF polymer solution used and to the different electrospinning parameters applied.

4.3.2. DCMD experiments of the prepared ENMs

As stated previously, all the prepared ENMs have been used in desalination by DCMD configuration. Fig. 4.5 shows the obtained DCMD permeate fluxes (J_w) and the NaCl rejection factors ($\alpha = \left(1 - C_{b,p} / C_{b,f}\right) 100$, where $C_{b,p}$ and $C_{b,f}$ are the salt concentration of the bulk permeate and feed solutions, respectively). As it is well known in MD, the permeate flux of all prepared membranes decreased with the increase of the salt concentration in the feed aqueous solution because of the reduction of the transmembrane driving force due to the decrease of the water vapour pressure at the feed/ENM interface and the effect of the concentration polarization [62]. The permeate flux of the DL-ENMs is higher than that of the PVDF SL-ENM and it increased with increasing the thickness of the PSF layer or which is the same the decrease of the PVDF layer. This result is also related with the reduction of the total thickness and the increase of both the inter-fiber space and the void volume fraction of the DL-ENMs with the increase of the electrospinning time of the PSF polymer solution. On the other hand, due to the more open structure of the PSF layer and its high wetting propensity compared to PVDF layer, distilled water may enter the inter-fiber space of the PSF layer reducing therefore the distance between the liquid/vapour interfaces formed at both side of the DL-ENMs and finally the permeate flux is enhanced [49-52].

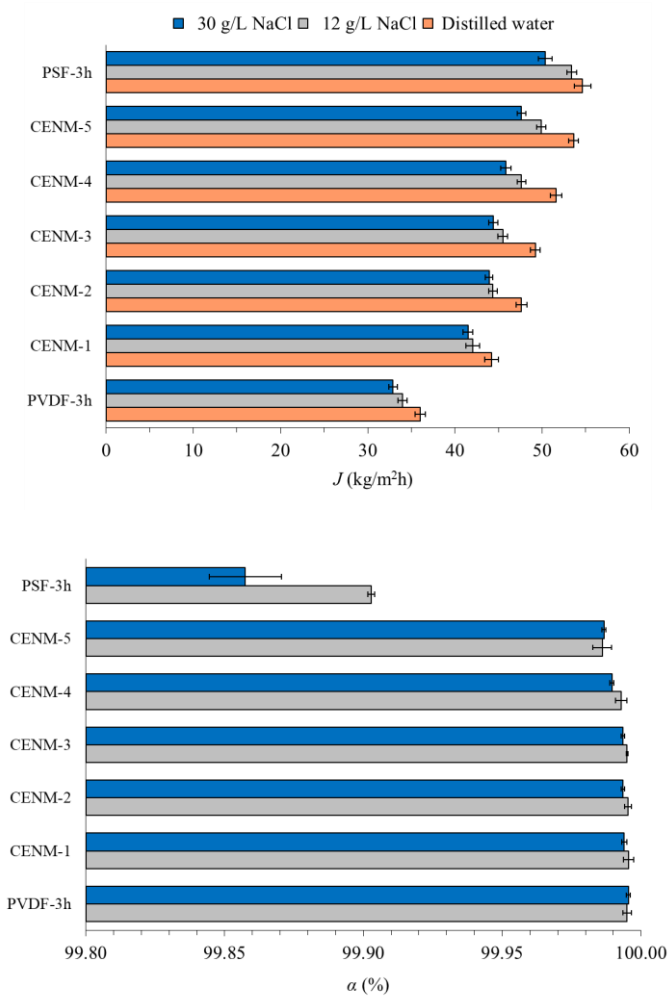

***Figure 4.5**. DCMD permeate flux (Jw) and salt rejection factor (α) of both the DL-ENMs and the PSF and PVDF SL-ENMs for distilled water and different feed concentrations of NaCl in water (12 and 30 g/L). The stirring rate of the feed and permeate liquid solutions is 500 rpm and the permeate (Tb,p) and feed (Tb,f) temperatures are 20ºC and 80ºC, respectively.*

In general, the obtained NaCl rejection factor of the DL-ENMs and the PVDF SL-ENM is greater than 99.99%. However, that of the PSF SL-ENM is smaller (i.e. the permeate electrical conductivity of this membrane increased from 2.96 to 73.49 µS/cm and from 4.98 to 180.0 µS/cm during only 3 h DCMD operation of 12 g/L and 30 g/L, respectively). This is attributed to the low *LEP* values of this membrane (see Table 4.6). Therefore, this membrane is not adequate for MD applications.

Table 4.7 summarizes the highest permeate fluxes obtained in DCMD for some laboratory prepared single, double and triple layered ENMs. As it can be seen, the DL-ENMs prepared in this study exhibit higher desalination performance than those ENMs proposed so far for desalination by DCMD. This is due to the considered double layer design and the high void volume fraction together with the size of the inter-fiber space.

Table 4.7. *Properties (mean size of the inter-fiber space, r, water contact angle, θ_w, void volume fraction, ε, and thickness, δ) as well as MD desalination performance (i.e. permeate flux, J_w and salt rejection factor, α) of different types of single, double and triple layered ENMs reported in the literature.*

Membrane		MD configuration	*r* (μm)	θ_w (º)	*ε* (%)	δ (μm)	Feed solution		Permeate[a]	J_w (kg m^{-2} h^{-1})	*α* (%)	Ref.
							NaCl (g/L)	T_f (ºC)	T_p(ºC)			
SL-ENMs	PVDF	DCMD	0.18	138	71.4	71	35	50	20	11	>99.99	[30]
	PVDF (Heat press)		0.21	136	53.7	42				21		
	PVDF	DCMD	3.6	87.5	93	144	30	60	20	17.3	99.99	[36]
								80	20	35.3		
	PVDF	DCMD	0.58	128	82	300	35	60	17	1.7	98.3	[37]
								80	17	5.3		
	PVDF/clay (Cloisite 20A)		0.64	154	81	300	35	60	17	2.2	99.95	
								80	17	5.8		
	PVDF	AGMD	–[b]	130	–[b]	–[b]	35	62	22	4.3	99.4	[29]
								82	22	11.2	99.2	
	PVDF	DCMD	0.39	128	95	228	30	55	10	12.44	99.99	[63]
	PVDF-HFP		0.34	125	90	55				13.28		
	PVDF/SiO_2	DCMD	0.69	156	82	102	35	60	20	18.1	>99.9[c]	[64]
	PVDF/SiO_2	DCMD	0.61	152	80	100	35	60	20	41.1	>99.99	[65]
	PVDF/SiO_2	DCMD	0.23	152	79	173	35	60	15	25	99.99	[39]
	PVDF/DPA/Ag	DCMD	0.34	153	77	47	35	60	20	31.6	99.99	[66]
	PVDF-HFP (Heat press)	DCMD	0.42	148	86	90	35	60	20	29	99.99	[46]
	PVDF-HFP/SiO_2	DCMD	0.42	150	–[b]	–[b]	58 (1 M)	60	20	13	>99.99	[67]

Table 4.7 (continuation). *Properties (mean size of the inter-fiber space, r, water contact angle, θ_w, void volume fraction, ε, and thickness, δ) as well as MD desalination performance (i.e. permeate flux, J_w and salt rejection factor, α) of different types of single, double and triple layered ENMs reported in the literature.*

Membrane		MD configuration	*r* (μm)	θ_w (º)	*ε* (%)	δ (μm)	Feed solution		Permeate[a]	J_w (kg m^{-2} h^{-1})	*α* (%)	Ref.
							NaCl (g/L)	T_f (ºC)	T_p(ºC)			
	PVDF-HFP /graphene	AGMD	0.86	162	89	100	35	60	20	22.9	>99.99	[44]
	F-POD	DCMD	1.7	153	–[b]	–[b]	Red Sea water	60	22	41	99.95	[68]
								80	22	78		
	F-PT		2.7	162	–[b]	–[b]		60	22	42	99.95	
								80	22	85		
	PA6(3)T	AGMD	0.07	151	–[b]	55	35	60	25	10	99.98	[69]
	Matrimid 5218	DCMD	2.15	130	–[b]	–[b]	30	60	20	23	99.99	[70]
DL-ENMs	PVDF-SiO_2/PVDF	DCMD	0.32	154	80	72	35	60	20	24.6	99.99	[34]
	FS-PVDF-SiO_2/PET		0.36	150	64	76				21		
	PVDF-SiO_2/PVDF	DCMD	2.1	139		61	35	27.5	15	6.8	99.98	[71]
	PVDF-SiO_2/PVDF (SiO_2+PDMS)	DCMD	0.21	163	81	159	35	60	20	27.5	99.99	[39]
	PVDF-HFP (2 layers)	DCMD	0.26	125	58	110	10	65	24	21	98	[72]
	PVDF-HFP (2 layers Heat press)		0.51	124	55	170		50	24	9	98	
	PVDF-HFP/PVA	AGMD	0.13	122.4	86.7	94.1	35	60	20	13	98.5	[47]

Table 4.7 (Continuation). *Properties (mean size of the inter-fiber space, r, water contact angle, θ_w, void volume fraction, ε, and thickness, δ) as well as MD desalination performance (i.e. permeate flux, J_w and salt rejection factor, α) of different types of single, double and triple layered ENMs reported in the literature.*

Membrane		MD configuration	*r* (μm)	θ_w (º)	*ε* (%)	δ (μm)	Feed solution		Permeate[a]	J_w (kg m^{-2} h^{-1})	*α* (%)	Ref.
							NaCl (g/L)	T_f (ºC)	T_p(ºC)			
	PVDF-HFP/Nylon		0.18	126.3	85.3	92.7		60	20	15.5	99.3	
								80	20	25	97.0	
	PVDF-HFP/PAN		0.27	128.5	81.1	96.3		60	20	10	98	
	PVDF-HFP/PAN	DCMD	1	150	90	82	35	60	20	30	>99	[48]
	PVDF-HFP-CNT/PP	DCMD	0.29	158	84	81	35	60	20	29.5	>99.99	[38]
	This work (CENM-5)	DCMD	0.94	140.5	92	407	30	60	20	19.5	99.98	
								80	20	47.7	99.99	
TL-ENMs	PVDF/PVDF-PVP/PET	AGMD	0.1	145	–[b]	175	35	60	15-20	10.2	99.8	[35]
								80	15-20	15.2	99.8	

[a] Permeate solution was distilled water or tap water
[b] The data was not shown in the paper
[c] The data was estimated from electrical conductivity data
PVDF: Polyvinylidene fluoride; PVDF-HFP: Polyvinylidene fluoride-co-hexafluoropropylene; DPA: Dopamine; F-POD: Aromatic fluorinated polyoxadiazoles; F-PT: Polytriazoles; PA6(3)T: Poly(trimethyl hexamethylene terephthalamide); FS: Fluorolink S10; PET: Polyethylene terephthalate; PDMS: Polydimethylsiloxane (SYLGARD184); PVA: Polyvinyl alcohol; PAN: Polyacrylonitrile; CNT: Carbon nanotubes; PP: Polypropylene; PVP: Polyvinylpyrrolidone

4.4. Conclusions

In this paper we demonstrated that dual layered ENMs (DL-ENMs) consisting of two polymers of different hydrophobicities had better DCMD desalination performance than single layer ENMs (SL-ENMs) prepared under the same electrospinning time.

The prepared DL-ENMs exhibited a strong cohesive fibrous structure with a random fiber distribution and more open PSF layer web structure than the PVDF layer. Although the total electrospinning time of the DL-ENMs was maintained at 3 h, the total thickness was decreased with the increase of the PSF layer.

Because PSF is an amorphous polymer, the enthalpy of melting (ΔH_m) and crystallization (ΔH_c) as well as the degree of crystallinity of the DL-ENMs were decreased with increasing the PSF layer thickness.

The decrease of the thickness of the PVDF layer resulted in a gradual enhancement of the Young´s modulus of the DL-ENMs towards that of the single layer PSF ENM. For all DL-ENMs the breaking of the PSF layer occurred before the PVDF layer.

The *LEP* of the DL-ENMs was decreased with the increase of the thickness of the PSF layer whereas the void volume fraction (ε) was gradually increased. This is attributed to the open structure of PSF due to the fact that the deposited layer of the ENM over the metallic collector acted as an electric insulator affecting the dissipation of the electric charges to the collector and caused the formed fibers to repel each other resulting in a loosely packed fibrous web. PSF is less electrically conductive than PVDF, hence the increase of the PSF thickness layer resulted in a less packed structure.

The DCMD permeate flux of the DL-ENMs was found to be higher than that of the single layer PVDF ENM and it increased with increasing the thickness of the PSF layer. This is due not only to the reduction of the total thickness and to the increase of both the inter-fiber space and the void volume fraction of the DL-ENMs with the increase of the electrospinning time of the PSF polymer solution; but also to the more open structure of the PSF layer, which had higher wetting propensity compared to PVDF layer, reducing therefore the path between the liquid/vapour interfaces formed at both sides of the DL-ENMs and finally enhancing the permeate flux.

The DCMD permeate flux of the DL-ENMs reached values of 53.6, 49.9 and 47.7 kg/m^2.h and 99.99% NaCl rejection factors for the membrane CENM-5 with a feed temperature of 80ºC, a permeate temperature of 20ºC and an NaCl concentration of 0, 12 and 30 g/L, respectively. However, under the same conditions, the DCMD permeate flux of the electrospun single layer PVDF ENM was lower (i.e. 36.1, 34.0 and 32.9 kg/m^2.h) with also high NaCl rejection factors.

Compared to all ENMs reported so far for DCMD, the PVDF/ PSF DL-ENMs prepared in this study exhibited higher desalination performance.

4.5 References

[1] Y. Dzenis, Spinning continuous fibers for nanotechnology, Science, 304 (2004) 1917-1919.
[2] X. Wang, B. Ding, J. Yu, M. Wang, Engineering biomimetic superhydrophobic surfaces of electrospun nanomateriales, Nano Today, 6 (2011) 510-530.
[3] X.R. Li, J.W. Xie, J. Lipner, X.Y. Yuan, S. Thomopoulos, Y.N. Xia, Nanofiber scaffolds with gradations in mineral content for mimicking the tendom-to-bone insertion site, Nano Lett. 9 (2009) 2763-2768.
[4] E.R. Kenawy, G.L. Bowlin, K. Mansfield, J. Layman, D.G. Simpson, E.H. Sanders, G.E. Wnek, Release of tetracycline hydrochloride from electrospun poly(ethylene-co-vinylacetate), poly(lactic acid), and a blend, J. Control. Release 81 (2002), 57-64.
[5] A. Yang, X.M. Tao, R.X. Wang, S.C. Lee, C. Surya, Room temperature gas sensing properties of SnO2/multiwall-carbon-nanotube composite nano-fibers, Appl. Phys. Lett. 91 (2007) 133110-1, 133110-3.
[6] S.W. Choi, S.M. Jo, W.S. Lee, Y.R. Kim, An electrospun poly(vinylidene fluoride) nanofibrous membrane and its battery applications, Adv. Mater. 15 (2003) 2027-2032.
[7] C. Drew, X. Wang, K. Senecal, H. Schreuder-Gibson, J. He, J. Kumar, L.A. Samuelson, Electrospun photovoltaic cells, J. Macromol. Sci. Pure Appl. Chem. 39 (2002) 1085-1094.
[8] X. Yan, G. Liu, F. Liu, B.Z. Tang, H. Peng, A.B. Pakhomov, C.Y. Wong, Superparamagnetic triblock copolymer/Fe2O3 hybrid nano-fibers, Angew. Chem. Int. Ed. 40 (2001) 3593-3596.
[9] R. Gopal, S. Kaur, Z. Ma, C. Chan, S. Ramakrishna, T. Matsuura, Electrospun nanofibrous filtration membrane, J. Membr. Sci., 281 (2006) 581-586.
[10] R.S. Barhate, S. Ramakrishna, Nanofibrous filtering media: Filtration problems and solutions from tiny materials: Review, J. Membr. Sci., 296 (2007) 1-8.
[11] F.E. Ahmed, B.S. Lalia, R. Hashaikeh, A review on electrospinning for membrane fabrication: Challenges and applications, Desalination, 356 (2015) 15-30.
[12] S.L. Tao, T.A. Desai, Aligned arrays of biodegradable poly (epsiloncaprolactone) nanowires and nanofibers by template synthesis, Nano Lett., 7 (2007) 1463-1468.
[13] P.X. Ma, R. Zhang, Synthetic nano-scale fibrous extracellular matrix, J. Biomed. Mater. Res., 46 (1999) 60-72.
[14] J.D. Hartgerink, E. Beniash, S.I. Stupp, Self-assembly and mineralization of peptide-amphiphile nanofibers, Science, 294 (2001) 1684-1688.
[15] D.A. Rollings, S. Tsoi, J.C. Sit, J.G. Veinot, Formation and aqueous surface wettability of polysiloxane nanofibers prepared via surface initiated vapor-phase polymerization of organotrichlorosilanes, Langmuir, 23 (2007) 5275-5278.
[16] J.M. Deitzel, J. Kleinmeyer, J.K. Hirvonen, N.C. Beck Tan, Controlled deposition of electrospun poly (ethylene oxide) fibers, Polymer, 42 (2001) 8163-8170.
[17] J.C. Chen, J.A. Wu, K.H. Lin, P.J. Lin, J.H. Chen, Preparation of microfiltration membranes with controlled pore sizes by interfacial polymerization on electrospun nanofibrous membranes, Polym. Eng. Sci., 54 (2014) 430–437.
[18] R. Gopal, S. Kaur, Z. Ma, C. Chan, S. Ramakrishna, T. Matsuura, Electrospun nanofibrous filtration membrane, J. Membr. Sci., 281 (2006) 581–586.
[19] P. Arribas, M. Khayet, M.C. García-Payo, L. Gil, Self-sustained electro-spun polysulfone nano-fibrous membranes and their surface modification by interfacial polymerization for micro- and ultra-filtration, Sep. Purif. Technol.., 138 (2014) 118-129.
[20] Z.W. Ma, M. Kotaki, S. Ramarkrishna, Surface modified nonwoven poly- sulphone (psu) fiber mesh by electrospinning: a novel affinity membrane, J. Membr. Sci., 272 (2006) 179–187.

[21] N.N. Bui, M.L. Lind, E.M.V. Hoek, J.R. McCutcheon, Electrospun nanofiber supported thin film composite membranes for engineered osmosis, J. Membr. Sci. 385–386 (2011) 10–19.
[22] S.F. Pan, Y. Dong, Y.M. Zheng, L.B. Zhong, Z.H. Yuan, Self-sustained hydrophilic nanofiber thin film composite forward osmosis membranes: Preparation, characterization and application for simulated antibiotic wastewater treatment, J. Membr. Sci., 523 (2017) 205-215.
[23] X. Song, Z. Liu, D.D. Sun, Nano gives the answer: breaking the bottleneck of internal concentration polarization with a nanofiber composite forward osmosis membrane for a high water production rate, Adv. Mater., 23 (2011) 3256–3260.
[24] M. Tian, R. Wang, K. Goh, Y. Liao, A.G. Fane, Synthesis and characterization of high-performance novel thin film nanocomposite PRO membranes with tiered nanofiber support reinforced by functionalized carbon nanotubes, J. Membr. Sci., 486 (2015) 151-160.
[25] M. Khayet, M.C. García-Payo, Nanostructured Flat membranes for Direct Contact Membrane Distillation. PCT/ES2011/000091, WO/2011/117443 (2011).
[26] L.D. Tijing, J.S. Choi, S. Lee, S.H. Kim, H.K. Shon, Recent progress of membrane distillation using electrospun nanofibrous membrane, J. Membr. Sci., 453 (2014) 435-462.
[27] M. Khayet, T. Matsuura, Membrane Distillation: Principles and Applications, Elsevier, The Netherlands, 2011.
[28] M. Khayet, Membranes and theoretical modeling of membrane distillation: a review, Adv. Colloid Interface Sci., 164(1-2) (2011) 56-88.
[29] C. Feng, K.C. Khulbe, T. Matsuura, R. Gopal, S. Kaur, S. Ramakrishna, M. Khayet, Production of drinking water from saline water by air-gap membrane distillation using polyvinylidene fluoride nanofiber membrane, J. Membr. Sci., 311 (2008) 1-6.
[30] Y. Liao, R. Wang, M. Tian, C. Qiu, A.G. Fane, Fabrication of polyvinylidene fluoride (PVDF) nanofiber membranes by electro-spinning for direct contact membrane distillation, J. Membr. Sci., 425-426 (2013) 30-39.
[31] M. Essalhi, M. Khayet, Self-sustained webs of polyvinyliden fluoride electrospun nano-fibers: Effects of polymer concentration and desalination by direct contact membrane distillation, J. Membr. Sci., 454 (2014) 133-143.
[32] C. Feng, K.C. Khulbe, S. Tabe, Volatile organic compound removal by membrane gas stripping using electro-spun nanofiber membrane, Desalination, 287 (2012) 98-102.
[33] Z.Q. Dong, X.H. Ma, Z.L. Xu, W.T. You, F.B. Li, Superhydrophobic PVDF–PTFE electrospun nanofibrous membranes for desalination by vacuum membrane distillation, Desalination, 347 (2014) 175-183.
[34] Y. Liao, C.H. Loh, R. Wang, A.G. Fane, Electrospun superhydrophobic membranes with unique structures for membrane distillation, ACS Appl. Mater. Interfaces, 6 (2014) 16035-16048.
[35] J.A. Prince, V. Anbharasi, T.S. Shanmugasundaram, G. Singh, Preparation and characterization of novel triple layer hydrophilic-hydrophobic composite membrane for desalination using air gap membrane distillation, Sep. Purif. Technol., 118 (2013) 598-603.
[36] M. Essalhi, M. Khayet, Self-sustained webs of polyvinylidene fluoride electrospun nanofibers at different electrospinning times: 1. Desalination by direct contact membrane distillation, J. Membr. Sci., 433 (2013) 167-179.
[37] J.A. Prince, G. Singh, D. Rana, T. Matsuura, V. Anbharasi, T.S. Shanmugasundaram, Preparation and characterization of highly hydrophobic poly(vinylidene fluoride)-clay nanocomposite nanofiber membranes (PVDF-clay NNMs) for desalination using direct contact membrane distillation, J. Membr. Sci., 397-398 (2012) 80-86.
[38] L.D. Tijing, Y.C. Woo, W.G. Shim, T. He, J.S. Choi, S.H. Kim, H.K. Shon, Superhydrophobic nanofiber membrane containing carbon nanotubes for high-performance direct contact membrane distillation, J. Membr. Sci., 502 (2016) 158-170.
[39] C. Su, J. Chang, K. Tang, F. Gao, Y. Li, H. Cao, Novel three-dimensional superhydrophobic and strength-enhanced electrospun membranes for long-term membrane distillation, Sep. Purif. Technol., 178 (2017) 279-287.

[40] E.J. Lee, A.K. An, T. He, Y.C. Woo, H.K. Shon, Electrospun nanofiber membranes incorporating fluorosilane-coated TiO2 nanocomposite for direct contact membrane distillation, J. Membr. Sci., 520 (2016) 145-154.
[41] Y.C. Woo, Y. Chen, L.D. Tijing, S. Phuntsho, T. He, J.S. Choi, S.H. Kim, H.K. Shon, CF4 plasma-modified omniphobic electrospun nanofiber membrane for produced water brine treatment by membrane distillation, J. Membr. Sci., 529 (2017) 234-242.
[42] A.K. An, J. Guo, E.J. Lee, S. Jeong, Y. Zhao, Z. Wang, T. Leikne, PDMS/PVDF hybrid electrospun membrane with superhydrophobic property and drop impact dynamics for dyeing wastewater treatment using membrane distillation, J. Membr. Sci., 525 (2017) 57-67.
[43] E.J. Lee, A.K. An, P. Hadi, S. Lee, Y.C. Woo, H.K. Shon, Advanced multi-nozzle electrospun functionalized titanium dioxide/polyvinylidene fluoride-co-hexafluoropropylene (TiO2/PVDF-HFP) composite membranes for direct contact membrane distillation, J. Membr. Sci., 524 (2017) 712-720.
[44] Y.C. Woo, L.D. Tijing, W.G. Shim, J.S. Choi, S.H. Kim, T. He, E. Drioli, H.K. Shon, Water desalination using graphene-enhanced electrospun nanofiber membrane via air gap membrane distillation, J. Membr. Sci., 520 (2016) 99-110.
[45] L.F. Ren, F. Xia, J. Shao, X. Zhang, J. Li, Experimental investigation of the effect of electrospinning parameters on properties of superhydrophobic PDMS/PMMA membrane and its application in membrane distillation, Desalination, 404 (2017) 155-166.
[46] M. Yao, Y.C. Woo, L.D. Tijing, W.G. Shim, J.S. Choi, S.H. Kim, H.K. Shon, Effect of heat-press conditions on electrospun membranes for desalination by direct contact membrane distillation, Desalination, 378 (2016) 80-91.
[47] Y.C. Woo, L.D. Tijing, M.J. Park, M. Yao, J.S. Choi, S. Lee, S.H. Kim, K.J. An, H.K. Shon, Electrospun dual-layer nonwoven membrane for desalination by air gap membrane distillation, Desalination, 403 (2017) 187-198.
[48] L.D. Tijing, Y.C. Woo, M.A.H. Johir, J.S. Choi, H.K. Shon, A novel dual-layer bicomponent electrospun nanofibrous membrane for desalination by direct contact membrane distillation, Chem. Eng. J., 256 (2014) 155-159.
[49] M. Khayet, T. Matsuura, Application of surface modifying macromolecules for the preparation of membranes for membrane distillation, Desalination, 158 (2003) 51-56.
[50] M. Khayet, T. Matsuura, J.I. Mengual, Porous hydrophobic/hydrophilic composite membranes: Estimation of the hydrophobic-layer thickness, J. Membr. Sci., 266 (2005) 68-79.
[51] M. Qtaishat, M. Khayet, T. Matsuura, Guidelines for preparation of higher flux hydrophobic/hydrophilic composite membranes for membrane distillation, J. Membr. Sci., 329 (2009) 193-200.
[52] M. Essalhi, M. Khayet, Surface segregation of fluorinated modifying macromolecule for hydrophobic/hydrophilic membrane preparation and application in air gap and direct contact membrane distillation, J. Membr. Sci., 417-418 (2012) 163-173.
[53] J. Zuo, T.S. Chung, G.S. O'Brien, W. Kosar, Hydrophobic/hydrophilic PVDF/Ultem® dual-layer hollow fiber membranes with enhanced mechanical properties for vacuum membrane distillation, J. Membr. Sci., 523 (2017) 103-110.
[54] F. Edwie, M.M. Teoh, T.S. Chung, Effects of additives on dual-layer hydrophobic-hydrophilic PVDF hollow fiber membranes for membrane distillation and continuous performance, Chem. Eng. Sci., 68 (2012) 567–578.
[55] M.M. Teoh, T.S. Chung, Y.S. Yeo, Dual-layer PVDF/PTFE composite hollow fibers with a thin macrovoid-free selective layer for water production via membrane distillation, Chem. Eng. J., 171 (2011) 684–691.
[56] S. Bonyadi, T.S. Chung, Flux enhancement in membrane distillation by fabrication of dual layer hydrophilic-hydrophobic hollow fiber membranes, J. Membr. Sci. 306 (2007) 134–146.

[57] M. Essalhi, M. Khayet, Self-sustained webs of polyvinylidene fluoride electrospun nanofibers at different electrospinning times: 2. Theoretical analysis, polarization effects and thermal efficiency, J. Membr. Sci., 433 (2013) 180-191.
[58] G. Mago, D.M. Kalyon, F.T. FISHER, Membranes of polyvinylidene fluoride and PVDF nanocomposites with carbon nanotubes via immersion precipitation, J. Nanomaterials, Article ID 759825 (2008) 759825.
[59] Y.J. Park, Y.S. Kang, C. Park, Micropatterning of semicrystalline poly(vinylidene fluoride) (PVDF) solutions, Eur. Polymer J., 41 (2005) 1002-1012.
[60] L Eykens, I. Hitsov, K. De Sitter, C. Dotrement, L. Pinoy, I. Nopens, B. Van der Bruggen, Influence of membrane thickness and process conditions on direct contact membrane distillation at different salinities, J. Membr. Sci., 498 (2016) 353-364.
[61] CRC Handbook of Chemistry and Physics, CRC PRESS, INC., David R. Lide (Editor-in-Chief, 73RD Edition 1992-1993
[62] J. Xu, W.B. Singh, G.L. Amy, N. Ghaffour, Effect of operating parameters and membrane characteristics on air gap membrane distillation performance for the treatment of highly saline water, J. Membrane Sci., 512 (2016) 73-82.
[63] C.I. Su, J.H. Shih, M.S. Huang, C.M. Wang, W.C. Shih, Y.S. Liu, A study of hydrophobic electrospun membrane applied in seawater desalination by membrane distillation, Fiber Polym., 13 (2012) 698-702.
[64] Y. Liao, R. Wang, A.G. Fane, Fabrication of bioinspired composite nanofiber membranes with robust superhydrophobicity for direct contact membrane distillation, Environ. Sci. Technol. 48 (2014) 6335−6341.
[65] X. Li, X. Yu, C. Cheng, L. Deng, M. Wang, X. Wang, Electrospun superhydrophobic organic/inorganic composite nanofibrous membranes for membrane distillation ACS Appl. Mater. Interfaces 2015, 7, 21919−21930.
[66] Y. Liao, R. Wang, A.G. Fane, Engineering superhydrophobic surface on poly(vinylidene fluoride) nanofiber membranes for direct contact membrane distillation, J. Membr. Sci. 433 (2013) 77-87.
[67] J. Lee, C. Boo, W.H. Ryu, A.D. Taylor, M. Elimelech, Development of omniphobic desalination membrane using a charged electrospun nanofiber scaffold, ACS Appl. Mater. Interfaces, 8 (2016) 11154-11161.
[68] H. Maab, L. Francis, A. Al-saadi, C. Aubry, N. Ghaffour, G. Amy, S.P. Nunes, Synthesis and fabrication of nanostructured hydrophobic polyazole embranes for low-energy water recovery, J. Membr. Sci., 423-424 (2012) 11-19.
[69] F. Guo, A. Servi, A. Liu, K.K. Gleason, G.C. Rutledge, Desalination by membrane distillation using electrospun polyamide fiber membranes with surface fluorination by chemical vapor deposition, ACS Appl. Mater. Interfaces 7 (2015) 8225−8232.
[70] L. Francis, H. Maab, A. AlSaadi, S. Nunes, N. Ghaffour, G.L. Amy, Fabrication of electrospun nanofibrous membranes for membrane distillation application, Desalination Water Treat. 51 (2013) 1337-1343
[71] J. E. Efome, D. Rana, T., C.Q. Lan, Enhanced performance of PVDF nanocomposite membrane by nanofiber coating: A membrane for sustainable desalination through MD, Water Res. 89(2016) 39-49.
[72] B.S. Lalia, E. Guillen-Burrieza, H.A. Arafat, R. Hashaikeh, Fabrication and characterization of polyvinylidenefluoride-co-hexafluoropropylene (PVDF-HFP) electrospun membranes for direct contact membrane distillation, J. Membr. Sci., 428 (2013) 104-115

Chapter 5

Electrospun Nanostructured Membrane Engineering Using Reverse Osmosis Recycled Modules: Membrane Distillation Application

As a consequence of the increase in reverse osmosis (RO) desalination plants, the number of discarded RO modules for 2020 was estimated to be 14.8 million annually. Currently, these discarded modules are disposed of in nearby landfills generating high volumes of waste. In order to extend their useful life, in this research study, we propose recycling and reusing the internal components of the discarded RO modules, membranes and spacers, in membrane engineering for membrane distillation (MD) technology. After passive cleaning with a sodium hypochlorite aqueous solution, these recycled components were reused as support for polyvinylidene fluoride nanofibrous membranes prepared by electrospinning technique. The prepared membranes were characterized by different techniques and, finally, tested in desalination of high saline solutions (brines) by direct contact membrane distillation (DCMD). The effect of the electrospinning time, which is the same the thickness of the nanofibrous layer, was studied in order to optimize the permeate flux together with the salt rejection factor and to obtain robust membranes with stable DCMD desalination performance. When the recycled RO membrane or the permeate spacer were used as supports with 60 min electrospinning time, good permeate fluxes were achieved, 43.2 and 18.1 kg m−2 h−1, respectively; with very high salt rejection factors, greater than 99.99%. These results are reasonably competitive compared to other supported and unsupported MD nanofibrous membranes. In contrast, when using the feed spacer as support, inhomogeneous structures were observed on the electrospun nanofibrous layer due to the special characteristics of this spacer resulting in low salt rejection factors and mechanical properties of the electrospun nanofibrous membrane

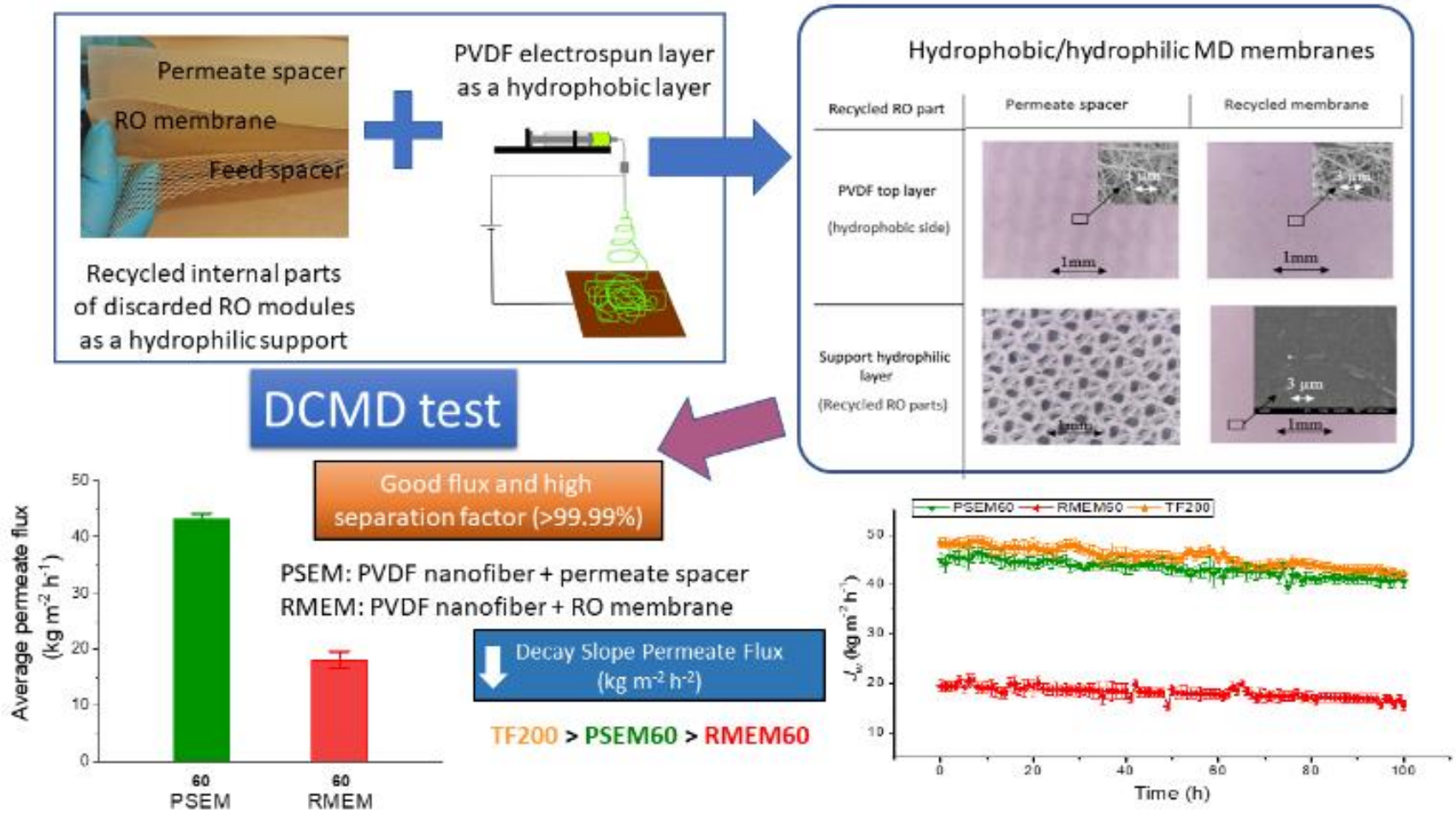
Permeate spacer
RO membrane
Feed spacer
Recycled internal parts of discarded RO modules as a hydrophilic support
PVDF electrospun layer as a hydrophobic layer
Hydrophobic/hydrophilic MD membranes
Recycled RO part
Permeate spacer
Recycled membrane
PVDF top layer
(hydrophobic side)
Support hydrophilic layer
(Recycled RO parts)
1mm
3 µm
DCMD test
Good flux and high separation factor (>99.99%)
PSEM: PVDF nanofiber + permeate spacer
RMEM: PVDF nanofiber + RO membrane
Decay Slope Permeate Flux (kg m-2 h-2)
TF200 > PSEM60 > RMEM60
Average permeate flux (kg m-2 h-1)
60 PSEM
60 RMEM
PSEM60
RMEM60
TF200
Time (h)

5.1. Introduction

Reverse osmosis (RO) is a well-established industrial membrane technology for water treatment, especially for desalination of seawater and brackish water with a 48% increase in installed capacity between 2017 and 2020. In the past year, the installed capacity was 148.4 million m^3 per day, while in 2017, the installed capacity was 99.8 million m^3 per day [1,2]. Although RO technology is undergoing continuous advances, there are still many aspects for improvement and some issues yet to be solved. One of the problems inherent to this technology is its high energy consumption associated to the high hydrostatic pressure required for the separation process especially for the treatment of high osmotic saline solutions. This problem has been already studied [3] and different strategies have been adopted to reduce this energy consumption [4]. Another intrinsic problem of this technology that needs a prompt resolution is the discharge of brines (i.e., aqueous saline solutions with an overall concentration in the range 50–82 g L^{-1}) [5].

The continuous growth of RO technology all around the world induces a critical and irreversible increase in the quantity of discarded membrane modules, generating a large amount of waste. The replacement rate of RO modules is 20% or 10% per year, depending on whether seawater or brackish water is used as feed, respectively [6]. This replacement is normally done when the RO modules present irreversible membrane fouling and a decline of their efficiency parameters [7]. For the desalination of 1000 m^3 per day, an average of 100 RO modules is needed [8]. Therefore, based on the installed capacity in 2020, an approximate number of 2.2 million annual waste RO modules is possible if 15% is taken as an average of the replacement rate of RO modules per year. Normally, the discarded modules are disposed of in nearby landfills. However, in order to comply with the EU regulations regarding the hierarchy of waste management (Directive 2008/98/CE: reduce, reuse, recycle, treat and recover energy), another strategy must be adopted. Taking into consideration that RO is a technology in full development, waste reduction is not possible. Some few studies have been proposed on the reuse of discarded RO modules, but without applying any previous membrane or module cleaning [9–11].

In 2017, more than 66% of the modules installed in RO plants were made of thin film composite (TFC)-polyamide (PA) membranes [1]. A typical TFC PA membrane is made by a support of polyester (PET) material over which a porous polysulfone (PSf) substrate is deposited by phase inversion method. Then, an active PA layer is formed on the porous PSf layer by interfacial polymerization technique [12]. This type of RO membrane was recycled using PA oxidizing agents such as sodium hypochlorite (NaOCl) to fully or partially degrade the PA layer responsible of irreversible fouling [8,10,13-20,21,22]. By applying different

exposure doses to the oxidizing agent, quantified by units of parts per million of NaOCl used in the cleaning solution multiplied by the exposure time in hours (ppm·h), discarded RO membranes have been transformed to membranes for microfiltration (MF), ultrafiltration (UF) or nanofiltration (NF) separation processes [10,13,15–18,23]. In other research studies, after exposing the RO modules to NaClO oxidizing aqueous solution, the membranes were transformed to anion or cation exchanged membranes for electrodialysis (ED) or to microsystin-degrading biofilms for membrane bioreactors by applying adequate approaches [19–22,24].

Membrane distillation (MD) is a non-isothermal separation process of emerging interest. In last decade, the interest in its development based on the number of the annual published manuscripts has grown by 702.1%. Porous and hydrophobic membranes with high porosity (i.e., void volume fraction), low thermal conductivity and high liquid entry pressure (*LEP*) are required in this process in which the temperature difference, or which is the same the vapor pressure difference, is the driving force. Different MD configurations (direct contact, DCMD; air gap, AGMD; vacuum, VMD; and sweeping gas, SGMD) were considered to establish this necessary driving force. It is applied in different fields, such as in food industry and desalination. [25]. Recent studies show the interest in the development of new nanofibrous membranes derived from ecological resources or using ion exchange polymers for the treatment of industrial and textile wastewaters as an increasingly essential research area [26,27]. For instance, treatment of RO brines by MD technology is one of the feasible solutions, enabling zero liquid discharge to the environment [28]. The combination of RO and MD technologies is a solution to RO brines disposal as it can increase water recovery [29], decrease the specific energy consumption (i.e., necessary energy per volume of produced water) [30] and protect the environment. Therefore, being able to recycle and reuse parts of discarded RO modules in MD membrane engineering for the treatment of RO brines is doubly beneficial for the environment, favoring the awaited circular economy.

The objective of the present study is to apply parts of discarded RO modules, membrane and spacers, as hydrophilic supports to MD membranes. In fact, dual-layered hydrophobic/hydrophilic membranes exhibit various advantages for the MD separation process, including their high permeate flux associated with the thin hydrophobic layer and low mass transfer resistance of the hydrophilic support, their high thermal efficiency associated to the low heat transfer by conduction through the thick hydrophilic support, and their high mechanical properties. These were proved in previous research reports [31,32]. In this study, the internal components of the discarded RO modules, membranes and spacers, were cleaned and recycled as supports for the preparation MD membranes. The necessary hydrophobic layer for the MD membranes was prepared by electrospinning

polyvinylidene fluoride (PVDF) nanofibrous layer over each recycled support, membrane, permeate and feed spacers. The electrospinning technique is commonly used for the preparation of nanostructured polymeric materials for different applications, including MD membrane engineering [31–35]. The prepared membranes were characterized by different techniques and tested in desalination of high saline solutions, brines, by DCMD.

5.2. Materials and Methods

5.2.1. End-of-Life RO Membrane Module and Hydrophilic Supports for Nanostructured MD Membranes

The discarded RO membrane modules used in a real plant located in Almeria (Spain) for brackish water treatment (spiral wound TFC-PA, 8" diameter, TM720-400, Toray Industries, Inc.,Tokyo, Japan) were cleaned and their internal parts (i.e., membrane, permeate and feed spacers) were used as supports for MD membrane preparation.

The applied cleaning procedure was as follows. At the end of their useful life, the discarded RO modules were preserved in sodium bisulphite (500–1000 ppm). After their autopsy, these modules were washed out and stored in Milli-Q water. The used discarded RO module in this study has a water permeability of 2.04 ± 0.06 L m^{-2} h^{-1} bar^{-1}, a salt rejection factor of 98.31 ± 0.24%, a colloidal fouling composition of 84% inorganic compounds and 16% organic compounds on the active layer of the RO membrane having a water contact angle of 46 ± 2° [15,16,36]. The initial water production rate of this type of membrane modules indicated by the manufacturer is 38.6 m^3/day with a salt rejection factor of 99.7% for 37 m^2 membrane area and 2 g L^{-1} salt (NaCl) aqueous feed solution subjected to 1.55 MPa. The discarded RO modules were then disassembled and all their internal parts were subjected to a passive cleaning procedure by submerging them in a sodium hypochlorite solution (6200 ppm of free chlorine) for 48 h (i.e., a total exposure dose of 300,000 ppm·h) in order to ensure the total oxidation of the PA layer of the RO membrane [15]. In order to confirm the total degradation of PA layer in the active layer of the recycled RO membrane, Attenuated Total Reflectance Fourier Transform Infrared Spectroscopy (ATR-FTIR) analysis was carried out for both the pristine and the recycled RO membrane. A Nicolet iS50 device (ThermoFisher Scientific Inc, Waltham, MA, USA equipped with the deuterated triglycine sulfate–potassium bromide (DTGS–KBr) detector and a KBr beam splitter was used and the obtained spectra are shown in Fig. 5.1.

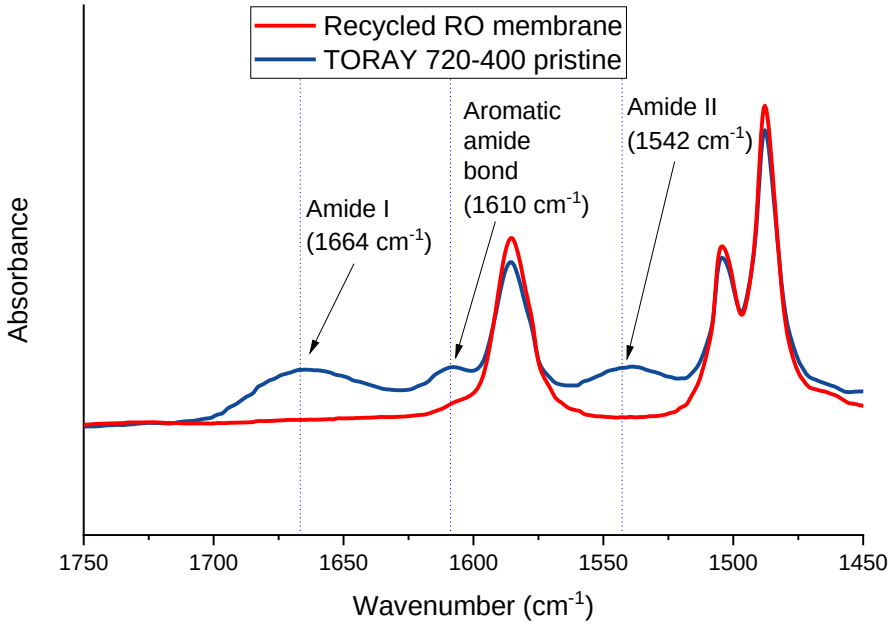

Figure 5.1. *ATR-FTIR spectra of the recycled RO and TM720-400 pristine membranes.*

The peaks corresponding to the PA (amide I and amide II bands and the C=C stretching vibrations of the aromatic amide bonds at 1664, 1542 and 1610 cm^{-1}, respectively [17]) were clearly identified in the spectra of the pristine TM720-400 commercial RO membrane but were not detected in the spectra of the recycled RO membrane confirming the total elimination of the PA layer.

In this study, the permeate PET spacer (a in Fig. 5.2), the TFC membrane with degraded PA layer (b in Fig. 5.2) and the feed polypropylene (PP) spacer (c in Fig. 5.2) were reused [37].

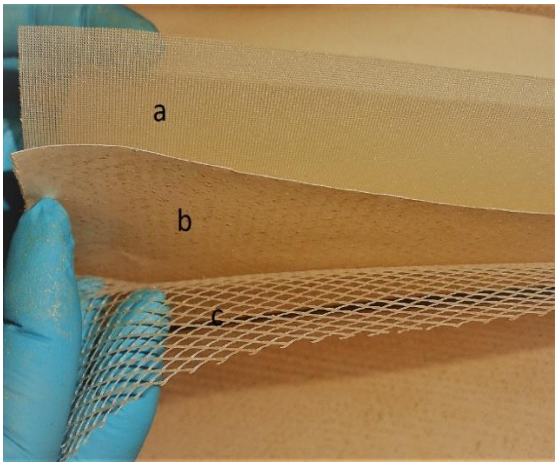

Figure 5.2. *Internal parts of the discarded RO module reused as supports for the nanofibrous MD membranes: (a) permeate spacer, (b) RO membrane and (c) feed spacer.*

5.2.2. Preparation of Nanofibrous Supported Hydrophobic/Hydrophilic MD Membranes

For the preparation of nanofibrous MD membranes, a polymer solution was prepared by dissolving 25 wt% PVDF (M_w = 275 kg mol^{-1} and M_n = 107 kg mol^{-1}) in a solvent mixture containing 20 wt% acetone and 80 wt% N,N-dimethyl acetamide, following the optimal procedure reported by Essalhi and Khayet [38]. All chemicals were purchased from Sigma-Aldrich. The polymer solution was characterized in terms of its viscosity, electrical conductivity and surface tension at room temperature (293 K) using a viscosimeter (Brookfield, DV-I+, Brookfield Ametek Co., Middleboro, MA, USA), an electrical conductivity meter (Cyber Scan con11 Conductivity/TDS/°C, Eutech Instruments, Vernon Hills, IL, USA), and CAM 100 (a contact angle system with CAM 200 Software, KSV Instruments Ltd., Monroe, CT, USA), respectively [38]. The obtained electrical conductivity, viscosity and surface tension of the polymer solution were 9.53 ± 0.03 µS cm^{-1}, 3.03 ± 0.01 Pa·s and 33.6 ± 0.6 mN m^{-1}, respectively. These data are similar to those reported by Essalhi and Khayet [38] for the same polymer solution (9.57 ± 0.03 µS cm^{-1}, 3.108 ± 0.005 Pa·s and 32.0 ± 1 mN m^{-1} for the electrical conductivity, viscosity and surface tension, respectively).

The applied electrospinning conditions were the optimal parameters claimed by Essalhi et al. [39]. An electric pump (Fisherbrand™ Single Syringe Pump, Fisher Scientific Co., Pittsburgh, PA, USA) was used to establish a flow rate of the polymer solution of 1.23 ml h^{-1} throughout a stainless-steel needle of 0.6 mm inner diameter. The electric voltage was fixed at 24.1 kV (Iseg; model T1CP 300 304P; Iseg Spezialelektronik GmbH, Radeberg, Germany), and the air gap distance between the needle tip and the copper collector was 27.7 cm. Fig. 5.3 shows the used electrospinning set-up for the preparation of the hydrophobic nanofibrous layer over the selected recycled RO hydrophilic supports. When using the recycled RO membrane as support, the PVDF nanofibers were deposited on the PET layer rather than on the PSf layer because of the risk to dissolve PSf layer during nanofibers deposition. The electrospinning time was varied from 30 to 90 min, and all prepared membranes were finally subjected to a thermal post-treatment at 333 K for 10 min in order to remove any residual solvents and improve the compact structure of the nanofibrous hydrophobic layer.

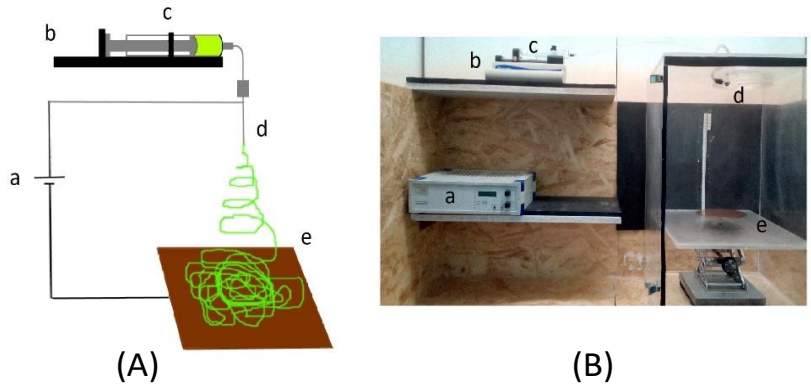

Figure 5.3. *Schema (A) and photographs (B) of the electrospinning set-up (high electric voltage source (a), circulation pump (b), syringe (c), stainless steel needle (d) and cooper collector (e).*

The electrospun nanofibrous membranes were named hereafter, RMEM, FSEM and PSEM when using the recycled RO membrane, feed spacer and permeate spacer, respectively, in which n refers to the electrospinning time 30, 60 or 90 min. For sake of comparison, unsupported hydrophobic nanofibrous membrane, NSEM, was also prepared under the same electrospinning conditions. For example, PSEM60 designates the MD membrane using the recycled permeate spacer as support and an electrospinning time of 60 min.

5.2.3. Membrane Characterization

The water contact angle was measured at 293 K with a CAM 100 Contact Angle System that captures water drop image, which is then analyzed by CAM 200 Software (KSV Instruments Ltd., Monroe, CT, USA). Twenty-five readings were considered for each membrane, and the average water contact angle together with its standard deviation are reported.

The thickness of the recycled supports (i.e., hydrophilic layer) and the total thickness of the electrospun nanofibrous membranes (i.e., hydrophobic/hydrophilic layers) were measured using a digital micrometer (model 1724-502 series, Helios-Preisser Instruments, Gammertingen, Germany). For each sample, thirty measurements were performed in different points of each sample, and the average thickness together with its standard deviation are reported.

To determine the mean size of the inter-fiber space, the porometer POROLUX™ 100 (Porometer, Eke, Belgium) was used following the protocol detailed elsewhere [38]. Three samples of each membrane were employed and the average value with its standard deviation were calculated.

The membrane porosity or void volume fraction was determined by measuring the density of the membrane using pycnometer witch isopropyl alcohol (IPA) that penetrates the void volume of the membrane and distilled water that does not. The followed procedure was detailed in our previous study [40]. Three samples of each membrane were considered to calculate the average void volume fraction together with its standard deviation.

The LEP_w of the MD membrane is the minimum pressure applied over distilled water before it penetrates into its pores having maximum size. The used set-up and the followed procedure were described in detail in our previous study [41]. In this study, an initial pressure (0.01×10^5 Pa) was applied for 30 min then, the pressure was increased in steps of 0.02×10^5 Pa for an interval of 10 min until water drops appear at the permeate side of the membrane. For each membrane, three samples were used, and the average value with its standard deviation were calculated.

The digital microscope (VHX Digital Microscope, Keyence VH-Z100R, Itasca, IL, USA) and the field emission scanning electron microscope (FESEM, JEOL Model JSM-6335F, Jeol Ltd., Tokyo, Japan) were used in to study the surface of the samples. For SEM analysis, the membrane sample was coated with a thin gold layer using a sputter-coater (EMITECH K550 X, Emitech Groupe, Montigny, France) for 1 min under 25 mA. The nanofiber diameter was measured by the image analysis software (tpsDIG2 version 2.32, State University of New York, Stony Brook, NY, USA). In this case, two different SEM images were used for each sample, and for each image more than 100 measurements were carried out to determine the average fiber diameter and its standard deviation as described elsewhere [42]. The ENMs cross section images were obtained by previously fracturing the samples in liquid nitrogen and, later, gold coated as reported elsewhere [43].

The Instron dynamometer (model 3366, Instron Ltd., Norwood, MA, USA) was used to study the mechanical properties of the prepared membranes according to ASTMA D 3379-75 specifications at 295 K.

Direct contact membrane distillation (DCMD) configuration was considered in this study to test both the unsupported and the supported electrospun nanofibrous membranes prepared in this study using recycled supports. For comparison, the same DCMD experiments were carried out for the commercial membrane TF200 (PALL Gelman Corp., New York, NY, USA). This membrane has been widely characterized in our previous studies [39] and has 165 µm thickness, 0.23 µm mean pore size, 2.8 bar LEP_w and 69% porosity. The used DCMD set-up was described in details elsewhere [32,44]. It has an effective membrane area of 1.59×10^{-3} m^2. The stirring rate was 1000 rpm, the feed temperature was 353 K and the permeate temperature was 293 K. Distilled water and NaCl aqueous solutions with different concentrations varying from 6 to 150 g L^{-1} were used as feed, while distilled water

was introduced in the permeate side of the membrane. The feed and permeate temperatures were controlled by two thermostats connected to the double-wall jacketed feed and permeate chambers of the DCMD set-up, respectively. The weight of the produced permeate (Δm) for a predetermined time (Δt) was measured using a precision balance (SI-2002, Denver Instrument Company, Arvada, CO, USA), and the permeate flux (J_w) was determined as:

$$J_w = \frac{\Delta m}{A_m \Delta t} \tag{5.1}$$

where A_m is the effective membrane area.

The above procedure was repeated three times for each membrane, and the average J_w with its standard deviation was calculated. To determine the salt concentration in both the feed and permeate chambers, the electrical conductivity (Metrohm 712Ω, Herisau, Switzerland) was measured before and after each permeate flux measurement and the salt rejection factor was calculated using the expression:

$$\alpha = \left(1 - \frac{C_p}{C_f}\right) * 100 \tag{5.2}$$

where C_p is the concentration of the permeate solution and C_f is the concentration of the feed solution.

5.2.4. Long-Term DCMD Desalination Tests

Long-term DCMD desalination tests of the prepared membranes showing adequate performance were performed using the system schematized in Fig. 5.4. The initial concentration of the feed aqueous solution was 65 g L^{-1} while the permeate was distilled water. This initial NaCl feed concentration was selected as it is an average concentration of RO brines of seawater desalination plants (50–82 g L^{-1} [5]). The membrane with an effective area of 1.26 × 10^{-3} m^2 was placed between the double wall jacketed feed and permeate chambers. The feed temperature was maintained at 353 K while that of the permeate was 293 K by means of a thermostat (TE-8D, Techne Inc., Burlington, NJ, USA) and a cryostat (N0691883 Recirculator, Poly Science®, IL, USA), respectively. The temperatures were measured by two pt100 sensors placed inside the chambers of the membrane module. A double head peristaltic pump (model 323S, Watson-Marlow Fluid Technology Group, Wilmington, DE, USA) was used for the circulation of both the feed and permeate solutions

with a flow rate of 0.8 L min^{-1}. The collected permeate each minute was measured by a precision balance (Sartorius Lab Instruments GmbH & Co., Goettingen, Germany, respectively) connected to a computer. The electrical conductivity of both the feed and permeate solutions was measured every hour (Metrohm 712 Ω, Herisau, Switzerland). The permeate flux and the salt rejection factor were also determined using Equations (1) and (2), respectively. The data were recorded every minute and then the mass differences and their associated permeate fluxes were determined. From these data, the average J_w was calculated each hour with its standard deviation.

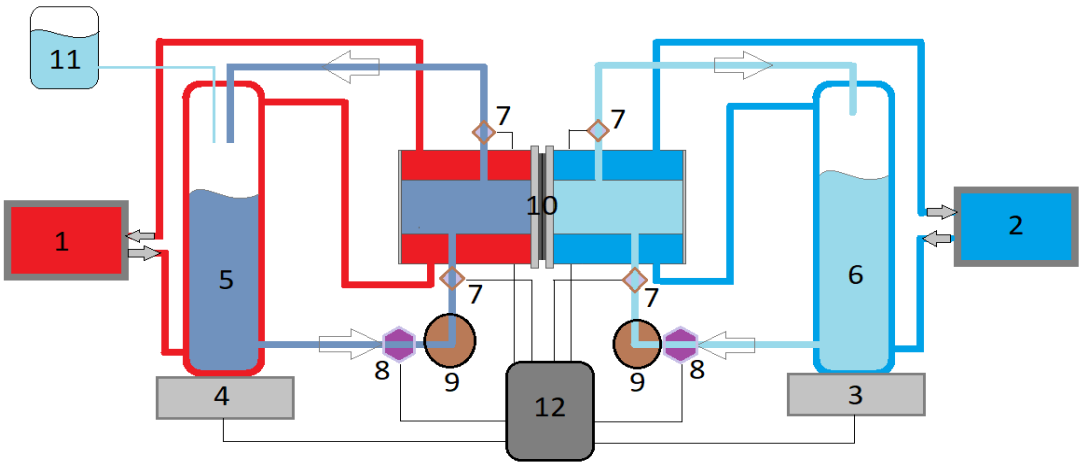

Figure 5.4. *Schema of the long-term DCMD experimental system: 1. thermostat connected to the feed container; 2. cryostat connected to the permeate container; 3. precision balance; 4. precision balance; 5. feed container; 6. permeate container; 7. temperature sensors; 8. flow rate sensors; 9. double head peristatic pump; 10. membrane module; 11. reservoir; 12. computer.*

Two types of long-term DCMD tests, regeneration test and exhaustion test, were carried out. For the first test, the feed salt concentration was kept constant around 65 g L^{-1} by introducing an adequate amount of distilled water in the feed tank comparable to that of the permeate; the second test consists of the concentration of the feed solution as much as possible until the whole feed solution was recovered, except the dead-end feed volume (around 300 mL and over 160 g L^{-1} concentration). In both DCMD tests, the initial feed volume was 2 L. In this test, a linear behavior was considered to quantify the decline of the permeate flux with time, and the corresponding absolute value of the slope was taken as the decay slope of the permeate flux (DS_{Jw}). The exhaustion operating time and the final feed concentration correspond to a substantial decline of the permeate flux with time (i.e., a reduction of the slope presenting the permeate flux with time by around 10%). These two

tests are complementary and permit us to know the permeate fluxes at different salt concentrations together with the maximum feed concentration that each membrane can reach, as well their DCMD performance and long-term stability.

5.3. Results and Discussions

5.3.1. Membrane Characterization

The morphological structure of the recycled supports and the nanostructured membranes are shown in Fig. 5.5, and the results of the characterization tests of the electrospun nanofibrous membranes for 30 min are summarized in Table 5.1.

Table 5.1. *Characteristics of electrospun unsupported and supported nanofibrous membranes for 30 min electrospinning time: Thickness (δ) and water contact angle (ϑ_w) of the top and bottom surfaces of the membrane, total thickness (δ_t), mean inter-fiber space (d_i), void volume fraction (ε), liquid entry pressure of water (LEP_w), Young´s modulus (Y_M), tensile strength (T_s) and elongation at break (E_b).*

Membrane Code	Bottom Layer (Hydrophilic Support)		Top Layer (PVDF Hydrophobic Membrane)		δ_t (μm)	d_i (μm)	ε (%)	LEP_w (10^3 Pa)	Y_M (MPa)	Ts (MPa)	E_b (%)
	δ_S (μm)	$(\vartheta_w)_S$ (°)	δ_{PVDF} (μm)	$(\vartheta_w)_{PVDF}$ (°)							
NSEM30	-	-	28 ± 5	139 ± 5	28 ± 5	2.02 ± 0.01	82 ± 1	14 ± 2	17 ± 1	4 ± 1	77± 15
RMEM30	98 ± 3	65 ± 7	31 ± 7	140 ± 5	128 ± 4	<0.1 [c]	64 ± 1	65 ± 4	3721 ± 86	93 ± 3	8 ± 1
PSEM30	221 ± 5	- [b]	33 ± 10	140 ± 2	255 ± 4	2.43 ± 0.08	80 ± 4	15 ± 1	881 ± 42	32 ± 1	15 ± 1
FSEM30	774 ± 7 [a]	- [b]	32 ± 16	132 ± 5	806 ± 9 [a]	3.58 ± 0.17	78 ± 4	7 ± 2	11 ± 1	3 ± 1	88 ± 8

[a] Thickness measured at the nodes of the mesh. [b] 100% hydrophilic nets with open structures (see the corresponding images in Fig. 5.5). [c] Mean size below the measurable limit of Porolux100 (100 nm).

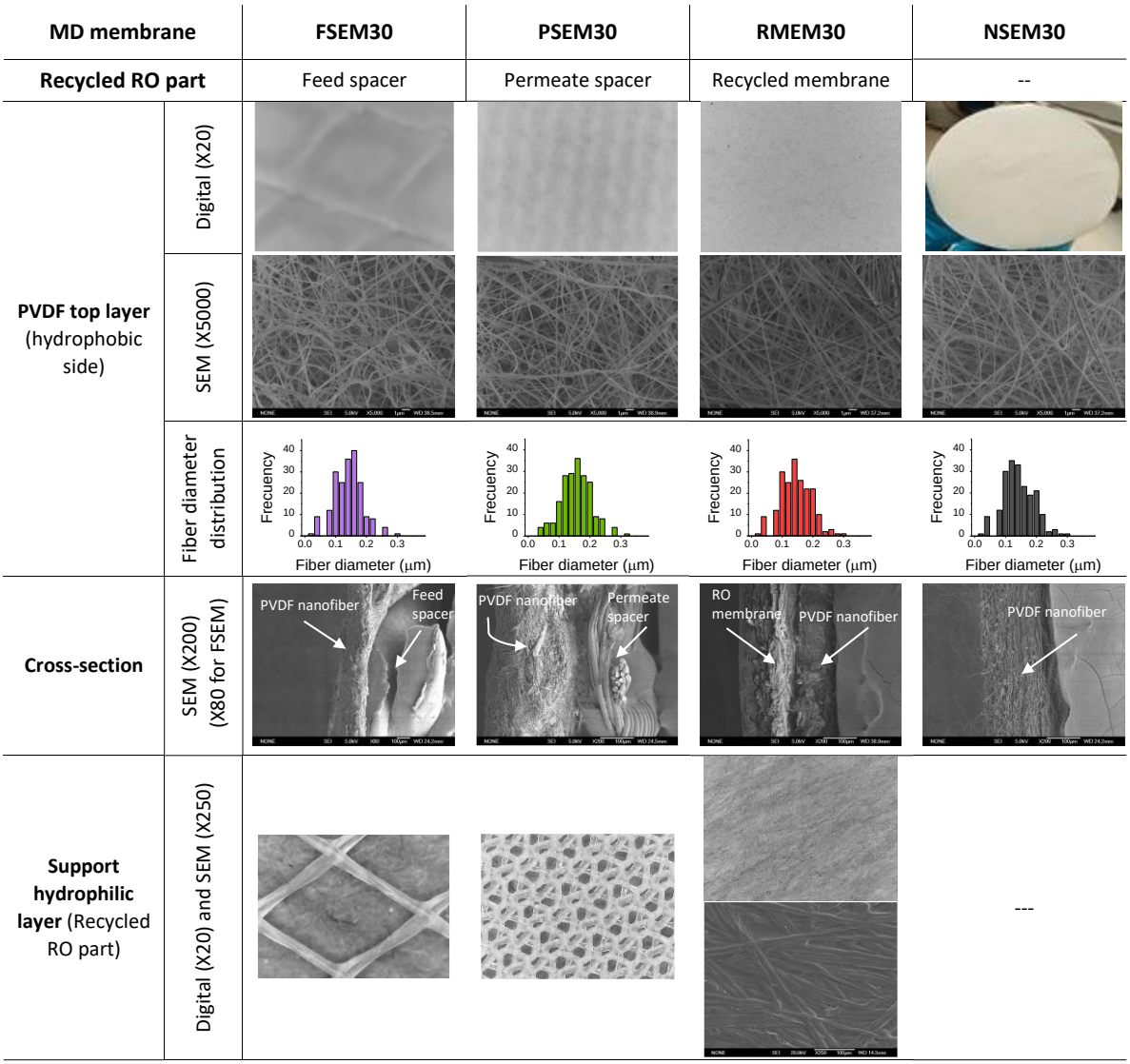

Figure 5.5. *Digital and SEM images of the top surface of the unsupported membrane (NSEM30), feed spacer supported membrane (FSEM30), permeate spacer supported membrane (PSEM30) and RO recycled supported membrane (RMEM30) with the corresponding fiber diameter distribution of the electrospun PVDF top layer and their cross-sections SEM images and the digital images of the feed and permeate spacers and the RO membrane of the discarded RO modules reused as support of the PVDF ENMs.*

The morphological structure of the used supports is evident from the digital microscopic images shown in Fig. 5.5. From the FSEM30 images, a large accumulation of nanofibers could be observed on the mesh nodes of the recycled feed spacer. This agrees with the thickness measurements as will be discussed later on, and it is associated to the more open structure of this spacer. When using the permeate spacer as a support, whose mesh structure is denser and more compact, this problem was not detected, and an even and homogeneous electrospun PVDF nanostructure was formed as shown by the

corresponding SEM image (PSEM30). Similar to NSEM30 and PSEM30, an even and homogeneous PVDF nanostructure was electrospun on the recycled RO membrane RMEM30. The fiber diameter distributions of the electrospun PVDF ENMS presented in Fig. 5.5 were found to be similar and independent on the used support (i.e., the average fiber diameter was 0.15 ± 0.05, 0.16 ± 0.05, 0.15 ± 0.05 and 0.15 ± 0.05 µm, for FSEM30, PSEM30, RMEM30 and NSEM 30 membranes, respectively).

The representative cross-sectional SEM images of NSEM30 membrane and the supported membranes (FSEM30, PSEM30, RMEM30) shown in Fig. 5.5 confirmed further the previously discussed structural characteristics of the membranes. The PVDF nanofibrous top layer exhibited a randomly oriented 3D non-woven nanofibrous structure. Regarding the junction between the PVDF nanofibrous top layer and the different hydrophilic supports used, it is clearly confirmed that the PVDF nanofibrous layer was not attached adequately to the feed spacer although the joints of the feed spacer bounded the PVDF nanofibrous layer. The best junction between the top and bottom layers was achieved for the RMEM30 using the PET side of the recycled RO membrane as contact layer for the PVDF nanofibrous in the electrospinning process.

Taking into consideration the standard deviation, the thickness of the hydrophobic PVDF layer of all electrospun nanofibrous membranes is similar. This is attributed partly to the comparable diameter of the formed PVDF nanofibers, 0.15 ± 0.05 µm, of all membranes regardless of the recycled support. The observed difference of their total thickness is associated to that of the recycled support, which varies in the order: recycled RO membrane < permeate spacer < feed spacer. Compared to the other electrospun nanofibrous membranes, the high standard deviation obtained for the total thickness of the FSEM30 membrane is associated with the open structure of the feed spacer resulting in an uneven thickness of this membrane (see Fig. 5.5). Both the feed and permeate spacers are totally hydrophilic as the water drop cannot stand over them, while the water contact angle of the PSf side of the RO recycled support is 65°, which is much lower than that of the PVDF nanofibrous layer (132–140°). The lower water contact angle of the FSEM30 membrane (i.e., 6% lower) compared to that of the other nanofibrous membranes, which was around 140°, may be attributed to the inhomogeneous and uneven nanostructure of the electrospun PVDF layer of this membrane. This is also confirmed by its higher inter-fiber space, lower LEP_w and poor mechanical properties as is discussed later on.

From the membrane characteristics shown in Table 5.1, it can be seen that the used recycled support affects the nanostructure of the electrospun PVDF layer although the same electrospinning conditions were applied. Compared to the unsupported PVDF nanofibrous membrane, NSEM30, taken as reference, the inter-fiber space of the PSEM30 and FSEM30

was greater, while that of the RMEM30 was smaller due to the different structures of the recycled supports as can be seen in Fig. 5.5. The RMEM30 membranes exhibited a very small inter-fiber space because of the low pore size and compact structure of the PSf layer of the recycled support. This also affected the void volume fraction of this membrane, which was much smaller than that of the other electrospun nanofibrous membranes.

The void volume fraction of the NSEM30 membrane is in accordance with those reported elsewhere [24,30]. The two recycled permeate and feed spacers reduced only slightly the void volume fraction, 2.4 and 4.9%, respectively; whereas this reduction was much higher, 22.0%, when using the recycled RO membrane as support.

Compared to other nanofibrous membranes [38,41], the LEP_w value of the NSEM30 is smaller due to the lower electrospinning time and heat post-treatment applied in this study. The RMEM30 membrane exhibits the highest LEP_w value because of its lowest inter-fiber space as explained previously. In contrast, the FSEM30 presents the lowest LEP_w value because of its highest inter-fiber space and lowest hydrophobic character of the PVDF nanofibrous layer. Both NSEM30 and PSEM30 membranes showed almost the same LEP_w value. This may be attributed to the same hydrophobic character of these two membranes although the inter-fiber space of the NSEM30 membrane is 16.9% smaller.

The mechanical properties of the prepared membranes are also summarized in Table 5.1, and the corresponding stress/strain curves are plotted in Fig. 5.6. Based on the mechanical characteristics reported for other PVDF nanofibrous membranes [41], NSEM30 showed the expected values for Young's modulus (Y_M) and tensile strength (T_s),17 ± 1 MPa and 4 ± 1 MPa, respectively. This membrane was prepared with 30 min electrospinning time, and it is known that the mechanical properties of electrospun nanofibrous membranes are improved with the increase in the electrospinning time, which enhances the membrane thickness. One of the advantages of the use of supports is to improve the membrane mechanical properties. In this case, the use of the recycled RO membrane (RMEM30) and the permeate spacer as supports (PSEM30) induced a considerable enhancement of Y_M and T_s compared to those of the unsupported NSEM30 membrane. However, the elongation at break (E_b) of these membranes was reduced. This is attributed to the stiffness and low elasticity of their corresponding recycled supports made up with PET polymer and to the morphological structure of the permeate spacer composed of a fine mesh and a high number of nodes. On the contrary, for the FSEM30, both Y_M and T_s were decreased indicating a worse mechanical strength compared to the other membranes. This is attributed to the uneven structure of the PVDF nanofibrous structure and to the open and wide web structure of the corresponding PP support.

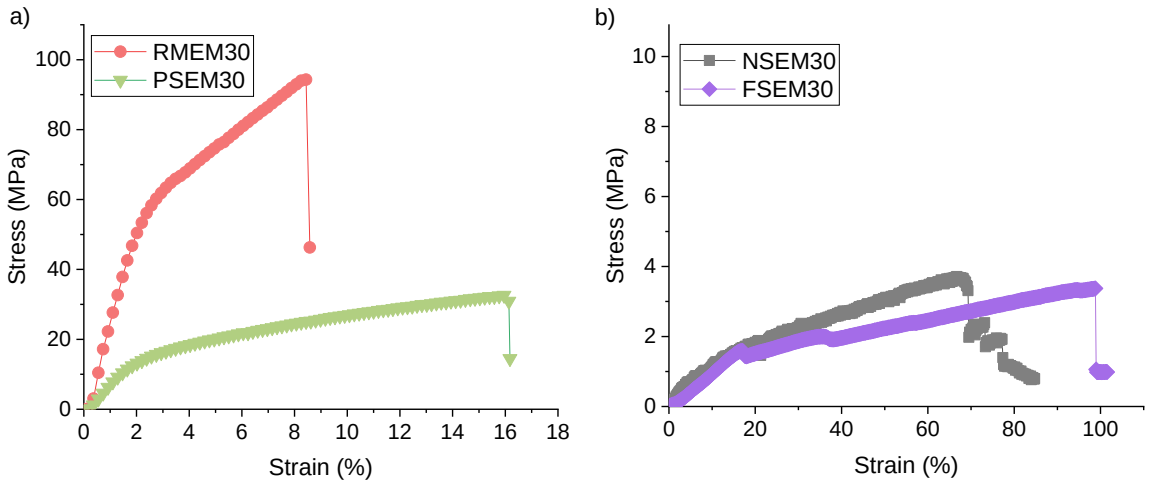

Figure 5.6 *Stress–strain curves of the unsupported and supported electrospun nanofibrous membranes for 30 min electrospinning time. (a) RMEM and PSEM using the RO membrane and permeate spacer, respectively, with 30 min electrospinning time; (b) NSEM and FSEM using unsupported and feed spacer, respectively, with 30 min electrospinning time.*

Table 5.2 shows the DCMD permeate flux and the salt rejection factor of the unsupported and supported nanostructured membranes prepared with 30 min electrospinning time for different NaCl feed concentrations. For sake of comparison, the corresponding permeate flux of the commercial membrane TF200 is also presented. It can be seen that the PSEM30 and NSEM30 membranes exhibit the highest permeate fluxes even higher than those of the commercial membrane TF200 (i.e., over 28%). However, the salt rejection factor of these NSEM30 and PSEM30 membranes were lower than those of TF200. This is due partly to the low thickness of the PVDF nanofibrous layer and low LEP_w values inducing wetting of large size inter-fiber space of the PVDF layer. Compared to TF200, the FSEM30 membrane has almost similar permeate fluxes, but much lower salt rejection factors, even lower than those of the NSEM30 and PSEM30 membranes. This is due to its lower LEP_w and its uneven and inhomogeneous PVDF nanostructured layer. The permeate flux of the RMEM30 membrane was the lowest but it exhibited high salt rejection factors due to its smallest inter-fiber space and void volume fraction compared to the other membranes. As it is well known, the decrease in the permeate flux with the increase in the NaCl concentration of the feed solution from 0 to 150 g L^{-1} is due to the reduction of the vapor pressure of the feed solution and the concentration polarization effect resulting in a decline of the driving force for DCMD. The observed different reduction rates of the permeate flux with the increase in the feed salt concentration (40% for RMEM30, 25% for NSEM30, 26% for PSEM30, 30% for FSEM30 and 22% for TF200) may be attributed to the

different supports used and to the membrane characteristics affecting the temperature and concentration polarization effects.

Table 5.2. *DCMD permeate flux (Jw) and salt rejection factor (α) of the unsupported and supported nanostructured membranes prepared with 30 min electrospinning time together with that of the commercial membrane TF200 for different NaCl feed concentrations.*

NaCl Concentration (g L^{-1})	NSEM30		RMEM30		PSEM30		FSEM30		TF200	
	J_w (kg m^{-2} h^{-1})	α (%)	J_w (kg m^{-2} h^{-1})	α (%)	J_w (kg m^{-2} h^{-1})	α (%)	J_w (kg m^{-2} h^{-1})	α (%)	J_w (kg m^{-2} h^{-1})	α (%)
0	72.5 ± 0.6	-	29.2 ± 0.2	-	74.7 ± 0.8	-	63.4 ± 0.5	-	55.9 ± 0.1	-
6	69.1 ± 0.4	99.97	25.7 ± 0.3	99.98	70.0 ± 0.2	99.98	58.3 ± 0.1	99.78	52.4 ± 0.1	99.99
12	66.6 ± 0.4	99.94	24.7 ± 0.2	99.97	68.5 ± 0.2	99.93	54.9 ± 0.2	99.74	51.6 ± 0.1	99.99
30	64.8 ± 1.1	99.94	23.6 ± 0.2	99.97	66.5 ± 0.3	99.93	51.3 ± 0.2	99.78	51.0 ± 0.3	99.99
60	61.9 ± 0.2	99.95	22.1 ± 0.2	99.99	63.6 ± 0.1	99.95	49.3 ± 0.4	99.71	50.0 ± 0.1	99.99
90	59.3 ± 0.3	99.95	20.9 ± 0.2	99.99	59.7 ± 0.2	99.95	46.5 ± 0.3	99.79	48.6 ± 0.1	99.99
120	56.6 ± 0.2	99.96	19.8 ± 0.5	99.99	57.7 ± 0.1	99.95	45.8 ± 0.3	99.77	46.3 ± 0.1	99.99
150	54.8 ± 0.3	99.97	17.3 ± 0.2	99.99	55.2 ± 0.1	99.95	44.0 ± 0.3	99.66	43.8 ± 0.1	99.99

5.3.2. Long-Term DCMD Desalination Tests

Based on the characterization results presented in the previous section, the FSEM30 membrane prepared with the recycled feed spacer as a support was discarded for further long-term DCMD desalination tests. As is mentioned in the previous section, this is because of the uneven and inhomogeneous nanostructure of its electrospun PVDF layer, low LEP_w, bad mechanical properties, large inter-fiber space and overall low salt rejection factors.

The PVDF nanostructured layer thickness of the other three membranes (NSEM, RMEM, PSEM) was increased by prolonging the electrospinning time to 60 and 90 min. These membranes were then characterized and tested for long-term DCMD desalination tests, as explained previously. The obtained results are shown in Table 5.3. As was expected, the membranes prepared with larger electrospinning time were thicker. The measured water

contact angles of the top (137–140°) and bottom layers of the prepared membranes were the same as those of the membranes prepared with 30 min electrospinning time (Table 5.1). Both the inter-fiber space and LEP_w vary with the electrospun thickness independently of the recycled support used or whether the membrane is supported or not. The inter-fiber space decreased, whereas the LEP_w increased with the increase in the electrospinning time from 30 to 90 min. These results were already observed by Essalhi and Khayet for the unsupported PVDF nanofibrous membranes prepared with electrospinning time varying from 1 to 4 h [41,45]. In addition to the significant increase in the LEP_w with electrospinning time (i.e., 300% for NSEM and PSEM membranes and 24.6% for RSEM membranes when the electrospinning time was increased from 30 to 60 min), the LEP_w values of the supported nanofibrous membranes, RMEM and PSEM, are greater than those of the self-sustained NSEM membranes. These results are attributed to the used recycled support and to the reduction of the maximum inter-fiber space with electrospinning time (i.e., increase in the PVDF nanostructured layer) provided that the hydrophobic character of the PVDF layer is maintained almost the same (i.e., the water contact angle was maintained around 138°). The highest LEP_w values were obtained for RMEM membranes because of the PSf layer of the corresponding recycled support that induced smaller inter-fiber space of the electrospun PVDF layer. However, no clear trend was detected for the void volume fraction with electrospinning time. This may be attributed to the short electrospinning time variation in this study (30–90 min) and the effect of the recycled supports. Essalhi and Khayet [41,45] reported a gradual and slight enhancement of the void volume fraction with the increase in the electrospinning time or which is the same the increase in the thickness of unsupported PVDF nanofibrous membranes (i.e., an enhancement of 9% when the electrospinning time was increased from 1 h to 4 h). This was attributed to the fact that the continuous deposited nanofibrous layer on the metallic collector acted as an electric insulator towards the dissipation of the electric charges to the collector resulting in a less packed nanofiber network. For a thicker nanofibrous layer or support, more electrostatic charges accumulated in the formed nanofibers causing them to repel each other so that a more loosely packed nanofibrous structure was induced resulting in a higher void volume fraction.

Table 5.3. *Characteristics of the electrospun unsupported and supported nanofibrous membranes prepared with 60 and 90 min electrospinning time: Thickness (δ) and water contact angle (ϑw) of the top and bottom surfaces of the membrane, total thickness (δt), mean inter-fiber space (di), void volume fraction (ε) and liquid entry pressure of water (LEPw).*

Membrane Code	Bottom Layer (Hydrophilic Support)		Top Layer (PVDF Hydrophobic Membrane)		δ_t (μm)	d_i (μm)	ε (%)	LEP_w (10^3 Pa)
	δ_S (μm)	$(\vartheta_w)_s$ (°)	δ_{PVDF} (μm)	$(\vartheta_w)_{PVDF}$ (°)				
NSEM60	-	-	68 ± 5	140 ± 2	68 ± 5	1.49 ± 0.28	87 ± 1	44 ± 3
NSEM90	-	-	125 ± 6	139 ± 4	125 ± 6	1.14 ± 0,35	84 ± 1	56 ± 2
RMEM60	98 ± 3	65 ± 7	74 ± 9	137 ± 2	171 ± 6	<0.1 [b]	69 ± 2	71 ± 2
RMEM90	98 ± 3	65 ± 7	111 ± 10	139 ± 2	209 ± 7	<0.1 [b]	65 ± 4	81 ± 3
PSEM60	221 ± 5	- [a]	84 ± 19	137 ± 3	306 ± 14	2.14 ± 0.78	77 ± 3	49 ± 1
PSEM90	221 ± 5	- [a]	142 ± 20	138 ± 6	363 ± 15	1.46 ± 0.23	82 ± 3	60 ± 3

[a] 100% hydrophilic nets with open structures (see the corresponding images in Fig. 5.4). [b] Mean size below the measurable limit of Porolux100 (100 nm).

The results of the long-term DCMD exhaustion test of the NSEM, RMEM, PSEM and TF200 are plotted in Fig. 5.7. As stated previously, this test consists of the concentration of the feed solution from 65 g L^{-1} up to a maximum concentration over 160 g L^{-1}. In order to compare all the membranes, the exhaustion operating time and the final feed salt concentration ($C_{f,f}$) were considered when the slope of the permeate flux changed significantly (around 10%). For all membranes, these results showed how the DCMD operating time increases, and the average permeate flux decreases with increasing the electrospinning time of the PVDF nanostructured layer. This was expected since the increase in the PVDF layer thickness, reduces the permeate flux and prolong the necessary time for the concentration of the feed solution over 160 g L^{-1}. When the recycled membrane was used as a support, the obtained permeate flux for the RMEM membranes was the lowest compared to the other membranes. The highest final feed salt concentrations achieved for these membranes was up to 190 g L^{-1} for the membranes RMEM30 and RMEM60. When the permeate spacer was used as a support (PSEM), the final feed salt concentration and the necessary DCMD operating time were similar to those of the unsupported NSEM membranes and lower than those of the RMEM membranes. In this case, the PSEM60 and NSEM60 exhibited the same DCMD operating time to that of the membrane TF200 with almost the same average permeate flux but greater final feed salt concentrations.

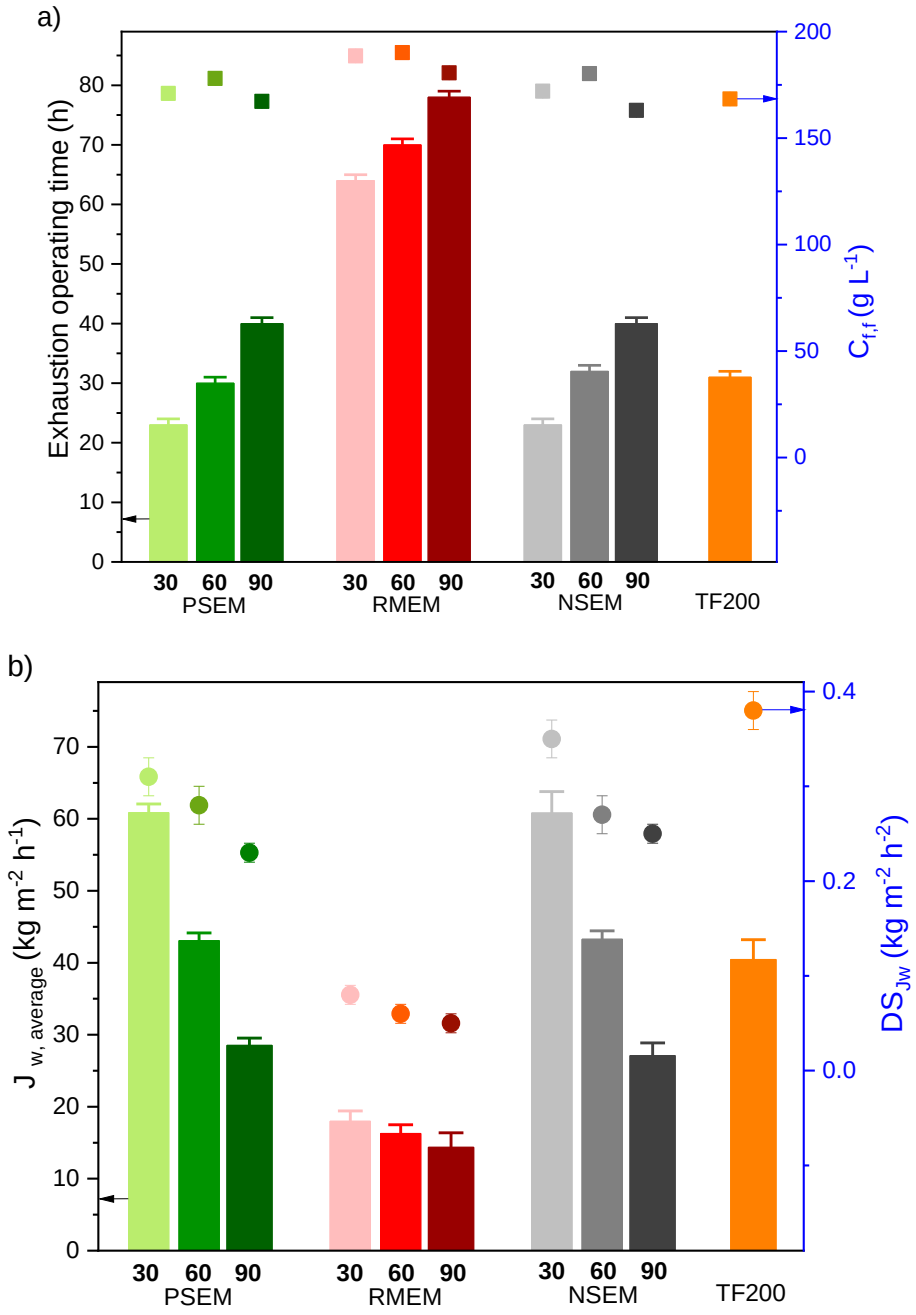

Figure 5.7. *Long-term DCMD exhaustion test of the unsupported, NSEM, the supported electrospun nanofibrous membranes, PSEM and RMEM, and the commercial membrane TF220: (a) operating time (vertical bar) and final feed salt concentration ($C_{f,f}$; symbols) (b) average permeate flux (J_w, average, vertical bars) and decay slope of the permeate flux (DS_{Jw}, symbols). Experimental conditions: T_f = 80 °C, T_p = 20 °C, Am=1.26 × 10^{-3} m^2, feed and permeate flow rate fixed at 0.8 L min^{-1}, distilled water as permeate and initial C^f at 65 g L^{-1}.*

For all prepared membranes, the slight decrease in the final concentration of the feed solution of the nanofibrous membranes prepared with 90 min electrospinning time, compared to those prepared with 30 and 60 min, is due partly to the corresponding lower slope of the permeate flux decay with time (DS_{Jw}) and to the thermal post-treatment that

might be insufficient to induce the necessary junction points between nanofibers of the thicker membranes prepared with 90 min electrospinning time increasing, therefore, scaling phenomenon and causing an earlier membrane collapse. The permeate fluxes obtained for all PSEM membranes are similar to NSEM membranes and those prepared with 30 and 60 min electrospinning exhibited superior permeate fluxes to that of the commercial TF200 membrane. All prepared membranes exhibited lower DS_{Jw} values than that of the membrane TF200 being those of the RMEM membranes the lowest. This indicates the more stable DCMD performance with time and with the increase in the feed concentration of the membranes prepared with recycled supports.

For the long-term DCMD regenerative test, in which the feed salt concentration was maintained at 65 g L^{-1}, only the electrospun nanofibrous membranes with 60 and 90 min electrospinning time were considered together with the commercial TF200 membrane. The prepared membranes with 30 min electrospinning time could not withstand 100 h DCMD operation because of the inter-fiber space wetting and the passage of salt to the permeate resulting in a low salt rejection factor of 90% after only 56 h DCMD operation. Fig. 5.8 shows the permeate flux over 100 h DCMD operation for the unsupported (NSEM60, NSEM90), the supported (PSEM60, PSEM90, RMEM60, RMEM90) nanofibrous membranes and the commercial membrane TF200. The salt rejection factor of all these membranes was maintained greater than 99.99%. A strong dependence of the permeate flux with the electrospinning time was detected (i.e., decrease in the permeate flux with the electrospinning time or thickness of the PVDF nanofibrous layer). From Fig. 5.8, three groups of membranes can be classified from higher to lower permeate fluxes: (TF200, PSEM60, NSEM60) > (PSEM90, NSEM90) > (RMEM60, RMEM90). A considerable permeate flux decline was observed for the first two groups whereas practically the same permeate flux was maintained (≈19 kg m^{-2} h^{-1}) for the third group presented by the RMEM60 and RMEM90 membranes. The calculated slope of the permeate flux decay with time (DS_{Jw}) was 0.062 ± 0.002, 0.049 ± 0.002 and 0.031 ± 0.002 kg m^{-2} h^{-2} for the TF200, PSEM60, NSEM60 membranes, 0.029 ± 0.002 and 0.023 ± 0.002 kg m^{-2} h^{-2} for the PSEM90 and NSEM90 membranes and 0.029 ± 0.002, 0.006 ± 0.001 kg m^{-2} h^{-2} for the RMEM60 and RMEM90 membranes, respectively. This decreased with the increasing of the electrospinning time, and all prepared membranes showed lower DS_{Jw} values than the commercial TF200 membrane. Among all prepared membranes, RMEM90 exhibited the lowest permeate flux decay with time while the PSEM60 membrane presented the highest one maintaining very high and stable salt rejection factors.

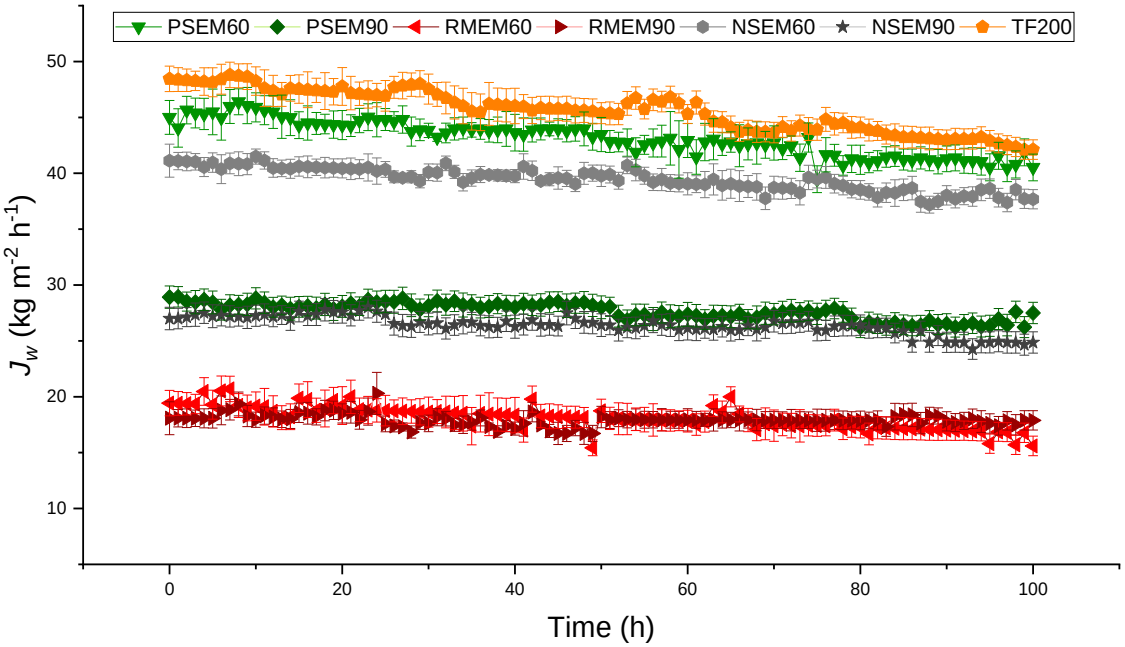

Figure 5.8. *Long-term DCMD regenerative test of the unsupported (NSEM60, NSEM90), and the supported electrospun nanofibrous membranes (PSEM60, PSEM90, RMEM60, RMEM90) and the commercial membrane TF200). Experimental conditions: T_f = 80 °C, T_p = 20 °C, Am = 1.26 x 10^{-3} m^2, feed and permeate flow rate fixed at 0.8 L min^{-1}, Cf at 65 g L^{-1} and distilled water as permeate.*

Taking into consideration the achieved high salt rejection factors greater than 99.99%, the reduction of the permeate flux with time may be attributed to scaling effect, which was more pronounced for the group of membranes exhibiting high permeate fluxes since the measured electrical conductivity of the permeate throughout the experiments showed very small variations (6–14 µS cm^{-1}). In addition, some inter-fiber spaces of some membranes may be wetted reducing slightly the permeate flux and maintaining the salt rejection factor higher than 99.99%.

The DCMD performance of the prepared nanostructured membranes in this study, both the unsupported (NSEM60) and the supported ones using the recycled RO membrane (RMEM60) and the permeate spacer (PSEM60), were compared in Table 5.4 to other PVDF and polyvinylidenefluoride-co-hexafluoropropyle (PVDF-HFP) electrospun nanofibrous MD membranes reported in other manuscripts [31,41,46–54]. It can be confirmed that both RMEM60 and PSEM60 exhibit DCMD permeate fluxes within the range of those reported for PVDF and PVDF-FHP nanofibrous membranes (13.3–54.4 kg m^{-2} h^{-1}) with good and stable salt rejection factors.

Table 5.4. *DCMD performance and characteristics of optimized electrospun nanofibrous membranes reported in other studies together with the best ones obtained in the present study for the supported PVDF nanofibrous membranes using the recycled RO membrane (RMEM60) and the permeate spacer (PSEM60), and the unsupported PVDF nanofibrous membrane (NSEM60).*

Material	Support	Membrane Characteristics	DCMD Conditions	Permeate Flux (kg m^{-2} h^{-1})	Salt Rejection Factor (%)	Ref.
PVDF	Recycled RO permeate spacer (PSEM60)	ε: 77%; δ: 306 µm; LEP_w: 0.49 bar; ϑ_w: 137°.	c_f: 65 g/L; ΔT = 60 K	43.2 ± 1.5	99.99	This study
PVDF	Recycled RO membrane (RMEM60)	ε: 69%; δ: 171 µm; LEP_w: 0.71 bar; ϑ_w: 137°.	c_f: 65 g/L; ΔT = 60 K	18.1 ± 0.9	99.99	This study
PVDF	Unsupported (NSEM60)	ε: 87%; δ: 68 µm; LEP_w: 0.44 bar; ϑ_w: 140°.	c_f: 65 g/L; ΔT = 60 K	39.4 ± 1.1	99.99	This study
PVDF	Unsupported	ε: 86%; δ: 144.4 µm; LEP_w: 0.63 bar; ϑ_w : 139.7°.	c_f: 12 g/L; ΔT = 60 K	15.2	99.7	[41]
PVDF-HFP	Unsupported	ε: 90%; δ: 55 µm; Θw: 128°.	c_f: 30 g/L; ΔT = 55 K	13.3	99.99	[46]
PVDF	PSf nanofibers	ε: 92%; δ: 407 µm; LEP_w: 0.79 bar; ϑ_w : 140.5°.	c_f: 30 g/L; ΔT = 60 K	47.7	99.99	[31]
PVDF	Polyester mesh (big square pores)	ε: 88.6%; δ: 190 µm; LEP_w: 0.45 bar; ϑ_w : 145°.	c_f: 35 g/L; ΔT = 60 K	49.3	99.99	[47]
PVDF/TBAC/FA	Unsupported	ε: 71.28%; δ: 60 µm; LEP_w:2.1 bar; ϑ_w : 137°.	c_f:3 5 g/L; ΔT = 40 K	54.4	99.5	[48]
PVDF/SiO_2NPs	Unsupported	ε: 80%; δ: 129 µm; LEP_w: 0.842 bar; ϑ_w : 156.4°.	c_f: 30 g/L; ΔT = 60 K	30.7	99.9	[49]
PVDF-HFP	Unsupported	ε: 58%; δ: 65 µm; LEP_w: 1.3 bar; ϑ_w : 120°.	c_f: 35 g/L; ΔT = 41 K	22	98	[50]
PVDF-HFP/CNT	Unsupported	ε: 89%; δ: 83 µm; LEP_w: 0.4 bar; ϑ_w : 150.4°.	c_f: 35 g/L; ΔT = 40 K	48.1	99.99	[51]
PVDF-HFP/AC	Nylon flat sheet	ε: 90%; δ: 200 µm; LEP_w: 1.36 bar; ϑ_w : 142.7°.	c_f: 35 g/L; ΔT = 45 K	45.6	99.99	[52]
PVDF-HFP	PAN nanofibers	ε: 90%; δ: 82 µm; LEP_w: 0.94 bar; ϑ_w : 150°.	c_f: 35 g/L; ΔT = 40 K	30	98.5	[53]
PVDF-HFP/SiF	Unsupported	ε: 71%; δ: 130 µm; LEP_w: 2.7 bar; ϑ_w : 100°.	c_f: 35 g/L; ΔT = 50 K	26	99.99	[54]

PVDF-HFP: polyvinylidenefluoride-co-hexafluoropropylene; TBAC: tetrabutylammonium chloride; FA: fluorinated acrylate copolymer; SiO_2NPs: silica nanoparticles; PS: polystyrene; SBS: styrene-butadiene-styrene; CNT: carbon nanotubes; AC: activated carbon; PAN: polyacrylonitrile; SiF: silica fibers; ε: porosity; δ: thickness; ϑ_w: water contact angle; LEP_w: liquid entry pressure; ΔT: temperature difference between the feed and permeate; c_f: feed salt concentration.

5.4. Conclusions

In this study, we propose recycling and reusing RO membranes and spacers of discarded RO modules as supports in MD membrane engineering, extending their useful life cycle and contributing to the awaited circular economy of waste management. In addition,

the proposed membranes were tested for the treatment of high saline aqueous solutions, near saturation, in order to check their ability to process RO brines, which is also beneficial for the environment favoring the noted zero liquid discharge for RO desalination plants.

The recycled RO membrane and the permeate spacer of the RO discarded module used as hydrophilic supports for the PVDF nanofibrous membranes exhibit suitable characteristics for MD separation process. The MD membranes supported by the recycled RO membrane (RMEMs) have a smaller inter-fiber space and a greater LEP_w than the membrane supported by the permeate spacer (PSEMs). Compared to the unsupported PVDF membrane, the use of these two supports enhanced both Young´s modulus (Y_M) and tensile strength (T_s). The DCMD tests showed higher salt rejection factors for the RMEMs and similar permeate fluxes to those of the unsupported PVDF membranes were observed for the PSEMs. Both supported membranes exhibited stable DCMD performance with time.

The recycled feed spacer of the RO discarded module caused a large accumulation of PVDF nanofibers on its mesh nodes due to its open structure resulting in an uneven thickness of the PVDF nanostructured membranes (FSEMs). Therefore, this type of membrane showed lower LEP_w value, a greater inter-fiber space, lower Y_M and T_s values and a lower salt rejection factor than the other membranes.

Compared to other PVDF or PVDF-HFP electrospun nanofibrous membranes reported in the literature, the prepared membranes, RMEM60 and PSEM60, with 60 min electrospinning time presented reasonably good DCMD performance (i.e., 43.2 and 18.1 kg/m^2 h with high salt rejection factors for RMEM60 and PSEM60, respectively).

5.5. References

[1] IDA and GWI desalData. IDA Desalination Yearbook 2017–2018; Media Analytics Ltd.: Oxford, UK, 2017; ISBN 978-1-907467-52-3.

[2] IDA and GWI desalData. The IDA Water Security Handbook 2020–2021; Media Analytics Ltd.: Oxford, UK, 2020; ISBN 978-1-907467-62-2.

[3] Kim, J.; Park, K.; Yang, D.R.; Hong, S. A comprehensive review of energy consumption of seawater reverse osmosis desali-nation plants. Appl. Energy 2019, 254, 113652.

[4] Park, K.; Kim, J.; Yang, D.R.; Hong, S. Towards a low-energy seawater reverse osmosis desalination plant: A review and theoretical analysis for future directions. J. Membr. Sci. 2020, 595, 117607.

[5] Panagopoulos, A.; Haralambous, K.-J. Minimal Liquid Discharge (MLD) and Zero Liquid Discharge (ZLD) strategies for wastewater management and resource recovery—Analysis, challenges and prospects. J. Environ. Chem. Eng. 2020, 8, 104418.

[6] Greenlee, L.F.; Lawler, D.F.; Freeman, B.D.; Marrot, B.; Moulin, P. Reverse osmosis desalination: Water sources, technology, and today's challenges. Water Res. 2009, 43, 2317–2348.

[7] García, N.P.; del Vigo, F.; Chesters, S.; Armstrong, M.; Wilson, R.; Fazel, M. A Study of the Physical and Chemical Damage on Reverse Osmosis Membranes Detected by Autopsies. In Proceedings of the The International Desalination Association World Congress on Desalination and Water Reuse, Tianjin, China, 20–25 October 2013.

[8] Lawler, W.; Bradford-Hartke, Z.; Cran, M.J.; Duke, M.; Leslie, G.; Ladewig, B.P.; Le-Clech, P. Towards new opportunities for reuse, recycling and disposal of used reverse osmosis membranes. Desalination 2012, 299, 103–112.
[9] Ould Mohamedou, E.; Penate Suarez, D.B.; Vince, F.; Jaouen, P.; Pontie, M. New lives for old reverse osmosis (RO) mem-branes. Desalination 2010, 253, 62–70.
[10] Pontié, M. Old RO membranes: Solutions for reuse. Desalin. Water Treat. 2015, 53, 1492–1498.
[11] Prince, C.; Cran, M.; Le-Clech, P.; Uwe-Hoehn, K.; Duke, M. Reuse and recycling of used desalination membranes. Proc. OzWater 2011, 11, 1–8.
[12] Hailemariam, R.H.; Woo, Y.C.; Damtie, M.M.; Kim, B.C.; Park, K.-D.; Choi, J.-S. Reverse osmosis membrane fabrication and modification technologies and future trends: A review. Adv. Colloid Interface Sci. 2020, 276, 102100
[13] Lawler, W.; Antony, A.; Cran, M.; Duke, M.; Leslie, G.; Le-Clech, P. Production and characterisation of UF membranes by chemical conversion of used RO membranes. J. Membr. Sci. 2013, 447, 203–211.
[14] Landaburu-Aguirre, J.; García-Pacheco, R.; Molina, S.; Rodríguez-Sáez, L.; Rabadán, J.; García-Calvo, E. Fouling prevention, preparing for re-use and membrane recycling. Towards circular economy in RO desalination. Desalination 2016, 393, 16–30.
[15] Molina, S.; Landaburu-Aguirre, J.; Rodríguez-Sáez, L.; García-Pacheco, R.; de la Campa, J.G.; García-Calvo, E. Effect of so-dium hypochlorite exposure on polysulfone recycled UF membranes and their surface characterization. Polym. Degrad. Stab. 2018, 150, 46–56.
[16] Molina, S.; García Pacheco, R.; Rodriguez-Sáez, L.; García-Calvo, E.; Campos, E.; Zarzo Martinez, D.; de la Campa, J.G.; de Abajo, J. Transformation of end-of-life RO membranes into recycled NF and UF membranes, surface characterization. In Proceedings of the International Desalination Association Word Congress, IDAWC15, San Diego, CA, USA, 30 August–4 September 2015; Volume 15WC-51551.
[17] García-Pacheco, R.; Landaburu-Aguirre, J.; Terrero-Rodríguez, P.; Campos, E.; Molina-Serrano, F.; Rabadán, J.; Zarzo, D.; García-Calvo, E. Validation of recycled membranes for treating brackish water at pilot scale. Desalination 2018, 433, 199–208.
[18] Moradi, M.R.; Pihlajamäki, A.; Hesampour, M.; Ahlgren, J.; Mänttäri, M. End-of-life RO membranes recycling: Reuse as NF membranes by polyelectrolyte layer-by-layer deposition. J. Membr. Sci. 2019, 584, 300–308.
[19] Lejarazu-Larrañaga, A.; Molina, S.; Ortiz, J.M.; Navarro, R.; García-Calvo, E. Circular economy in membrane technology: Using end-of-life reverse osmosis modules for preparation of recycled anion exchange membranes and validation in elec-trodialysis. J. Membr. Sci. 2020, 593, 117423.
[20] Morón-López, J.; Nieto-Reyes, L.; Senán-Salinas, J.; Molina, S.; El-Shehawy, R. Recycled desalination membranes as a sup-port material for biofilm development: A new approach for microcystin removal during water treatment. Sci. Total Environ. 2019, 647, 785–793.
[21] Morón-López, J.; Nieto-Reyes, L.; Molina, S.; Lezcano, M.Á. Exploring microcystin-degrading bacteria thriving on recycled membranes during a cyanobacterial bloom. Sci. Total Environ. 2020, 736, 139672.
[22] Morón-López, J.; Molina, S. Optimization of Recycled-Membrane Biofilm Reactor (R-MBfR) as a sustainable biological treatment for microcystins removal. Biochem. Eng. J. 2020, 153, 107422.
[23] García-Pacheco, R.; Landaburu-Aguirre, J.; Molina, S.; Rodríguez-Sáez, L.; Teli, S.B.; García-Calvo, E. Transformation of end-of-life RO membranes into NF and UF membranes: Evaluation of membrane performance. J. Membr. Sci. 2015, 495, 305–315.
[24] Morón-López, J.; Nieto-Reyes, L.; Aguado, S.; El-Shehawy, R.; Molina, S. Recycling of end-of-life reverse osmosis mem-branes for membrane biofilms reactors (MBfRs). Effect of chlorination on the membrane surface and gas permeability. Chemosphere 2019, 231, 103–112.
[25] Khayet, M.; Matsuura, T. Chapter 1—Introduction to Membrane Distillation. In Membrane Distillation; Khayet, M., Matsuura, T., Eds.; Elsevier: Amsterdam, The Netherlands, 2011; pp. 1–16. ISBN 978-0-444-53126-1.

[26] Topuz, F.; Holtzl, T.; Szekely, G. Scavenging organic micropollutants from water with nanofibrous hypercrosslinked cy-clodextrin membranes derived from green resources. Chem. Eng. J. 2021, 419, 129443.
[27] Cseri, L.; Topuz, F.; Abdulhamid, M.A.; Alammar, A.; Budd, P.M.; Szekely, G. Electrospun Adsorptive Nanofibrous Mem-branes from Ion Exchange Polymers to Snare Textile Dyes from Wastewater. Adv. Mater. Technol. 2021, 2000955.
[28] Soliman, M.N.; Guen, F.Z.; Ahmed, S.A.; Saleem, H.; Khalil, M.J.; Zaidi, S.J. Energy consumption and environmental impact assessment of desalination plants and brine disposal strategies. Process Saf. Environ. Prot. 2021, 147, 589–608.
[29] Alrehaili, O.; Perreault, F.; Sinha, S.; Westerhoff, P. Increasing net water recovery of reverse osmosis with membrane distil-lation using natural thermal differentials between brine and co-located water sources: Impacts at large reclamation facilities. Water Res. 2020, 184, 116134.
[30] Bindels, M.; Carvalho, J.; Gonzalez, C.B.; Brand, N.; Nelemans, B. Techno-economic assessment of seawater reverse osmosis (SWRO) brine treatment with air gap membrane distillation (AGMD). Desalination 2020, 489, 114532.
[31] Khayet, M.; García-Payo, M.C.; García-Fernández, L.; Contreras-Martínez, J. Dual-layered electrospun nanofibrous mem-branes for membrane distillation. Desalination 2018, 426, 174–184.
[32] Khayet, M.; Mengual, J.I.; Matsuura, T. Porous hydrophobic/hydrophilic composite membranes: Application in desalination using direct contact membrane distillation. J. Membr. Sci. 2005, 252.
[33] Thenmozhi, S.; Dharmaraj, N.; Kadirvelu, K.; Kim, H.Y. Electrospun nanofibers: New generation materials for advanced applications. Mater. Sci. Eng. B 2017, 217, 36–48.
[34] Wang, X.; Hsiao, B.S. Electrospun nanofiber membranes. Curr. Opin. Chem. Eng. 2016, 12, 62–81.
[35] Eykens, L.; De Sitter, K.; Dotremont, C.; Pinoy, L.; Van der Bruggen, B. Membrane synthesis for membrane distillation: A review. Sep. Purif. Technol. 2017, 182, 36–515.
[36] García-Pacheco, R.; Rabadán, F.J.; Terrero, P.; Molina Martínez, S.; Martínez, D.; Campos, E.; Molina, F.; Rodríguez, L.; Ortíz de Lejarazu, A.; Landaburu-Aguirre, J.; et al. Life+13 transfomem: A recycling example within the desalination world. In Proceedings of the XI AEDYR International Congress, Valencia, Spain, 19–21 October 2016; VAL-112-16.
[37] Lawler, W.; Alvarez-Gaitan, J.; Leslie, G.; Le-Clech, P. Comparative life cycle assessment of end-of-life options for reverse osmosis membranes. Desalination 2015, 357, 45–54.
[38] Essalhi, M.; Khayet, M. Self-sustained webs of polyvinylidene fluoride electrospun nano-fibers: Effects of polymer concen-tration and desalination by direct contact membrane distillation. J. Membr. Sci. 2014, 454, 133–143.
[39] Essalhi, M.; Khayet, M.; Cojocaru, C.; García-Payo, M.C.; Arribas, P. Response surface modeling and optimization of elec-trospun nanofiber membranes. Open Nanosci. J. 2013, 7, 8–17.
[40] Khayet, M.; Matsuura, T. Chapter 8—MD Membrane Characterization. In Membrane Distillation; Khayet, M., Matsuura, T., Eds.; Elsevier: Amsterdam, The Netherlands, 2011; pp. 189–225. ISBN 978-0-444-53126-1.
[41] Essalhi, M.; Khayet, M. Self-sustained webs of polyvinylidene fluoride electrospun nanofibers at different electrospinning times: 1. Desalination by direct contact membrane distillation. J. Membr. Sci. 2013, 433, 167–179.
[42] Arribas, P.; García-Payo, M.C.; Khayet, M.; Gil, L. Heat-treated optimized polysulfone electrospun nanofibrous membranes for high performance wastewater microfiltration. Sep. Purif. Technol. 2019, 226, 323–336.
[43] Li, X.; García-Payo, M.C.; Khayet, M.; Wang, M.; Wang, X. Superhydrophobic polysulfone/polydimethylsiloxane electro-spun nanofibrous membranes for water desalination by direct contact membrane distillation. J. Membr. Sci. 2017, 542, 308–319.
[44] Godino, P.; Peña, L.; Mengual, J.I. Membrane distillation: Theory and experiments. J. Membr. Sci. 1996, 121, 83–93.

[45] Essalhi, M.; Khayet, M. Self-sustained webs of polyvinylidene fluoride electrospun nanofibers at different electrospinning times: 2. Theoretical analysis, polarization effects and thermal efficiency. J. Membr. Sci. 2013, 433, 180–191.
[46] Su, C.-I.; Shih, J.-H.; Huang, M.-S.; Wang, C.-M.; Shih, W.-C.; Liu, Y. A study of hydrophobic electrospun membrane applied in seawater desalination by membrane distillation. Fibers Polym. 2012, 13, 698–702.
[47] Li, K.; Hou, D.; Fu, C.; Wang, K.; Wang, J. Fabrication of PVDF nanofibrous hydrophobic composite membranes reinforced with fabric substrates via electrospinning for membrane distillation desalination. J. Environ. Sci. 2018, 75, 277–288.
[48] Li, Z.; Liu, Y.; Yan, J.; Wang, K.; Xie, B.; Hu, Y.; Kang, W.; Cheng, B. Electrospun polyvinylidene fluoride/fluorinated acry-late copolymer tree-like nanofiber membrane with high flux and salt rejection ratio for direct contact membrane distilla-tion. Desalination 2019, 466, 68–76.
[49] Nthunya, L.N.; Gutierrez, L.; Verliefde, A.R.; Mhlanga, S.D. Enhanced flux in direct contact membrane distillation using superhydrophobic PVDF nanofibre membranes embedded with organically modified SiO2 nanoparticles. J. Chem. Technol. Biotechnol. 2019, 94, 2826–2837.
[50] Lalia, B.S.; Guillen-Burrieza, E.; Arafat, H.A.; Hashaikeh, R. Fabrication and characterization of polyvinylidenefluo-ride-co-hexafluoropropylene (PVDF-HFP) electrospun membranes for direct contact membrane distillation. J. Membr. Sci. 2013, 428, 104–115.
[51] Kyoungjin An, A.; Lee, E.-J.; Guo, J.; Jeong, S.; Lee, J.-G.; Ghaffour, N. Enhanced vapor transport in membrane distillation via functionalized carbon nanotubes anchored into electrospun nanofibres. Sci. Rep. 2017, 7, 41562.
[52] Zhao, L.; Wu, C.; Lu, X.; Ng, D.; Truong, Y.B.; Xie, Z. Activated carbon enhanced hydrophobic/hydrophilic dual-layer nano-fiber composite membranes for high-performance direct contact membrane distillation. Desalination 2018, 446, 59–69.
[53] Tijing, L.D.; Woo, Y.C.; Johir, M.A.H.; Choi, J.S.; Shon, H.K. A novel dual-layer bicomponent electrospun nanofibrous membrane for desalination by direct contact membrane distillation. Chem. Eng. J. 2014, 256, 155–159.
[54] Makanjuola, O.; Anis, S.F.; Hashaikeh, R. Enhancing DCMD vapor flux of PVDF-HFP membrane with hydrophilic silica fibers. Sep. Purif. Technol. 2021, 263, 118361.

Chapter 6

Recycled Reverse Osmosis Membranes for Forward Osmosis Technology

An alternative use of end-of-life reverse osmosis (RO) membranes is proposed for forward osmosis (FO) application as recycled FO (RFO) membranes and transformed recycled FO (TRFO) membranes. Different passive cleaning protocols in pilot plant and laboratory scale were followed using sodium hypochlorite (NaClO) at different concentrations and exposure time. The RFO with the best performance was selected for its transformation by interfacial polymerization (IP) technique to improve further the FO performance. Both the morphological structure and transport properties of the RFO and TRFO membranes were studied by means of different characterization techniques. Although the RFO membranes are suitable for FO, the TRFO membranes are more competitive. The highest FO water permeate fluxes (12.21 kg/m2h and 15.12 kg/m2h) were obtained for the membrane recycled applying the highest NaClO exposure dose applied in pilot plant (106 ppm·h) followed by IP of a thin polyamide layer. These permeate fluxes were better or at least comparable to commercial membranes used under the same FO conditions. The results indicated that it is possible to use discarded RO membranes in FO technology for wastewater treatment after adequate treatment procedures extending their lifetime and contributing to a circular economy and sustainability in membrane science and related materials.

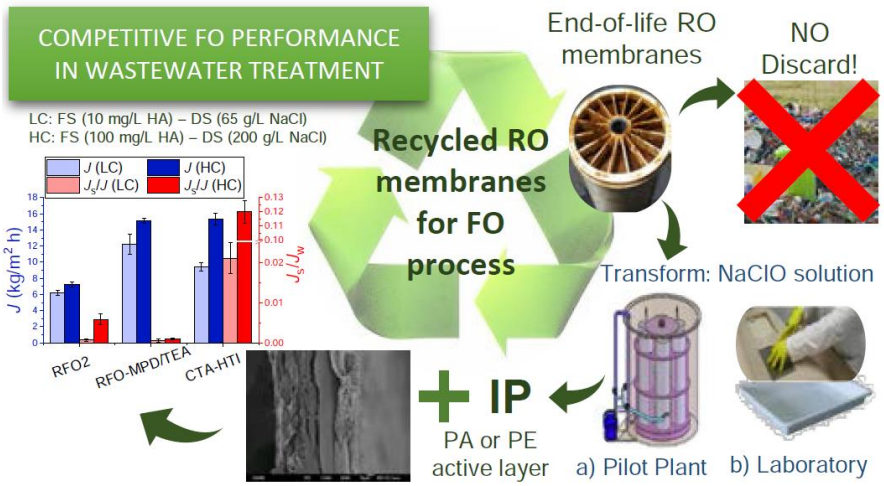

6.1. Introduction

Both the demographic increase and the climatic change aggravate the global situation of water scarcity and the search for unconventional resources is demanded [1]. Desalination and wastewater reuse are two viable cost-effective ways of achieving water security in many regions of the world. Membrane-based technologies have been applied significantly for water treatment because of their high sustainability criteria in terms of environmental impacts, land usage, ease of use, flexibility and adaptability, compared to other techniques such as thermal and chemical approaches [2].

The worldwide total desalination capacity of clean water per day is 99.8 Hm^3 among which 70% are represented by reverse osmosis (RO) desalination plants in which the spiral wound thin film composite (TFC)-polyamide (PA) membrane modules are the most used [3]. However, RO desalination technology has some environmental drawbacks that need to be addressed and resolved. The major environmental challenge associated to energy consumption of fossil resources because of their repercussion in climate change, together with both the inland and coastal discharges of high concentrated brines and their adversely negative environmental impacts are the principal issues of RO technology. Some strategies have been proposed for the treatment of RO brines taking into consideration their high osmotic pressure [4]. In addition, the short lifespan of the used membrane modules, which is about six year average [5], is nowadays another environmental issue of this technology. In RO desalination plants, it is required a membrane replacement rate of about 5 – 20 % each year even if different strategies are considered to control and mitigate fouling of RO membrane modules [6]. More than 840000 end-of-life RO membrane modules are discharged annually worldwide [7]. The most common management of the discarded membrane modules is their deposition in landfills near desalination plants. The European Union (EU) in the Directive 2008/98/CE clearly established the following hierarchy for wastes serving as an order of priorities in legislation and policy in favor of prevention and waste management (prevention, preparation for reuse, recycling, energy recovery and final disposal) [8]. Therefore, it is necessary to find out new ways to properly manage this large amount of solid waste by reusing and recycling discarded RO membrane modules.

Different recycling techniques of end-of-life RO membranes modules have been proposed recently [5, 7, 9, 10]. These techniques include chemical conversion using different oxidative agents of the dense polyamide (PA) active layer of the RO membranes by means of active recirculation or passive immersion. The dense PA layer of the discarded RO membranes can be partially or completely degraded depending on the concentration of the oxidative agent used and its exposure time. As consequence, discarded RO membranes can be

converted into NF or UF membranes, depending on the degree of exposure of the membrane to free chlorine [11].

Sodium hypochlorite (NaClO) has been proposed as an oxidative agent of PA because its main effect is the degradation and separation of the thin PA layer from PSf layer through hydroxide-induced amide link scission [12]. Different concentrations of free chlorine (i.e. hypochlorous acid and hypochlorite ion) and its exposure time were considered depending on the type and observed effects of membrane fouling. By using this agent, the recovery of discarded RO modules for their reuse in nanofiltration (NF), ultrafiltration (UF), electrodialysis (ED) and membrane bioreactors (MBR) were reported [11, 13-15]. Therefore, the use of recycled membranes contributes to the circular economy scheme. Senán-Salinas et al. [16] evaluated recycled RO membranes with Life Cycle Assessment (LCA) and cost effectiveness analysis. LCA results showed that the most environmentally interesting transformations are passive systems with recycling costs of € 25.9 – 41.5 per membrane module. It must be pointed out that NaClO has not been used yet to recover discarded modules for their reuse in forward osmosis (FO) technology.

FO is a separation process of emerging interests during last decade for wastewater treatments [17-20]. It allows the concentration of feed aqueous solutions by the application of an osmotic pressure difference through a semipermeable membrane using a draw solution with very low chemical potential of water [21]. Compared to RO, FO technology requires less specific energy consumption since water flux takes place naturally by means of the osmotic driving force through a semi-permeable membrane from a low osmotic pressure solution to a high osmotic pressure solution. Other advantages of FO are its lower fouling tendency, resulting in easier cleaning, extending therefore membrane lifetime; and its higher selectivity compared to RO [22, 23]. However, the product of FO is not potable water but a diluted draw solution that requires a regenerating step to extract clean water [22]. It is worth quoting that FO, alone or in combination with other processes [17, 19, 24-27], has been proposed as an appropriate technology for wastewater treatment [19, 28, 29] with a high energy efficiency [20, 30].

A suitable membrane for FO process must exhibit among others a high hydrophilic character, a high water permeance, a highly selective thin layer with a support having a low tortuosity factor and a high porosity [31]. Maximizing the permeate water flux while minimizing the reverse solute permeate flux that causes a decline of the transmembrane osmotic pressure gradient is one of the proposed objectives in FO membrane engineering [32]. Various types of membranes were developed to optimize FO separation process [25, 33, 34]. Some new FO membranes exhibit a thin-film composite (TFC) structure similar to that of RO membranes [35]. Tiraferri et al. [36] studied the influence of the TFC membrane support

layer structure on FO performance and concluded that both the active layer transport properties and the support layer structural characteristics should be optimized in order to achieve a high FO performance.

In the present study, an attempt has been made for the first time to recycle discarded RO membranes for their application in FO process. This avoids their disposal in landfills giving them a new use. For their cleaning, different concentrations of the NaClO oxidative agent and exposure time have been considered. The recycled FO membranes (RFO) were first characterized and tested in FO for the treatment of humic acid (HA) solutions. Then, the RFO membrane with the best FO performance was selected as support of the TFC FO membranes. Transformed recycled FO membranes (TRFO) were prepared by interfacial polymerization (IP) technique in order to improve its FO performance. It is worth quoting that various research studies have been already carried out on IP using different types of monomers in both the aqueous solution and organic solution [37, 38]. The obtained TRFO membranes were also characterized and tested in FO for the treatment of HA solutions and finally compared to FO commercial membranes.

6.2. Materials and Methods

6.2.1. RO modules and recycled forward osmosis membranes (RFO)

End-of-life spiral wound RO modules (TM720-400 by Toray Industries, Inc., Japan) discarded by a brackish water desalination plant located in Almeria (Spain) were used in this study. These modules have 8" (equivalent to 0.2032 m) diameter and contain a TFC–PA membrane composed of three layers: a PE support layer, a PSf porous intermediate layer and a selective PA dense top layer. The water permeance and salt rejection factor of the discarded RO membrane modules are 2.04 ± 0.06 L/m^2·h·bar and 98.31 ± 0.24%, respectively. The RO tests for evaluating the discarded RO membranes were carried out for 5 min with a feed aqueous solution containing NaCl (2,000 ppm), $MgSO_4$ (2,000 ppm) and dextrose (250 ppm) at 303 K under a transmembrane pressure of 5 bar. After their autopsy, the membranes of the discarded RO modules presented a clay-like appearance (i.e. brown color, odorless with a colloidal fouling texture composed by 84% inorganic and 16% organic compounds) and a water contact angle of the active layer of 46 ± 2° without any superficial damage [39-41]. The discarded RO modules were conserved in sodium bisulphite (500-1000 ppm). Prior their characterization, membrane coupons were first extracted from the modules, washed and conserved in Milli-Q water. For the present study, two types of recycled membranes were

used according to the followed passive cleaning procedure using free chlorine as PA degradant at basic pH (Table 6.1).

Table 6.1. *Free chlorine exposure doses to obtain RFO membranes.*

Membrane code	Cleaning in pilot plant			Cleaning in lab			Total dose level (ppm·h)
	Exposure Time (h)	Free chlorine (ppm)	Dose level (ppm·h)	Exposure Time (h)	Free chlorine (ppm)	Dose level (ppm·h)	
RFO1	65	$12.4 \cdot 10^3$	$8 \cdot 10^5$	-	-	-	$8 \cdot 10^5$
RFO2	81	$12.4 \cdot 10^3$	10^6	-	-	-	10^6
RFO3	65	$12.4 \cdot 10^3$	$8 \cdot 10^5$	7	$7 \cdot 10^3$	$49 \cdot 10^3$	$8 \cdot 10^5 + 49 \cdot 10^3$
RFO4	81	$12.4 \cdot 10^3$	10^6	7	$7 \cdot 10^3$	$49 \cdot 10^3$	$10^6 + 49 \cdot 10^3$

The choice of free chlorine was motivated by the low tolerance of RO membranes to it (< 1000 ppm·h using a free chlorine concentration of 1 ppm) [42]. NaClO solutions were prepared by diluting NaClO in water until achieving the free chlorine concentration set for the experiments (12385 ppm for cleaning in pilot plant and 7000 ppm for cleaning in lab) [41]. In the pilot plant, the free chlorine concentration was controlled according to the in-situ determination of pH, conductivity and redox in order to guarantee a constant concentration in each assay. In laboratory, the free chlorine concentration was measured by a Pharo 100 Spectroquant spectrophotometer (Merck). The NaClO solutions presented a high physical and chemical stability together with a high capacity to be reused in successive treatments. The lowest applied exposure dose was $3 \cdot 10^5$ ppm·h because UF-like membranes from discarded RO membranes were previously obtained following the laboratory cleaning procedure [43]. In addition, starting from this exposure dose, the elimination of the PA layer could be guaranteed obtaining a recycled membrane formed by a PSf layer supported on a PE backing material [43].

The first type of RFO membranes (RFO1 and RFO2) was subjected to a passive cleaning process in the pilot plant with NaClO solution of 12,385 ppm of free chlorine at different exposure times [41]. Under this cleaning protocol it was not necessary to disassemble the discarded RO modules. The second type of RFO membranes (RFO3 and RFO4) were cleaned twice, first in the pilot plant and then in the laboratory. The second cleaning in laboratory was carried out by a passive cleaning using NaClO (6,200 ppm of free chlorine) under a total level dose of $49 \cdot 10^3$ ppm·h [41]. In this case, it was necessary to disassemble the RO membrane module and cut the necessary membrane coupons for their immersion in the oxidative agent´s solution, increasing therefore the recycling cost with respect to the previous cleaning protocol and limiting the reuse of the complete module as well. Under these high total

exposure doses, the final degradation of the PA layer of the RO membranes was ensured as demonstrated elsewhere [11]. The complete degradation of the PA layer is necessary since it is supposed to be the fouled layer of the RO membrane [44]. Therefore, the remained supported PSf membrane (as shown in Fig. 9.1c of the Appendix B) was proposed for the first set of FO separation tests and characterization.

For sake of comparison of the efficiency of the different cleaning protocols, one more type of RFO membrane (RFO5) was prepared skipping the first cleaning in pilot plant and cleaning the discarded RO membrane only under laboratory protocol with a total exposure dose of $3 \cdot 10^5$ ppm·h. All related details can be found in the Appendix B (section 9.6).

6.2.2. Interfacial polymerization (IP) of the recycled forward osmosis membrane (TRFO)

Interfacial polymerization (IP) is a well-studied membrane modification method exhibiting various advantages as it allows the formation of TFC membranes with excellent performance in RO, NF, MF and FO applications. Different monomers with different concentrations and application time were considered. Compared to CTA membrane, TFC-FO membranes prepared by IP display promising characteristics due mainly to the benefits of both the active skin layer and the support layer.

TFC membranes were prepared by IP using as support the RFO membrane with the best FO performance (RFO2 membrane as will be discussed later on). In our previous study [38], IP was followed to prepare PA or PE thin layer on commercial polyethersulfone (PES) filtration membrane (HPWP Merk Millipore, 0.45 µm pore size) using different monomers in the aqueous phase for the formation of the PA layer (m-phenylenediamine, MPD; piperazine, PIP; and combinations of trimethylamine, TEA and polyvinyl alcohol, PVA) and bisphenol A (BPA) for the formation of the PE layer while TMC was the monomer used in the organic phase. These TFC membranes showed high selectivity to humic acid feed aqueous solutions. In the present study, the same solutions and procedure were followed using as support the selected RFO membrane in order to improve further its FO performance. The employed monomers, their concentrations and combinations together with the reaction time of the IP and membrane names are summarized in Table 6.2.

Table 6.2. *IP parameters used to prepare thin film composite membranes (TRFO) using as support the selected RFO2 membrane.*

Membrane	TFC type	Aqueous phase			Organic phase		
		Material	w/v (%)	Time (min)	Material	w/v (%)	Time (min)
RFO-MPD	PA	MPD	2	60	TMC	2.5	15
RFO-MPD/TEA	PA	MPD-TEA	1-1	60	TMC	2.5	15
RFO-PIP	PA	PIP	2	60	TMC	2.5	15
RFO-PIP/TEA	PA	PIP-TEA	1-1	60	TMC	2.5	15
RFO-PIP/PVA	PA	PIP-PVA	1-1	60	TMC	2.5	15
RFO-BPA	PE	BPA	2	60	TMC	2.5	15

To prepare the thin layer (PA or PE), the PSf layer of the selected RFO membrane was brought into contact first with the aqueous solution for 1 h, then with the organic solution for 15 min. Subsequently, it was air-dried in a dark environment for 24 h at room temperature (293 K) before characterization. More details of the IP technique can be found elsewhere [38]. All the above cited chemicals were purchased from Sigma-Aldrich Chemical Co. St. Louis, Massachusetts, USA.

6.2.3. Commercial membranes

For sake of comparison, two asymmetric FO commercial PA (TFC-HTI) and cellulose triacetate CTA (CTA-HTI) membranes supplied by Hydration Technology Innovations (HTI™, LLC, Albany, USA) were used. Both membranes are embedded in a PE mesh as shown in Figs. 9.1a and 9.1b of the Appendix B. The CTA-HTI membrane has been used extensively in various research studies [45-49]. The characteristics of the prepared membranes were also compared with those of the pristine TM720-400 membrane supplied by Toray Industries, Inc., Japan.

6.2.4. Membrane characterization

Water contact angle (ϑ_w) of membrane samples was measured at room temperature by a CAM 100 Contact Angle Meter (KSV Instruments Ltd., Monroe, Connecticut, USA). The membrane thickness (δ) was measured by a digital micrometer (model 1724-502 series, Helios-Preisser Instruments, Gammertingen, Germany). Scanning electron microscopy (SEM, JEOL Model JSM-6335F, Jeol Ltd., Tokyo, Japan) was used to get images of both the surface

and cross-section of the membranes. Previously, the membrane samples were cut in liquid nitrogen and then coated with a thin layer of gold using a sputter coater (EMITECH K550 X, Emitech Groupe, Montigny, France) with a current of 25 mA during 1 min.

To quantify the surface charge of the membranes streaming potential measurements were performed with SURPASS equipment (Anton Paar GmbH, Austria). All measurements were conducted with an adjustable-gap cell where two membrane samples of 20 mm × 10 mm were fixed on sample holders using double-sided adhesive tape. In this study, a flow channel gap of 100 µm was set between the sample surfaces. First, the samples were thoroughly rinsed with the testing electrolyte (1 mM KCl aqueous solution) and the pH was adjusted to the required value using 0.1 M HCl or 0.1 M NaOH solution. All zeta potential (ζ-potential) measurements were carried out at 25 ± 2 ºC and the pH range was varied from 5.5 to 2.5 with a step of 0.3. Three ζ-potential values were obtained for each pH value.

Attenuated Total Reflectance Fourier Transform Infrared Spectroscopy (ATR-FTIR) was used to confirm the total degradation of the PA layer of the discarded RO membranes after cleaning and to analyze the chemical composition of the prepared TRFO membranes. The measurements were carried out with a Nicolet iS50 device equipped with the deuterated triglycine sulfate-potassium bromide (DTGS-KBr) detector, a KBr beam splitter and an infrared source (Ever-Glo); and having a maximum resolution of 0.09 cm^{-1}.

Solute separation transport tests were performed using polyethylene glycol (PEG) and polyethylene oxide (PEO) of different molecular weights. The selected molecular weights were 0.4, 1, 6, 10, 12, 20 and 35 kg/mol for PEGs and 100 and 200 kg/mol for PEOs [50]. The set-up used was described in our previous paper [51]. The detailed procedure together with the obtained results of water permeance (*WP*) and solute rejection factor (α) are included in Appendix B, Section 9.3. All products were purchased from Sigma-Aldrich Chemical Co. St. Louis, Massachusetts, USA. The feed temperature, pressure and solute concentration were 296 K, 1.04 bar and 200 ppm, respectively.

As it was described in [52], the mean pore size and the geometric standard deviation were determined from the plot of the solute rejection factor as a function of the solute diameter and their correlation according to the log-normal probability function. The mean pore size (μ_p) and the molecular weight cut-off (*MWCO*) correspond to the Einstein-Stokes diameters of 50% and 90% solute rejection factors, respectively. The geometric standard deviation is the ratio between the Einstein-Stokes diameters of 84.13% and 50% rejection factors. The pore density (*N*) and porosity (ε) were determined from the permeance data of PEG and PEO aqueous solution as it is explained in the Supporting Information (Eqs. (9.4) and (9.5) of the Appendix B).

To estimate the tortuosity factor (τ), Bruggeman correlation, which has been proved to be a good approximation relating τ with ε, was employed [53]:

$$\tau = \varepsilon^{-0.5} \tag{6.1}$$

The structural parameter (S) is commonly considered as an important characteristic of FO membranes because of its influence on the internal concentration polarization (ICP) phenomenon and membrane´s structural resistance to solute mass transport. S, often called the "intrinsic" structural parameter, S_{int}, was described as the average diffusive path length through the membrane support layer as follows [54, 55]:

$$S_{int} = \frac{\tau\delta}{\varepsilon} \tag{6.2}$$

6.2.5. Forward osmosis (FO) experiments

All membranes were tested in the FO set-up (Lewis cell) shown in Fig. 6.1. This is composed of two stainless steel cylindrical chambers having an internal volume of 250 mL. The membrane, with an effective area of $1.59 \cdot 10^{-3}$ m^2, is placed between the two chambers with its selective layer facing the feed side (FO mode). Both chambers are double walled so that a thermostatic liquid can circulate through them and keep constant the temperature of both the feed and permeate at 296 K.

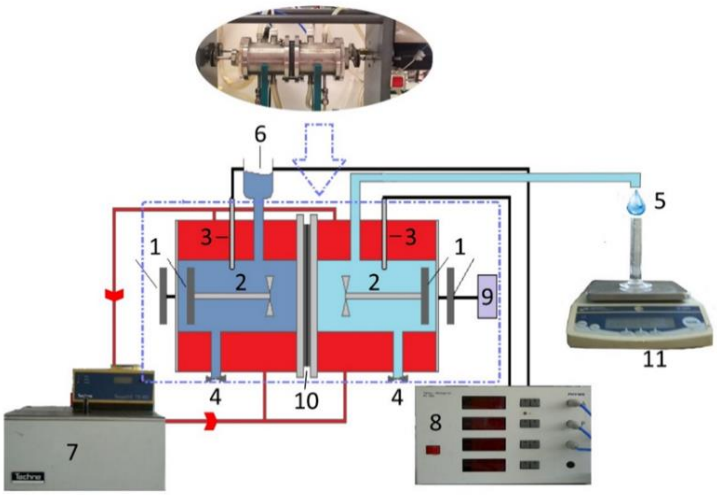

Figure 6.1. *FO experimental set-up: 1. magnets; 2. stirrers; 3. temperature sensors (pt100 probes); 4. inlets; 5. permeate; 6. reservoir; 7. thermostat (TE-8D, Techne Inc., New Jersey, USA); 8. digital temperature indicator (Temp. Meßgerät pt100, PHYWE Systeme GmbH und Co. KG, Göttingen,*

Germany); 9. electric motor with speed control (K50640, Kelvin S.A., Madrid, Spain); 10. Membrane support; 11. Balance (SI-2002, Denver Instrument Company, Arvada, USA).

6.2.5.1. Evaluation of the effective structural parameter, S_{eff}, from FO experiments

As stated earlier, the structural parameter, *S* (Eq. (6.2)), is widely used as an assessment of FO membrane structural characteristics. However, measuring porosity and tortuosity is a challenging task. Most researchers have adopted a fitted parameter mass transfer model to determine S_{eff} from RO test obtaining the membrane water permeance (parameter *A*) and the membrane salt permeance (parameter *B*). This method is questionable since *A* and *B* are different in RO process subjected to much higher pressure than in FO process. Furthermore, the solute concentration at the membrane selective layer is much higher in RO test than in FO because of the higher applied hydrostatic pressure in RO [54]. In addition, FO membranes are not generally designed to bear high hydrostatic pressures like those applied in RO and therefore the permselective properties of the FO membrane could be altered during RO test (i.e. the *A* and *B* values could be different) [49]. To estimate an "effective" or fitted structural parameter, semi-empirical models, based on fitted parameter mass transfer equations from FO experimental flux measurements, have been used [54]:

$$S_{eff} = \frac{D}{J_w} \ln\left(\frac{B + A\pi_{D,b}}{B + J_w + A\pi_{F,m}}\right) \tag{6.3}$$

where, *D* is the solute coefficient diffusion, J_w is the average water flux, *A* is the water permeance coefficient of the membrane, *B* is the solute permeance coefficient of the membrane, $\pi_{D,b}$ is the osmotic pressure of the bulk draw solution, and $\pi_{F,m}$ is the osmotic pressure of the feed solution at the membrane side. It is worth noting that both the water and solute permeance coefficients (*A* and *B*, respectively) are typically obtained from additional RO tests using different applied pressures.

In FO experiments, water together with a little quantity of feed solute permeate from the feed to the draw solution, which becomes diluted within the membrane and draw solution/membrane boundary layer causing both internal concentration polarization (ICP) and external concentration polarization (ECP). In fact, ECP occurs externally at both sides of the membrane surface. At the same time, draw solute diffuses from the draw solution through the membrane to the feed solution boundary layer [56]. Therefore, the effects of both the selective layer side and the draw side of the membrane must be taken into account in theoretical modelling. Tiraferri *et al*. [57] derived a transport model for FO taking into

account both the concentrative ECP on the feed side, the dilutive ICP and the reverse solute flux as:

$$J_w = A\left\{\frac{\pi_D \exp\left(-\frac{J_w S_{eff}}{D}\right) - \pi_F \exp\left(\frac{J_w}{k}\right)}{1 + \frac{B}{J_w}\left[\exp\left(\frac{J_w}{k}\right) - \exp\left(-\frac{J_w S_{eff}}{D}\right)\right]}\right\} \tag{6.4}$$

$$J_s = B\left\{\frac{C_D \exp\left(-\frac{J_w S_{eff}}{D}\right) - C_F \exp\left(\frac{J_w}{k}\right)}{1 + \frac{B}{J_w}\left[\exp\left(\frac{J_w}{k}\right) - \exp\left(-\frac{J_w S_{eff}}{D}\right)\right]}\right\} \tag{6.5}$$

where k is the feed mass transfer coefficient and *D* is the bulk diffusion coefficient of the draw solution. Note that the terms $\exp\left(\frac{J_w}{k}\right)$ and $\exp\left(-\frac{J_w S_{eff}}{D}\right)$ are related to the concentrative external concentration polarization (ECP) and dilutive internal concentration polarization (ICP) phenomena, respectively. Tiraferri *et al*. [57] designed an alternative and simple methodology to estimate the parameters *A*, *B* and S_{eff} solely from FO experiments using different concentrations of a given draw solution and distilled water as feed. In this study, the S_{eff} structural parameter of RFO, TRFO and FO commercial membranes was determined using the FO experimental results (*J* and J_s as will be explained in Eqs. (6.7) and (6.8)) obtained at different NaCl concentrations of the NaCl draw solution (15, 40, 65 and 90 g/L) while Milli-Q water was employed as feed. By using the salt osmotic pressure at different NaCl concentrations and the Excel spreadsheet provided by Tiraferri *et al*. [57] the parameters *A, B* and S_{eff} were calculated.

By using van't Hoff approximation, the osmotic pressure of the draw solution was assumed to be linearly proportional to the concentration:

$$\pi = icRT \tag{6.6}$$

where *c* is the molarity (in mM), *T* is the absolute temperature (in K), *R* is the ideal gas constant and *i* is the van´t Hoff factor presenting the number of ionic species dissociated in the aqueous solution, feed or draw solution. For NaCl aqueous solution, *i* = 2.

Since S_{int} depends only on the geometrical factors of the membrane (see Eq. (6.2)), it can be assumed independent on the solute transport rates [55]. It is to be noted that although in general S_{eff} and S_{int} are assumed to be identical, some researchers claimed their discrepancy [21, 54, 55, 58, 59].

6.2.5.2. Wastewater treatment by FO separation process

Sodium chloride (NaCl, Scharlau Chemicals Co., Barcelona, Spain) aqueous solutions of 65 g/L and 200 g/L were used as draw solutions and HA (Sigma-Aldrich Chemical Co. St. Louis, Massachuset, USA) aqueous solutions with 10 mg/L and 100 mg/L concentrations were used as feed wastewater model solutions. Dilute HA solutions were prepared from a standard HA concentrated solution of 1 g/L and the pH was adjusted to 11 (Metrohm pH/Ion meter 692, Herisau, Suiza) by adding 2 M hydrochloric acid (HCl) aqueous solution as needed [38]. Taking into consideration that the ζ-potential of both PSf layer of the RFO membranes, and the PA and PE layers of the TRFO membranes formed by IP are very electronegative at high pH [38, 60] a higher feed pH was selected to minimize the adsorption phenomenon of HA. In other words, at high pH values both the membrane and the HA feed solution have negative electrical charges that generate electrical repulsion between them [61]. Two types of FO tests were carried out using low concentrations of NaCl (65 g/L) and HA (10 mg/L) and high concentrations of NaCl (200 g/L) and HA (100 mg/L) solutions.

The feed and permeate temperatures were measured inside each chamber by pt100 sensors connected to a digital meter. Both chambers contain magnetic stirrers set in this study at 750 rpm for all tests. To determine the permeate flux (J) through the effective membrane area (A_m), the collected permeate (Δm) was weighed in a precision balance for a predetermined time (Δt) and then calculated as [48, 62]:

$$J = \frac{\Delta m}{A_m \Delta t} \tag{6.7}$$

The permeate flux measurements were made in triplicate and for each membrane two samples were tested for 30 min. A mean permeate flux was finally determined with its corresponding standard deviation.

The HA and salt concentrations of the both the feed and draw solutions were measured at the beginning and at the end of each experiment for all samples. From these measurements, the reverse salt permeate flux (J_s) was calculated using the following equation [48, 62]:

$$J_S = \frac{C_{s,\mathrm{F},t} V_{F,t} - C_{s,\mathrm{F},0} V_{F,0}}{A_m \Delta t} \tag{6.8}$$

where $C_{s,F,0}$ an $C_{s,F,t}$ are the initial and final feed salt concentrations, respectively; and $V_{F,0}$ and $V_{F,t}$ are the initial and final feed volumes, respectively. During the FO experiments, the feed volume was maintained constant (250 mL) by the feed reservoir (Fig. 6.1).

The HA rejection factor (R_{HA}) was evaluated using the following equation [63]:

$$R_{HA}\,(\%) = \left(1 - \frac{C_{HA,D,t}}{C_{HA,F,0}}\right) \cdot 100 \tag{6.9}$$

where $C_{HA,D,t}$ is the final HA concentration of the draw solution and $C_{HA,F,0}$ the initial HA concentration of the feed solution.

Another parameter considered to evaluate the membrane performance is the HA concentration factor (CF_{HA}) defined as [64, 65]:

$$CF_{HA} = \left(\frac{C_{HA,F,t}}{C_{HA,F,0}}\right) \tag{6.10}$$

where $C_{HA,F,t}$ and $C_{HA,F,0}$ are the HA concentrations of the feed solution at the initial and final of the FO experiment, respectively. For sake of comparison, the total experimental time for each membrane was maintained the same (30 min). Since two different HA initial concentrations were considered in FO, CF_{HA} values could reflect the effectiveness of FO membranes during the concentration processes depending on the feed solutions. Furthermore, this parameter can be taken into consideration to figure out whether feed contaminants could be adsorbed at the membrane or not [64].

To determine the concentration of NaCl and HA, both the electrical conductivity and absorbance of the feed and draw solutions were measured using a conductivity meter (Metrohm 712Ω, Herisau, Suiza) and a spectrophotometer (Genesis 10S UV-Vis, Thermo Scientific Inc., Massachusetts, USA), respectively. It is worth quoting that the HA absorption spectrum has no characteristic peak so in this study the absorbance measurements of HA were taken at 254 nm as reported elsewhere [51]. The HA and NaCl concentrations were determined by comparing the obtained absorbance and electrical conductivity data with appropriate calibration curves presenting the absorbance or electrical conductivity as a function of the HA or NaCl concentration, respectively. The effects of HA on the electrical conductivity of NaCl solutions was verified by measuring the electrical conductivity of the studied saline solutions at different HA concentrations (Fig. 9.2 of the Appendix B). Moreover, for all studied HA solutions the absorbance was measured at different NaCl concentrations (Fig. 9.3 of the Appendix B).

6.3. Results and Discussions

6.3.1. Characteristics of recycled forward osmosis (RFO) membranes

The water contact angles (θ_w) of both the active top layer and support layer of the RFO membranes together with the total thickness (δ) and the isoelectric point (IEP) are summarized in Table 6.3. All RFO membranes exhibit similar results regardless of the followed cleaning procedure and the total dose level applied.

Table 6.3. *Water contact angle (θ_w) of the active layer (AL) and support layer (SL), thickness (δ) and isoelectric point (IEP) of the RFO membranes and the commercial membranes TM720-400, CTA-HTI and TFC-HTI.*

Membrane	$(\theta_w)_{AL}$ (º)	$(\theta_w)_{SL}$ (º)	δ (µm)	*IEP* (pH)
TM720-400	54 ± 3	64 ± 2	110 ± 3	--
RFO1	78 ± 3	65 ± 2	100 ± 6	3.55
RFO2	79 ± 2	65 ± 5	97 ± 4	3.63
RFO3	76 ± 2	69 ± 2	96 ± 5	3.96
RFO4	78 ± 2	65 ± 5	96 ± 5	3.88
CTA-HTI	60 ± 1	69 ± 6	72 ± 5	4.12
TFC-HTI	26 ± 4	N/A	83 ± 4	3.21

The water contact angle of the support layer of the RFO membranes is similar to that of the pristine TM720-400 membrane (i.e. 64 ± 2º). However, an increase of the water contact angle of the active layer from 54º to 78º was detected for the discarded RO membranes after NaClO cleaning. This value corresponds to the water contact angle of PSf layer confirming therefore the removal of the PA top layer from the surface of the RFO membranes [66, 67]. The obtained results indicate the low hydrophilic character of the RFO membranes compared to the pristine TM720-400 membrane and both CTA-HTI and TFC-HTI membranes. The measured water contact angle of the commercial membranes (CTA-HTI and TFC-HTI) agree well with those reported by [68] (i.e. the active layer water contact angle was 60 ± 1° and 26° ± 4 for CTA-HTI and TFC-HTI membranes, respectively). The thickness of all RFO membranes is almost similar taking into consideration their error intervals. Compared to the thickness of the TM720-400 pristine membrane (110 ± 2 µm), the RFO membranes are thinner (96 – 100 µm) indicating the 10 to 14 µm PA layer thickness.

From the SEM images of the RFO membranes shown in Fig. 6.2, it can be seen that the surface cleaning improved with the increase of the exposure time (from RFO1 to RFO2) and

by adding the laboratory cleaning step (RFO3 and RFO4) although the effect of this last step is not significant for cleaning improvement compared to the increase of the exposure dose in the pilot plant. However, this second cleaning step requires disassembling the membrane module and results in an increase of the cleaning cost. In fact, the SEM images of the RFO2 and RFO4 membranes are similar although the last membrane was subjected to laboratory cleaning.

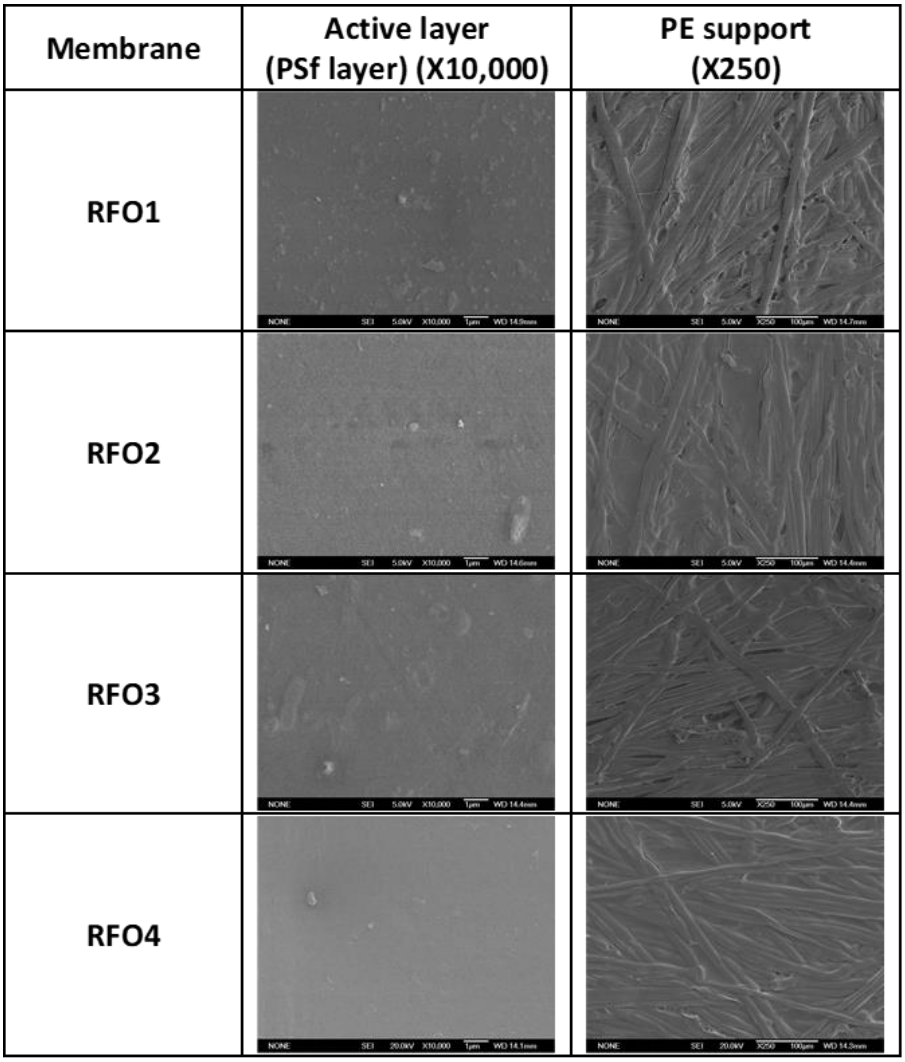

Figure 6.2. *SEM images of the PSf layer and PE support of the RFO membranes.*

The ζ-potential and *IEP* of the RFO membranes and commercial membranes, CTA-HTI and TFC-HTI, are presented in Fig. 6.3 and Table 6.3, respectively. The obtained values of the commercial membranes (CTA-HTI and TFC-HTI) agreed well with those presented in previous studies [47, 49, 69]. The TFC-HTI membrane was more negatively charged than the CTA-HTI membrane as it was observed elsewhere [70]. In general, the ζ-potential and *IEP* of the RFO membranes are quite similar and all *IEP* values of the RFO membranes were between those

of TFC-HTI and CTA-HTI. Small differences of the ζ-potential and *IEP* were detected between the RFO membranes. The membranes previously cleaned in the laboratory (RFO3 and RFO4) exhibited slightly higher values than those cleaned in the pilot plant (RFO1 and RFO2). This could be due to the existence of small persistent PA residues on the membrane surface of the RFO membranes cleaned in the pilot plant, which seems to be eliminated after laboratory cleaning step.

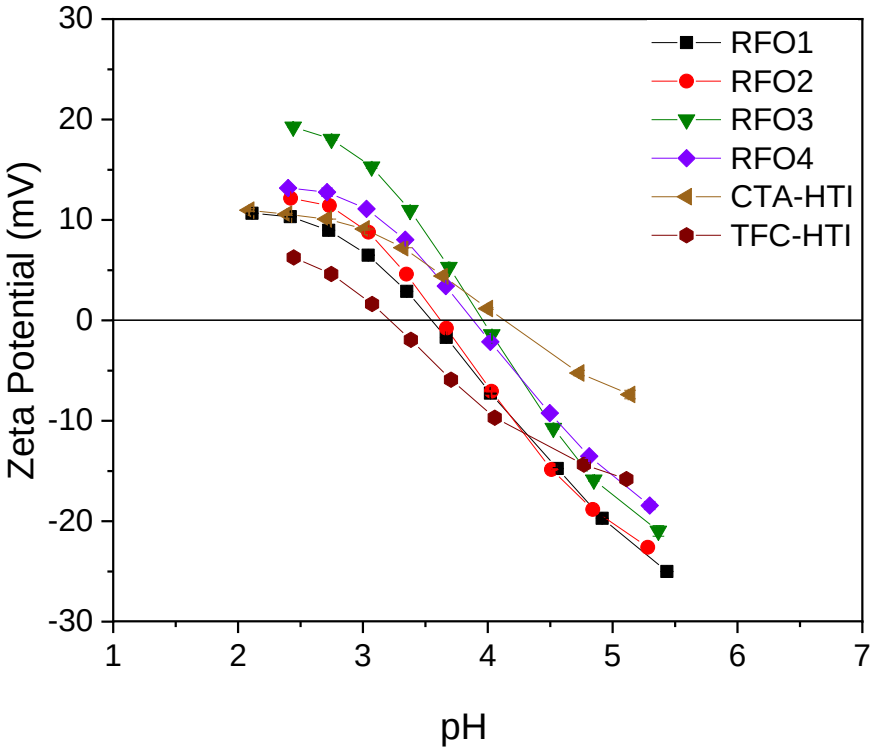

Figure 6.3. *ζ-potential of the RFO membranes together with that of CTA-HTI and TFC-HTI commercial membranes at different pH values.*

In order to confirm if the total degradation of the PA top layer occurs, the RFO membranes were characterized by ATR-FTIR and their spectra were compared to the pristine TM720-400 membrane spectrum. From Fig. 6.4, it can be seen that the peaks corresponding to the amide I and amide II bands and the C = C stretching vibrations of the aromatic amide bonds (1664, 1542 and 1610 cm^{-1}, respectively [41]) were clearly detected in the spectrum of the pristine TM720-400 membrane but not in the spectra of the RFO membranes. This indicates the degradation of the PA layer. It is to be noted that no significant difference was detected between the spectra of the RFO3 and RFO4 membranes, while in the RFO1 and RFO2 membranes some absorbance was detected in amide bands. It must be mentioned that several ATR-FTIR spectra were carried out in different parts of the RFO membranes. Depending on the analysed section of the RFO1 and RFO2 membrane samples, the absorbance at the amide bands appeared or not. This is probably attributed to PA residual

left deep suggesting that the pilot plant cleaning did not completely remove the PA layer of the discarded RO membranes.

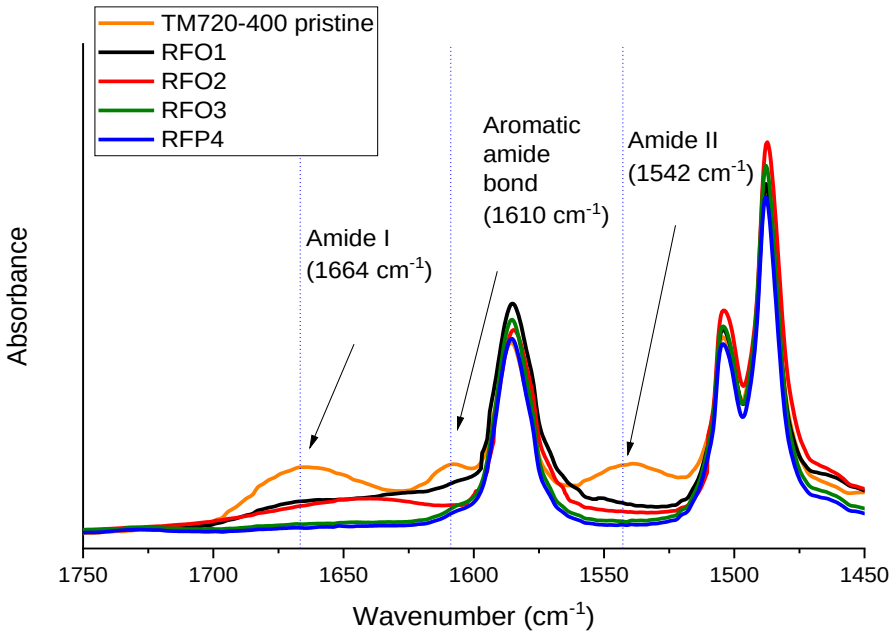

Figure 6.4. *ATR-FTIR spectra of the RFO membranes and the pristine TM720-400 commercial membrane.*

Prior to solute transport experiments with PEG and PEO, the water permeance (*WP*) was determined for each RFO membrane and the results are summarized in Table 9.1 of the Appendix B. By increasing the cleaning exposure time (RFO1 and RFO2 membranes) or adding the laboratory cleaning step (RFO1 and RFO3 membranes) the *WP* value was increased by 17% and 11%, respectively. However, for the RFO2 membrane no enhanced *WP* was detected after the addition of the laboratory cleaning step (i.e. both RFO2 and RFO4 membranes exhibit the same *WP*). It must be stated that the obtained *WP* of the RFO2 membrane is in good agreement, within 3% deviation, with that reported elsewhere for a similar membrane and for the same cleaning procedure followed to prepare RFO2 membrane [41]. Similar *WP* values were reported for UF recycled end-of-life RO membranes [13, 43].

The solute separation results are also presented in Table 9.1 of the Appendix B. With the application of the laboratory cleaning step, a slight reduction of the solute rejection factor (α) was detected. The RFO1 and RFO2 membranes reached 50% rejection for PEG6, while for the same PEG the rejection factor of the other membranes, RFO3 and RFO4, was lower than 50%. All RFO membranes presented a 100% rejection factor when using PEO200 and between 96-99% for PEO100. For all recycled membranes, an average rejection factor of 35% was obtained when using PEG0.4. This high degree of separation for such low molecular weight

compound indicates that RFO membranes preserved NF characteristics after recycling procedure. The use of NF-like FO membranes has been already reported elsewhere [71-73].

In Fig. 9.4 of the Appendix B the rejection factor was plotted as a function of the solute diameter according to log-normal probability function. The determined mean pore size (μ_p), its geometric standard deviation (σ_p), pore density (N), porosity (ε) and molecular weight cut-off ($MWCO$) from the solute transport tests, as well as the tortuosity (τ, obtained from Eq. (6.1)) and the "intrinsic" structural parameter (S_{int}, from Eq. (6.2)) are summarized in Table 6.4. The related cumulative pore size distribution and the probability density function curves are presented in Fig. 9.5 of the Appendix B.

Table 6.4. *Mean pore size (μp), geometric standard deviation (σp), pore density (N), porosity (ε), molecular weight cut-off (MWCO), tortuosity (τ) and "intrinsic" structural parameter factor (Sint) of the RFO membranes obtained from the solute transport test.*

Membrane	μ_p (nm)	σ_p (-)	N (pores/μm^2)	ε (%)	$MWCO$ (kDa)	τ (-)	S_{int} (μm)
RFO1	3.6	2.6	5037	26	33.9	2.15	824
RFO2	3.4	2.1	4910	30	29.5	1.97	631
RFO3	4.1	2.6	4446	28	39.8	2.08	725
RFO4	3.7	2.6	5467	30	38.0	1.98	629

Since the PA layer was removed, the obtained mean pore size of the RFO membranes were larger than the typical pore size of RO membranes (< 1nm) and similar to those of NF-like membranes [74]. Almost similar pore sizes were obtained when increasing the cleaning exposure time in the pilot plant (i.e. reduction of less than 6% of the pore size of the membrane RFO2 compared to the membrane RFO1) but the *MWCO* was decreased 12.8%. This is attributed to the reduction of the tail of the probability density function curve of the RFO2 membrane. However, when comparing the RFO1 membrane with the RFO3 membrane, and the RFO2 membrane with the RFO4 membrane, slight enhancements of both the pore size and the *MWCO* were detected when the laboratory cleaning step was added after the pilot plant cleaning protocol (i.e. 13.9% and 8.8% increase of the pore size and 17.5% and 28.9% increase of the *MWCO* for the RFO3 and RFO4 membranes, respectively). Note that the CTA-HTI membrane has an average pore size of 0.3 nm [75]. Therefore, the pore size of the RFO membranes is an order of magnitude greater than that of the CTA-HTI membrane. A broad range of pore size (0.2 – 7 nm) for FO membranes is reported in the literature [74-79]. In addition, the porosity (ε) of the RFO membranes was found to be within the values expected for a typical FO membrane. A porosity of 40 ± 3 % was reported for CTA-HTI

membrane [45] while porosity values between 16% and 21% were reported for the PSf support of the TFC-PA RO membranes prepared with different PSf concentrations [80].

The pore density decreased by 12% for the RFO3 compared to the RFO1 membrane whereas that of the RFO4 membrane increased by 11% compared to the RFO2 membrane. This indicates that the pore density does not show any relationship with the followed laboratory cleaning protocol. The tortuosity was estimated from Eq. (6.1) in order to determine the "intrinsic" or geometrical structural parameter, S_{int}. A slightly lower tortuosity was obtained for the recycled RFO membranes (RFO2 and RFO4) applying the lower exposure dose in pilot plant cleaning. A tortuosity factor of 4.69 was reported in [45] for the commercial membrane CTA-HTI using the structural parameter (620 μm) estimated by RO tests and Eq. (6.2). If Eq. (6.1) were used to estimate the tortuosity factor from the value of the porosity (40%) also reported in [45], an estimated lower value of 1.69 would be obtained. This indicates that the applied model gives tortuosity values lower than the estimated from RO test and, as a consequence, lower S_{int} values are obtained. Membranes with low S_{int} values are preferred for FO membranes in order to reduce the ICP effect. Therefore, the ratio τ/ε must be as low as possible. In general, to decrease the structural parameter of the TFC-FO membranes, a thin support layer with a high porosity should be used. The porosity of the support layer of a given FO membrane exerts a significant effect on both J and J_s (i.e. both permeate fluxes increase with the increase of the porosity). For active layers with low porosity values, J and J_s are more sensitive to the support layer porosity [81]. It must be pointed out that increasing porosity or decreasing tortuosity is not always desirable since increasing J also increases J_s.

6.3.2. FO experiments of recycled forward osmosis (RFO) membranes

The RFO membranes and the two commercial membranes (CTA-HTI and TFC-HTI) were tested in FO using HA aqueous solutions as feed and NaCl aqueous solutions as draw solutions (i.e. low concentration: 10 mg/L HA aqueous solution and 65 g/L NaCl aqueous solution; and high concentration: 100 mg/L HA aqueous solution and 200 g/L NaCl aqueous solution). The results represented in Figs. 6.5 and 6.6.

The permeate flux (J) of each RFO membrane is quite similar for both the high (3.3-7.2 kg/m^{2}h) and low (3.2-6.3 kg/m^{2}h) concentrations tests, although slightly greater values could be detected for the high concentration test because of the enhanced osmotic pressure of the draw solution with the increase of the NaCl concentration (i.e. FO driving force) [82]. Longer exposure time during cleaning in the pilot plant (RFO1 and RFO2 membranes) improves the permeate flux. However, the addition of the laboratory cleaning step (RFO1 and RFO3 membranes, RFO2 and RFO4 membranes) does not provide any significant enhancement of

the permeate flux, but it increases slightly the specific reverse salt flux J_s/J. This could be due to the existence of PA residues in the PSf pores of RFO1 and RFO2 membranes (Fig.6.4) reducing the reverse draw solute transport (J_s) while increasing slightly the water transport (J) and rendering the membrane semi-permeable.

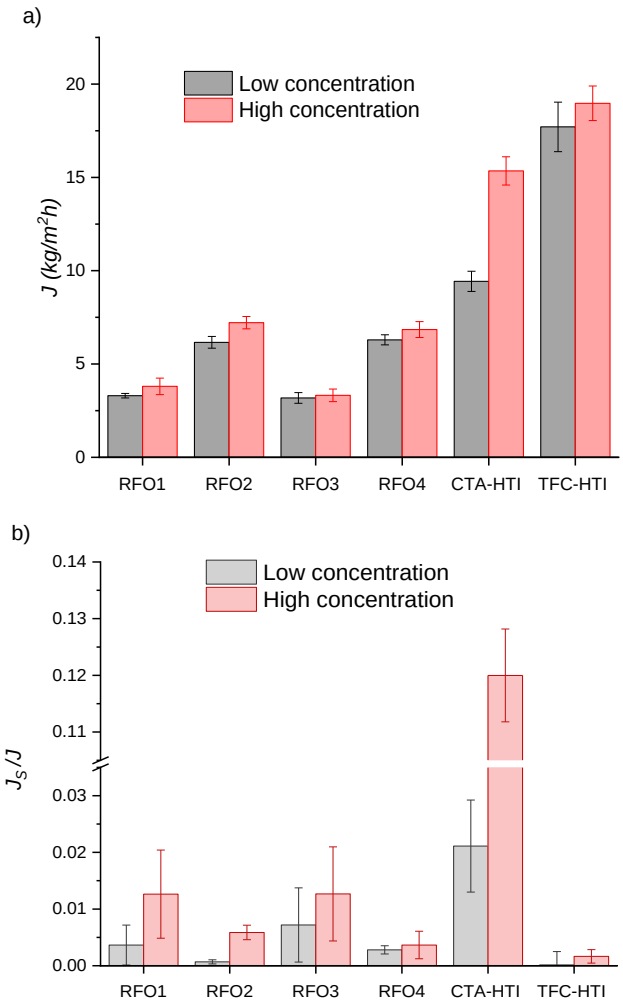

Figure 6.5. *a) FO permeate flux (J) and b) specific reverse salt flux (Js/J) of the RFO membranes and commercial membranes (CTA-HTI and TFC-HTI) for low concentration (10 mg/L HA feed aqueous solution and 65 g/L NaCl draw aqueous solution) and high concentration (100 mg/L HA feed aqueous solution and 200 g/L NaCl draw aqueous solution).*

The specific reverse salt flux (J_s/J) is a quantitative factor that indicates the bi-directional diffusion in the FO process. Higher (J_s/J) reflects a decrease of the selectivity and efficiency of the membrane. As can be seen in Fig. 6.5b, J_s/J depends on the NaCl concentration of the draw solution. For a higher NaCl concentration, a greater J_s/J value was obtained because the osmotic pressure (i.e. the FO driving force) is higher. Similar results were reported in [83]. In order to compare the draw solute loss due to the reverse salt flux for both high and low concentrations, a normalized reverse salt transfer (RT_s) was defined as

the ratio of the NaCl concentration transported through the FO membrane to the feed side and the initial draw concentration (Section 9.4, Fig. 9.6a of the Appendix B). For the low concentration test, the RFO membranes cleaned only in the pilot plant (RFO1 and RFO2 membranes) have significantly lower RT_s values than the other RFO membranes cleaned also following the laboratory scale protocol (RFO3 and RFO4 membranes), confirming therefore that small PA residues in the PSf pores of RFO1 and RFO2 membranes could prevent reverse draw solute transport reducing both the RT_s and J_s values.

The best FO performance (i.e. high J, low J_s/J and low RT_s) for the low concentration test was obtained with the RFO2 membrane. However, this membrane presents 35% and 65% lower permeate flux than those of the commercial membranes CTA-HTI and TFC-HTI, respectively. The J_s/J of the RFO2 membrane is smaller than that of the commercial membrane CTA-HTI and comparable with the best result obtained for the commercial membrane TFC-HTI. For the high concentration test, the RFO2 membrane also presents the highest J flux among all RFO membranes. In general, the above results show that the RFO2 membrane is optimal for both high and low concentrations tests.

The observed lower J values of the RFO membranes compared to the commercial ones (CTA-HTI and TFC-HTI) may be due to their lower surface porosity and pore density as well as to their lower hydrophilic character as discussed earlier. In addition, the highest permeate flux of the TFC-HTI membrane compared to the CTA-HTI membrane may be due to its lower electronegativity at pH 11 that results in greater electrostatic repulsive forces to HA favouring therefore water permeation through the membrane. The obtained J and J_s/J data of the membranes TFC-HTI and CTA-HTI for low concentration test were found to be within the expected values reported in the literature (i.e. less than 10% deviation) although different experimental systems and FO operating conditions were considered [46, 48, 54, 70].

The humic acid rejection factor (R_{HA}) of both low and high concentration tests are plotted in Fig. 6.6a. For high concentration test, the R_{HA} of all RFO membranes is at least 99.3 %, which is higher than that of the commercial membranes (TFC-HTI, 98.9 % and CTA-HTI 97.7 %). The RFO2 membrane has the highest R_{HA} value for the low concentration test, which is 0.6% and 1.9% higher than that of the commercial membranes TFC-HTI and CTA-HTI, respectively. It can be seen from the R_{HA} data of the RFO1 and RFO3 membranes, as well as those of the RFO2 and RFO4 membranes, that the laboratory cleaning step does not improve R_{HA}. This also supports that the existence of the PA residues in the PSf pores retards the diffusion of the HA from the feed to the draw solution [22].

The calculated HA concentration factor (CF_{HA}) of all membranes by Eq. (6.10) at 30 min running time is shown in Fig. 6.6b for both low and high concentration tests. The CF_{HA} factor takes into account both J and R_{HA} results (i.e. sufficiently high J and R_{HA} values results

in a high CF_{HA} factor). For all membranes, it was observed lower CF_{HA} factor for the high concentration test than for the low concentration test. This is because CF_{HA} is inversely proportional to the initial HA concentration of the feed solution although both *J* and R_{HA} are greater for the high concentration value than for the low concentration test.

Among all tested membranes, the commercial membrane TFC-HTI exhibits the best CF_{HA} factors while the CTA-HTI membrane shows the worst factors. For the high concentration test, the RFO membranes also show comparable values to those of the membrane TFC-HTI. Again, the RFO membranes cleaned only in the pilot plant (RFO1 and RFO2 membranes) have slightly better CF_{HA} factors than the other RFO membranes cleaned also following laboratory protocol (RFO3 and RFO4 membranes).

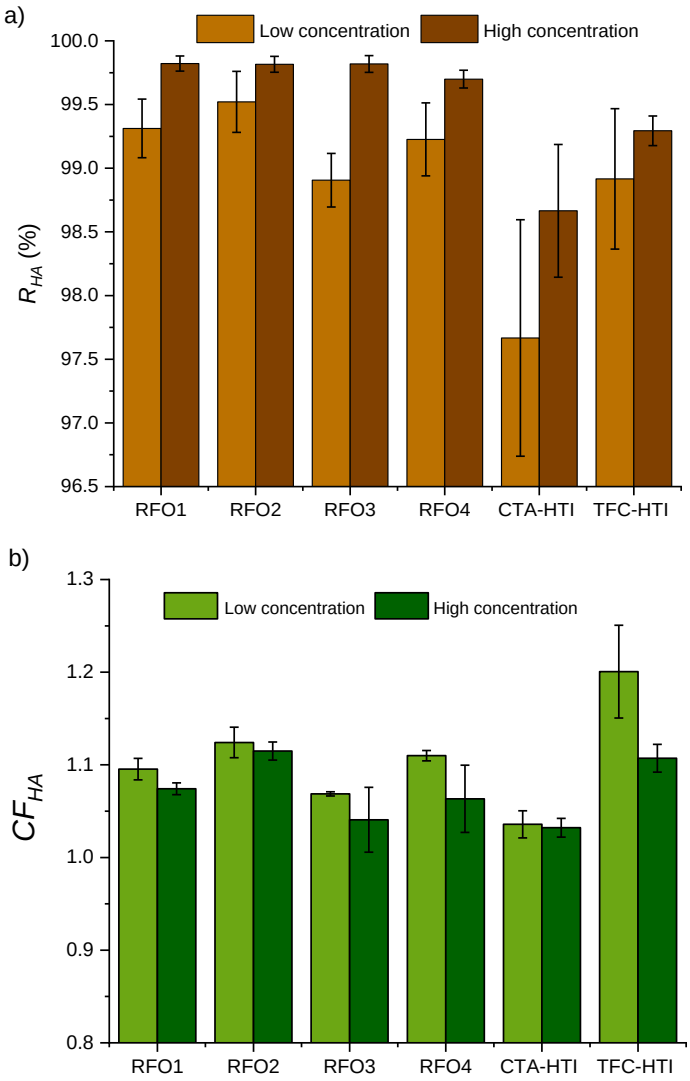

Figure 6.6. *HA rejection factor (RHA) (a) and HA concentration factor (CFHA) at 30 min (b) of the RFO membranes and commercial CTA-HTI and TFC-HTI membranes for low concentration (10 mg/L HA feed aqueous solution and 65 g/L NaCl draw aqueous solution) and high concentration (100 mg/L HA feed aqueous solution and 200 g/L NaCl draw aqueous solution).*

In general, the RFO2 membrane cleaned only in pilot plant with an exposure dose level of 10^6 ppm·h presents among all RFO membranes the best FO results (Table 9.2 of the Appendix B). This membrane exhibits reasonably high water permeate fluxes compared to the FO commercial membranes and much lower permeate fluxes ratio (J_s/J) than those of the CTA-HTI membrane. Note that in pilot plant cleaning procedure, it is not necessary to disassemble the membrane module allowing therefore the reuse of the complete RO discarded membrane in FO after an appropriate modification. Therefore, as explained previously in section 6.2.2, this membrane was selected as support for the preparation of TFC-RFO membranes by interfacial polymerization (IP) in order to improve further the FO performance.

6.3.3. Characteristics of TRFO membranes

The water contact angle of the active and support layers of the prepared TRFO membranes are summarized in Table 6.5 together with their total thickness. The water contact angle of the support layer of all TRFO membranes is the same as that of the RFO2 membrane (i. e. 65 ± 5º). However, a decrease of the water contact angle of the active layer from 79º to 55-29º was detected after the surface modification of the RFO2 membrane by IP showing their improved hydrophilic character. Taking into consideration the standard deviation of the measured water contact angles, all TRFO membranes with the new PA active layer presented similar water contact angle values (i.e. a mean value of 32 ± 2 º) clearly lower than that of the new PE active layer (55 ± 5 º). The lower hydrophilic character of PA compared to PE was already observed in other studies [38]. The total thickness of all TRFO membranes can also be considered the same taking into account the associated errors, even it was maintained the same as that of the RFO2 membrane (97 ± 4 μm). Therefore, a very thin active (PA or PE) layer can be assumed.

Table 6.5. *Water contact angle (θw) of both the active layer (AL) and support layer (SL) and thickness of the TRFO membranes.*

Membrane	$(\theta_w)_{AL}$ (º)	$(\theta_w)_{SL}$ (º)	δ (μm)
RFO-MPD	31 ± 5	65 ± 4	98 ± 2
RFO-MPD/TEA	33± 5	65 ± 4	99 ± 4
RFO-PIP	35 ± 2	66 ± 4	97 ± 3
RFO-PIP/TEA	29 ± 6	65 ± 5	98 ± 4
RFO-PIP/PVA	29 ± 3	63 ± 3	96 ± 5
RFO-BPA	55 ± 5	64 ± 3	97 ± 5

Fig. 6.7 shows the SEM images of the top surface (PA or PE active layer) of the TRFO membranes. A PA formed layer on the top surface of the RFO2 substrate was observed and as a consequence, the resultant TRFO membranes exhibited a dense top surface. Noticeable morphological differences of the active layers (PA with MPD, PA with PIP or PE) of the TRFO membranes were detected. The formed PA layer using MPD presented the typical characteristic of an interfacial polymerized PA membrane consisting of ‘‘ridge-and-valley’’ morphological structure [77, 79, 84, 85]. It must be noted that TFC-FO membranes are commonly prepared with MPD as aqueous phase in the IP process. The surface morphology of the transformed membranes by PIP (RFO-PIP, RFO-PIP/TEA and RFO-PIP/PVA) were also rough with granular-like-structure morphology. Using TEA or PVA in the aqueous phase together PIP induced a smooth granular top surface. When PE layer was formed on the top surface of the RFO2 substrate, a less dense layer was observed. This could be attributed to the fact that PA residual in the pores of PSf substrate of the RFO2 membrane facilitated the penetration of the aqueous phase (MPD or PIP) into the substrate but hindered BPA that was used to form PE layer. Chi et al. [85] prepared a TFC FO membrane supported by polyimide (PI) microporous nanofiber membrane using two IP steps. In the first IP step, only few amounts of PA could be deposited on the nanofibers without forming a PA layer. These PA deposits facilitated the formation of a dense and thin PA layer in the second IP step.

The obtained ATR-FTIR spectra of the TRFO membranes and that of the RFO2 membrane are presented in Fig. 6.8. All PA modified TRFO membranes showed an absorption peak corresponding to the C = C stretching vibrations of the aromatic amide bonds at 1610 cm^{-1} (Fig. 6.8a and 6.8b). The amide I and amide II absorbance peaks at 1664 and 1542 cm^{-1}, respectively, were clearly detected for the RFO-MPD and RFO-MPD/TEA membranes as presented in Fig. 6.8a. However, these peaks were not detected for the transformed membranes by PIP (RFO-PIP, RFO-PIP/PVA and RFO-PIP/TEA) in Fig. 6.8b since the amine salts were consumed as catalyst and was not integrate into the poly(piperazine-amide) layer [86]. The broad peak centred at 3313 cm^{-1} for the membranes RFO-MPD and RFO-MPD/TEA or at 3440 cm^{-1} for the membranes RFO-PIP, RFP-PIP/TEA and RFO-PIP/PVA was due to O–H stretching that could arise from the partial hydrolysis of the acyl chloride unit of TMC [87, 88].

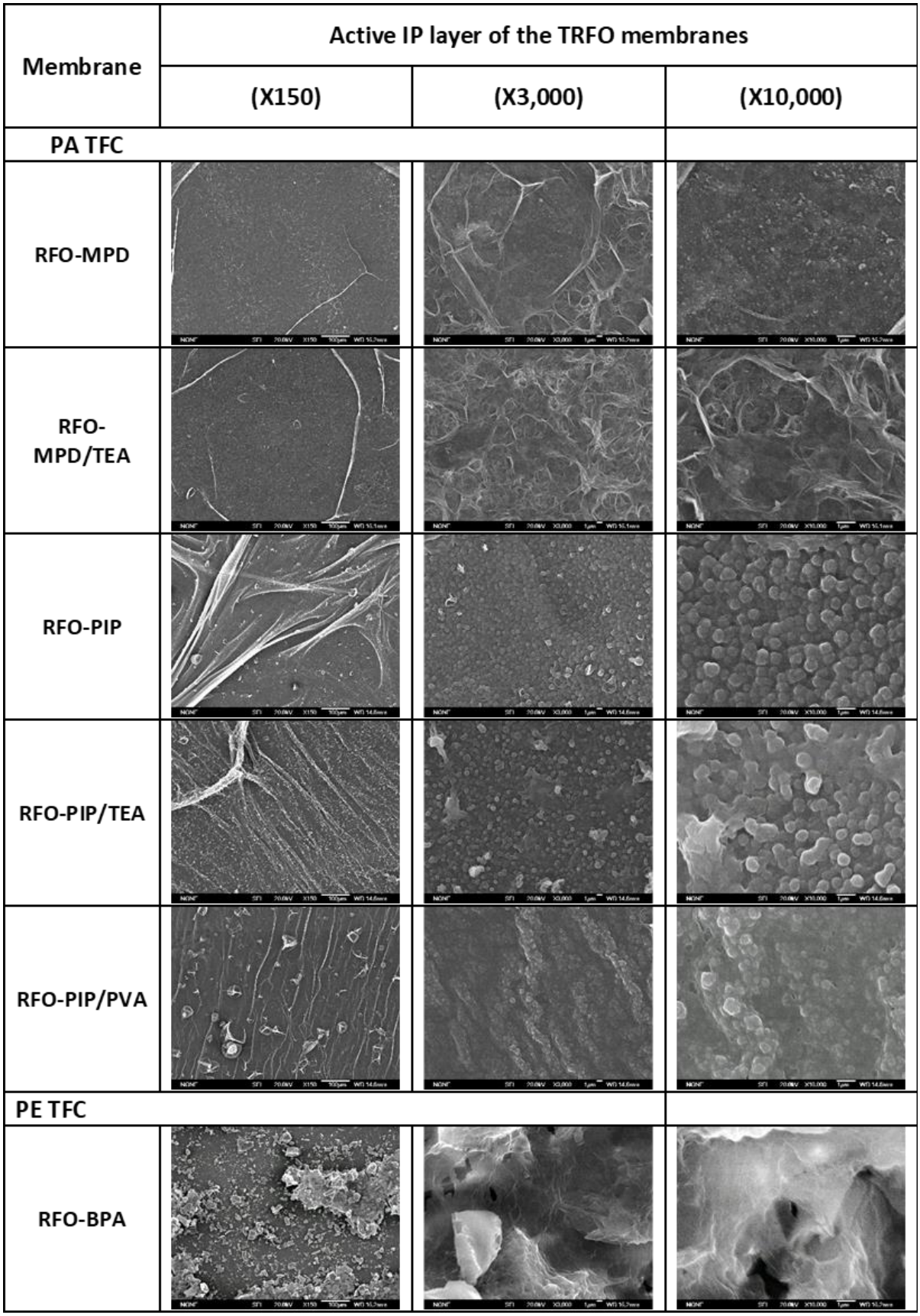

Figure 6.7. *Top-surface SEM images (active IP layer) of the TRFO membranes.*

The spectrum of the membrane RFO-BPA (Fig. 6.8c) shows an absorption peak at 1720 cm^{-1}, which correspond to C=O stretching vibrations of the ester groups. This absorption peak was not detected in the spectra of the RFO2 membrane indicating the correct formation of the PE thin layer [89]. Similarly, a broad adsorption peak appeared at 3393 cm^{-1} due to the asymmetry stretching vibration of the hydroxyl groups (-OH) [90] that could arise from the unreacted hydroxyl groups of BPA in the membrane or from the partial hydrolysis of the acyl chloride unit of TMC. In general, it can be confirmed the correct formation of both the PA and PE thin layers on the top surface of the RFO2 membrane and the successful preparation of TRFO membranes.

Table 6.6 summarizes the transport parameters *A*, *B* and the "effective" structural parameter, S_{eff}, calculated from the model developed in [57] as stated earlier in section 6.2.5.1. Lower S_{eff} values were obtained for the commercial CTA-HTI and TFC-HTI membranes compared with those reported in the literature using RO test to determine *A* and *B* parameters for the same membranes. The calculated average S_{eff} factor of the CTA-HTI membrane obtained by means of RO test in other studies is 520 $\pm$ 163 μm [45, 46, 48, 49, 54, 91-93]. For the TFC-HTI membrane, the reported S_{eff} value was 533 μm [70]. It was also observed that S_{eff} of the CTA-HTI membrane obtained by means of FO test varied with the type, concentration and temperature of the draw and feed solutions in the range between 200 and 500 μm [92]. Moreover, the determined S_{eff} for the CTA-HTI membrane based on FO test was found to be 498 ± 37 μm [57]. The S_{eff} value, 402 μm, obtained in our study for this membrane applying FO test is close to these values confirming therefore the validity of the followed procedure.

As it was expected, the RFO2 membrane exhibited higher S_{eff} value than that of the TRFO membranes. In addition, all TRFO membranes exhibited lower S_{eff} values than that of the CTA-HTI commercial membrane. The lowest S_{eff} values were obtained for the membranes RFO-MPD and RFO-MPD/TEA (i.e. 269 μm). The *A* value of all TRFO membranes was slightly greater than that of the membrane RFO2. As mentioned previously, for TFC-FO membranes both the selective IP layer as well as the support are key factors determining their FO performance. Typically, the active layer accounts for the solute rejection, while the support dominates the permeate fluxes (both *J* and J_s) because of the *ICP* effects [22]. Among all tested membranes, the RFO-MPD/TEA membrane was found to have the highest *A* value (0.42 L/m^2 h bar) whereas the lowest *B* value was obtained for the membrane RFO-MPD, showing both desirable characteristics for FO performance. The results of the solute permeance (*B*) of the TRFO membranes indicated that the IP increased *B* value except for the two membranes RFO-MPD and RFO-BPA.

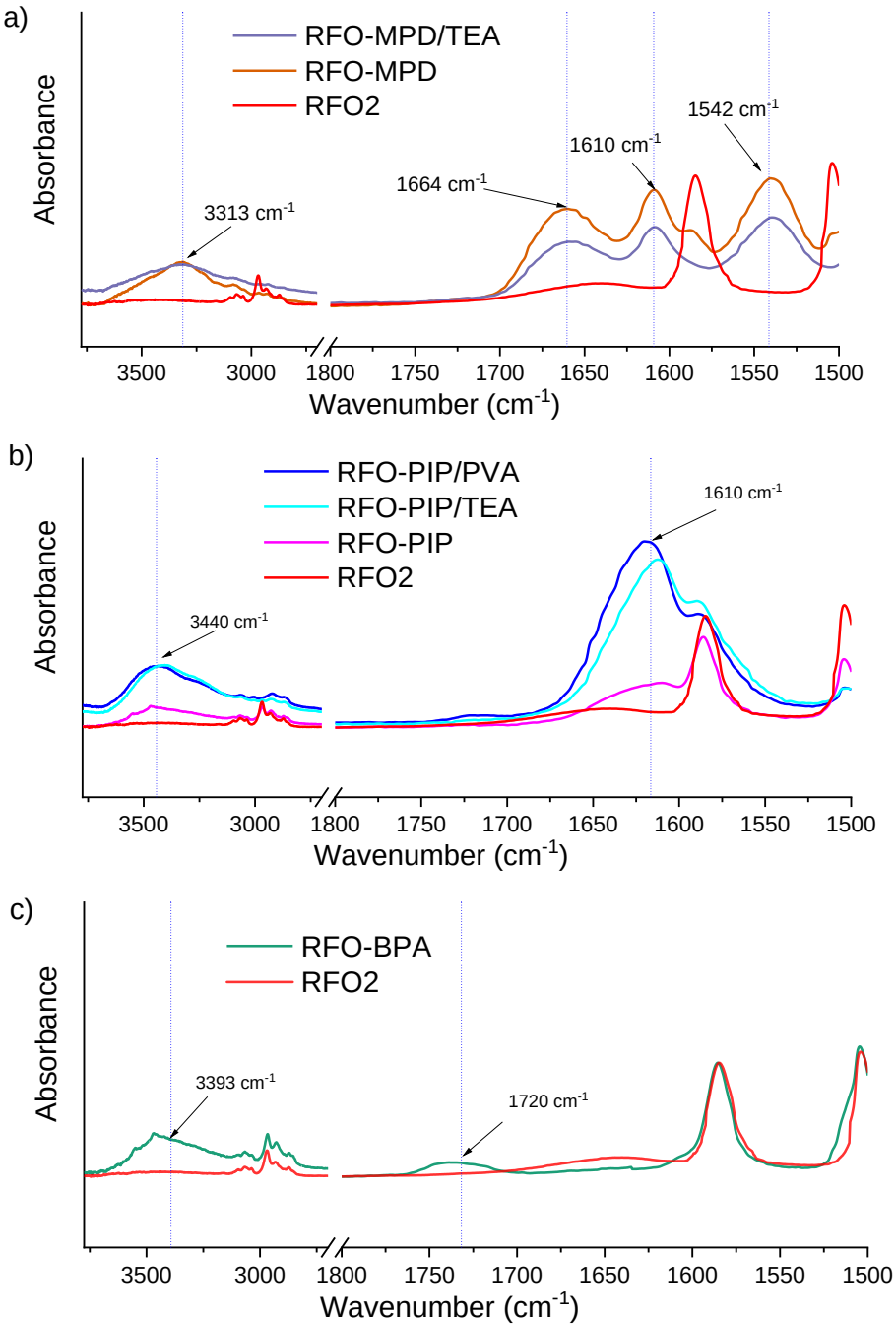

Figure 6.8. *ATR-FTIR spectra of the TRFO membranes: a) RFO-MPD and RFO-MPD/TEA, b) RFO-PIP, RFO-PIP/TEA and RFO-PIP/PVA and c) RFO-BPA, together the spectra of the RFO2 membrane.*

Table 6.6. *Water permeance (A), solute permeance (B) coefficients and "effective" structural parameter (Seff) of the TRFO membranes together with the RFO2 membrane and commercial membranes (CTA-HTI and TFC-HTI).*

Membrane	*A* (L/m²h bar)	*B* (L/m²h)	S_{eff} (μm)
RFO-MPD	0.33	0.15	269
RFO-MPD/TEA	0.42	0.26	269
RFO-PIP	0.27	0.56	362
RFO-PIP/TEA	0.31	0.79	322
RFO-PIP/PVA	0.30	0.88	374
RFO-BPA	0.33	0.17	297
RFO2	0.23	0.17	551
CTA-HTI	0.32	0.92	402
TFC-HTI	0.62	0.057	245

6.3.4. FO experiments of TRFO membranes

Similar to RFO membranes, the TRFO membranes were also tested in FO to treat HA aqueous solutions following the same procedure. The results are plotted in Fig. 6.9 together with those of the membrane RFO2 and the commercial membranes CTA-HTI and TFC-HTI.

The permeate flux (*J*) of all TRFO membranes, for both low and high concentration tests, were found to be higher than that of the membrane RFO2. This is attributed to the effects of the prepared IP layer of PA or PE, which reduces the water contact angle increasing its hydrophilic character, and as a consequence, decreasing the structural parameter, S_{eff}. This increase in *J* with respect to the non-transformed RFO membrane confirms the successful IP coating layer since the membrane becomes more semi-permeable.

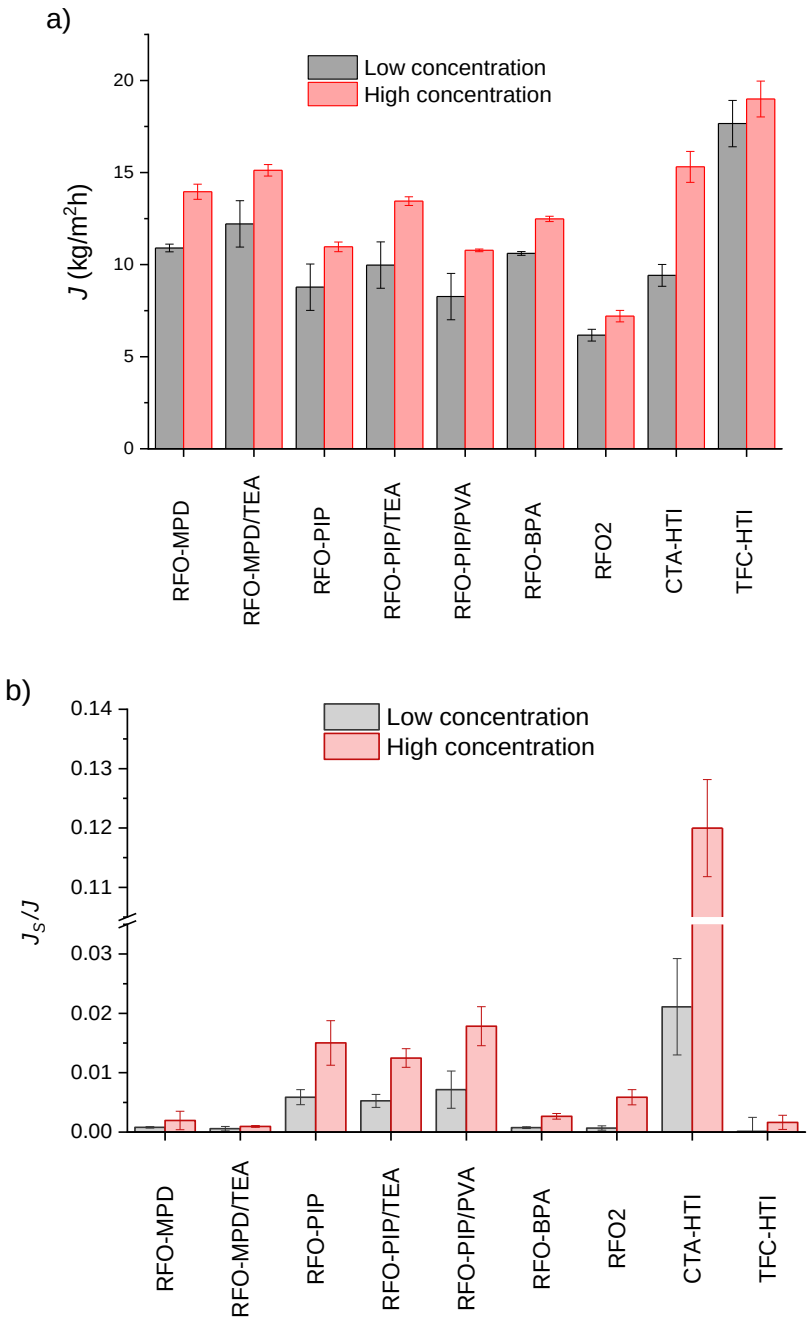

Figure 6.9. *a) FO permeate flux (J) and b) the specific reverse salt flux (Js/J) of the TRFO membranes together with those of the membrane RFO2 and the commercial membranes (CTA-HTI and TFC-HTI) for low concentration (10 mg/L HA feed aqueous solution and 65 g/L NaCl draw aqueous solution) and high concentration (100 mg/L HA feed aqueous solution and 200 g/L NaCl draw aqueous solution).*

All TRFO membranes exhibited a higher *J* value for high concentration test (10.8-15.1 kg/m^{2}h) than for low concentration test (8.3-12.2 kg/m^{2}h). This was also observed for the RFO membranes and the commercial membranes. As stated earlier, this is due to the enhancement of the osmotic pressure with the increase of the salt concentration of the draw solution. The permeate flux of the PA modified TRFO membranes using MPD alone or mixed

with TEA was better than that of the PA modified membranes using PIP or its mixture with TEA or PVA. This is because the use of the MPD monomer in IP process provides very good transport properties as well as antifouling characteristics making it one of the most used monomers in FO membrane synthesis [37, 94]. In addition, using either MPD or the mixture MPD/TEA results in a significant reduction of J_s/J compared to PIP or its mixture with TEA or PVA.

The PE modified membrane (RFO-BPA) showed J values lower than those of the RFO-MPD or RFO-MPD/TEA membranes, but higher than those of the of the TRFO membranes modified using PIP or its mixed with TEA or PVA. Likewise, the J_s/J values of the RFO-BPA membrane was similar to that of the TRFO-MPD membrane and slightly higher than that of the TRFO-MPD/TEA membrane, but much lower than that of the TRFO membranes modified using PIP.

In order to compare the draw solute loss (i.e. reduction of the driving force) due to the reverse salt flux for both high and low concentrations, a normalized reverse salt transfer (RT_s) was determined (Fig. 9.6b of the Appendix B). No significant difference in the obtained RT_s values was detected for all TRFO membranes although these values were lower than those of the RFO2 membrane, and even lower than those of TFC-HTI membrane.

Among all TRFO membranes, the best FO performance, for both low and high concentration tests, was achieved by the membrane RFO-MPDA/TEA (i.e. (high J and low J_s/J). Compared to the commercial membrane CTA-HTI, this membrane showed a competitive behaviour since its permeate flux for low concentration test was 30% higher, and the J_s/J value was 97% lower for both low and high concentration tests. Phuntsho et al. [95] compared both J and J_s/J of FO and RO membranes in the FO process of several feed and draw solutions. The J values for CTA-HTI membrane was regularly more than 20 times higher than that of the RO membrane, while the J_s/J values of CTA-HTI were also significantly higher by several orders of magnitude than that of the RO membrane. Therefore, the TRFO membranes considerably improved the FO performance of the RO membranes and could depict a good alternative to reuse end-of-life RO membranes.

The obtained R_{HA} values of the TRFO membranes for both low and high concentration tests are plotted in Fig. 6.10a. For the low concentration test, all performed surface modifications of the RFO2 membrane, did not improve the R_{HA} value. In this case, the high R_{HA} values obtained for the membranes RFO-MPD and RFO-MPD/TEA were lower than those of the membranes RFO2 and TFC-HTI but higher than that of the CTA-HTI membrane. For high concentrations, these two TRFO membranes together with the membrane RFO-PIP/PVA presented R_{HA} results similar to those of the membrane RFO2 and superior to those of the commercial membranes CTA-HTI and TFC-HTI. These results showed greater affinity of the IP

thin layers to HA regardless of the monomers used than the PSf layer of the RFO membranes (i.e. RFO2 membrane in this case). This effect is more noticeable for the low concentration test than for the high concentration test.

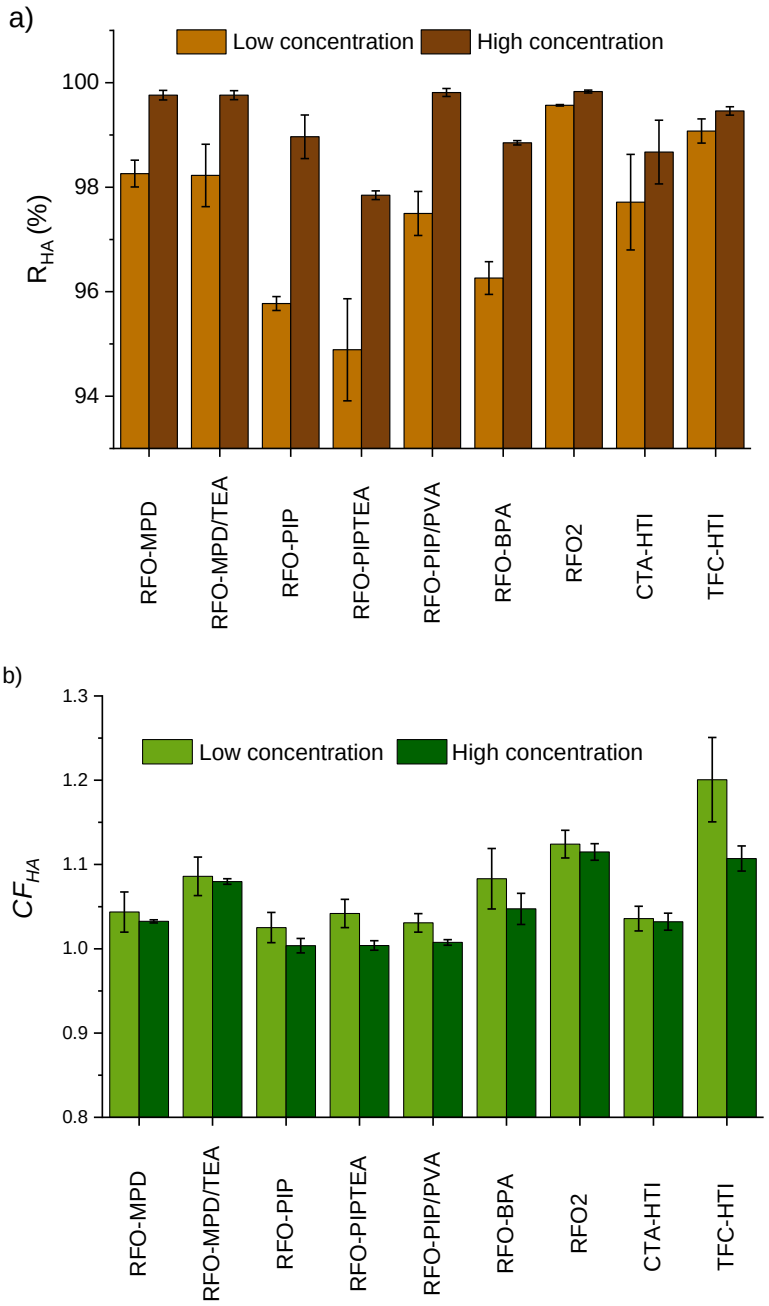

Figure 6.10. *HA rejection factor (RHA) (a) and HA concentration factor (CFHA) at 30 min (b) of the TRFO membranes together with the those of the membrane RFO2 and the commercial membranes (CTA-HTI and TFC-HTI) for low concentration (10 mg/L HA feed aqueous solution and 65 g/L NaCl draw aqueous solution) and high concentration (100 mg/L HA feed aqueous solution and 200 g/L NaCl draw aqueous solution).*

The calculated CF_{HA} values at 30 min FO tests of the TRFO membranes are shown in Fig. 6.10b together with those of the membrane RFO2 and the commercial membranes CTA-

HTI and TFC-HTI. As observed for the other RFO membranes (Fig. 6.6b), the CF_{HA} value of the TRFO membranes decreases with the increase of both HA and salt concentrations. As stated previously, this is due partly to the fact that CF_{HA} is inversely proportional to the initial HA concentration of the feed solution and both *J* and R_{HA} are not high enough to enhance CF_{HA} over that of the low concentration test. The highest CF_{HA} was obtained using the membrane TFC-HTI for the low concentration test and the membrane RFO2 for the high concentration test. All TRFO membranes show lower CF_{HA} values than that of the membrane RFO2 being that of the membrane RFO-MPD/TEA the highest among all TRFO membranes. This decrease in CF_{HA} value is due to the increase of HA transport through TRFO membranes, obtaining lower R_{HA} values.

For sake of comparison, Table 6.7 summarizes both *J* and J_s fluxes reported in other studies for different FO membranes used in wastewater treatment with different concentrations of salt as draw solutions. It can be seen that the RFO2 membrane exhibits reasonably good FO performance and the PA modified membrane, RFO-MPD/TEA, exhibits outstanding FO performance compared to other FO membranes. Compared to the previously reported data for different FO membranes used for wastewater treatment, the TRFO membranes proved to be competitive rendering the reuse of discarded RO membrane modules feasible for FO technology extending as consequence their life cycle.

Table 6.7. *FO fluxes, J and Js, reported for different membranes used in wastewater treatment with different concentrations of salt as draw solutions and different FO configurations.*

Feed Solution	Draw solution	Membrane material	*J* (kg/m²h)	J_s (kg/m²h)	Ref.
Wastewater model (10 mg/L HA)	65 g/L NaCl	RFO2	6.2	0.009	This study
Wastewater model (100 mg/L HA)	200 g/L NaCl	RFO2	7.2	0.042	This study
Wastewater model (10 mg/L HA)	65 g/L NaCl	RFO-MPD/TEA	12.21	0.006	This study
Wastewater model (100 mg/L HA)	200 g/L NaCl	RFO-MPD/TEA	15.12	0.014	This study
Municipal wastewater	synthetic seawater	CTA	7.95	0.004	[96]
Textile wastewater	35 g/L NaCl	CTA	6.5	--	[20]
Wastewater model (50 mg/L HA)	30 g/L NaCl	CA	5.1	--	[69]
Dairy wastewater pretreated	60 g/L NaCl	TFC-PA	8.4	--	[97]
Municipal wastewater	synthetic seawater	TFC-PA	15.1	--	[98]

6.4. Conclusions

According to the main waste management principles, membrane recycling should be considered as an environmental action to enhance the sustainability of membrane technology and minimize the ecological impact. The main aim of this study was to recycle and transform end-of-life RO membranes in FO membranes at lab scale for wastewater treatment. The obtained morphological and structural characteristics of the recycled FO membranes (RFO) and transformed RFO membranes (TRFO) by interfacial polymerization indicated their validity and suitability for FO process. Their intrinsic structural parameters were found to be quite similar to those of commercial FO membranes.

The highest FO water permeate fluxes for RFO membranes were obtained for the RFO2 membrane recycled with the highest NaClO exposure dose applied in pilot plant (10^6 ppm·h) indicating that it is not necessary a second laboratory cleaning step. The permeate fluxes of the RFO2 membrane were comparable to those of the commercial CTA-HTI membrane operated under the same FO conditions.

Among all prepared TRFO membranes, the PA surface modified membranes using MPD or its mixture with TEA showed better transport properties than those prepared using PIP or its mixture with TEA or PVA, and PE surface modified membrane using BPA. The best FO performance was achieved by the membrane RFO-MPD/TEA (J = 15.12 kg/m^{2}h, Js = 0.014 kg/m^{2}h, and R_{HA} greater than 99%). These values were found to be superior to those of the commercial membrane CTA-HTI membrane and comparable to those the commercial membrane TFC-HTI.

It is demonstrated that it is possible to use discarded RO membrane modules in FO separation technology after an adequate treatment procedure. This extends their lifetime contributing therefore to a circular economy and sustainability in membrane science and related materials. However, this research area is relatively new and further studies are necessary such as its environmental impact using Life Cycle Assessment (LCA) and cost effectiveness analysis as well as the possibility to apply IP without disassembling the RO membrane modules.

6.5. References

[1] UNWWAP, United Nations World Water Assessment Programme. The United Nations World Water Development Report 2015: Water for a Sustainable World, Paris, UNESCO, (2015).

[2] A. Yusuf, A. Sodiq, A. Giwa, J. Eke, O. Pikuda, G. De Luca, J.L. Di Salvo, S. Chakraborty, A review of emerging trends in membrane science and technology for sustainable water treatment, J. Clean. Prod., 266 (2020) 121867.

[3] G.W.I. IDA, IDA Desalination Yearbook, in: Ed. Media Analytics Ltd, UK, 2017.

[4] J.A. Sanmartino, M. Khayet, M.C. García-Payo, H. El-Bakouri, A. Riaza, Treatment of reverse osmosis brine by direct contact membrane distillation: Chemical pretreatment approach, Desalination, 420 (2017) 79-90.
[5] W. Lawler, Z. Bradford-Hartke, M.J. Cran, M. Duke, G. Leslie, B.P. Ladewig, P. Le-Clech, Towards new opportunities for reuse, recycling and disposal of used reverse osmosis membranes, Desalination, 299 (2012) 103-112.
[6] L.F. Greenlee, D.F. Lawler, B.D. Freeman, B. Marrot, P. Moulin, Reverse osmosis desalination: Water sources, technology, and today's challenges, Water Res., 43 (2009) 2317-2348.
[7] J. Landaburu-Aguirre, R. García-Pacheco, S. Molina, L. Rodríguez-Sáez, J. Rabadán, E. García-Calvo, Fouling prevention, preparing for re-use and membrane recycling. Towards circular economy in RO desalination, Desalination, 393 (2016) 16-30.
[8] EPC, European Commisssion. Directive 2008/98/EC of the European Parliament and of the Council of 19 November 2008 on waste and repealing certain directives. doi:2008/98/EC.; 32008L0098., in, Off. J. Eur. Union L13 2008, pp. 3-30.
[9] E. Coutinho de Paula, M.C. Santos Amaral, Environmental and economic evaluation of end-of-life reverse osmosis membranes recycling by means of chemical conversion, J. Clean. Prod., 194 (2018) 85-93.
[10] M. Pontié, S. Awad, M. Tazerout, O. Chaouachi, B. Chaouachi, Recycling and energy recovery solutions of end-of-life reverse osmosis (RO) membrane materials: A sustainable approach, Desalination, 423 (2017) 30-40.
[11] R. García-Pacheco, J. Landaburu-Aguirre, S. Molina, L. Rodríguez-Sáez, S.B. Teli, E. García-Calvo, Transformation of end-of-life RO membranes into NF and UF membranes: Evaluation of membrane performance, J. Membr. Sci., 495 (2015) 305-315.
[12] J.M. Gohil, A.K. Suresh, Chlorine attack on reverse osmosis membranes: Mechanisms and mitigation strategies, J. Membr. Sci., 541 (2017) 108-126.
[13] W. Lawler, A. Antony, M. Cran, M. Duke, G. Leslie, P. Le-Clech, Production and characterization of UF membranes by chemical conversion of used RO membranes, J. Membr. Sci., 447 (2013) 203-211.
[14] J. Morón-López, L. Nieto-Reyes, S. Aguado, R. El-Shehawy, S. Molina, Recycling of end-of-life reverse osmosis membranes for membrane biofilms reactors (MBfRs). Effect of chlorination on the membrane surface and gas permeability, Chemosphere, 231 (2019) 103-112.
[15] A. Lejarazu-Larrañaga, S. Molina, J.M. Ortiz, R. Navarro, E. García-Calvo, Circular economy in membrane technology: Using end-of-life reverse osmosis modules for preparation of recycled anion exchange membranes and validation in electrodialysis, J. Membr. Sci., 593 (2020) 117423.
[16] J. Senán-Salinas, R. García-Pacheco, J. Landaburu-Aguirre, E. García-Calvo, Recycling of end-of-life reverse osmosis membranes: Comparative LCA and cost-effectiveness analysis at pilot scale, Resour. Conserv. Recycl., 150 (2019) 104423.
[17] T.-S. Chung, L. Luo, C.F. Wan, Y. Cui, G. Amy, What is next for forward osmosis (FO) and pressure retarded osmosis (PRO), Sep. Purif. Technol., 156, Part 2 (2015) 856-860.
[18] N. Akther, A. Sodiq, A. Giwa, S. Daer, H.A. Arafat, S.W. Hasan, Recent advancements in forward osmosis desalination: A review, Chem. Eng. J., 281 (2015) 502-522.
[19] K. Lutchmiah, A.R.D. Verliefde, K. Roest, L.C. Rietveld, E.R. Cornelissen, Forward osmosis for application in wastewater treatment: A review, Water Res., 58 (2014) 179-197.
[20] J. Korenak, C. Hélix-Nielsen, H. Bukšek, I. Petrinić, Efficiency and economic feasibility of forward osmosis in textile wastewater treatment, J. Clean. Prod., 210 (2019) 1483-1495.
[21] T.Y. Cath, A.E. Childress, M. Elimelech, Forward osmosis: Principles, applications, and recent developments, J. Membr. Sci., 281 (2006) 70-87.
[22] M. Mohammadifakhr, J. de Grooth, H.D.W. Roesink, A.J.B. Kemperman, Forward Osmosis: A Critical Review, Processes, 8 (2020) 404.
[23] M. Xie, L.D. Nghiem, W.E. Price, M. Elimelech, Comparison of the removal of hydrophobic trace organic contaminants by forward osmosis and reverse osmosis, Water Res., 46 (2012) 2683-2692.

[24] R. Valladares Linares, Z. Li, S. Sarp, S.S. Bucs, G. Amy, J.S. Vrouwenvelder, Forward osmosis niches in seawater desalination and wastewater reuse, Water Res., 66 (2014) 122-139.
[25] D.L. Shaffer, J.R. Werber, H. Jaramillo, S. Lin, M. Elimelech, Forward osmosis: Where are we now?, Desalination, 356 (2015) 271-284.
[26] Y. Zhou, M. Huang, Q. Deng, T. Cai, Combination and performance of forward osmosis and membrane distillation (FO-MD) for treatment of high salinity landfill leachate, Desalination, 420 (2017) 99-105.
[27] S. Lee, Y. Kim, S. Hong, Treatment of industrial wastewater produced by desulfurization process in a coal-fired power plant via FO-MD hybrid process, Chemosphere, 210 (2018) 44-51.
[28] P.S. Goh, A.F. Ismail, A review on inorganic membranes for desalination and wastewater treatment, Desalination, 434 (2018) 60-80.
[29] A.J. Ansari, F.I. Hai, W.E. Price, J.E. Drewes, L.D. Nghiem, Forward osmosis as a platform for resource recovery from municipal wastewater - A critical assessment of the literature, J. Membr. Sci., 529 (2017) 195-206.
[30] S.M. Iskander, S. Zou, B. Brazil, J.T. Novak, Z. He, Energy consumption by forward osmosis treatment of landfill leachate for water recovery, Waste Manage., 63 (2017) 284-291.
[31] D. Li, Y. Yan, H. Wang, Recent advances in polymer and polymer composite membranes for reverse and forward osmosis processes, Prog. Polym. Sci., 61 (2016) 104-155.
[32] S. Zou, M. Qin, Z. He, Tackle reverse solute flux in forward osmosis towards sustainable water recovery: reduction and perspectives, Water Res., 149 (2019) 362-374.
[33] W. Xu, Q. Chen, Q. Ge, Recent advances in forward osmosis (FO) membrane: Chemical modifications on membranes for FO processes, Desalination, 419 (2017) 101-116.
[34] Q. Yang, J. Lei, D.D. Sun, D. Chen, Forward Osmosis Membranes for Water Reclamation, Sep. Purif. Rev., 45 (2016) 93-107.
[35] N.Y. Yip, A. Tiraferri, W.A. Phillip, J.D. Schiffman, M. Elimelech, High performance thin-film composite forward osmosis membrane, Environ. Sci. Technol., 44 (2010) 3812-3818.
[36] A. Tiraferri, N.Y. Yip, W.A. Phillip, J.D. Schiffman, M. Elimelech, Relating performance of thin-film composite forward osmosis membranes to support layer formation and structure, J. Membr. Sci., 367 (2011) 340-352.
[37] M.D. Firouzjaei, S.F. Seyedpour, S.A. Aktij, M. Giagnorio, N. Bazrafshan, A. Mollahosseini, F. Samadi, S. Ahmadalipour, F.D. Firouzjaei, M.R. Esfahani, A. Tiraferri, M. Elliott, M. Sangermano, A. Abdelrasoul, J.R. McCutcheon, M. Sadrzadeh, A.R. Esfahani, A. Rahimpour, Recent advances in functionalized polymer membranes for biofouling control and mitigation in forward osmosis, J. Membr. Sci., 596 (2020) 117604.
[38] P. Arribas, M.C. García-Payo, M. Khayet, L. Gil, Improved antifouling performance of polyester thin film nanofiber composite membranes prepared by interfacial polymerization, J. Membr. Sci., 598 (2020) 117774.
[39] R. García-Pacheco, F.J. Rabadán, P. Terrero, S.M. Martínez, D. Martínez, E. Campos, e. al., Life+13 transfomem: a recycling example within the desalination world, in: XI AEDYR Int. Congr., Valencia, Spain, 2016.
[40] S. Molina, R. Garcia-Pacheco, L. Rodriguez-Sáez, E. Garcia-Calvo, E. Campos, D. Zarzo, e. al., Transformation of end-of-life RO membranes into recycled NF and UF membranes, surface characterization, in: International Desalination Asociation Word Congress, IDAWC15, San Diego, California, 2015.
[41] R. García-Pacheco, J. Landaburu-Aguirre, P. Terrero-Rodríguez, E. Campos, F. Molina-Serrano, J. Rabadán, D. Zarzo, E. García-Calvo, Validation of recycled membranes for treating brackish water at pilot scale, Desalination, 433 (2018) 199-208.
[42] R. García-Pacheco, J. Landaburu-Aguirre, A. Lejarazu-Larrañaga, L. Rodríguez-Sáez, S. Molina, T. Ransome, E. García-Calvo, Free chlorine exposure dose (ppm·h) and its impact on RO membranes ageing and recycling potential, Desalination, 457 (2019) 133-143.

[43] S. Molina, J. Landaburu-Aguirre, L. Rodríguez-Sáez, R. García-Pacheco, J.G. de la Campa, E. García-Calvo, Effect of sodium hypochlorite exposure on polysulfone recycled UF membranes and their surface characterization, Polym. Degrad. Stab., 150 (2018) 46-56.
[44] P.A. Araújo, J.C. Kruithof, M.C.M. Van Loosdrecht, J.S. Vrouwenvelder, The potential of standard and modified feed spacers for biofouling control, J. Membr. Sci., 403-404 (2012) 58-70.
[45] X. Song, Z. Liu, D. Sun, Nano Gives the Answer: Breaking the Bottleneck of Internal Concentration Polarization with a Nanofiber Composite Forward Osmosis Membrane for a High Water Production Rate, Adv. Mater., 23 (2011) 3256-3260.
[46] W.A. Phillip, J.S. Yong, M. Elimelech, Reverse draw solute permeation in forward osmosis: modeling and experiments, Environ. Sci. Technol., 44 (2010) 5170-5176.
[47] G. Blandin, H. Vervoort, P. Le-Clech, A.R.D. Verliefde, Fouling and cleaning of high permeability forward osmosis membranes, J. Water Process Eng., 9 (2016) 161-169.
[48] S. Lim, M.J. Park, S. Phuntsho, L. Tijing, G. Nisola, W.-G. Shim, W.-J. Chung, H.K. Shon, Dual-layered nanocomposite membrane based on polysulfone/graphene oxide for mitigating internal concentration polarization in forward osmosis, Polymer, 110 (2017) 36-48.
[49] G. Blandin, H. Vervoort, A. D'Haese, K. Schoutteten, J.V. Bussche, L. Vanhaecke, D.T. Myat, P. Le-Clech, A.R.D. Verliefde, Impact of hydraulic pressure on membrane deformation and trace organic contaminants rejection in pressure assisted osmosis (PAO), Process Saf. Environ. Prot., 102 (2016) 316-327.
[50] T. Liu, S. Xu, D. Zhang, S. Sourirajan, T. Matsuura, Pore size and pore size distribution on the surface of polyethersulfone hollow fiber membranes, Desalination, 85 (1991) 1-12.
[51] P. Arribas, M. Khayet, M.C. García-Payo, L. Gil, Self-sustained electro-spun polysulfone nano-fibrous membranes and their surface modification by interfacial polymerization for micro- and ultra-filtration, Sep. Purif. Technol., 138 (2014) 118-129.
[52] S. Singh, K.C. Khulbe, T. Matsuura, P. Ramamurthy, Membrane characterization by solute transport and atomic force microscopy, J. Membr. Sci., 142 (1998) 111-127.
[53] L. Pisani, Simple Expression for the Tortuosity of Porous Media, Transp. Porous Med., 88 (2011) 193-203.
[54] S.S. Manickam, J.R. McCutcheon, Model thin film composite membranes for forward osmosis: Demonstrating the inaccuracy of existing structural parameter models, J. Membr. Sci., 483 (2015) 70-74.
[55] P.K. Kang, W. Lee, S. Lee, A.S. Kim, Origin of structural parameter inconsistency in forward osmosis models: A pore-scale CFD study, Desalination, 421 (2017) 47-60.
[56] J.R. McCutcheon, M. Elimelech, Influence of concentrative and dilutive internal concentration polarization on flux behavior in forward osmosis, J. Membr. Sci., 284 (2006) 237-247.
[57] A. Tiraferri, N.Y. Yip, A.P. Straub, S. Romero-Vargas Castrillon, M. Elimelech, A method for the simultaneous determination of transport and structural parameters of forward osmosis membranes, J. Membr. Sci., 444 (2013) 523-538.
[58] S.S. Manickam, J.R. McCutcheon, Understanding mass transfer through asymmetric membranes during forward osmosis: A historical perspective and critical review on measuring structural parameter with semi-empirical models and characterization approaches, Desalination, 421 (2017) 110-126.
[59] N.N. Bui, J.T. Arena, J.R. McCutcheon, Proper accounting of mass transfer resistances in forward osmosis: Improving the accuracy of model predictions of structural parameter, J. Membr. Sci., 492 (2015) 289-302.
[60] M.J. Ariza, J. Benavente, Streaming potential along the surface of polysulfone membranes: a comparative study between two different experimental systems and determination of electrokinetic and adsorption parameters, J. Membr. Sci., 190 (2001) 119-132.
[61] I. Christl, R. Kretzschmar, Relating ion binding by fulvic and humic acids to chemical composition and molecular size. 1. Proton binding, Environ. Sci. Technol., 35 (2001) 2505-2511.

[62] N.Z.S. Yahaya, M.Z.M. Pauzi, N. Mu'ammar Mahpoz, M.A. Rahman, K.H. Abas, A.F. Ismail, M.H.D. Othman, J. Jaafar, Chapter 10 - Forward Osmosis for Desalination Application, in: A.F. Ismail, M.A. Rahman, M.H.D. Othman, T. Matsuura (Eds.) Membrane Separation Principles and Applications, Elsevier, 2019, pp. 315-337.
[63] S. Engelhardt, J. Vogel, S.E. Duirk, F.B. Moore, H.A. Barton, Urea and ammonium rejection by an aquaporin-based hollow fiber membrane, J. Water Process Eng., 32 (2019) 100903.
[64] G. Blandin, F. Ferrari, G. Lesage, P. Le-Clech, M. Heran, X. Martinez-Llado, Forward Osmosis as Concentration Process: Review of Opportunities and Challenges, Membranes (Basel), 10 (2020).
[65] E.M. Garcia-Castello, J.R. McCutcheon, Dewatering press liquor derived from orange production by forward osmosis, J. Membr. Sci., 372 (2011) 97-101.
[66] M.S. Fahmey, A.-H.M. El-Aassar, M. M.Abo-Elfadel, A.S. Orabi, R. Das, Comparative performance evaluations of nanomaterials mixed polysulfone: A scale-up approach through vacuum enhanced direct contact membrane distillation for water desalination, Desalination, 451 (2019) 111-116.
[67] D. Song, J. Xu, Y. Fu, L. Xu, B. Shan, Polysulfone/sulfonated polysulfone alloy membranes with an improved performance in processing mariculture wastewater, Chem. Eng. J., 304 (2016) 882-889.
[68] N.M. Mazlan, P. Marchetti, H.A. Maples, B. Gu, S. Karan, A. Bismarck, A.G. Livingston, Organic fouling behaviour of structurally and chemically different forward osmosis membranes – A study of cellulose triacetate and thin film composite membranes, J. Membr. Sci., 520 (2016) 247-261.
[69] M. Xie, L.D. Nghiem, W.E. Price, M. Elimelech, Impact of humic acid fouling on membrane performance and transport of pharmaceutically active compounds in forward osmosis, Water Res., 47 (2013) 4567-4575.
[70] J. Ren, J.R. McCutcheon, A new commercial thin film composite membrane for forward osmosis, Desalination, 343 (2014) 187-193.
[71] W.N.A.S. Abdullah, S. Tiandee, W. Lau, F. Aziz, A.F. Ismail, Potential use of nanofiltration like-forward osmosis membranes for copper ion removal, Chin. J. Chem. Eng., 28 (2020) 420-428.
[72] P.S. Goh, A.F. Ismail, B.C. Ng, M.S. Abdullah, Recent Progresses of Forward Osmosis Membranes Formulation and Design for Wastewater Treatment, Water, 11 (2019) 2043.
[73] Y.-N. Wang, K. Goh, X. Li, L. Setiawan, R. Wang, Membranes and processes for forward osmosis-based desalination: Recent advances and future prospects, Desalination, 434 (2018) 81-99.
[74] D.M. Warsinger, S. Chakraborty, E.W. Tow, M.H. Plumlee, C. Bellona, S. Loutatidou, L. Karimi, A.M. Mikelonis, A. Achilli, A. Ghassemi, L.P. Padhye, S.A. Snyder, S. Curcio, C. Vecitis, H.A. Arafat, J.H.t. Lienhard, A review of polymeric membranes and processes for potable water reuse, Prog. Polym. Sci., 81 (2016) 209-237.
[75] Y. Fang, L. Bian, Q. Bi, Q. Li, X. Wang, Evaluation of the pore size distribution of a forward osmosis membrane in three different ways, J. Membr. Sci., 454 (2014) 390-397.
[76] S. Xiong, S. Xu, S. Zhang, A. Phommachanh, Y. Wang, Highly permeable and antifouling TFC FO membrane prepared with CD-EDA monomer for protein enrichment, J. Membr. Sci., 572 (2019) 281-290.
[77] W. Xu, Q. Ge, Novel functionalized forward osmosis (FO) membranes for FO desalination: Improved process performance and fouling resistance, J. Membr. Sci., 555 (2018) 507-516.
[78] R.C. Ong, T.-S. Chung, J.S. de Wit, B.J. Helmer, Novel cellulose ester substrates for high performance flat-sheet thin-film composite (TFC) forward osmosis (FO) membranes, J. Membr. Sci., 473 (2015) 63-71.
[79] Z. Alihemati, S.A. Hashemifard, T. Matsuura, A.F. Ismail, N. Hilal, Current status and challenges of fabricating thin film composite forward osmosis membrane: A comprehensive roadmap, Desalination, 491 (2020) 114557.
[80] M.E. Yakavalangi, S. Rimaz, V. Vatanpour, Effect of surface properties of polysulfone support on the performance of thin film composite polyamide reverse osmosis membranes, J. Appl. Polym. Sci., 134 (2017) 44444.

[81] M. Kahrizi, J. Lin, G. Ji, L. Kong, C. Song, L.F. Dumée, S. Sahebi, S. Zhao, Relating forward water and reverse salt fluxes to membrane porosity and tortuosity in forward osmosis: CFD modelling, Sep. Purif. Technol., 241 (2020) 116727.
[82] W.R. Smith, F. Moučka, I. Nezbeda, Osmotic pressure of aqueous electrolyte solutions via molecular simulations of chemical potentials: Application to NaCl, Fluid Phase Equilib., 407 (2016) 76-83.
[83] J.T. Martin, G. Kolliopoulos, V.G. Papangelakis, An improved model for membrane characterization in forward osmosis, J. Membr. Sci., 598 (2020) 117668.
[84] X. Liu, H.Y. Ng, Fabrication of layered silica–polysulfone mixed matrix substrate membrane for enhancing performance of thin-film composite forward osmosis membrane, J. Membr. Sci., 481 (2015) 148-163.
[85] X.-Y. Chi, P.-Y. Zhang, X.-J. Guo, Z.-L. Xu, A novel TFC forward osmosis (FO) membrane supported by polyimide (PI) microporous nanofiber membrane, Appl. Surf. Sci., 427 (2018) 1-9.
[86] J. Xiang, Z. Xie, M. Hoang, K. Zhang, Effect of amine salt surfactants on the performance of thin film composite poly(piperazine-amide) nanofiltration membranes, Desalination, 315 (2013) 156-163.
[87] N. Misdan, W.J. Lau, A.F. Ismail, Physicochemical characteristics of poly(piperazine-amide) TFC nanofiltration membrane prepared at various reaction times and its relation to the performance, J. Polym. Eng., 35 (2015) 71-78.
[88] P.S. Singh, S.V. Joshi, J.J. Trivedi, C.V. Devmurari, A.P. Rao, P.K. Ghosh, Probing the structural variations of thin film composite RO membranes obtained by coating polyamide over polysulfone membranes of different pore dimensions, J. Membr. Sci., 278 (2006) 19-25.
[89] B. Tang, Z. Huo, P. Wu, Study on a novel polyester composite nanofiltration membrane by interfacial polymerization of triethanolamine (TEOA) and trimesoyl chloride (TMC): I. Preparation, characterization and nanofiltration properties test of membrane, J. Membr. Sci., 320 (2008) 198-205.
[90] X. Wei, X. Kong, J. Yang, G. Zhang, J. Chen, J. Wang, Structure influence of hyperbranched polyester on structure and properties of synthesized nanofiltration membranes, J. Membr. Sci., 440 (2013) 67-76.
[91] T.Y. Cath, M. Elimelech, J.R. McCutcheon, R.L. McGinnis, A. Achilli, D. Anastasio, A.R. Brady, A.E. Childress, I.V. Farr, N.T. Hancock, J. Lampi, L.D. Nghiem, M. Xie, N.Y. Yip, Standard Methodology for Evaluating Membrane Performance in Osmotically Driven Membrane Processes, Desalination, 312 (2013) 31-38.
[92] M.C.Y. Wong, K. Martinez, G.Z. Ramon, E.M.V. Hoek, Impacts of operating conditions and solution chemistry on osmotic membrane structure and performance, Desalination, 287 (2012) 340-349.
[93] M. Xie, L.D. Nghiem, W.E. Price, M. Elimelech, A Forward Osmosis–Membrane Distillation Hybrid Process for Direct Sewer Mining: System Performance and Limitations, Environ. Sci. Technol., 47 (2013) 13486-13493.
[94] H. Jain, M.C. Garg, Fabrication of polymeric nanocomposite forward osmosis membranes for water desalination—A review, Environ. Technol. Innov., 23 (2021) 101561.
[95] S. Phuntsho, S. Sahebi, T. Majeed, F. Lotfi, J.E. Kim, H.K. Shon, Assessing the major factors affecting the performances of forward osmosis and its implications on the desalination process, Chem. Eng. J., 231 (2013) 484-496.
[96] Y. Sun, J. Tian, Z. Zhao, W. Shi, D. Liu, F. Cui, Membrane fouling of forward osmosis (FO) membrane for municipal wastewater treatment: A comparison between direct FO and OMBR, Water Res., 104 (2016) 330-339.
[97] B.K. Pramanik, F.I. Hai, F.A. Roddick, Ultraviolet/persulfate pre-treatment for organic fouling mitigation of forward osmosis membrane: Possible application in nutrient mining from dairy wastewater, Sep. Purif. Technol., 217 (2019) 215-220.

[98] M. Zhan, G. Gwak, B.G. Choi, S. Hong, Indexing fouling reversibility in forward osmosis and its implications for sustainable operation of wastewater reclamation, J. Membr. Sci., 574 (2019) 262-269.

Chapter 7

Conclusions and Future Research Studies

7.1. Conclusions

Different dual-layer polymeric membranes have been developed in this PhD thesis for water treatment by different membrane separation processes of emerging interests, membrane distillation (MD), pervaporation (PV) and forward osmosis (FO). Provided that the design of dual-layer membranes must meet certain specific requirements for each membrane process, these were prepared applying different techniques: electrospinning, dip-coating and interfacial polymerization (IP). In addition, first attempts have been made in this PhD thesis to recycle and reuse end-of-life reverse osmosis (RO) membranes for MD and FO processes. Recycling different internal components such as the feed and permeate spacers of RO membrane modules and their transformation into dual-layer MD membranes were also explored. The important drawn conclusions of the performed research studies are summarized below.

Dual-layer PV membranes composed of a highly porous electrospun polyvinylidene fluoride (PVDF) support and a thin selective layer of organophilic polymer of intrinsic microporosity (PIM-1) were prepared by dip-coating in Chapter 3. These thin film composite (TFC) membranes were applied for the separation of n-butanol/water mixtures by PV. The high porosity of the PVDF support and the thin layer of organophilic PIM-1 allowed an exceptionally high flux membrane. The results showed that the penetration of PIM-1 into the nanofibrous support during the preparation of thin film composite membranes played an

important role on the formation of the PIM-1 thin layer and, as a consequence, on the PV membrane performance. The impregnation the PVDF nanofibrous support with ethanol or methanol prior to coating avoided infiltration but small pinholes were created upon the formation of the PIM-1 thin layer, reducing n-butanol/water separation factors. However, the impregnation of the support with chloroform led to the formation of a thin and non-fragile PIM-1 layer, which resulted in a membrane with a total permeate flux of 16.1 kg/m^{2}h and a separation factor of n-butanol/water of 8, as well as a PV separation index (*PSI*) of 112.7 kg/m^{2}h. The total permeate flux was much higher than those reported by other membranes in literature, while the obtained separation factor was within the reported range. Under similar PV operating conditions, the calculated *PSI* was greater than that of most commercial membranes.

The energy requirements were also estimated in Chapter 3 by applying numerical simulations using Aspen HYSYS in a PV-distillation hybrid process and a conventional stand-alone distillation process for the recovery of n-butanol. The increase of n-butanol concentration in the feed aqueous solution of the stand-alone distillation column decreased the energy demand for the separation process. A PV process to pre-concentrate n-butanol before it enters the distillation column was proposed using the prepared PMI-1 TFC membranes. In the simulated PV-distillation process, it could be verified that the reduction of the energy demand as the separation factor of the PIM-1 TFC membranes was increased, obtaining similar energy demands to those reported for other membranes. Because the energy requirements depend basically on the separation factors, the developed higher permeate flux PIM-1 TFC membranes allow to decrease the total membrane area, reducing their manufacturing, installation and maintenance costs.

In Chapter 4, dual-layer electrospun nanofibrous membranes (DL-ENMs) were prepared using the hydrophobic polymer polyvinylidene fluoride (PVDF) as a bottom layer and polysulfone (PSF) as a hydrophilic top layer by electrospinning technique with different ratio of PVDF/PSF electrospinning time maintaining the total electrospinning time at 3 h. The DL-ENMs exhibited better direct contact membrane distillation (DCMD) desalination performance than single-layer nanofibrous membranes (SL-ENMs) electrospun from each of the polymers considering the same electrospinning time. These DL-ENMs presented a strong cohesive structure, being the PSF layer web structure more open. By increasing the thickness of the PSF layer, it was observed a decrease of the enthalpy of fusion, enthalpy of crystallization and *LEP* values whereas the Young's modulus and the void volume fraction of these DL-ENMs were increased. These results were attributed to the open structure of the PSF nanofibrous layer due to the fact that PSF is less electrically conductive than PVDF, acting as an insulator and resulting in loosely packed web.

DL-ENMs showed higher permeate fluxes (53.6, 49.9 and 47.7 kg/m^{2}h with a feed temperature of 80 °C, a permeate temperature of 20 °C and an aqueous NaCl concentration of 0, 12 and 30 g/L, respectively) than single-layer PVDF ENM (36.1, 34.0 and 32.9 kg/m^{2}h) carried out at the same experimental conditions. Both types of ENMs (DL-ENMs and SL-ENMs) presented NaCl rejection factors greater than 99.99 %. The DCMD permeate flux of the DL-ENMs was also found to be higher when the thickness of the PSF layer was increased. Event it is greater than that of all ENMs reported in the literature for DCMD. This is due to the thin hydrophobic layer of DL-ENMs compared to SL-ENMs, the reduction of the total thickness of the DL-ENMs compared to SL-ENMs prepared with the same electrospinning time, and the increase of both the inter fiber space and the void volume fraction with increasing the thickness of the PSF layer. Moreover, the more open structure of the hydrophilic PSF layer also improved wetting of this layer reducing therefore the path between the liquid/vapor interfaces formed at both sides of the PVDF layer of DL-ENMs, and finally enhancing the permeate flux.

To contribute to the awaited circular economy waste management in the field of membrane science and its involved materials, an attempt has been made in Chapter 5 to recycle and reuse some internal components of RO membrane modules (RO membrane, feed spacer and permeate spacer) as hydrophilic supports for MD membranes. These were dual-layer hydrophobic/hydrophilic membranes prepared by electrospinning a hydrophobic PVDF top layer on the above cited hydrophobic supports after their cleaning. The recycled RO membranes were first subjected to a passive cleaning procedure by submerging them in a sodium hypochlorite solution (total exposure dose of 300,000 ppm·h) to ensure the total oxidation of the PA layer of the RO membrane. The knowledge acquired for the preparation of polymeric dual-layer membranes explored in Chapters 3 and 4, aided to fix the optimized electrospinning parameters to tailor suitable MD membranes. In this cases, different electrospinning times (30, 60 and 90 min) were considered for the preparation of the hydrophobic nanofibrous PVDF layer over the mentioned recycled hydrophilic supports. These dual-layer membranes were tested for the treatment of high saline aqueous solutions, near saturation, in order to check their ability to treat RO brines by MD technology enabling zero liquid discharge to the environment. The dual-layer membranes prepared by the recycled RO membrane and the permeate spacer exhibited appropriate characteristics for MD separation process. The use of these two hydrophilic recycled supports improved the mechanical properties of the membranes compared to the unsupported PVDF electrospun membrane. The dual-layer membrane with the recycled RO membrane as support showed the highest NaCl rejection factor while the greatest permeate fluxes were obtained for the dual-layer membrane supported by the RO permeate spacer. These permeate fluxes were

found to be similar to those obtained for the unsupported PVDF electrospun membrane prepared with the same electrospinning time. A stable performance over time was observed for both dual-layer membranes, prepared on RO recycled membrane and permeate spacer, in long term DCMD regenerative tests. In contrast, the dual-layer membranes prepared using the RO feed spacer showed the worst results (i.e. very low LEP_w values, poor mechanical properties and bad salt rejection factors) because of its open structure resulting in an uneven thickness and defective PVDF nanostructured membranes. Compared to other PVDF or PVDF-HFP electrospun nanofibrous membranes reported in the literature, the dual-layer membranes prepared with RO recycled membrane or permeate spacer of RO membrane modules and 60 min electrospinning time exhibited reasonably good DCMD performance (i.e., 43.2 and 18.1 kg/m^2 h with high salt rejection factors, 99.99 %).

In Chapter 6, another attempt has been made to recycle and transform end-of-life RO membranes to FO membranes. Different passive cleaning protocols in pilot plant and laboratory scale were followed using sodium hypochlorite (NaClO) at different concentrations and exposure time in order to remove the fouled and clay-like PA layer. The recycled RO membrane (RFO) with the best FO performance was selected for different transformations by interfacial polymerization (IP) technique to obtain TFC membranes (TRFO) with even better FO performance. The validity of these membranes in the treatment of wastewater (humic acid (HA) aqueous solutions and RO brines as model feed and draw solutions, respectively) was tested and discussed.

Among all prepared TRFO membranes, the best FO performance was achieved by the RFO membrane with a cleaning step in the pilot plant of 10^6 ppm·h NaClO exposure dose and a subsequent IP modification using a mixture of m-phenylenediamine (MPD) and trimethylamine (TEA) as aqueous solution to form a new selective PA layer. The best FO performance results were a permeate flux of 15.12 kg/m^{2}h, a specific reverse salt flux of 0.014 kg/m^{2}h, and a HA rejection factor greater than 99%. These values were found to be superior to those of the commercial CTA-HTI membrane and comparable to those the commercial TFC-HTI membrane, both supplied by Hydration Technology Innovations (HTI™, LLC, Albany, USA). The prepared FO dual-layer membranes exhibited similar structural parameter (S_{eff} between 269 and 374 μm) to that of the commercial membranes CTA-HTI (S_{eff} = 402 μm) and TFC-HTI (S_{eff} = 245 μm).

It is demonstrated in Chapters 5 and 6 that it is possible to recycle and reuse the internal components of end-of-life RO membrane modules in both MD and FO separation technologies after adequate cleaning and modification procedures. This allowed to extend their lifetime contributing therefore to a circular economy and sustainability in membrane science and related materials. Furthermore, the recycled FO and MD membranes were found

to be suitable for the treatment of RO brines. This opens a window for the implantation of FO and MD in the RO desalination plant where the modules are discarded. However, this research area is relatively new and further studies are necessary such as its environmental impact using Life Cycle Assessment (LCA) and cost effectiveness analysis. In the case of TRFO membranes, it will be exceptionally interesting to study the possibility to apply IP without disassembling the RO membrane modules in order to reduce further the cost of the membrane transformation/modification.

7.2. Future research studies

Some promising research studies in the field of dual-layer membranes and their application in different membrane processes of emerging interest (PV, MD and FO) were derived from this PhD thesis as summarized in the following paragraphs. Other than the discarded RO membrane modules considered in this PhD thesis, another attempt of important interest for the circular economy in membrane science and technology can be made by recycling and reusing other end-of-life membranes and modules. The following topics are some proposed research projects to be explored in near future or already under development stage in our research group.

Taking into consideration the excellent properties of the prototypical polymer of intrinsic microporosity (PIM-1) used in Chapter 3 that exhibits a good selectivity towards organophilic components, other polymers such as polysulfone (PSF), polyethersulfone (PES) or polyetherimide (PEI) can be considered in order to prepare suitable electrospun supports for PIM-1 coated PV membranes. Both the intrinsic microporosity of the PIM-1 and the ideal features of nanofibrous supports may improve both the PV permeate flux and organic/water selectivity. The effect of the PIM-1 content in the coating solution can also be studied to obtain an enhanced PV index performance. Moreover, blends of PIM-1 with one of the above mentioned polymers PSF, PES or PEI can be explored to prepare highly porous membranes for other purposes such as filtration (e.g. microfiltration, MF, ultrafiltration, UF or nanofiltration, NF), solar evaporation or membrane distillation (MD) as supports subjected to further surface modification if needed. Preliminary PIM-1/PSF blended electrospun membranes have already been prepared successfully in our research group. The measured water contact angles of these membranes were found to be around 138º. The effects of the PIM-1 content in the polymer blend and the electrospinning parameters on the morphological structure and characteristics of these nanofibrous membranes should be investigated.

Another interesting research study can be the development of electrospun dual-layer hydrophobic/hydrophilic nanofibrous membranes for MD separation process considering

other polymers with different hydrophobic characters rather than those used in this PhD thesis in Chapter 4 (e.g. poly (vinylidene/tetrafluoroethylene) fluoride (PVDF-*co*-F4ET), poly(lactic acid) (PLA)). Polymers with different degree of hydrophilicity such as polyethersulfone (PES) or modified PES (i.e. hydroxyl, -OH, grafted on PES, sulfonated PES), polyetherimide (PEI), polyamide (PA) or poly(ethylene oxide) (PEO) can be studied. The affinity of the hydrophobic and hydrophilic polymers must be studied to reduce the undesirable delamination effect. Furthermore, the incorporation of nano-additives such as silica nanoparticles in the hydrophobic layer can also be explored to improve further the characteristics of the dual-layer MD membranes and their performance. Some research groups have already started working in this membrane engineering topic.

Once the technical validity of recycling discarded RO membranes for MD and FO applications has been shown, it is necessary to carry out life cycle and life cost assessments to verify the environmental and economic viability of the recycling procedures proposed in this PhD thesis for discarded RO membranes. Recently, a life cycle assessment (LCA) for recycled membranes applied to FO processes presented in this PhD thesis has been performed. The obtained results point out the interest in recycling end-of-life RO membrane modules for FO applications as an innovative alternative to boost the awaited circular economy in membrane science, even if discarded RO membrane modules are disassembled and chemically treated and modified. This developed study has already been compiled in a manuscript and submitted for publication as indicated in section List of publication (see page XVII of this PhD thesis).

Recycling and adapting discarded RO membrane modules in FO technology seems to be an interesting research line to which future efforts should be devoted. This would require the study of the most favorable recycling and transformation protocols without disassembling the RO membrane modules to improve the recycling economical assessment. Both cleaning and IP steps can be carried out without disassembling the membrane module. However, RO modules consist of one inlet (i.e. feed) and two outlets (i.e. retentate and permeate), whereas FO modules require two inlets and two outlets for feed and draw solutions. Therefore, an adequate adaptation of the RO modules to FO modules design is necessary and consequently merits a through and adequate investigation.

Discarded membranes and modules by other technologies rather than RO like nanofiltration (NF) and ultrafiltration (UF) should also be explored. These can be recycled and transformed to FO membranes by IP. It is expected that the resultant FO dual-layer membranes can exhibit lower structural parameters (S) than that obtained when recycling RO membranes since S is inversely proportional to the porosity or void volume fraction and proportional to the thickness (i.e. compared to UF and NF membranes, RO membranes tend

to be thicker to bear the higher hydrostatic pressure required, with smaller pore size and porosity). In fact, a lower support layer structural parameter results in a higher FO performance.

The study of the combination of MD and FO processes using recycled RO membranes for the treatment of RO brines is a promising strategy to meet zero liquid discharge (ZLD) with a minimal environmental impact. It would be very appropriate to use RO brines as draw solution in FO process for wastewater treatment. Because of the dilution of the draw solution, another separation process such as MD can be used as a second step for draw solution regeneration and water production. In order to maintain constant the salt concentration of the draw solution, the MD permeate flux must be similar to that of FO. An adequate hybrid FO/MD laboratory set-up should be developed and optimized membrane surface area and operating parameters of both processes should be determined. Depending on the results obtained on a laboratory scale, an FO/MD pilot plant should be designed and constructed for the treatment of RO brines using recycled RO membranes.

Appendix A

8. Supplementary Information of Chapter 3

8.1. Electrospun PVDF support characterization

The morphology of the electrospun PVDF support was studied by SEM (Fig. 8.1). A micrograph of its top surface showing a bead-free nanofibrous mesh is displayed inset together with nanofiber size distribution.

The thickness of the electrospun nanofiber support depends on the concentration of the polymer in the dope solution, the electrospinning time, and the nanofiber diameter. A nanofibrous support with small nanofibers diameters has more ability to transfer the electric charges to the stainless-steel collector, decreases the repulsion force between nanofibers and results in a highly packed support with low void volume fraction or porosity and thickness. However, for greater nanofibers sizes a more loosely packed structure is obtained [1]. In this case, for a PVDF concentration of 25 wt.%, an electrospinning time of 70 min, and diameter of nanofibers of 500 ± 20 nm.

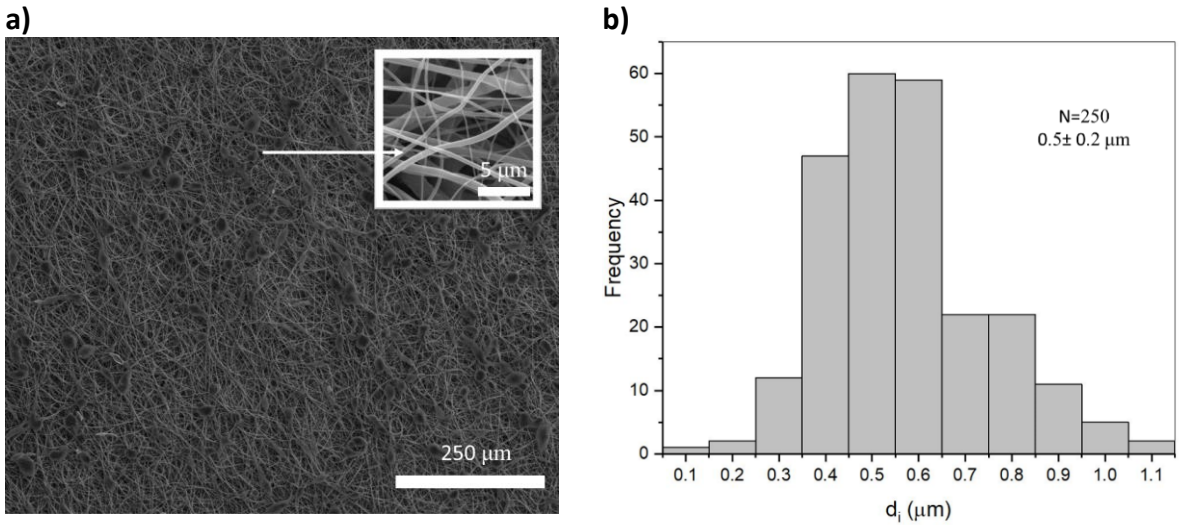

Figure 8.1. *a) SEM image of the surface of the electrospun PVDF support (higher magnification SEM image at inset), b) a histogram representing the distribution of the nanofiber diameters measured from the SEM image considering a total of 250 measurements.*

LEP$_W$ of the electrospun PVDF support was found to be 52 ± 1 kPa. This value is similar to that obtained for commercial PVDF membrane prepared by the phase inversion method [2] and electrospun PVDF nanofibrous membranes [1], reported to be 58 kPa and 46.5 kPa, respectively. The differences between the *LEP*$_W$ can be attributed mainly to the different maximum pore sizes.

8.2. Vapor-liquid equilibrium data of chloroform/methanol (MeOH) and chloroform/ethanol (EtOH) mixtures

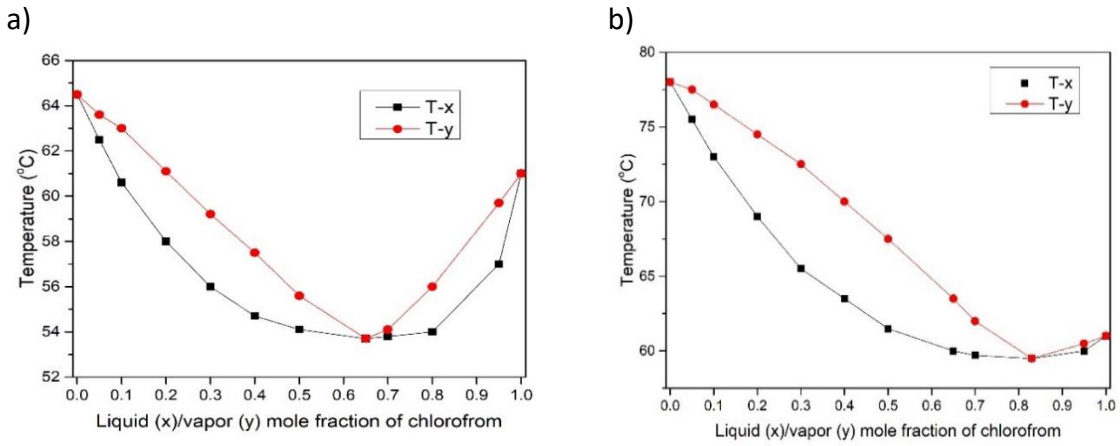

Figure 8.2. *T-xy diagram of a) chloroform/MeOH and b) chloroform/EtOH.*

8.3. Hansen Solubility Parameters

The interaction and miscibility between two liquids can be related with their Hansen solubility parameters (HSP). The following equation can be used to estimate the affinity of two solvents.

$$Ra^2 = 4(\delta_{d_2} - \delta_{d_1})^2 + (\delta_{p_2} - \delta_{p_1})^2 + (\delta_{h_2} - \delta_{h_1})^2 \qquad (8.1)$$

where δ_p, δ_h and δ_d are the polar, hydrogen, and dispersive solubility parameters, respectively. For *Ra* closer to zero, the components have a higher affinity with each other. The HSP values of the liquids are mentioned in Table 8.1. The calculated *Ra* values for chloroform/EtOH and chloroform/MeOH are 15.3 and 19.7 $MPa^{0.5}$, respectively. Therefore, chloroform has more affinity to ethanol than methanol. The solubility parameter value for PIM-1 is 19.4 ($MPa^{0.5}$) [3].

Table 8.1. *Hansen Solubility Parameters of the used liquids [4].*

Liquid	***δ_d ($MPa^{0.5}$)***	***δ_p ($MPa^{0.5}$)***	***δ_h ($MPa^{0.5}$)***
Chloroform	*17.8*	*3.1*	*5.7*
Ethanol	*15.9*	*8.8*	*19.4*
Methanol	*15.1*	*12.3*	*22.3*

8.4. Surface SEM images

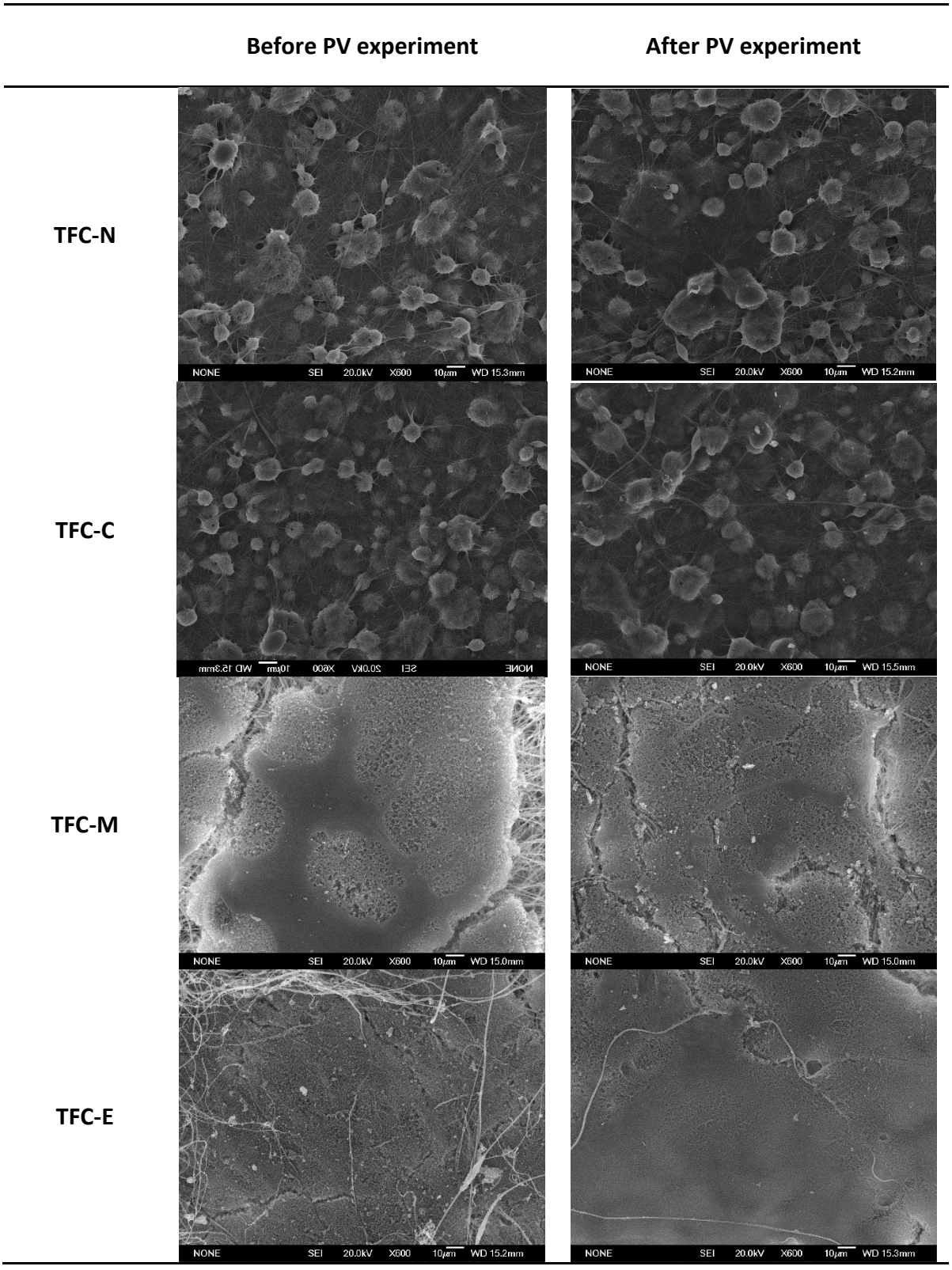

Figure 8.3. *Surface SEM images of the prepared membranes before and after the PV process.*

8.5. EDX mapping

TFC-N

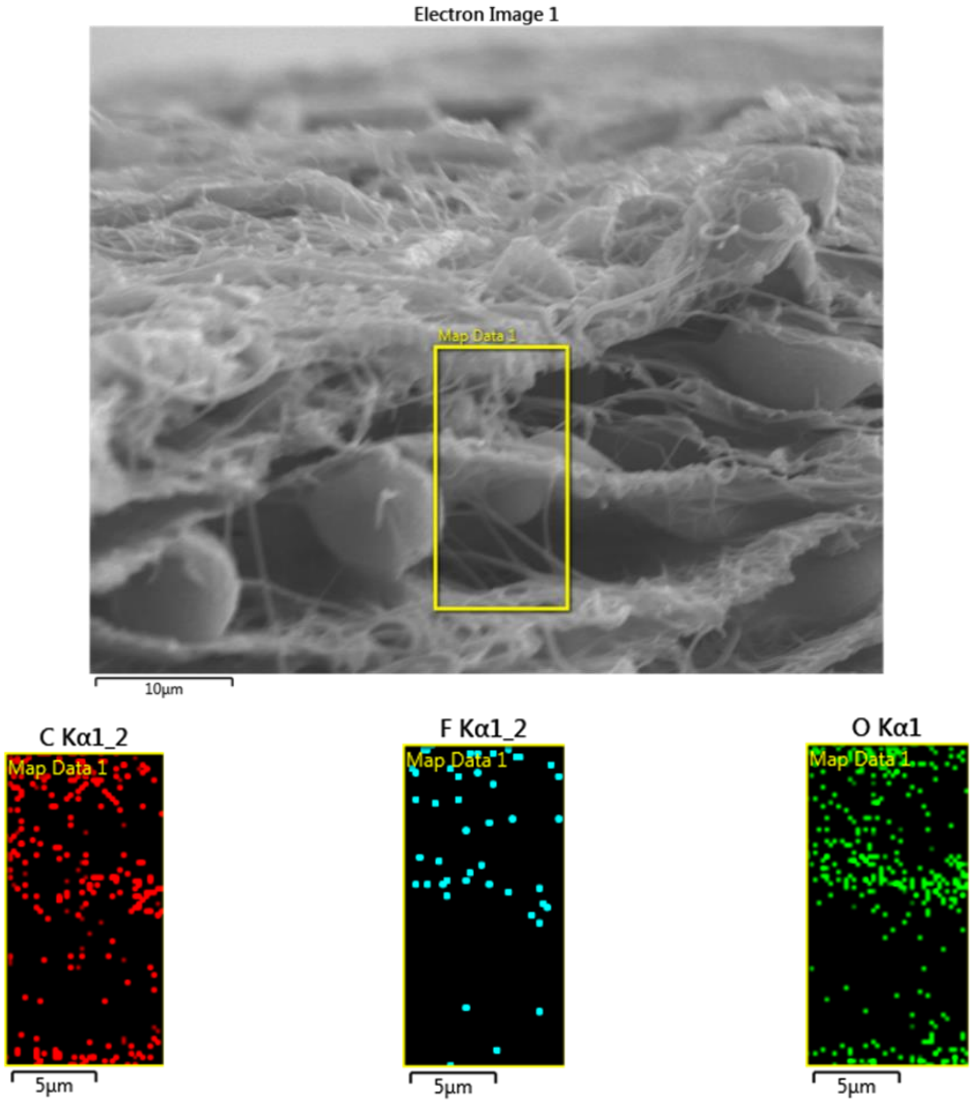

Figure 8.4. *Energy-dispersive X-ray spectroscopy (EDX) for TFC-N (thin film composite membrane prepared using a non-impregnated PVDF support). Mapping for carbon, fluorine and oxygen for the selected area on the SEM image. Oxygen (O), which corresponds just to the PIM-1 layer, is distributed with the same intensity at the top and middle of the membrane.*

TFC-E

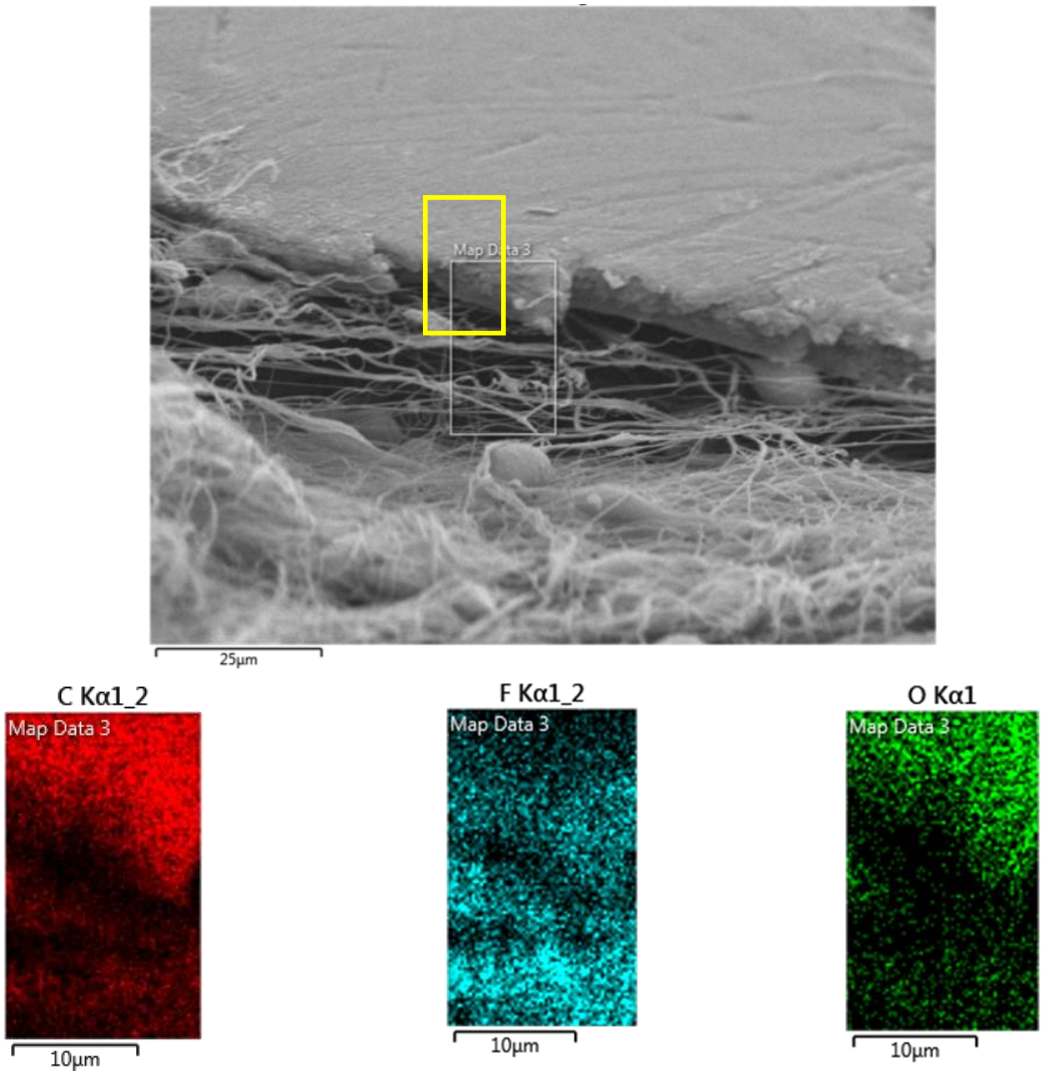

Figure 8.5. *Energy-dispersive X-ray spectroscopy (EDX) for TFC-E (thin film composite membrane prepared using an ethanol-impregnated PVDF support). Mapping for carbon, fluorine and oxygen for the selected area on the SEM image. The intensity of O, which corresponds just to the PIM-1 layer, is higher at the top, and the intensity of fluorine (F), which corresponds just to PVDF, is high at the bottom of the membrane (membrane support).*

8.6. Digital images of the top and bottom sides of TFC membranes

The digital images of both the top and bottom sides of the prepared TFC membranes after the pervaporation (PV) experiment are shown in Figure 8.6. As can be seen from the backside yellow images of the TFC-C and TFC-N membranes, PIM-1 penetrated into the inter-fiber volume of the PVDF support. However, based on the lighter yellow color of the bottom side of the TFC-C membrane compared to that of the TFC-N membrane, less PIM-1 penetration occurred in TFC-C. For both membranes, the PIM-1 layer was stable and did not detach from the PVDF support. In contrast, no PIM-1 could be detected at the bottom side of the TFC-M and TFC-E membranes (see white color of the bottom side of these membranes similar to that of the pristine PVDF nanofibrous support).

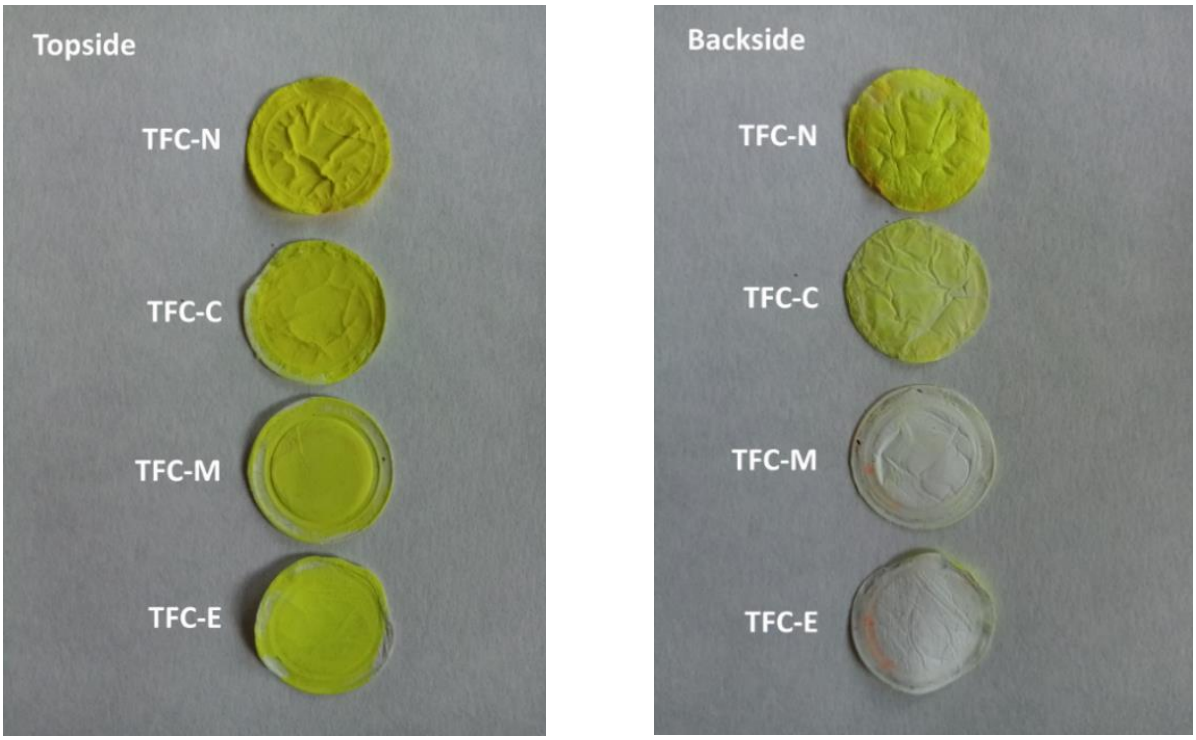

Figure 8.6. *Digital images of the top and bottom sides of the prepared TFC membranes.*

8.7. Feed conditions and performance of the membranes for butanol recovery

Table 8.2. *Comparison of PV performance of various types of membranes used for n-butanol recovery from aqueous solutions. Feed concentration and temperature (T_f), total permeate flux (J_T), n-butanol separation factor ($\beta_{BuOH/w}$) and PV separation index (PSI).*

Membrane	Feed conc. (wt%)	T_f (°C)	J_T (kg m^{-2} h^{-1})	$\beta_{BuOH/w}$	PSI (kg m^{-2} h^{-1})	Ref.
TFC-N	5	65	19.4	7.1	118.3	This study
TFC-C	5	65	16.1	8	112.7	This study
TFC-M	5	65	30.2	4.8	114.8	This study
TFC-E	5	65	35.4	4.8	134.5	This study
PIM-1 freestanding	5	65	1.85	19.6	34.4	[5]
PIM-1/PVDF (2% PIM-1) (TFC)	5	65	9.08	13.3	111.7	[5]
PIM-1/ 0.1rGO-OA freestanding	5	65	1.36	32.9	43.4	[6]
PIM-1 (TFC)	5	65	4.19	13.4	52.0	[7]
PIM-1/ 0.1rGO-OA (TFN)	5	65	5.34	12.5	61.4	[7]
PDMS (Pervatech BV)	5	65	5.25	9.9	46.7	[5]
PDMS1 (PERVAP™ 4060)	5	65	3.8	16.4	58.5	[6]
PDMS2 (PERVAP™ 4060)	5	50	3.4	39	129.2	[8]
Silica-filled PTMSP/PVDF (VITO®)	5	50	9.5	104	978.5	[8]
PIM-1freestanding	5	50	0.26	40	10.1	[9]
PTMSP freestanding	6	70	2.10	41	83.6	[10]
PDMS/CNT (10%)	1.5	80	0.24	32.9	7.7	[11]
PDMS/PE	2	37	0.13	32	4.0	[12]
PDMS/20% ZIF-7	1	60	1.69	65	107.5	[13]
PDMS/40% ZIF-7	1	60	1.46	36	51.1	[13]
PEBA/25% ZIF-71	1	40	0.43	22.3	9.2	[14]
PDMS (PERVAP™ 1070)	<0.5	55	0.36	34.5	12.1	[15]
PDMS (Pervatech BV)	2	40	1.03	9	8.2	[16]
PDMS (MEM-100™)	2	52	0.17	46	7.7	[17]
PDMS/Ceramic	1	40	0.5	25	12.0	[18]
PTFE	1.25	40	0.17	8.5	1.3	[19]
Silicalite/Silicon	1	78	0.09	90	8.0	[20]

8.8. PV-distillation hybrid simulation conditions: temperature and composition of the feed aqueous solution, permeate pressure and activation energy

Table 8.3. *Composition ($x_{BuOH,feed}$) and temperature ($T_{PV\text{-}inlet}$) of the feed solution, permeate side pressure ($P_{vacuum\ Pump}$) and activation energy of n-butanol (E_{BuOH}) and water (E_w) for the studied membranes in PV-distillation hybrid simulation.*

Membrane	$X_{BuOH,feed}$	$T_{PV\text{-}inlet}$ (°C)	$P_{vacuum\ Pump}$ (bar)	E_{BuOH} (kJ mol^{-1})	E_w (kJ mol^{-1})	Ref
TFC-C	0.05	65	0.01	70.6	34.5	This work
TFC-E	0.05	65	0.01	70.6	34.5	This work
PIM-1 (TFC)	0.05	65	0.01	70.6	34.5	[7]
PIM-1/PVDF (2% PIM-1) (TFC)	0.05	65	0.01	68	25.6	[7]
PDMS (Pervatech BV)	0.05	65	0.01	42.7[a]	32.3[a]	[5]
PDMS1 (PERVAP™ 4060)	0.05	65	0.01	42.7 [a]	32.3 [a]	[7]
PDMS2 (PERVAP™ 4060)	0.05	50	4×10^{-5}[b]	42.7[a]	32.3[a]	[8]
PDMS/Ceramic	0.01	40	Not mentioned (0.01 assumed)	25.82	27.45	[18]
PDMS/20% ZIF-7	0.01	60	Not mentioned (0.01 assumed)	30.23	31.48	[13]
Silicalite/Silicon	0.01	78	0.007	66.14	12	[20]

[a] The activation energy was obtained from Ref [17].
[b] It should be mentioned that vacuum pressure less than 10 mbar is unlikely to be achievable on the industrial scale [21].

8.9. Capital and utility cost calculations

The PV unit includes a membrane, membrane module, a refrigeration system (to condense permeate), and a vacuum pump. A freestanding PIM-1 membrane (80 µm) with an area of 0.002 m^2 contains 0.14 g PIM-1 polymer.[22] Therefore, to prepare 1 m^2 TFC membrane with a 5 µm thick PIM-1 film (thickness of the prepared membrane in this study), 4.3 g of PIM-1 is required. By knowing the price of monomers and solvents used in the PIM-1 synthesis procedure, the cost of the PIM-1 is estimated 3.5 \$ g^{-1}. In this study by considering

the cost of support and nonwoven fabric the TFC membrane cost is assumed 50 $ m^2. The PDMS membrane cost is also assumed the same.

The installed purchase cost of the refrigeration unit is calculated by the following equation [23]:

$$C_2 = C_1(\frac{S_2}{S_1})^n \times f \tag{8.2}$$

where, C_1 and C_2 are the capital cost of a plant with capacity S_1 and S_2, respectively. The constant exponent *n* is 0.8. The cost of a refrigeration system with a capacity of 15 kW is 2000 $.[24] The installation factor (*f*) which considers the cost of piping, electrical, installation, instrumental, and control, etc. [25] equals 3.5 for a refrigeration system.[23] This factor is 2.27 for membrane. It should be mentioned that for simplicity the same equation has been used to calculate the purchase cost of refrigeration systems for PDMS2 (PERVAP 3060) and TFC-C membranes, however, the evaporation temperature is -55 ˚C, and 5.4 ˚C, respectively.

The purchase cost of vacuum pump is evaluated according to the following equation [26]:

$$C_{\mathrm{vp}} = \frac{\text{CEPCI index in 2019}}{\text{CEPCI in 1994}} \times 4200(\frac{60GRT}{P})^{0.55} \times f \tag{8.3}$$

where, *P* and *T* are pressure and temperature at the standard condition (10^5 Pa, 273 K). *R* is the gas constant (8.314 kPa m^3 $kmol^{-1}$ K^{-1}) and G (kmol s^{-1}) is the inlet molar flow rate of the pump. The purchase cost of the equipment in the year 2019 can be estimated using the Chemical Engineering Plant Cost Index (CEPCI). CEPCI in 1994 and 2019 are 381.4 and 607, respectively. The installation factor (*f*) is 4.

The distillation column includes a vertical vessel, a reboiler, a condenser, and trays. The condenser and reboiler are assumed to be a shell and tube heat exchanger. The capital cost of the distillation column can be calculated according to the following equation [23]:

$$C = (a + bS^n) \times \frac{\text{CEPCI index in 2019}}{\text{CEPCI in 2007}} \times f \times f_{\mathrm{m}} \tag{8.4}$$

where, *C* is the equipment purchased cost. *a*, *b* and *n* are constant and *S* is the size parameter. The constant values in Jan. 2007 and the unit for size parameter are given in Table 8.4. The CEPCI index in the year 2007 is 509.7. The prices are for the equipment built from carbon steel except for vertical vessel. $f_{\mathrm{m}}$is the material cost factor which equals to 1.3 for 304 stainless steel (304 SS).

Table 8.4. *Purchased equipment cost*

Equipment	Unit for size (*S*)	*a*	*b*	*n*	*f*
Vertical vessel (304 stainless-steel)	shell mass (kg)	15000	68	0.85	4
Sieve tray	diameter (m)	110	380	1.8	-
Shell and tube heat exchanger	area (m^2)	24000	46	1.2	3.5
Centrifugal pump	Flow ($L\ s^{-1}$)	6900	206	0.9	4

The shell mass of the vertical column is calculated according to the following equation:

$$\text{Shell mass} = \pi D_c L_c t_w \rho$$

$$u_v = (-0.171 l_t^2 + 0.27 l_t - 0.047)\left[\frac{\rho_l - \rho_v}{\rho_v}\right]^{0.5} \quad (8.5)$$

$$D_c = \sqrt{\frac{4V_v}{\pi \rho_v u_v}} \quad (8.6)$$

$$L_c = l_t(NT - 1) + 2 \quad (8.7)$$

where, l_t (=0.6 m) is the spacing between trays. ρ_l and ρ_v are the densities of liquid and vapor, respectively obtained from Aspen-Hysys simulation. *NT* is the number of trays. V_v ($kg\ s^{-1}$) and u_v ($m\ s^{-1}$) are the maximum mass flow rate of vapor (obtained from the simulation) and maximum allowable vapor velocity. t_w is the thickness of the distillation column wall obtained from Table 8.5. ρ (=8000 $kg\ m^{-3}$) is the stainless steel density. D_c and L_c are the distillation column diameter and height, respectively.

Table 8.5. *Minimum wall thickness for distillation columns [23].*

Vessel diameter (m)	Minimum wall thickness (mm)
1	5
1-2	7
2-2.5	9
2.5-3	10
3-3.5	12

The area of a heat exchanger (*S* parameter in equation S4) can be calculated according to the following equation:

$$A = \frac{q}{U.LMTD} \quad (8.8)$$

$$LMTD = \frac{\Delta T_1 - \Delta T_2}{\ln\left(\frac{\Delta T_1}{\Delta T_2}\right)} \tag{8.9}$$

where, q is the heat flow (w), U is the overall heat transfer coefficient (w m^{-2} k^{-1}) obtained from Ref [23] and *LMTD* is the mean logarithmic temperature difference. The minimum temperature difference between the cold and hot stream in the heat exchanger is considered 5 ˚C.

The electricity price (required by the vacuum pump and refrigeration systems) is considered 40 $ MWh^{-1}[27, 28]. The price of low-pressure steam (130 ˚C), used in the heaters and distillation columns boiler, is 3.8 $ $MMBtu^{-1}$[28]. Cooling water (0.02 $ m^{-3}) at 25 ˚C was used as the coolant of the distillation column condenser. The shaft work required to supply cooling duty in the refrigeration unit can be calculated according to the following equation [23]:

$$\text{Shaft work required} = \frac{\text{Cooling duty}}{\text{COP}} \tag{8.10}$$

$$\text{COP} = \frac{T_1}{T_2 - T_1} \tag{8.11}$$

where, T_1 and T_2 are evaporator and condenser absolute temperature in the refrigerant cycle, respectively. COP is the refrigerator coefficient of performance for the Carnot cycle. COP of the real refrigeration system is considered 0.85 times of Carnot cycle [23]. COP for PDMS2 (PERVAP 4060) and TFC-C hybrid system is 1.9 ($= \frac{213}{303-213} \times 0.85$) and 7.7 ($= \frac{273}{303-213} \times 0.85$), respectively.

A plant running time of 8000 h $year^{-1}$ is considered and the calculations have been carried out based on 10 years depreciation. The total cost of the plant is calculated according to the following equation:

$$\text{Total cost } (\$\,\text{year}^{-1}\,\text{kg}_{\text{BuOH}}^{-1}) = \frac{\frac{\text{Capital cost } (\$)}{\text{depreciation time (year)}} + \text{operating cost } (\$\,\text{year}^{-1})}{\text{Produced BuOH (kg)}} \tag{8.12}$$

The capital cost is the summation of the purchased cost of the main plant equipment. The operating cost is the summation of utility cost, maintenance cost, and membrane replacement cost. It is assumed the membrane should be replaced every year. The maintenance cost of the equipment is considered 5% of the capital cost [29, 30].

An economic comparison of the hybrid systems at the optimum area with the standalone distillation column is shown in Table 8.6.

Table 8.6. *Installed equipment, utility, and maintenance costs of the main equipment for standalone distillation system and the hybrid units at the optimum membrane area.*

Item	TFC-C (1500 m^2) hybrid	PDM2 (PERVAP 4060) (4500 m^2) hybrid	Distillation
Water column1 ($)	-	-	1591048
Water column2 ($)	288090	179145	362276
Butanol column ($)	583616	987598	1501738
Membrane+module ($)	340500	1021500	-
Vacuum pump ($)	15085	11127	-
Centrifuge pump ($)	201925	198293	-
Condenser ($)	1216106	702980	-
Heat exchangers ($)	80437	672088	1505593
LP steam ($ $year^{-1}$)	1145321	554652	2293956
Cooling water ($ $year^{-1}$)	-	-	553884
Electricity ($ $year^{-1}$)	444900	653939	-
Maintenance ($ $year^{-1}$)	163601	130148	248032
Membrane replacement ($ $year^{-1}$)	170250	510750	-

8.10. References

[1] M. Essalhi, M. Khayet, Self-sustained webs of polyvinylidene fluoride electrospun nano-fibers: Effects of polymer concentration and desalination by direct contact membrane distillation, Journal of Membrane Science, 454 (2014) 133-143.

[2] M. Khayet, T. Matsuura, Chapter 8 - MD Membrane Characterization, in: M. Khayet, T. Matsuura (Eds.) Membrane Distillation, Elsevier, Amsterdam, 2011, pp. 189-225.

[3] S. Thomas, I. Pinnau, N. Du, M.D. Guiver, Pure-and mixed-gas permeation properties of a microporous spirobisindane-based ladder polymer (PIM-1), Journal of Membrane Science, 333 (2009) 125-131.

[4] C.M. Hansen, A.L. Smith, Using Hansen solubility parameters to correlate solubility of C60 fullerene in organic solvents and in polymers, Carbon, 42 (2004) 1591-1597.

[5] L. Gao, M. Alberto, P. Gorgojo, G. Szekely, P.M. Budd, High-flux PIM-1/PVDF thin film composite membranes for 1-butanol/water pervaporation, Journal of Membrane Science, 529 (2017) 207-214.

[6] M. Alberto, J.M. Luque-Alled, L. Gao, M. Iliut, E. Prestat, L. Newman, S.J. Haigh, A. Vijayaraghavan, P.M. Budd, P. Gorgojo, Enhanced organophilic separations with mixed matrix membranes of polymers of intrinsic microporosity and graphene-like fillers, Journal of Membrane Science, 526 (2017) 437-449.

[7] M. Alberto, R. Bhavsar, J.M. Luque-Alled, E. Prestat, L. Gao, P.M. Budd, A. Vijayaraghavan, G. Szekely, S.M. Holmes, P. Gorgojo, Study on the formation of thin film nanocomposite (TFN) membranes of polymers of intrinsic microporosity and graphene-like fillers: Effect of lateral flake size and chemical functionalization, Journal of Membrane Science, 565 (2018) 390-401.

[8] S. Claes, P. Vandezande, S. Mullens, K. De Sitter, R. Peeters, M.K. Van Bael, Preparation and benchmarking of thin film supported PTMSP-silica pervaporation membranes, Journal of Membrane Science, 389 (2012) 265-271.

[9] M. Žák, M. Klepic, L.Č. Šťastná, Z. Sedláková, H. Vychodilová, Š. Hovorka, K. Friess, A. Randová, L. Brožová, J.C. Jansen, Selective removal of butanol from aqueous solution by pervaporation with a PIM-1 membrane and membrane aging, Separation and Purification Technology, 151 (2015) 108-114.
[10] A.G. Fadeev, Y.A. Selinskaya, S.S. Kelley, M.M. Meagher, E.G. Litvinova, V.S. Khotimsky, V.V. Volkov, Extraction of butanol from aqueous solutions by pervaporation through poly(1-trimethylsilyl-1-propyne), Journal of Membrane Science, 186 (2001) 205-217.
[11] C. Xue, G.-Q. Du, L. Chen, J.-G. Ren, J.-X. Sun, F.-W. Bai, S.-T. Yang, A carbon nanotube filled polydimethylsiloxane hybrid membrane for enhanced butanol recovery, Scientific reports, 4 (2014) 5925.
[12] S.-Y. Li, R. Srivastava, R.S. Parnas, Separation of 1-butanol by pervaporation using a novel tri-layer PDMS composite membrane, Journal of Membrane Science, 363 (2010) 287-294.
[13] X. Wang, J. Chen, M. Fang, T. Wang, L. Yu, J. Li, ZIF-7/PDMS mixed matrix membranes for pervaporation recovery of butanol from aqueous solution, Separation and Purification Technology, 163 (2016) 39-47.
[14] S. Liu, G. Liu, X. Zhao, W. Jin, Hydrophobic-ZIF-71 filled PEBA mixed matrix membranes for recovery of biobutanol via pervaporation, Journal of Membrane Science, 446 (2013) 181-188.
[15] E.A. Fouad, X. Feng, Pervaporative separation of n-butanol from dilute aqueous solutions using silicalite-filled poly(dimethyl siloxane) membranes, Journal of Membrane Science, 339 (2009) 120-125.
[16] S. Van Wyk, A. Van der Ham, S. Kersten, Pervaporative separation and intensification of downstream recovery of acetone-butanol-ethanol (ABE), Chemical Engineering and Processing-Process Intensification, 130 (2018) 148-159.
[17] A. Fadeev, M. Meagher, S. Kelley, V. Volkov, Fouling of poly [-1-(trimethylsilyl)-1-propyne] membranes in pervaporative recovery of butanol from aqueous solutions and ABE fermentation broth, Journal of Membrane Science, 173 (2000) 133-144.
[18] L. Gongping, H. Dan, W. Wang, F. Xiangli, J. Wanqin, Pervaporation separation of butanol-water mixtures using polydimethylsiloxane/ceramic composite membrane, Chinese Journal of Chemical Engineering, 19 (2011) 40-44.
[19] D.L. Vrana, M.M. Meagher, R.W. Hutkins, B. Duffield, Pervaporation of model acetone-butanol-ethanol fermentation product solutions using polytetrafluoroethylene membranes, Separation science and technology, 28 (1993) 2167-2178.
[20] N. Qureshi, M. Meagher, R.W. Hutkins, Recovery of butanol from model solutions and fermentation broth using a silicalite/silicone membrane, Journal of Membrane Science, 158 (1999) 115-125.
[21] W. Van Hecke, H. De Wever, High-flux POMS organophilic pervaporation for ABE recovery applied in fed-batch and continuous set-ups, Journal of Membrane Science, 540 (2017) 321-332.
[22] A.W. Ameen, J. Ji, M. Tamaddondar, S. Moshenpour, A.B. Foster, X. Fan, P.M. Budd, D. Mattia, P. Gorgojo, 2D boron nitride nanosheets in PIM-1 membranes for CO2/CH4 separation, Journal of Membrane Science, (2021) 119527.
[23] R. Sinnott, G. Towler, Chemical engineering design: SI Edition, Butterworth-Heinemann, 2019.
[24] S.S. Alrwashdeh, H. Ammari, Life cycle cost analysis of two different refrigeration systems powered by solar energy, Case Studies in Thermal Engineering, 16 (2019) 100559.
[25] W. Hand, From flow sheet to cost estimate, Petroleum Refiner, 37 (1958) 331-334.
[26] W. Ji, A. Hilaly, S.K. Sikdar, S.-T. Hwang, Optimization of multicomponent pervaporation for removal of volatile organic compounds from water, Journal of membrane science, 97 (1994) 109-125.
[27] V. Van Hoof, L. Van den Abeele, A. Buekenhoudt, C. Dotremont, R. Leysen, Economic comparison between azeotropic distillation and different hybrid systems combining distillation with pervaporation for the dehydration of isopropanol, Separation and Purification Technology, 37 (2004) 33-49.

[28] F. Hamad, M. Qahtani, A. Ameen, M. Vaidya, S. Duval, A. Bahamdan, F. Otaibi, Treatment of highly sour natural gas stream by hybrid membrane-amine process: Techno-economic study, Separation and Purification Technology, 237 (2020) 116348.
[29] A.W. Ameen, P.M. Budd, P. Gorgojo, Superglassy Polymers to Treat Natural Gas by Hybrid Membrane/Amine Processes: Can Fillers Help?, Membranes, 10 (2020) 413.
[30] M. Di Luccio, C.P. Borges, T.L. Alves, Economic analysis of ethanol and fructose production by selective fermentation coupled to pervaporation: effect of membrane costs on process economics, Desalination, 147 (2002) 161-166.

Appendix B

9. Supplementary Information of Chapter 6

9.1. Cross-section SEM images of the asymetric FO commercial membranes and RFO2 membrane.

(a)

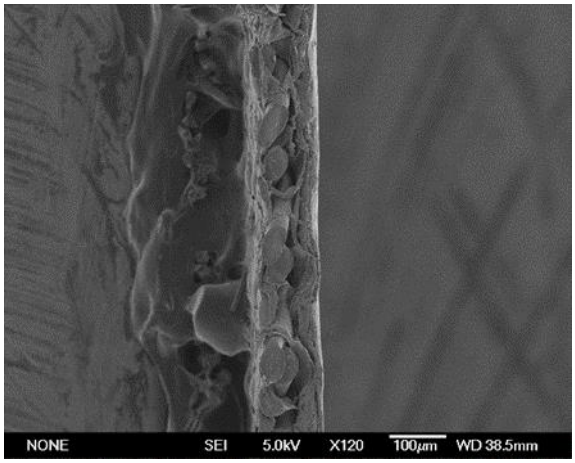

(b)

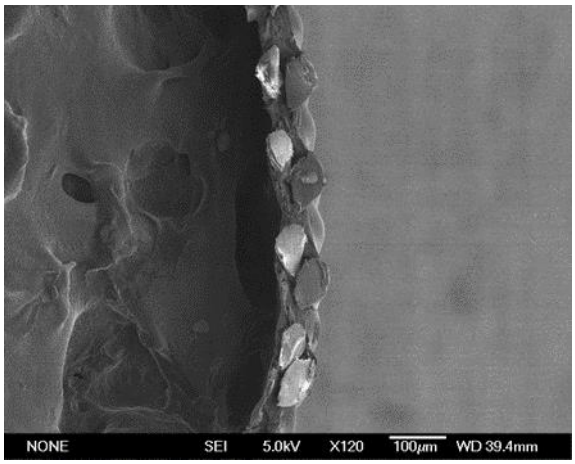

(c)

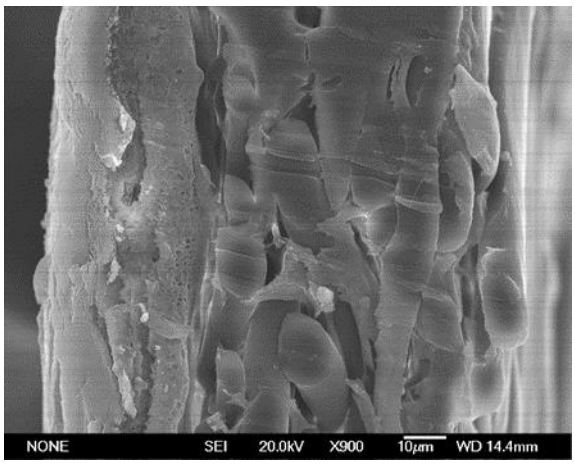

Figure 9.1. *Cross-section SEM images of the asymetric FO commercial (a) PA (TFC-HTI) and (b) CTA (CTA-HTI) membranes embedded in a polyster mesh supplied by Hydration Technology Innovations (HTI™, LLC, Albany, USA) and (c) the RFO2 membrane.*

9.2. Effects of HA on the electrical conductivity of NaCl solutions and NaCl on the absorbance of HA solutions.

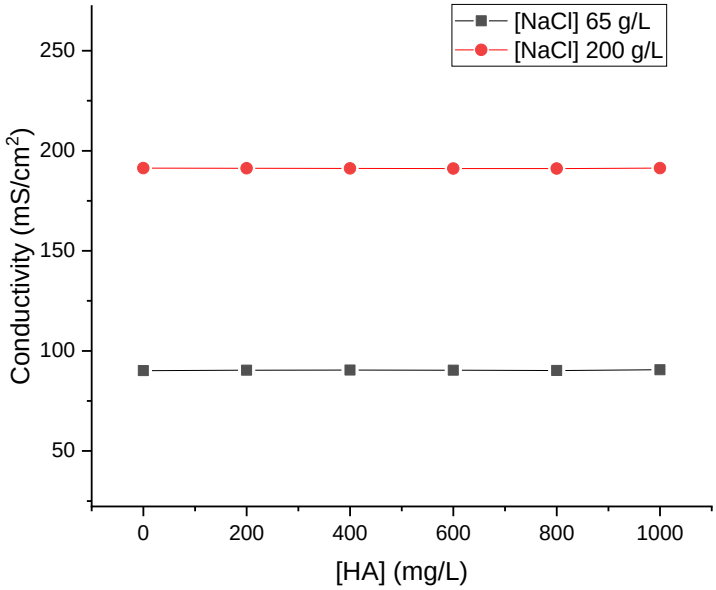

Figure 9.2. *Measured electrical conductivity of two NaCl concentrations (200 g/L and 65 g/L) at different concentrations of HA in water solutions.*

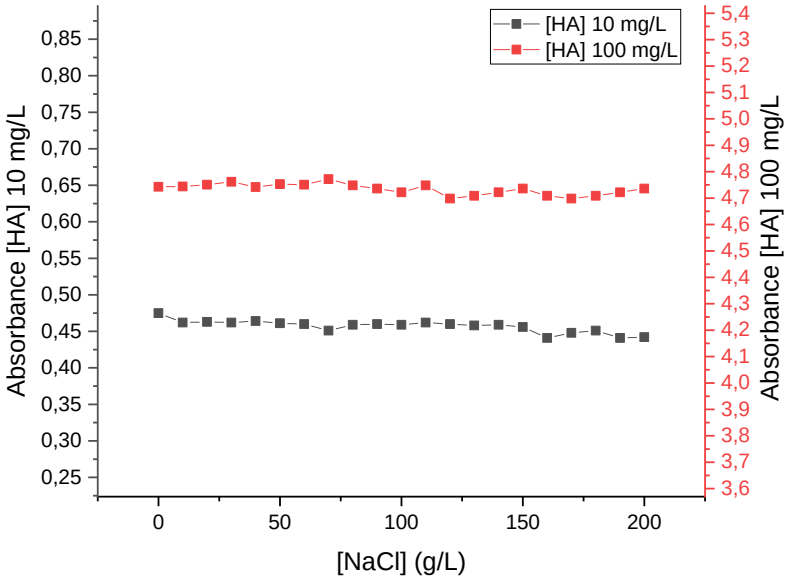

Figure 9.3. *Measured absorbance of two HA concentrations (100 mg/L and 10 mg/L) at different concentrations of NaCl in water.*

As can be seen in Figs. 9.2 and 9.3, no interaction of HA on the electrical conductivity of NaCl measurements was observed. Moreover, the absorbance of HA was kept almost constant for different NaCl concentrations (from 0 to 200 g/L of NaCl in water).

9.3. Solute transport tests using polyethylene glycol (PEG) and polyethylene oxide (PEO) of different molecular weights.

Solute separation transport tests were performed using polyethylene glycol (PEG) and polyethylene oxide (PEO) of different molecular weights. The selected molecular weights were 0.4, 1, 6, 10, 12, 20 and 35 kg/mol for PEGs and 100 and 200 kg/mol for PEOs [1]. The set-up used was described in our previous paper [2]. All chemicals were purchased from Sigma-Aldrich Chemical Co. St. Louis, Massachusetts, USA. The feed temperature, pressure and solute concentration were 296 K, 1.04 bar and 200 ppm, respectively.

First, pure water permeance (*WP*) of each membrane was determined using distilled water as feed. Then, PEG and PEO aqueous solutions were filtered through the membrane following an ascending order of their molecular weights for one hour each and the product permeation rate was determined. The PEG and PEO concentrations of both the feed and permeate were evaluated using the total organic carbon (TOC) analyzer (model CA16 for Skalar Analytical B.V., Breda, Netherlands). The solute rejection factor (α) was calculated as [3]:

$$\alpha = \left(1 - \frac{C_p}{C_f}\right) \cdot 100 \tag{9.1}$$

where C_p and C_f are the solute (PEG or PEO) permeate and feed concentrations, respectively.

To determinate the size of PEG and PEO, the following equations that relate the Einstein-Stokes radius to the molecular weight of PEG (Eq. (9.2)) and PEO (Eq. (9.3)) were considered [4]:

$$a_{r,PEG} = 16.73 \cdot 10^{-10} M^{0.557} \tag{9.2}$$

$$a_{r,PEO} = 10.44 \cdot 10^{-10} M^{0.587} \tag{9.3}$$

where *M* is the molecular weight in g/mol and a_r is the Einstein-Stokes radius in cm.

The obtained water permeance (*WP*) and solute rejection factor (α) of the RFO membranes are shown in Table 9.1.

Table 9.1. *Water permeance (WP) and solute rejection factor (α) of the RFO membranes obtained by solute transport experiments of aqueous solutions containing PEG and PEO of different molecular weights (Mw).*

Membrane	*WP* (L/m²·h·bar)	α (%)								
		PEG 0.4[a]	PEG 1[b]	PEG 6[c]	PEG 10[d]	PEG 12[e]	PEG 20[f]	PEG 35[g]	PEO 100[h]	PEO 200[i]
RFO1	37 ± 1	34 ± 1	44 ± 4	54 ± 4	64 ± 2	68 ± 3	80 ± 4	97 ± 2	98 ± 1	100
RFO2	43 ± 2	33 ± 1	37 ± 3	55 ± 5	68 ± 3	80 ± 3	93 ± 6	98 ± 2	99 ± 1	100
RFO3	41 ± 1	35 ± 1	36 ± 1	41 ± 4	51 ± 3	63 ± 4	74 ± 7	89 ± 2	99 ± 1	100
RFO4	43 ± 1	36 ± 1	37 ± 2	47 ± 6	58 ± 5	67 ± 3	79 ± 2	91 ± 3	96 ± 1	100

[a] PEG 0.4: *Mw* = 0.4 kg/mol, Einstein-Stoke radius (*ar,PEG*) = 0.94 nm; [b] PEG 1: *Mw* = 1 kg/mol, radius (*ar,PEG*) = 1.57 nm; [c] PEG 6: *Mw* = 6 kg/mol, radius (*ar,PEG*) = 4.26 nm; [d] PEG 10: *Mw* = 10 kg/mol, radius (*ar,PEG*) = 5.66 nm; [e] PEG 12: *Mw* = 12 kg/mol, radius (*ar,PEG*) = 6.26 nm; [f] PEG 20: *Mw* = 20 kg/mol, radius (*ar,PEG*) = 8.32 nm; [g] PEG 35: *Mw* = 35 kg/mol, radius (*ar,PEG*) = 11.36 nm; [h] PEO 100: *Mw* = 100 kg/mol, radius (*ar,PEO*) = 17.98 nm; [i] PEO 200: *Mw* = 200 kg/mol, radius (*ar,PEO*) = 27.01 nm.

The mean pore size and the geometric standard deviation were determined from the plot of the rejection factor as a function of the solute diameter and their correlation according to the log-normal probability function (Fig. 9.4) [4].

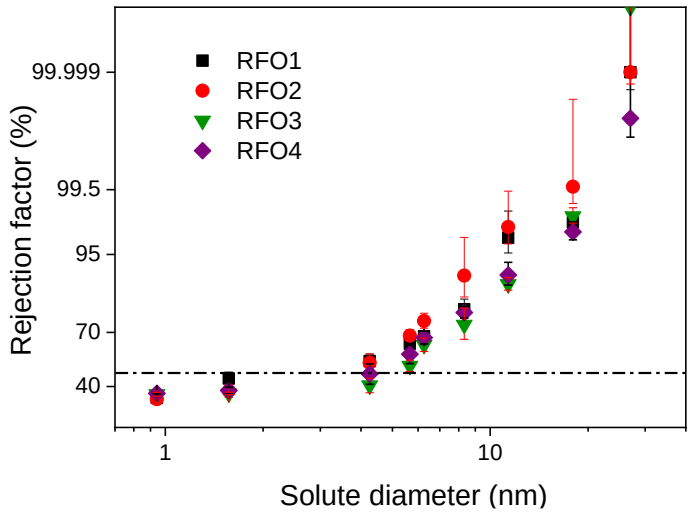

Figure 9.4. *Log-normal probability plot of the rejection factor of the RFO membranes as a function of solute diameter.*

The mean pore size (μ_p) and the molecular weight cut-off (*MWCO*) correspond to the Einstein-Stokes diameters of 50% and 90% rejection factors, respectively. The geometric standard deviation is the ratio between the Einstein-Stokes diameters corresponding to 84.13% and 50% rejection factors [4]. The pore density (*N*) and porosity (ε) were determined from the obtained permeance data using the following equations [4]:

$$N = \frac{128\eta\delta J_t}{\pi\Delta P \sum_{d_{min}}^{d_{max}} f_i d_i^4} \tag{9.4}$$

$$\varepsilon = \left(\frac{N\pi}{4}\sum_{d_{min}}^{d_{max}} f_i d_i^2\right)100 \tag{9.5}$$

where η is the solvent viscosity, δ is the pore length considered equivalent to the membrane thickness, ΔP is the pressure difference across the membrane, J_t is the total permeate flux and f_i the fraction of pores with diameter d_i.

From the mean pore size (μ_p) and the geometric standard deviation, the cumulative pore size distribution and the probability density function curves are presented in Fig. 9.5.

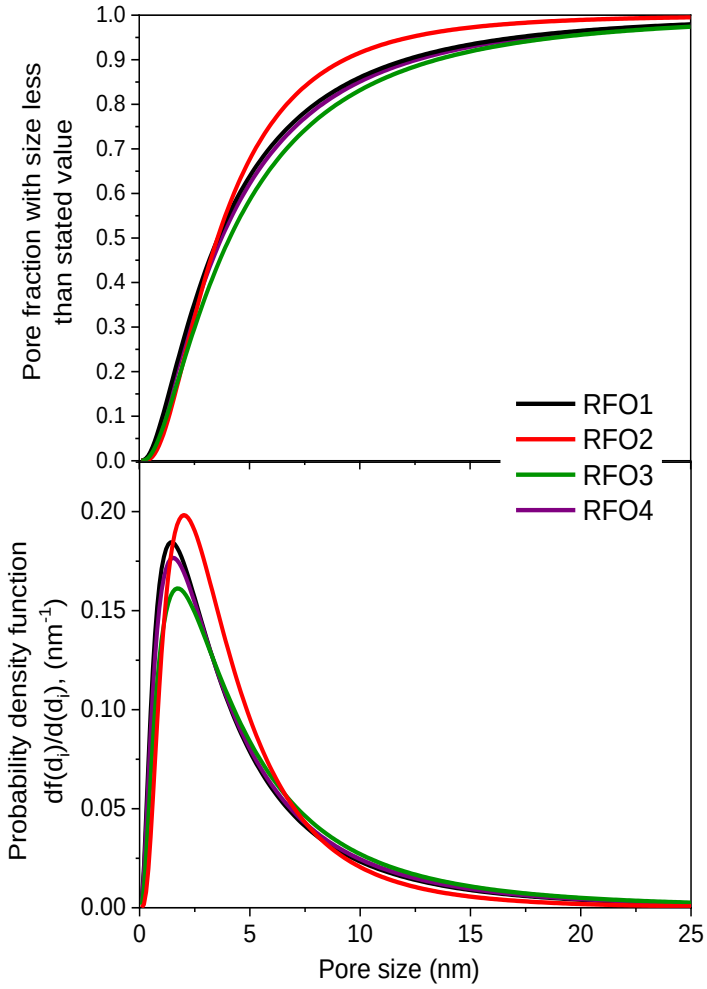

Figure 9.5. *Cumulative pore size distribution (a) and probability density function (b) curves of the RFO membranes.*

9.4. Reverse salt transfer factor (RTs) of the RFO and TRFO membranes

For FO membranes, NaCl is one of the most used draw solutes due to its small ion sizes and its high diffusivity in the FO membrane support. In this study, FO tests were carried out for low concentration (10 mg/L HA feed aqueous solution and 65 g/L NaCl draw aqueous solution) and high concentration (100 mg/L HA feed aqueous solution and 200 g/L NaCl draw aqueous solution). The specific reverse salt flux (J_s/J) is a quantitative factor indicating the bi-directional diffusion in the FO separation process. A reduced (J_s/J) value indicates an increase of the selectivity and efficiency of the membrane. However, as shown in Figs. 6.5b and 6.8b, J_s/J values depend on the NaCl concentration of the draw solution. A higher NaCl concentration of the draw solution induced a greater J_s/J value. Similar results were reported elsewhere [5]. The higher reverse draw solute flux detected for a higher NaCl concentration reduces further the driving force for water transport (i.e. decrease of the permeate flux).

In this study two different conditions of both the feed and draw solutions have been tested to evaluate the FO performance of RFO and TRFO membranes. In order to compare the draw solute loss due to the reverse salt flux for both high and low concentrations, a normalized reverse salt transfer (RT_s) parameter was defined as [6]:

$$RT_s\,(\%) = \left(\frac{C_{s,F,t}}{C_{s,D,0}}\right) \cdot 100 \tag{9.6}$$

where $C_{s,F,t}$ is the final salt (NaCl) concentration of the feed solution and $C_{s,D,0}$ is the initial salt concentration of the draw solution. RT_s reveals the amount of NaCl transported across the FO membrane to the feed side in relation to the initial draw concentration.

The obtained normalized reverse salt transfer (RT_s) of all membranes is shown in Fig. 9.6. In general, as it was expected, RT_s increases with the increase of the salt concentration in the draw solution except for the CTA-HTI membrane. Compared to all membranes, the commercial membrane TFC-HTI exhibits the lowest RT_s values while the CTA-HTI membrane showed the worst results (Fig. 9.6a). The RT_s values were found to be higher for the RFO membranes than for the TRFO membranes. For the low concentration test, the RFO membranes cleaned only in the pilot plant (RFO1 and RFO2 membranes) show significantly lower RT_s results than the other RFO membranes cleaned also following the laboratory scale protocol (RFO3 and RFO4 membranes). This can be due to the existence of the PA residues in the pores of the PSf support that retards the diffusion of the salt from the draw solution to the feed solution [7]. However, for the TRFO membranes no significant difference was observed (Fig. 9.6b).

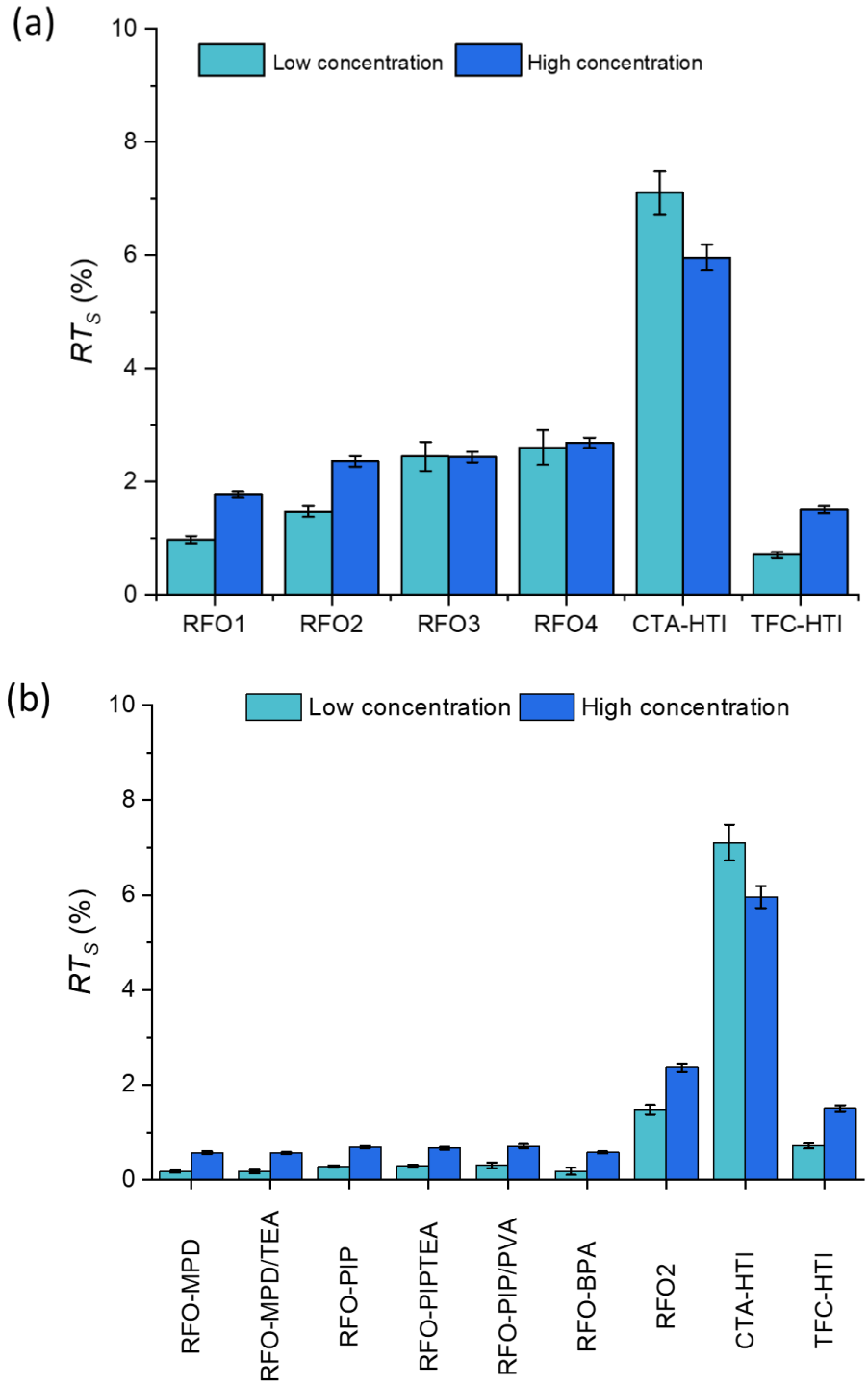

Figure 9.6. *Normalized reverse salt transfer (RTs) of the RFO (a) and TRFO (b) membranes together with that of the commercial CTA-HTI and TFC-HTI membranes for low concentration (10 mg/L HA feed aqueous solution and 65 g/L NaCl draw aqueous solution) and high concentration (100 mg/L HA feed aqueous solution and 200 g/L NaCl draw aqueous solution).*

9.5. FO results of the best RFO membrane (RFO2) subjected to a passive NaClO cleaning process in the pilot plant under a level dose of 10^6 ppm·h

Table 9.2. *FO results of the RFO2 membrane obtained for low (L_c) and high (H_c) concentration tests: permeate flux (J), reverse salt permeate flux (J_s), specific reverse salt flux (J_s/J), reverse salt transfer factor (RT_s), HA rejection factor (R_{HA}) and HA concentration factor (CF_{HA}).*

	J (kg/m²h)	J_s (10^{-3} kg/m²h)	J_s/J (10^{-3})	RT_s (%)	R_{HA} (%)	CF_{HA}
Lc	6.2 ± 0.3	4 ± 2	0.7 ± 0.4	1.48 ± 0.09	99.52 ± 0.24	1.12 ± 0.02
Hc	7.2 ± 0.3	42 ± 1	6 ± 1	2.36 ± 0.09	99.82 ± 0.06	1.11 ± 0.01

9.6. Study of passive cleaning under laboratory protocol with a total NaClO exposure dose of $3 \cdot 10^5$ ppm·h

To identify the efficacy of the followed cleaning protocols carried out either in the pilot plant, in the laboratory or both, cleaning was carried out only under the laboratory protocol. After disassembling the discarded modules, the membranes were exposed to an aqueous solution of NaClO at 6200 ppm·h for 48h, reaching a total exposure dose of $3 \cdot 10^5$ ppm.h. The membrane is named hereafter RFO5 membrane.

The membrane thickness and water contact angle of this membrane are summarized in Table 9.3. The obtained water contact angle of both sides of the membrane RFO5 as well as its thickness can be considered similar to the values obtained for the other RFO membranes (See Table 6.3). The IEP value obtained for the RFO5 membrane is slightly higher than that of the membranes RFO1 and RFO2 that were recycled following the pilot plant cleaning protocol, but comparable to that of the membranes RFO3 and RFO4 that were subjected to Laboratory cleaning after the pilot plant cleaning.

Table 9.3. *Water contact angle (θ_w) of the active layer (AL) and support layer (SL), thickness (δ) and isoelectric point (IEP) of the RFO5 membrane.*

Membrane	$(\theta_w)_{AL}$ (º)	$(\theta_w)_{SL}$ (º)	δ (µm)	*IEP* (pH)
RFO5	77 ± 3	65 ± 7	98 ± 3	4.01

From the SEM image (Fig. 9.7) it can be seen a similar surface to that of the RFO2 membrane (Fig. 6.2) recycled following only the pilot plant cleaning protocol under an exposure dose of 10^6 ppm·h.

Membrane	Active layer (PSf layer) (X10,000)	PE support (X250)
RFO5	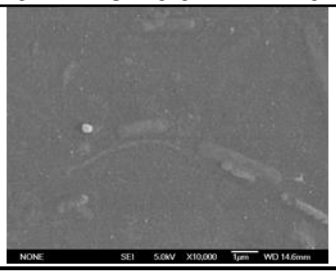	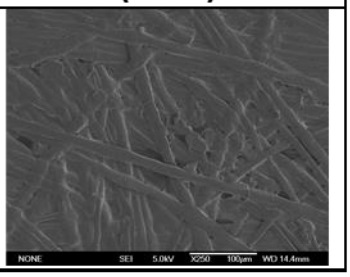

Figure 9.7. *SEM images of the support and active layer of the RFO5 membrane.*

The water permeance (*WP*) and the solute transport experiments with PEGs and PEOs were also determined for the membrane RFO5 and the results are summarized in Table 9.4. The *WP* values of the membranes RFO5 and RFO1 (Table 9.1) are similar indicating that the cleaning procedure in the laboratory is more efficient since less exposure time was applied compared to that in the pilot plant. The solute rejection factor values obtained in solute transport tests for the RFO5 membrane were similar to the values obtained for the RFO3 membrane (Table 9.1) and slightly lower than the values obtained for the RFO1 membrane (Table 9.1).

Table 9.4. *Water permeance (WP) and solute rejection factor (α) of the RFO5 membrane obtained by the solute transport experiments of aqueous solutions containing PEG and PEO of different molecular weights (Mw).*

WP **(L/m²·h·bar)**	**α (%)**								
	PEG 0.4[a]	**PEG 1[b]**	**PEG 6[c]**	**PEG 10[d]**	**PEG 12[e]**	**PEG 20[f]**	**PEG 35[g]**	**PEO 100[h]**	**PEO 200[i]**
38 ± 1	38 ± 2	45 ± 2	47 ± 3	54 ± 2	64 ± 2	71 ± 2	80 ± 4	99 ± 1	100

[a] PEG 0.4: M_w = 0.4 kg/mol, Einstein-Stoke radius ($a_{r,PEG}$) = 0.94 nm; [b] PEG 1: M_w = 1 kg/mol, radius ($a_{r,PEG}$) = 1.57 nm; [c] PEG 6: M_w = 6 kg/mol, radius ($a_{r,PEG}$) = 4.26 nm; [d] PEG 10: M_w = 10 kg/mol, radius ($a_{r,PEG}$) = 5.66 nm; [e] PEG 12: M_w = 12 kg/mol, radius ($a_{r,PEG}$) = 6.26 nm; [f] PEG 20: M_w = 20 kg/mol, radius ($a_{r,PEG}$) = 8.32 nm; [g] PEG 35: M_w = 35 kg/mol, radius ($a_{r,PEG}$) = 11.36 nm; [h] PEO 100: M_w = 100 kg/mol, radius ($a_{r,PEO}$) = 17.98 nm; [i] PEO 200: M_w = 200 kg/mol, radius ($a_{r,PEO}$) = 27.01 nm.

The membrane characteristics obtained from the solute transport experiments (mean pore size (μ_p), its geometric standard deviation (σ_p), density (N), porosity (ε) and molecular weight cut-off ($MWCO$), together with the tortuosity (τ, Eq. (6.1)) and the "intrinsic" structural parameter (S_{int}, from Eq. (6.2)) are presented in Table 9.5. The membrane RFO5 recycled with a lower total dose level following the laboratory cleaning protocol exhibits similar WP to those of the RFO1 membrane recycled with more than 2 times total dose level following the pilot plant cleaning (See Table 6.4). This is attributed mainly to the greater pore size of the membrane RFO5, which is 16% larger than that of the membrane RFO1. However, the pore density and porosity of the membrane RFO5 are lower than those of the other RFO membranes (i.e. 4446-5467 pores/μm^2 for the pore density and 26-30% for the porosity). In addition, among all recycled membranes studied, the MWCO, tortuosity and S_{int} values of the RFO5 membrane are the highest (See Table 9.5).

Table 9.5. *Mean pore size (μ_p), geometric standard deviation (σ_p), pore density (N), porosity (ε), molecular weight cut-off (MWCO), tortuosity (τ) and "intrinsic" structural parameter factor (S_{int}) of the RFO5 membrane obtained from solute transport experiments.*

Membrane	μ_p (nm)	σ_p (-)	N (pores/μm^2)	ε (%)	$MWCO$ (kDa)	τ (-)	S_{int} (μm)
RFO5	4.3	2.6	3191	23	46.5	2.33	1003

Table 9.6 summarized the results of the FO tests of the membrane RFO5. As can be seen from the FO results listed in Table 9.2, the membranes RFO2 and RFO5 exhibit similar J and J_s/J values for the low concentration FO test. This is due to the cleaning step in the laboratory that requires three times less total dose level than in the pilot plant to prepare recycled membranes with similar morphological characteristics. The observed increase of J (i.e. ΔJ = 0.1 kg/m^{2}h) of the RFO5 membrane for the high concentration test from that of the low concentration test is very low. This increase is 90% less than that observed for the membrane RFO2 (i.e. ΔJ = 1 kg/m^{2}h). The J_s/J value corresponding to the high concentration test of the RFO5 membrane is greater than that of the other RFO membranes. It could be caused by a high S_{int} structural parameter (low porosity and high tortuosity) of the RFO5 membrane inducing high ICP effects. The membranes RFO5 and RFO2 exhibit similar R_{HA} values for both low and high concentrations tests.

Table 9.6. *FO results of the RFO5 membrane obtained for low (L_c) and high (H_c) concentration tests: permeate flux (J), reverse salt permeate flux (J_s), specific reverse salt flux (J_s/J), reverse salt transfer factor (RT_s), HA rejection factor (R_{HA}) and HA concentration factor (CF_{HA}).*

	J (kg/m^{2}h)	J_s (10^{-3} kg/m^{2}h)	J_s/J (10^{-3})	RT_s (%)	R_{HA} (%)	CF_{HA}
Lc	6.2 ± 0.3	9 ± 3	1.4. ± 0.4	2.30 ± 0.07	98.57 ± 0.42	1.09 ± 0.05
Hc	6.3 ± 0.3	135 ± 7	21 ± 1	2.60 ± 0.05	99.89 ± 0.06	1.06 ± 0.02

In general, cleaning the discarded RO membrane following the laboratory protocol with an exposure dose three times lower than the pilot plant cleaning protocol resulted in a recycled membrane with very similar intrinsic characteristics, but different transport properties appreciated mainly in high concentration FO tests in which the J_s/J values obtained were higher.

9.7. References

[1] T. Liu, S. Xu, D. Zhang, S. Sourirajan, T. Matsuura, Pore size and pore size distribution on the surface of polyethersulfone hollow fiber membranes, Desalination, 85 (1991) 1-12.

[2] P. Arribas, M. Khayet, M.C. García-Payo, L. Gil, Self-sustained electro-spun polysulfone nano-fibrous membranes and their surface modification by interfacial polymerization for micro- and ultra-filtration, Sep. Purif. Technol., 138 (2014) 118-129.

[3] M. Khayet, C.Y. Feng, K.C. Khulbe, T. Matsuura, Preparation and characterization of polyvinylidene fluoride hollow fiber membranes for ultrafiltration, Polymer, 43 (2002) 3879-3890.

[4] S. Singh, K.C. Khulbe, T. Matsuura, P. Ramamurthy, Membrane characterization by solute transport and atomic force microscopy, J. Membr. Sci., 142 (1998) 111-127.

[5] J.T. Martin, G. Kolliopoulos, V.G. Papangelakis, An improved model for membrane characterization in forward osmosis, J. Membr. Sci., 598 (2020) 117668.

[6] B.R. Babu, N.K. Rastogi, K.S.M.S. Raghavarao, Effect of process parameters on transmembrane flux during direct osmosis, J. Membr. Sci., 280 (2006) 185-194.

[7] M. Mohammadifakhr, J. de Grooth, H.D.W. Roesink, A.J.B. Kemperman, Forward Osmosis: A Critical Review, Processes, 8 (2020) 404.

List of tables in order of appearance

Chapter 1

Chapter 2

Chapter 3

Chapter 4

Chapter 5

Chapter 6

Appendix A

Appendix B

Table 9.6. FO results of the RFO5 membrane obtained for low (L_c) and high (H_c) concentration tests: permeate flux (J), reverse salt permeate flux (J_s), specific reverse salt flux (J_s/J), reverse salt transfer factor (RT_s), HA rejection factor (R_{HA}) and HA concentration factor (CF_{HA}).

226

List of figures in order of appearance

Chapter 1

Chapter 2

Chapter 3

Chapter 4

Chapter 5

Chapter 6

Appendix A

Appendix B